

2-2.5

DOE/NASA/0806-79/1  
NASA CR-159663

*Wilson - 8/53.*

# HIGH-TEMPERATURE MOLTEN SALT THERMAL ENERGY STORAGE SYSTEMS

Randy J. Petri  
Terry D. Claar  
Ray R. Tison  
Leonard G. Marianowski  
Institute of Gas Technology

**February 1980**

Prepared for  
NATIONAL AERONAUTICS AND SPACE ADMINISTRATION  
Lewis Research Center  
Under Contract NAS 3-20806

for  
**U.S. DEPARTMENT OF ENERGY**  
**Office of Solar, Geothermal, Electric and Storage Systems**  
**Division of Energy Storage Systems**

## NOTICE

This report was prepared as an account of work sponsored by the United States Government. Neither the United States nor the United States Department of Energy, nor any of their employees, nor any of their contractors, subcontractors, or their employees, make any warranty, express or implied, or assume any legal liability or responsibility for the accuracy, completeness or usefulness of any information, apparatus, product or process disclosed, or represent that its use would not infringe privately owned rights.

DOE/NASA/0806-79/1  
NASA CR-159663

# HIGH-TEMPERATURE MOLTEN SALT THERMAL ENERGY STORAGE SYSTEMS

Randy J. Petri  
Terry D. Claar  
Ray R. Tison  
Leonard G. Marianowski  
Institute of Gas Technology  
Chicago, Illinois 60616

February 1980

Prepared for  
National Aeronautics and Space Administration  
Lewis Research Center  
Cleveland, Ohio 44135  
Under Contract NAS 3-20806

for  
U.S. DEPARTMENT OF ENERGY  
Office of Solar, Geothermal, Electric and Storage Systems  
Division of Energy Storage Systems  
Washington, D.C. 20545  
Under Interagency Agreement EC-77-A-31-1034

## ACKNOWLEDGMENT

The authors wish to thank John Dullea, Bernie D. Yudow and Abu Talib for their significant contributions to the organization and completion of Task 1. We thank Joseph G. Hermanek for his efforts and timely suggestions in the assembly and experimental data collection phase of the program. The authors are especially grateful to Alan Kardas for his cooperation, insight, and enthusiastic advice throughout the preparation of this report.

## ABSTRACT

Experimental results of comparative screening studies of candidate molten carbonate salts as phase-change materials (PCM) for advanced solar-thermal energy storage applications at 540° to 870°C (1004° to 1600°F) and steam-Rankine electric generation at 400° to 540°C (752° to 1004°F) are presented. Alkali carbonates are attractive as latent-heat storage materials because of their relatively high storage capacity and thermal conductivity, low corrosivity, moderate cost, and safe and simple handling requirements. Salts were tested in 0.1 kWhr lab-scale modules and evaluated on the basis of discharge heat flux, solidification temperature range, thermal cycling stability, and compatibility with containment materials. The feasibility of using a distributed network of high-conductivity material to increase the heat flux through the layer of solidified salt was experimentally evaluated. The thermal performance of an 8 kWhr thermal energy storage (TES) module containing  $\text{LiKCO}_3$  remained very stable throughout 5650 hours and 130 charge/discharge cycles at 480° to 535°C (896° to 995°F). A TES utilization concept of an electrical generation peaking subsystem composed of a multistage condensing steam turbine and a TES subsystem with a separate power conversion loop was defined. Conceptual designs for a 100 MW<sub>e</sub> TES peaking system providing steam at 316°, 427°, and 454°C (600°, 800°, and 850°F) at  $3.79 \times 10^6$  Pa (550 psia) were developed and evaluated. Areas requiring further investigation have also been identified.

## EXECUTIVE SUMMARY

The objectives of this TES program were to a) define and identify a high-temperature TES concept that can effectively utilize the high-quality thermal energy in a steam-electric power generating facility, b) investigate and test candidate TES salts, primarily carbonates, which are applicable to energy storage in both the superheat region (temperature range of 343° to 399°C, 649° to 750°F) of conventional electric-utility, water-Rankine power plants and in TES systems for solar-thermal power system applications in the temperature range of 538° to 871°C (1000° to 1600°F), and c) evaluate means of increasing the heat flux during thermal discharging. The work performed to achieve these objectives is described in two tasks.

- Task 1 System Definition

This section presents a TES peaking system concept to apply in fossil fuel-fired steam-electric plants. It discusses the design criteria used to develop the concept, the necessary operating characteristics from the TES unit, and the economics and general status of the technology. The principal features of the TES peaking system are 1) good system efficiency, 2) minimum degradation of the charging energy in the TES unit, and 3) minimum impact on the primary plant's operating procedures.

The results of the system studies performed here indicate that a phase-change TES material for application in a steam-Rankine cycle should have a transformation temperature less than 350°C (662°F).

- Task 2 TES Module Testing and Evaluation

Three engineering-scale modules were constructed and operated under Energy Research and Development Administration (ERDA) Contract No. EY-76-C-02-2888. The engineering-scale units were 0.305 m (1 ft) in outer diameter (OD) and 0.457 m (1.5 ft) high with a 0.0508-m (2-in.) diameter single-pass heat exchanger (HX) tube. They contained LiKCO<sub>3</sub> salt, which has a melting point of 505°C (940°F). One of these units, Unit No. 2, was cycled 30 times, which represented 1400 hours of operation. As a result of the already accumulated operating time, the unit was restarted and operation was continued under this contract to obtain system endurance data. This unit was then operated and discharged for a total of 5650 hours and 129 charge/discharge

cycles, with no significant losses of system performance. The  $\text{LiKCO}_3$  salt and AISI 316 stainless-steel containment and HX exhibited very good physical and chemical stability.

Salts were also investigated in this subtask for their applicability to latent heat storage in the low  $343^\circ$  to  $399^\circ\text{C}$  ( $650^\circ$  to  $750^\circ\text{F}$ ) temperature range, and the  $538^\circ$  to  $871^\circ\text{C}$  ( $1000^\circ$  to  $1600^\circ\text{F}$ ) range for solar-thermal applications. Emphasis was given to salt compositions based on  $\text{Li}_2\text{CO}_3$ ,  $\text{Na}_2\text{CO}_3$ , and  $\text{K}_2\text{CO}_3$ , from which congruent melting carbonate mixtures are available covering the temperature range  $397^\circ$  to  $898^\circ\text{C}$  ( $747^\circ$  to  $1648^\circ\text{F}$ ). From the work completed in Task 1, however, it was indicated that phase-change TES materials in a steam-Rankine cycle should also have transformation temperatures less than  $350^\circ\text{C}$  ( $662^\circ\text{F}$ ). Because this temperature is lower than the lowest melting carbonate eutectic known, and subsequent work was to be primarily with carbonates, the major experimental effort was at this point redirected to solar-thermal systems applications in the temperature range  $538^\circ$  to  $871^\circ\text{C}$  ( $1000^\circ$  to  $1600^\circ\text{F}$ ). These salts were tested in laboratory-scale units that were 0.0762 m (3 in.) in OD and 0.127 m (5 in.) high with a 0.0127-m (0.5-in.) diameter internal HX tube. The thermal performance of the laboratory-scale units was determined during charge/discharge cycles, using high-velocity ambient air as the working fluid. From this study, pure  $\text{Li}_2\text{CO}_3$  and  $\text{Na}_2\text{CO}_3$  emerged as strong congruent melting candidates for high-temperature solar-thermal applications, with a  $(\text{Li-Na-K})_2\text{CO}_3$  eutectic for the lower, steam-Rankine applications. Two alkali/alkaline earth carbonate mixtures,  $\text{Na}_2\text{CO}_3\text{-BaCO}_3$  and  $\text{Li}_2\text{CO}_3\text{-CaCO}_3$ , also exhibited extremely stable performance in the  $600^\circ$  to  $750^\circ\text{C}$  ( $1112^\circ$  to  $1382^\circ\text{F}$ ) range. The thermal response of these lab-scale storage units agreed well with that predicted by the heat-transfer model developed at the Institute of Gas Technology (IGT) under the previous ERDA contract.

At the flow rates investigated, the rate of discharge was limited by the transfer of heat between the salt and HX through the zone of solidified salt formed on the HX during discharge. Enhancement of this heat conduction was investigated and accomplished by installing a continuous, reticulated aluminum matrix into the  $(\text{Li-Na-K})_2\text{CO}_3$  salt and by testing an off-eutectic, 81.3 wt %  $\text{Na}_2\text{CO}_3$  - 18.7 wt %  $\text{K}_2\text{CO}_3$  incongruent melting slush. A porous carbon-based material tested as a heat conduction enhancement material was found to be incompatible with a  $\text{Na}_2\text{CO}_3\text{-K}_2\text{CO}_3$  melt at  $710^\circ\text{C}$  ( $1318^\circ\text{F}$ ).

A heat transfer model, originally developed at IGT in 1976 under ERDA Contract No. EY-76-C-02-2888, was also used in the scale-up of a TES subsystem conceptual design relevant to large, solar-thermal power system applications. A conceptual design based on use of  $\text{Li}_2\text{CO}_3$  PCM for a  $50 \text{ MW}_{\text{th}}$  system utilizing air charge/discharge fluid was completed.

It is recommended that further investigations focus on salt/containment compatibility using high-temperature alloys, development of cost-effective containment and insulation materials, long-term testing of larger units ( $\geq 10 \text{ kWhr}_{\text{th}}$ ) utilizing actual working fluids, continued cost/benefit analyses of thermal conductivity enhancement (TCE) materials, and heat-transfer modeling studies. In addition, interaction with ongoing TES systems design and analysis studies is necessary to provide effective feedback to salt/HX research and development efforts.

## TABLE OF CONTENTS

	<u>Page No.</u>
ABSTRACT	v
EXECUTIVE SUMMARY	vii
DETAILED DESCRIPTION OF TECHNICAL PROGRESS	1
Task 1. System Definition	1
Introduction	1
System Concept Development	1
Operating Conditions	5
Base Case — 316°C (600°F) Outlet Steam Temperature	5
Additional Designs — 427°C (800°F) and 454°C (850°F) Outlet Steam Temperatures	6
Economic Analysis	12
Status of Technology	13
Summary	26
Task 2. TES Module Testing	27
2.1 Engineering-Scale Testing	27
Introduction	27
Cyclic Endurance Testing	27
Post-Test Examination	33
2.2 Laboratory-Scale Testing	39
Introduction	39
Salt Selection	40
System Components: Construction, Operating Procedures and Data Collection	49
Construction	49
Operating Procedures and Data Collection	49
Salt TES Performance Evaluation	55

## TABLE OF CONTENTS, Cont.

	<u>Page No.</u>
Criteria for Performance Evaluation	55
Evaluation of Salts for Steam-Rankine Applications 343° to 399°C (650° to 750°F)	56
Evaluation of Salts for Solar-Thermal Applications 538° to 871°C (1000° to 1600°F)	63
Non-Carbonate Salts	96
Experimental Verification of Megerlin Analysis	100
Solidification of Pure $\text{Li}_2\text{CO}_3$ and $\text{Na}_2\text{CO}_3$ ; Movement of the Solid-Liquid Interface During System Discharge	102
Assessment of Salt TES Applicability	105
2.3 Evaluation of TCE Materials	107
Introduction	107
Experimental Testing	107
Corrosion Tests	109
Lab-Scale TCE Evaluation	111
Techno-Economic Considerations of TCE Materials	120
Conductivity Enhancement Factor	122
Cost, Performance, and Design Implications	123
2.4 Conceptual Design of TES Module for Solar-Thermal Power Station	130
Use of the Heat Transfer Model in Large-Scale TES Solar-Thermal Power System	130
Introduction	130
TES Subsystem for Large-Scale Solar-Thermal Power Plant (Air Fluid)	131

## TABLE OF CONTENTS, Cont.

	<u>Page No.</u>
CONCLUSIONS	144
Steam-Electric Power System Definition	144
Salts	144
Containment and HX Materials	145
TCE Materials	145
TES Module Thermal Performance	146
RECOMMENDATIONS FOR FUTURE RESEARCH	147
REFERENCES	148
APPENDIX A. Conversion Factors	151
APPENDIX B. Carbonate Phase Diagrams	155
APPENDIX C. Information for NASA	161

## LIST OF FIGURES

<u>Figure No.</u>		<u>Page No.</u>
1	Primary Plant With TES Peaking System	3
2	TES Subsystem With 316°C (600°F) Outlet Steam	7
3	Tentative Heat Balance for 100-MW Peaking Unit	8
4	Conceptual TES Unit With 427°C (800°F) Outlet Steam	10
5	TES Subsystem With 454°C (850°F) Outlet Steam	11
6	Tentative Heat Balances for 100-MW Peaking Unit With 427°C (800°F) Outlet Steam	13
7	Tentative Heat Balances for 100-MW Peaking Unit With 454°C (850°F) Outlet Steam	15
8	Target Costs for a TES Subsystem as a Function of Electrical Generation Subsystem Cost, Fixed Charge Rate, and Output Electricity Cost With 316°C (600°F) Outlet Steam	20
9	Target Costs for a TES Subsystem as a Function of Electrical Generation Subsystem Cost, Fixed Charge Rate, and Output Electricity Cost With 427°C (800°F) Outlet Steam	21
10	Target Costs for a TES Subsystem as a Function of Electrical Generation Subsystem Cost, Fixed Charge Rate, and Output Electricity Cost With 454°C (850°F) Outlet Steam	22
11	Engineering-Scale Thermal Energy Storage Unit	28
12	Engineering-Scale Unit Mounted in Testing Station	29
13	Schematic Diagram of the Engineering-Scale TES System	30
14	Discharge Performance of Engineering-Scale TES Unit 2 (LiKCO <sub>3</sub> Salt)	32
15	Appearance of Engineering Unit 2 After 5650 Hours of Elevated-Temperature Operation (Insulation and Cover Removed)	34

## LIST OF FIGURES, Cont.

<u>Figure No.</u>		<u>Page No.</u>
16	Appearance of $\text{LiKCO}_3$ Salt in Engineering Unit 2 After 129 Cycles and 5650 Hours of Elevated-Temperature Operation	35
17	Type 316 SS Containment From Engineering Unit 2 After 5650 Hours of Testing, Salt Side, Mid-Height ( $\text{FeCl}_3\text{-HCl-H}_2\text{O}$ Etchant)	38
18	Heat Content Curves for Selected Carbonates and MgO	43
19	Cross Section of Typical Lab-Scale Cannister	50
20	Final Design of TES Cannister	51
21	Four-Station TES Lab-Scale Test Stand	52
22	Schematic of Lab-Scale Module	54
23	Typical Discharge Performance of Lab-Scale Module L3-1 Containing Ternary $(\text{Li-Na-K})_2\text{CO}_3$ Eutectic	59
24	Typical Discharge Performance of $(\text{Li-Na-K})_2\text{CO}_3$ Ternary Eutectic at $5.1 \text{ m}^3/\text{hr}$ ( $180 \text{ ft}^3/\text{hr}$ ) Air Flow Rate	60
25	Experimental Heat Flux Curve for $(\text{Li-Na-K})_2\text{CO}_3$ System With No Conductivity Enhancement	61
26	Typical Discharge Performance of Module L1-1, 49.4 wt % $\text{Na}_2\text{CO}_3$ - 50.6 wt % $\text{K}_2\text{CO}_3$	65
27	Typical Discharge Performance of Module L1-1, 49.4 wt % $\text{Na}_2\text{CO}_3$ - 50.6 wt % $\text{K}_2\text{CO}_3$ at $5.1 \text{ m}^3/\text{hr}$ ( $180 \text{ ft}^3/\text{hr}$ ) Air Flow Rate	66
28	Experimental Heat Flux Curve for Module L1-1, 49.4 wt % $\text{Na}_2\text{CO}_3$ - 50.6 wt % $\text{K}_2\text{CO}_3$ at $5.1 \text{ m}^3/\text{hr}$ ( $180 \text{ ft}^3/\text{hr}$ ) Air Flow Rate	67
29	Typical Discharge Performance of $(\text{Na-K})_2\text{CO}_3$ System With $\text{Li}_2\text{CO}_3$ Added	69
30	Experimental Heat Flux Curve for $(\text{Na-K})_2\text{CO}_3$ System With $\text{Li}_2\text{CO}_3$ Added	70

## LIST OF FIGURES, Cont.

<u>Figure No.</u>		<u>Page No.</u>
31	Lifetime Discharge Performance of (Na-K) <sub>2</sub> CO <sub>3</sub> System With Li <sub>2</sub> CO <sub>3</sub> Added	71
32	Typical Discharge Performance of Li <sub>2</sub> CO <sub>3</sub> System (Module L2-1: Air Cover Gas) at 5.1 m <sup>3</sup> /hr (180 ft <sup>3</sup> /hr) Air Flow Rate	73
33	Experimental Heat Flux Curve for Li <sub>2</sub> CO <sub>3</sub> System (Module L2-1: Air Cover Gas) at 5.1 m <sup>3</sup> /hr (180 ft <sup>3</sup> /hr) Air Flow Rate	74
34	Typical Discharge Performance of Li <sub>2</sub> CO <sub>3</sub> System With CO <sub>2</sub> Cover Gas at 5.1 m <sup>3</sup> /hr (180 ft <sup>3</sup> /hr) Air Flow Rate	75
35	Experimental Heat Flux Curve for Li <sub>2</sub> CO <sub>3</sub> System With CO <sub>2</sub> Cover Gas at 5.1 m <sup>3</sup> /hr (180 ft <sup>3</sup> /hr) Air Flow Rate	76
36	Lifetime Discharge Performance of Li <sub>2</sub> CO <sub>3</sub> System With CO <sub>2</sub> Cover Gas	77
37	Transverse Cross Section Through Module L4-2 Li <sub>2</sub> CO <sub>3</sub> System After 672 Hours and 22 Cycles	79
38	Typical Discharge Performance of Na <sub>2</sub> CO <sub>3</sub> System at 5.1 m <sup>3</sup> /hr (180 ft <sup>3</sup> /hr) Air Flow Rate	81
39	Lifetime Discharge Performance of Na <sub>2</sub> CO <sub>3</sub> System	82
40	Transverse Cross Section Through Module L2-2 Na <sub>2</sub> CO <sub>3</sub> System After 288 Hours and 21 Cycles	83
41	Type 316 SS Containment After 288 Hours Exposure to Na <sub>2</sub> CO <sub>3</sub> And 21 Cycles at 807° to 907°C (1485° to 1665°F) Under CO <sub>2</sub> Cover Gas (FeCl <sub>3</sub> -HCl-H <sub>2</sub> O Etchant)	85
42	Typical Discharge Performance of Module L2-3 K <sub>2</sub> CO <sub>3</sub> System at 5.1 m <sup>3</sup> /hr (180 ft <sup>3</sup> /hr) Air Flow Rate	86
43	Experimental Heat Flux Curve for Module L2-3 K <sub>2</sub> CO <sub>3</sub> System at 5.1 m <sup>3</sup> /hr (180 ft <sup>3</sup> /hr) Air Flow Rate	87

## LIST OF FIGURES, Cont.

<u>Figure No.</u>		<u>Page No.</u>
44	Longitudinal Cross Section Through Module L2-3 K <sub>2</sub> CO <sub>3</sub> System That Failed After 96 Hours at 841° to 941°C (1546° to 1726°F) and 2 Cycles	89
45	Typical Discharge Performance of Na <sub>2</sub> CO <sub>3</sub> -BaCO <sub>3</sub> System at 5.1 m <sup>3</sup> /hr (180 ft <sup>3</sup> /hr) Air Flow Rate	90
46	Lifetime Discharge Performance of Na <sub>2</sub> CO <sub>3</sub> -BaCO <sub>3</sub> System Over 984 Hours	92
47	Transverse Cross Section Through Module L3-3 47.8 wt % Na <sub>2</sub> CO <sub>3</sub> - 52.2 wt % BaCO <sub>3</sub> After 984 Hours and 36 Cycles	93
48	Typical Discharge Performance of Li <sub>2</sub> CO <sub>3</sub> -CaCO <sub>3</sub> System at 5.1 m <sup>3</sup> /hr (180 ft <sup>3</sup> /hr) Air Flow Rate	94
49	Lifetime Average Instantaneous Heat Flux Curve for Li <sub>2</sub> CO <sub>3</sub> -CaCO <sub>3</sub> System	95
50	Module L3-4 After Filling With CaCl <sub>2</sub> and Holding at 725°C (1337°F) For 20 Hours	98
51	Module L4-3 After Filling With NaF-KF and Holding at 770°C (1418°F) for 6 Hours	99
52	Comparison of Li <sub>2</sub> CO <sub>3</sub> Experimental Solidification Profiles With Predictions of the Megerlin Solution	103
53	Comparison of Na <sub>2</sub> CO <sub>3</sub> Experimental Solidification Profiles With Predictions of the Megerlin Solution	104
54	Duocel Aluminum Material as Received (Left) and After 528 Hours Exposure to Molten (Li-Na-K) <sub>2</sub> CO <sub>3</sub> At 450°C (842°F) (Right)	110
55	Force-Fit Installation of Duocel Enhancement Material Into Cannister Containing (Li-Na-K) <sub>2</sub> CO <sub>3</sub> Eutectic	112
56	(Li-Na-K) <sub>2</sub> CO <sub>3</sub> (32-33-35 wt %) Discharge Profile Without and With Duocel TCE Material	114
57	Comparison of (Li-Na-K) <sub>2</sub> CO <sub>3</sub> Discharge Heat Flux Performance Without and With Conductivity Enhancement	115

## LIST OF FIGURES, Cont.

<u>Figure No.</u>		<u>Page No.</u>
58	Longitudinal Cross Section Through Module L3-1 and L3-2 (Li-Na-K) <sub>2</sub> CO <sub>3</sub> (32-33-35 wt %) After 816 Hours and 32 Cycles	116
59	Typical Discharge Performance of (Na-K) <sub>2</sub> CO <sub>3</sub> Slush at 5.1 m <sup>3</sup> /hr (180 ft <sup>3</sup> /hr) Air Flow Rate	118
60	Lifetime Discharge Heat Flux of (Na-K) <sub>2</sub> CO <sub>3</sub> Slush	119
61	Transverse Cross Section Through Module L1-3 81.3 wt % Na <sub>2</sub> CO <sub>3</sub> - 18.7 wt % K <sub>2</sub> Cl <sub>3</sub> After 1032 Hours and 38 Cycles	121
62	Thermal Conductivity of Porous Aluminum Duocel Material	124
63	Effective Thermal Conductivity of Porous Aluminum/Salt Composite Material (Calculated From Equation 33)	125
64	Enhancement Factor-to-Cost Ratio Versus Density of Porous Aluminum for Several Assumed Values of k <sub>S</sub>	127
65	Assumed Cost of Porous Aluminum Enhancement Material	128
66	Kinetics of Solidification of Annular PCM Layer From Within	129
67	Central Receiver Solar Power Plant Concept	132
68	Storage/Plant Schematic	133
69	Phase-Change TES Concept	134
70	Megerlin Plots for Determining Solidified PCM Thickness	137
71	Graphic Solution for the Design of a Multitube HX TES Subsystem Using Li <sub>2</sub> CO <sub>3</sub>	141
72	Cross Section of Latent-Heat Phase-Change TES Subsystem (Top View)	142

## LIST OF TABLES

<u>Table No.</u>		<u>Page No.</u>
1	Typical Power Plant Steam-Generator Conditions	4
2	Heat-Balance Information for 100-MW Peaking Unit With 316°C (600°F) Outlet Steam	9
3	Heat-Balance Information for 100-MW Peaking Unit With 427°C (800°F) Outlet Steam	14
4	Heat-Balance Information for 100-MW Peaking Unit With 454°C (850°F) Outlet Steam	16
5	EPRI-Recommended Levelized Fixed Charge Rates	17
6	Containment Vessel/HX Ceiling Costs as a Function of Salt Cost (Expressed in Terms of HX Heat Flux)	26
7	Experimental Results for Discharging of Engineering-Scale TES Unit 2 (LiKCO <sub>3</sub> Salt)	33
8	X-Ray Diffraction Analysis of Corrosion Product Scale From Engineering Unit 2	36
9	Chemical Analysis of LiKCO <sub>3</sub> Salt From Engineering-Scale Unit 2	37
10	Selected Properties of Alkali Carbonates	41
11	Selected Properties of Alkaline Earth Carbonates	45
12	Candidate Carbonate-Containing Salts Having Melting Points in the Range 398° to 898°C (750° to 1650°F)	47
13	Final Salts Selected for Lab-Scale TES Testing	48
14	DSC Results for the (Li-Na-K) <sub>2</sub> CO <sub>3</sub> Ternary and Ternary With Alkaline Earth Carbonate Additions	57
15	Lab-Scale TES Experimental Results	62
16	Pre- and Post-Test Chemical Analysis of Li <sub>2</sub> CO <sub>3</sub> System	78

## LIST OF TABLES, Cont.

<u>Table No.</u>		<u>Page No.</u>
17	Pre- and Post-Test Chemical Analysis of $\text{Na}_2\text{CO}_3$ System	84
18	Pre- and Post-Test Chemical Analysis of $\text{K}_2\text{CO}_3$ System	88
19	Comparison of Theoretical and Observed Solidification Behavior ( $\text{Li}_2\text{CO}_3$ and $\text{Na}_2\text{CO}_3$ )	102
20	Potential Heat Conduction Enhancement Materials	108
21	Results of Corrosion Testing of Aluminum Duocel in Ternary Eutectic 43.5 mol % $\text{Li}_2\text{CO}_3$ , 31.5 mol % $\text{Na}_2\text{CO}_3$ , 25.0 mol % $\text{K}_2\text{CO}_3$ , 450°C	109
22	(Na-K) $_2\text{CO}_3$ 81.3 - 18.7 wt % "Slush" Pre- and Post-Test Chemical Analysis	120
23	Design Parameters for Air Upgrading, Using $\text{Li}_2\text{CO}_3$ as the PCM	140

## DETAILED DESCRIPTION OF TECHNICAL PROGRESS

Task 1. System DefinitionIntroduction

Energy demands from baseload electrical generating plants vary throughout any given day, producing a variable demand on generating equipment. Because of this variation, a portion of a utility's baseload generation, which is generally coal- and nuclear-fueled, may be unused during low-demand periods. With baseload generation capacity available, the concept of storing energy becomes attractive, because energy storage can reduce the conventional peaking unit's (diesel and combustion turbines) requirements by allowing for the substitution of domestically available coal and uranium for the more expensive and increasingly difficult-to-obtain oil and natural gas. But storing electrical energy is both difficult and technologically limited. To date, pumped hydro has been the principal method of storing energy on a large scale; however, other methods of storing energy for utility application are being developed. One such method is thermal energy storage (TES), utilizing the latent heat of phase-change storage media.

The objectives of this task were to --

- Identify a range of operational latent-heat TES temperatures required for application with fossil fuel-fired steam-electric plants
- Define and identify a high-temperature TES concept that could utilize this high-temperature energy.

These objectives were accomplished by evaluating peaking energy availability from coal- and nuclear-fueled baseload plants, design criteria and operating and economic requirements of the TES unit, and the general status of the technology of TES systems. In considering peaking TES subsystems, particular attention was given to assuring minimum impact on the operating procedures of the primary generating plant, minimum degradation of the charging energy in the TES subsystem, and a realistically good overall system efficiency.

System Concept Development

Several concepts exist for integrating TES peaking systems into power plants. For example, a recent study by Grumman examined 10 different TES locations within nuclear and fossil fuel power plants, and Honeywell, Xerox,

and others<sup>1-6</sup> have proposed TES concepts for integration with solar-powered plants. In selecting a TES utilization concept for analysis, current literature on TES systems was reviewed, and a meeting was held with representatives of a major utility in order to define the selection criteria and limits that would prohibit TES application.<sup>7,8</sup> The criteria and limits defined were —

- Significant increases in the complexity of plant operations are undesirable.
- The introduction of additional thermal/mechanical stress on the primary plant's equipment is undesirable.
- Retrofit of current feedwater TES concepts, and possibly all other TES concepts that assume retrofit, may not be feasible because of downtime requirements for system installation.
- When the TES charging-steam circuit is such that at some point it passes through the plant's cooling tower, a portion of the energy rejected may have to be charged to the peaking system if fair energy-accounting practices are employed.
- Latent-heat storage is well suited to the boiling operation.

Based on these criteria, a TES peaking system concept that would allow considerable freedom in the specific design of the storage portion of the system, while taking advantage of the available information, was chosen. This TES peaking concept, shown in Figure 1, employs a separate power conversion loop (electrical generation subsystem) and a TES subsystem. During charging, steam coming directly from the primary plant's boiler is supplied to the TES subsystem, where it is condensed and returned as boiler feedwater. When discharging, the TES subsystem serves as a boiler, providing steam to the electrical generation subsystem — a conventional multistage condensing steam turbine.

With the separate power conversion loop TES peaking system concept, additional thermal/mechanical stress is not introduced into the primary plant's generation section, and increased control complexity is limited to throttling the charging and discharging fluid.

For this concept, the primary plant's steam generator determines, to a great extent, the TES subsystem's operating conditions. The operating pressure determines the temperature at which the steam will condense and, hence, the temperature at which a major portion of the energy is available during

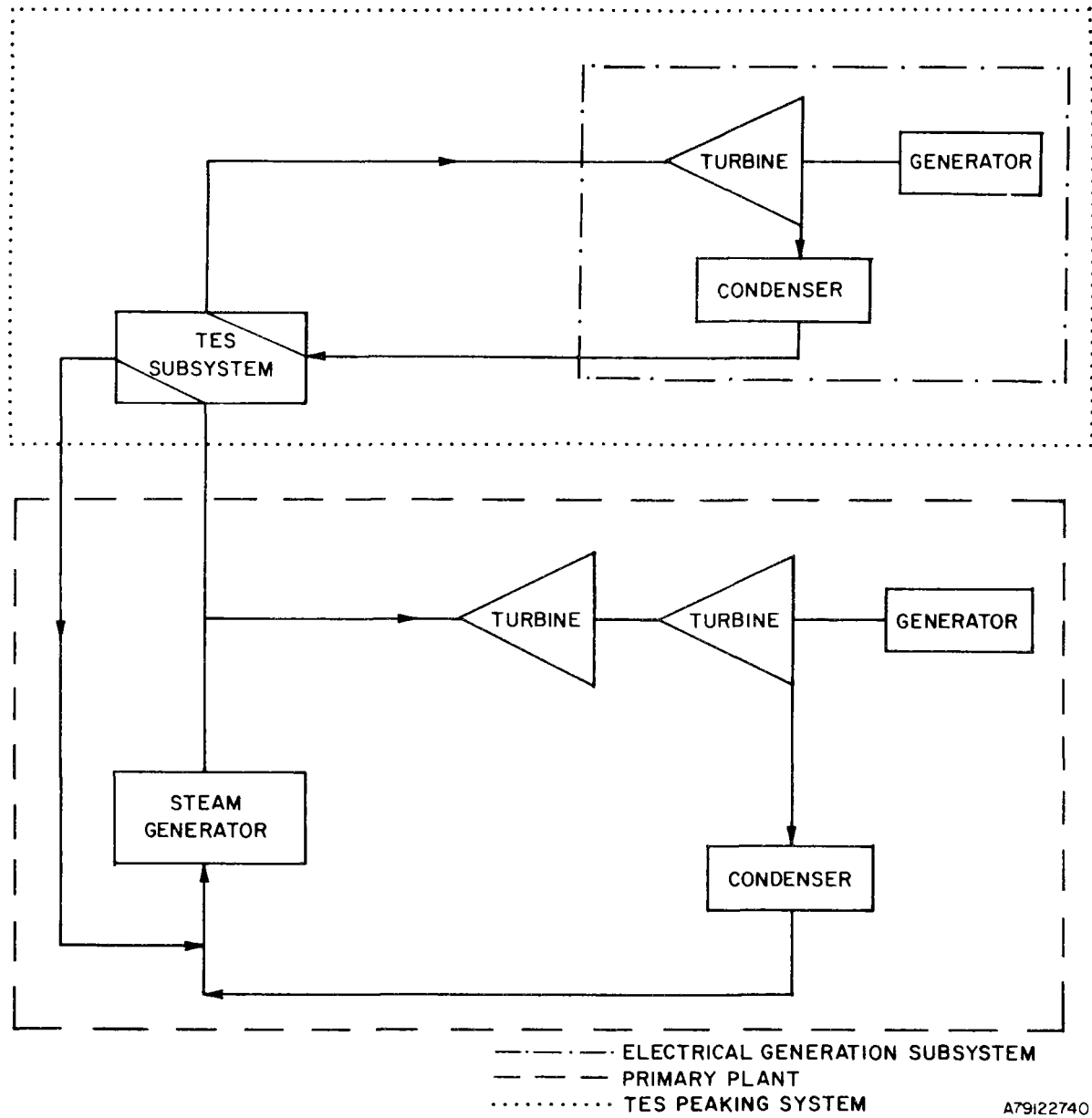


Figure 1. PRIMARY PLANT WITH TES PEAKING SYSTEM

charging. The output steam temperature influences the discharging output temperature, and the feedwater return temperature establishes a target temperature for the condensate returned from the TES subsystem during charging. Typical primary plant steam generator characteristics are shown generically in Table 1 for the two fossil- and two nuclear-fueled plants.

Table 1. TYPICAL POWER PLANT STEAM-GENERATOR CONDITIONS

	Conventional Fossil <sup>6</sup>	Supercritical Fossil <sup>6</sup>	Nuclear	
			PWR <sup>7</sup>	BWR <sup>8</sup>
Output Temperature, Steam, °C (°F)	538 (1000)	538 (1000)	266 (510)	288 (550)
Return Temperature, Water, °C (°F)	249 (480)	266 (510)	204 (400)	171 (340)
Pressure, Pa (psia)	1.7 X 10 <sup>7</sup> (2500)	1.3 X 10 <sup>7</sup> (3500)	2.5 X 10 <sup>6</sup> (690)	3.6 X 10 <sup>6</sup> (965)

A80020302

While it is desirable (and most likely possible) to combine a TES system with a pressurized water reactor (PWR) or a boiling water reactor (BWR) nuclear power plant, the low output steam temperature and pressure of just over 260°C (500°F) and  $4.826 \times 10^6$  Pa to  $6.957 \times 10^6$  Pa (700 to 1009 psia), respectively, prohibit the use of a separate power conversion loop TES peaking system. The conversion efficiency during discharge of the TES peaking system would be very low.

In contrast, the fossil-fueled plants have boiler output temperature and pressures of about 538°C (1000°F) and  $1.655 \times 10^7$  to  $2.413 \times 10^7$  Pa (2400 to 3500 psia), permitting a considerably higher efficiency during discharge. Thus, we have assumed the TES utilization concept to be mated with a power plant that can provide superheated steam at 538°C (1000°F) and  $1.655 \times 10^7$  Pa (2400 psia). Additionally, for a TES system designed to accept superheated steam and discharge water in the charging mode, a staged or phased TES subsystem will be needed to minimize the reduction in temperature availability from charging to discharging.

Simplistically, the TES subsystem can be viewed as a subsystem with a charge/discharge mode. Both modes can then be broken down into three stages, with the discharge mode performing the reverse of the charge mode, as follows:

<u>Stage</u>	<u>Charging Mode</u>	<u>Discharging Mode</u>
1	Desuperheating	Superheating
2	Condensing	Boiling
3	Condensate Cooling	Feedwater Heating

Although the desuperheating/superheating and condensate cooling/feedwater heating stages could employ non-isothermal energy storage in a sensible storage material with temperature gradients in the direction of charging fluid flow, the establishment and maintenance of these gradients in storage and during discharge to ensure the system's proper operation is uncertain. Thus, we have assumed all TES subsystem stages to be nearly isothermal, employing phase change materials.

In summary, the TES utilization concept selected consists of an electrical generation subsystem composed of a conventional multistage condensing steam turbine and a TES subsystem, with the subsystem employing at least three isothermal energy storage modules operating in series. Its only connection to the primary plant, which provides steam at 538°C (1000°F) and  $1.655 \times 10^7$  Pa (2400 psia), is a charging steam line and a feedwater return line.

#### Operating Conditions

##### Base Case - 316°C (600°F) Outlet Steam

In the TES subsystem, the charging steam is received from the primary plant's boiler at 538°C (1000°F) and  $1.655 \times 10^7$  Pa (2400 psia); at this pressure, the saturation temperature of the charging steam is about 350°C (662°F), which defines an upper boundary for the operating temperature of the condensing/boiling stage of the TES subsystem. The lower boundary is simply the highest temperature and associated pressure that can be obtained during discharge, allowing for a reasonable driving temperature difference during charging and discharging. Assuming a temperature difference of about 50°C (90°F) between the PCM in the condensing/boiling stage and the charging and discharging fluid, the saturation temperature of the discharge steam was set at 247°C (477°F), resulting in a system pressure of  $3.792 \times 10^6$  Pa (550 psia) and a melt temperature for the PCM of about 297°C (567°F). Operating temperatures of the remaining stages were set somewhat arbitrarily after a discharge output temperature was selected, with reasonable temperatures for the feedwater return during charging and feedwater input during discharging being known.

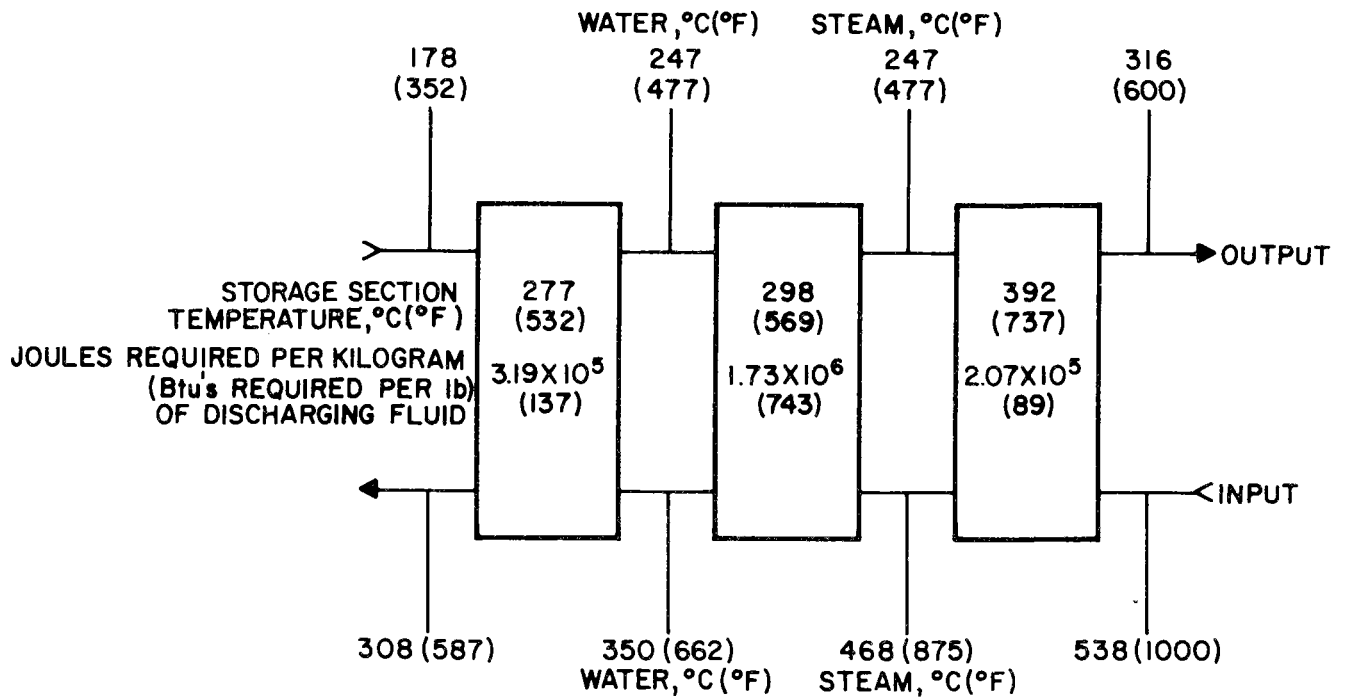
For a base-case, three-stage TES subsystem, the final temperature of the discharging fluid was conservatively set at 316°C (600°F), with feedwater input set at 178°C (352°F). Figure 2 conceptually shows the TES subsystem and its charging and discharging condition. With input steam conditions of 316°C (600°F) and  $3.792 \times 10^6$  (550 psia) to the electrical generation subsystem and exhaust conditions of  $6.895 \times 10^3$  Pa (1 psia) and 5% moisture, a tentative heat balance was calculated for a plant producing 100 MW of net electric power output (Figure 3). A heat rate of  $1.79 \times 10^7$  J/kWhr (16,972 Btu/kWhr) was obtained for a thermal-to-electric cycle efficiency of 20.1%. Table 2 provides additional cycle information.

The total heat required in storage to achieve an 8-hour discharge period at 100 MW is  $1.43 \times 10^{13}$  J ( $13.576 \times 10^9$  Btu). Discharging mass is  $6.355 \times 10^6$  kg (14,010,552 lb) with a charging mass of  $7.12 \times 10^6$  kg (15,691,818 lb). Discharging flow rate is  $7.94 \times 10^5$  kg/hr (1,751,319 lb/hr) for 8 hours. At a flow rate equal to the discharging rate, charging would require 8.96 hours.

Additional Designs: 427°C (800°F) and 454°C (850°F) Outlet Steam Temperatures

The base-case TES unit was assumed to provide steam at 316°C (600°F) and  $3.792 \times 10^6$  Pa (550 psia) via a multi-temperature storage unit. This TES unit was depicted as having nominally three isothermal sections to provide preheating, vaporization, and superheating to the discharging fluid. It is desirable, for efficient operation of the steam turbine, to increase the output temperature of the discharge fluid; this increase requires division into non-isothermal superheating and preheating sections or the division of these two sections into several isothermal sections.

Using the several isothermal sections approach, the number of isothermal storage sections and the charging-mass to discharging-mass ratio were varied to arrive at conceptual designs for TES units providing steam at  $3.792 \times 10^6$  Pa (550 psia), 427°C (800°F) and 454°C (850°F). Figures 4 and 5 show these designs. The 427°C (800°F) case requires six isothermal sections and has a charge-to-discharge mass ratio of 1.2 while the 454°C (850°F) case requires seven sections with a charge-to-discharge mass ratio of 1.3. The increased charging-mass to discharging-mass ratios [the 316°C (600°F) unit's 1.12 ratio is the reference base] were required to obtain enough high-temperature energy in storage for superheating during discharge.



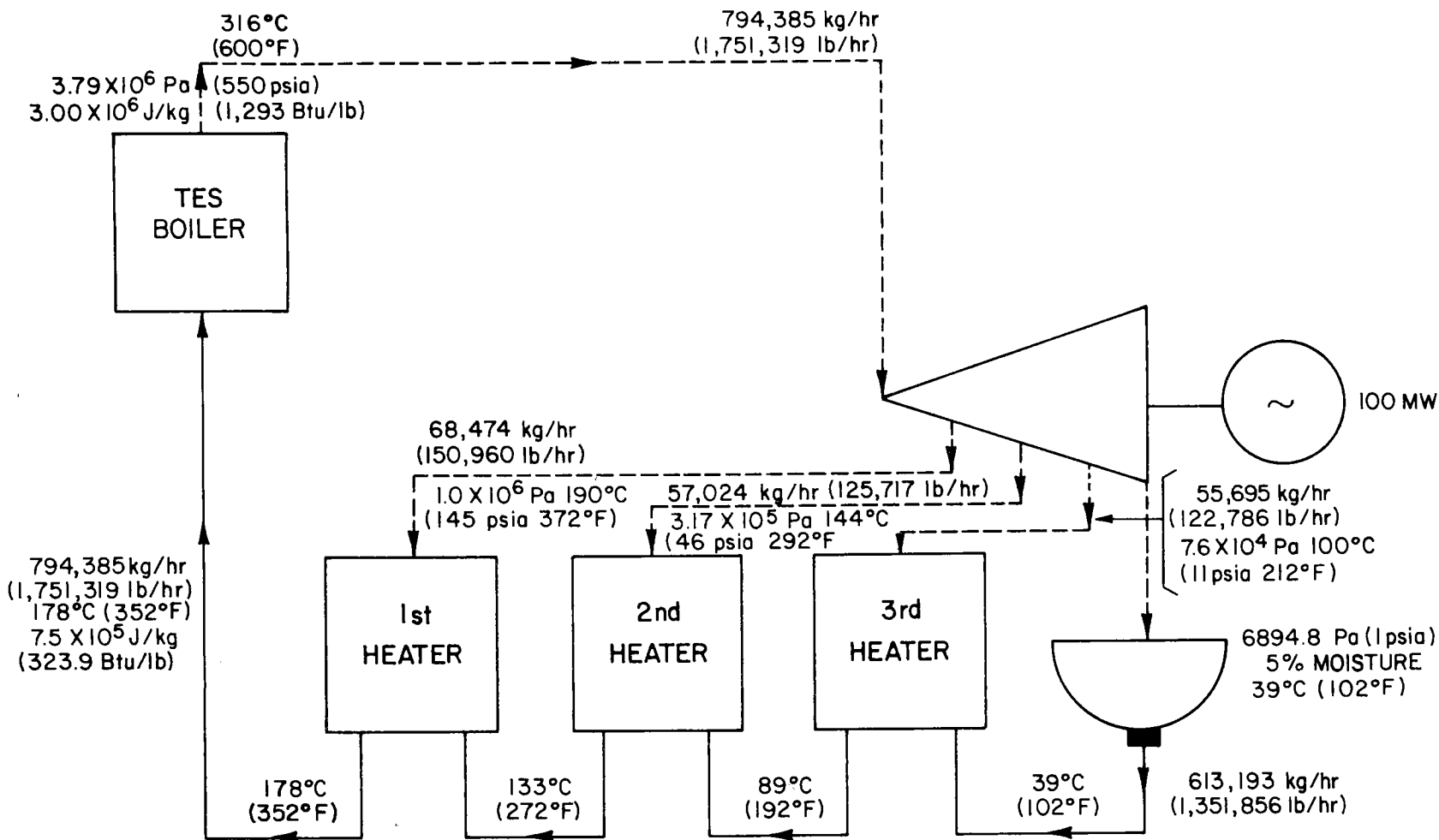
INPUT 538 °C (1000 °F), 1.65 X 10<sup>7</sup> Pa (2400 psia) STEAM

OUTPUT 316 °C (600 °F), 3.79 X 10<sup>6</sup> Pa (550 psia) STEAM

$$\frac{\text{CHARGING MASS}}{\text{DISCHARGING MASS}} = 1.12$$

A79112448

Figure 2. TES SUBSYSTEM WITH 316°C (600°F) OUTLET STEAM

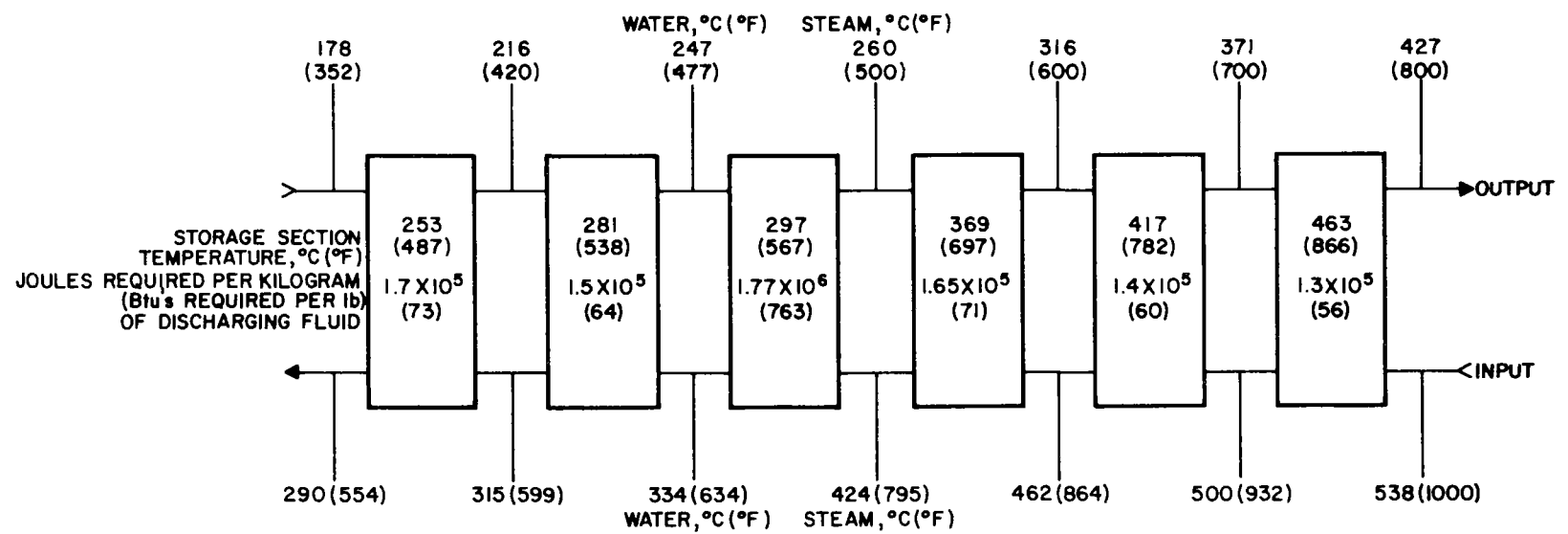


A80010225

Figure 3. TENTATIVE HEAT BALANCE FOR 100-MW PEAKING UNIT

Table 2. HEAT-BALANCE INFORMATION FOR 100-MW PEAKING UNIT  
WITH 316°C (600°F) OUTLET STEAM

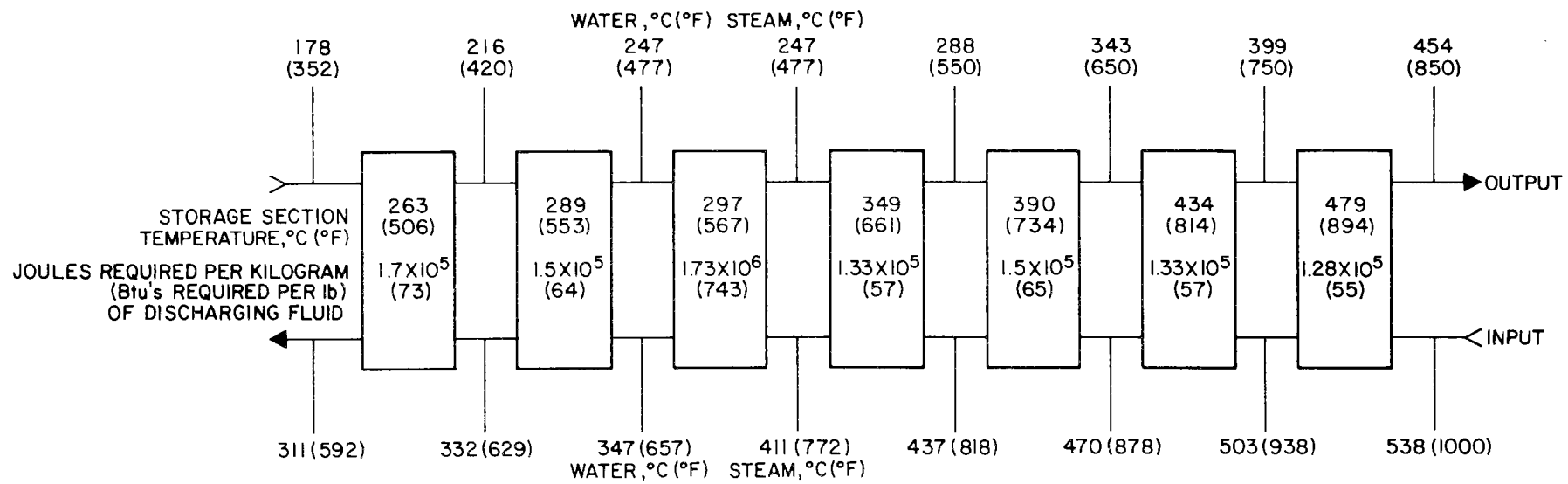
	<u>Full Throttle</u>	
<b>Turbine</b>		
Steam Flow, kg/hr (lb/hr)	794,385	(1,751,319)
Pressure, Pa (psia)	$3.79 \times 10^6$	(550)
Total Temperature, °C (°F)	316	(600)
<b>Condenser</b>		
Steam Flow, kg/hr (lb/hr)	613,193	(1,351,856)
Pressure, Pa (psia)	6894.8	(1.0)
<b>3rd Extraction Heater</b>		
Water Flow to Heater, kg/hr (lb/hr)	613,193	(1,351,856)
Turbine Stage Pressure, Pa (psia)	$7.6 \times 10^4$	(11.0)
Water Temperature Out, °C (°F)	89	(192)
Water Temperature In, °C (°F)	39	(102)
Extraction Enthalpy, J/kg (Btu/lb)	$2.7 \times 10^6$	(1160)
Extraction Required, kg/hr (lb/hr)	55,695	(122,786)
<b>2nd Extraction Heater</b>		
Water Flow to Heater, kg/hr (lb/hr)	668,886	(1,474,642)
Turbine Stage Pressure, Pa (psia)	$3.17 \times 10^5$	(46)
Water Temperature Out, °C (°F)	133	(272)
Extraction Enthalpy, J/kg (Btu/lb)	$2.74 \times 10^6$	(1180)
Extraction Required, kg/hr (lb/hr)	57,024	(125.717)
<b>1st Extraction Heater</b>		
Water Flow to Heater, kg/hr (lb/hr)	725,911	(1,600,359)
Turbine Stage Pressure, Pa (psia)	$1.0 \times 10^6$	(145)
Water Temperature Out, °C (°F)	178	(352)
Water Enthalpy In, J/kg (Btu/lb)	$7.54 \times 10^5$	(324)
Extraction Enthalpy, J/kg (Btu/lb)	$2.8 \times 10^6$	(1205)
Extraction Required, kg/hr (lb/hr)	68,474	(150,960)
Boiler Feed, kg/hr (lb/hr)	79,438	(1,751,319)
<b>Turbine Generator</b>		
Enthalpy at Throttle, J/kg (Btu/lb)	$3.0 \times 10^6$	(1293)
Work up to 1st Extraction Point, J/kg (Btu/lb)	$2.0 \times 10^5$	(88)
Work up to 2nd Extraction Point, J/kg (Btu/lb)	$2.6 \times 10^5$	(113)
Work up to 3rd Extraction Point, J/kg (Btu/lb)	$3.1 \times 10^5$	(133)
Exhaust Enthalpy, J/kg (Btu/lb)	$2.4 \times 10^6$	(1053)
<b>Plant Performance</b>		
Net Plant Sendout, kW	100,000	(100,000)
Plant Heat Supplied, $10^6$ J/hr ( $10^6$ Btu/hr)	$1.79 \times 10^6$	(1697.2)
Overall Plant Heat Rate, J/kWhr (Btu/kWhr)	$1.79 \times 10^7$	(16,972)



INPUT 538 °C (1000 °F), 1.65 × 10<sup>7</sup> Pa (2400 psia) STEAM  
 OUTPUT 427 °C (800 °F), 3.79 × 10<sup>6</sup> Pa (550 psia) STEAM  
 CHARGING MASS / DISCHARGING MASS = 1.2

A79112449

Figure 4. CONCEPTUAL TES UNIT WITH 427°C (800°F) OUTLET STEAM



INPUT 538°C (1000°F),  $1.65 \times 10^7$  Pa (2400 psia) STEAM  
 OUTPUT 454°C (850°F),  $3.79 \times 10^6$  Pa (550 psia) STEAM  
 $\frac{\text{CHARGING MASS}}{\text{DISCHARGING MASS}} = 1.3$

A79112450

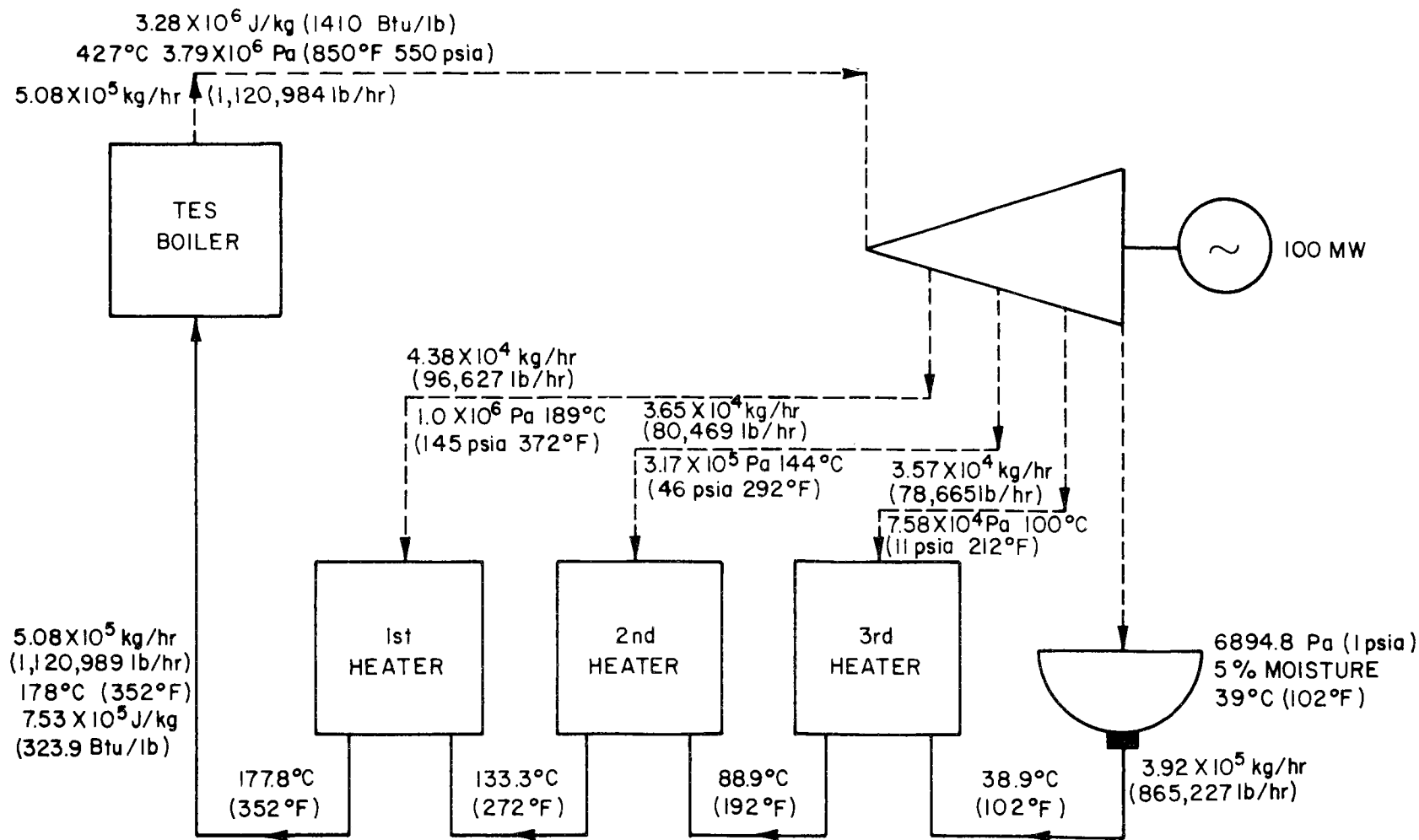
Figure 5. TES SUBSYSTEM WITH 454°C (850°F) STEAM OUTLET

Tentative heat balances for a 100-MW steam turbine with three stages of water preheat were calculated for steam at  $3.792 \times 10^6$  (550 psia) and at temperatures of 427° and 454°C (800° and 850°F). The resulting system efficiencies were approximately 28% and 30%, a substantial improvement over the 20% efficiency of the 316°C (600°F) base case. This improvement is significant considering that a 30% efficient TES peaking system operating with a 38% efficient primary plant has an effective efficiency equal to that of pumped hydro with an electricity-to-electricity efficiency of about 70%. These heat balances and additional cycle information are shown in Figure 6, Table 3, and Figure 7, Table 4, respectively.

Our original thinking was that the TES subsystem designs having output temperatures of 316°C (600°F) and 454°C (850°F) would provide a conservative to somewhat optimistic parameterization. But this may not be the case because the lowest log-mean temperature difference for the 454°C (850°F) case is about 39°C (70°F). Higher output temperatures could be obtained if lower log-mean temperature differences were affordable and higher charge-to-discharge mass ratios were acceptable. In addition, the system could be redesigned with more feedwater heating stages in the electrical generation subsystem, which would increase the efficiency of electrical generation and tend to eliminate part of the low-temperature sections of the TES subsystem. However, the temperature of the charging stream as it leaves the TES subsystem would increase (possibly increasing the total plant operation complexity) to fully utilize the remaining energy in the stream.

#### Economic Analysis

Because cost data for the TES subsystem are uncertain, an equation defining output energy cost as a function of the peaking system's total annual cost and energy output was given to establish allowable costs for the TES subsystem. This analysis was performed parametrically for a range of output energy costs (\$30 to \$80 million/kWh<sub>e</sub>), an electrical generation subsystem cost of \$200 and \$400 per installed kilowatt, and levelized fixed charge rates of 15% and 19% recommended by the Electric Power Research Institute (EPRI).<sup>9</sup> These fixed charge rates represent tax preference cases for a plant life of 20 years and no-tax preference cases, respectively. EPRI has recommended that the tax preference be excluded from long-term analyses, included for near-term analyses. Table 5 shows the EPRI-recommended levelized fixed charge rates

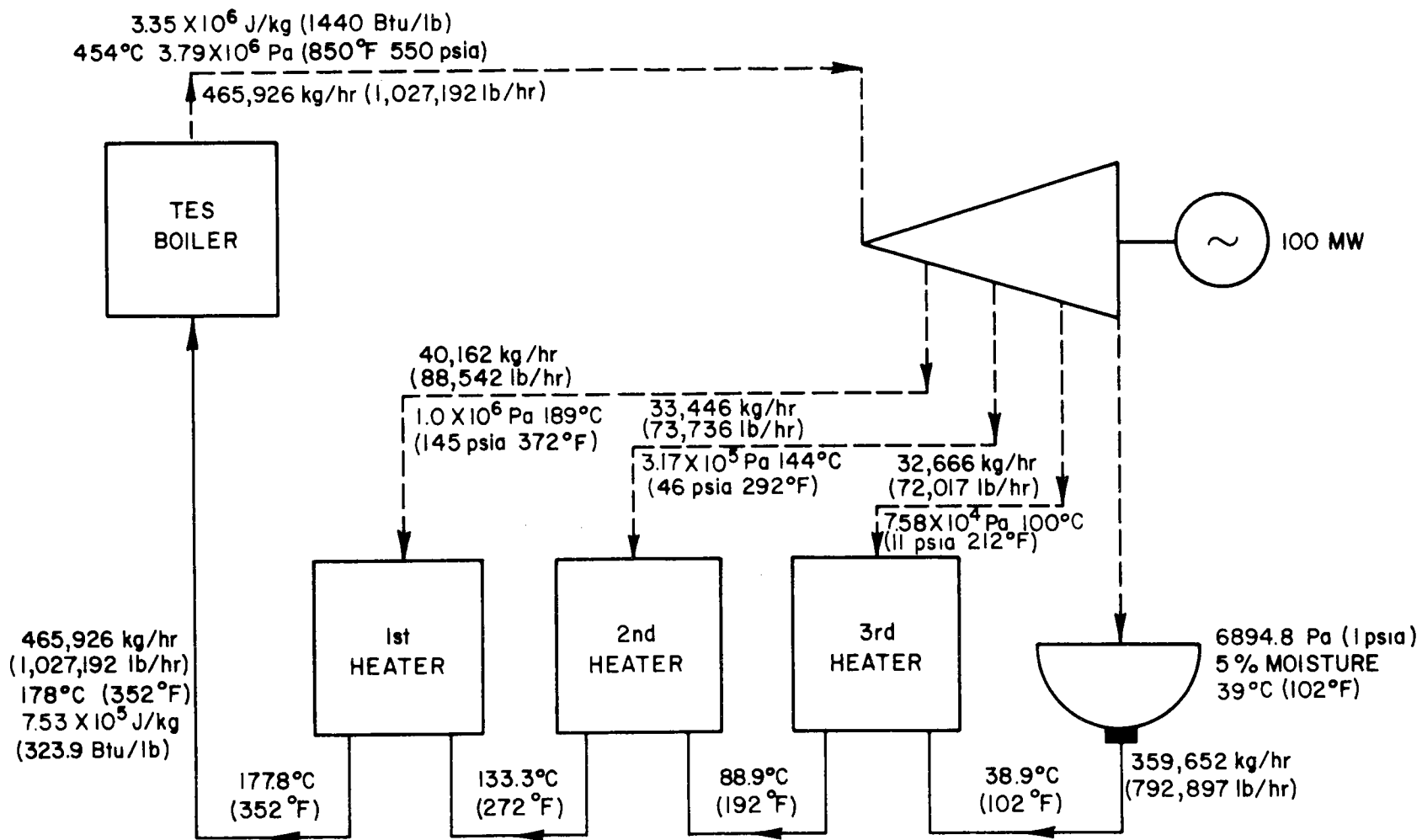


A79112451

Figure 6. TENTATIVE HEAT BALANCES FOR 100-MW PEAKING UNIT AT  $427^\circ\text{C}$  ( $800^\circ\text{F}$ ) OUTLET STEAM

Table 3. HEAT-BALANCE INFORMATION FOR 100-MW PEAKING UNIT  
WITH 427°C (800°F) OUTLET STEAM

	Full Throttle	
Turbine		
Steam Flow, kg/hr (lb/hr)	50,847	(1,120,989)
Pressure, Pa (psia)	$3.79 \times 10^6$	(550)
Total Temperature, °C (°F)	427	(800)
Condenser		
Steam Flow, kg/hr (lb/hr)	39,246	(865,227)
Pressure, Pa (psia)	6894.8	(1.0)
3rd Extraction Heater		
Water Flow to Heater, kg/hr (lb/hr)	39,246	(865,227)
Turbine Stage Pressure, Pa (psia)	$7.6 \times 10^4$	(11.0)
Water Temperature Out, °C (°F)	89	(192)
Water Temperature In, °C (°F)	39	(102)
Extraction Enthalpy, J/kg (Btu/lb)	$2.7 \times 10^6$	(1160)
Extraction Required, kg/hr (lb/hr)	35,682	(78,665)
2nd Extraction Heater		
Water Flow to Heater, kg/hr (lb/hr)	428,142	(943,892)
Turbine Stage Pressure, Pa (psia)	$3.17 \times 10^5$	(46)
Water Temperature Out, °C (°F)	133	(272)
Extraction Enthalpy, J/kg (Btu/lb)	$2.74 \times 10^6$	(1180)
Extraction Required, kg/hr (lb/hr)	36,500	(80,469)
1st Extraction Heater		
Water Flow to Heater, kg/hr (lb/hr)	464,642	(1,024,361)
Turbine Stage Pressure, Pa (psia)	$1.0 \times 10^6$	(145)
Water Temperature Out, °C (°F)	178	(352)
Water Enthalpy In, J/kg (Btu/lb)	$7.54 \times 10^5$	(324)
Extraction Enthalpy, J/kg (Btu/lb)	$2.8 \times 10^6$	(1205)
Extraction Required, kg/hr (lb/hr)	43,829	(96,627)
Boiler Feed, kg/hr (lb/hr)	508,472	(1,120,989)
Turbine Generator		
Enthalpy at Throttle, J/kg (Btu/lb)	$3.28 \times 10^6$	(1410)
Work up to 1st Extraction Point, J/kg (Btu/lb)	$4.77 \times 10^5$	(205)
Work up to 2nd Extraction Point, J/kg (Btu/lb)	$5.00 \times 10^5$	(215)
Work up to 3rd Extraction Point, J/kg (Btu/lb)	$5.93 \times 10^5$	(255)
Exhaust Enthalpy, J/kg (Btu/lb)	$2.45 \times 10^6$	(1053)
Plant Performance		
Net Plant Sendout, kW	100,000	(100,000)
Plant Heat Supplied, $10^6$ J/hr ( $10^6$ Btu/hr)	$1.28 \times 10^6$	(1217.5)
Overall Plant Heat Rate, J/kWhr (Btu/kWhr)	$1.28 \times 10^7$	(12,175)



A79112447

Figure 7. TENTATIVE HEAT BALANCES FOR 100-MW PEAKING UNIT WITH  $454^\circ\text{C}$  ( $850^\circ\text{F}$ ) OUTLET STEAM

Table 4. HEAT-BALANCE INFORMATION FOR 100-MW PEAKING UNIT  
WITH 454°C (850°F) OUTLET STEAM

	<u>Full Throttle</u>	
<b>Turbine</b>		
Steam Flow, kg/hr (lb/hr)	465,926	(1,027,192)
Pressure, Pa (psia)	$3.79 \times 10^6$	(550)
Total Temperature, °C (°F)	454	(850)
<b>Condenser</b>		
Steam Flow, kg/hr (lb/hr)	359,652	(792,897)
Pressure, Pa (psia)	6,894.8	(1.0)
<b>3rd Extraction Heater</b>		
Water Flow to Heater, kg/hr (lb/hr)	359,652	(792,897)
Turbine Stage Pressure, Pa (psia)	$7.6 \times 10^4$	(11.0)
Water Temperature Out, °C (°F)	89	(192.0)
Water Temperature In, °C (°F)	39	(102.0)
Extraction Enthalpy, J/kg (Btu/lb)	$2.7 \times 10^6$	(1160)
Extraction Required, kg/hr (lb/hr)	32,666	(72,017)
<b>2nd Extraction Heater</b>		
Water Flow to Heater, kg/hr (lb/hr)	392,318	(864,914)
Turbine Stage Pressure, Pa (psia)	$3.17 \times 10^5$	(46)
Water Temperature Out, °C (°F)	133	(272)
Extraction Enthalpy, J/kg (Btu/lb)	$2.74 \times 10^6$	(1180)
Extraction Required, kg/hr (lb/hr)	33,446	(73,736)
<b>1st Extraction Heater</b>		
Water Flow to Heater, kg/hr (lb/hr)	425,764	(938,650)
Turbine Stage Pressure, Pa (psia)	$1.0 \times 10^6$	(145)
Water Temperature Out, °C (°F)	178	(352)
Water Enthalpy In, J/kg (Btu/lb)	$7.54 \times 10^5$	(324)
Extraction Enthalpy, J/kg (Btu/lb)	$2.8 \times 10^6$	(1205)
Extraction Required, kg/hr (lb/hr)	40,162	(88,542)
Boiler Feed, kg/hr (lb/hr)	465,926	(1,027,192)
<b>Turbine Generator</b>		
Enthalpy at Throttle, J/kg (Btu/lb)	$3.35 \times 10^6$	(1440)
Work up to 1st Extraction Point, J/kg (Btu/lb)	$5.40 \times 10^5$	(232)
Work up to 2nd Extraction Point, J/kg (Btu/lb)	$5.70 \times 10^5$	(245)
Work up to 3rd Extraction Point, J/kg (Btu/lb)	$6.63 \times 10^5$	(285)
Exhaust Enthalpy, J/kg (Btu/lb)	$2.45 \times 10^6$	(1053)
<b>Plant Performance</b>		
Net Plant Sendout, kW	100,000	(100,000)
Plant Heat Supplied, $10^6$ J/hr ( $10^6$ Btu/hr)	$1.21 \times 10^6$	(1146.4)
Overall Plant Heat Rate, J/kWhr (Btu/kWhr)	$1.21 \times 10^7$	(11,464)

a function of assumed plant life. Additional assumptions made in this analysis are as follows:

- The peaking system size is 100 MW<sub>e</sub>.
- The peaking system is designed for operation at full capacity for 8 hours per day.
- The electrical generation subsystem investment cost is installed cost and includes turbine/generator, condenser, and feedwater heaters.
- The annual operating and maintenance cost for the electrical generator subsystem is \$0.003/kWhr.
- The annual operating and maintenance cost for the TES subsystem is 3% of the capital investment.
- The TES subsystem energy losses are zero.
- Plant availability is 85%.

Table 5. EPRI-RECOMMENDED LEVELIZED FIXED CHARGE RATES<sup>9</sup>

Facility Life, Years	Levelized Fixed Charges, %*	
	No Tax Preference	With Tax Preference
5	34	29
10	23	19
15	20	16
20	19	15
25	18	15
30	18	15
35	18	15
40	18	15
45	18	15
50	18	15

\* Includes return, depreciation, allowance for retirement dispersion, income taxes, other taxes, and insurance. Excludes operation and maintenance.

Essentially this economic analysis treated the break-even cost of such a system as an unknown and solved for it in terms of the electrical generation subsystem and desired electric power costs.

The derivation is as follows:

$$EC = K \frac{AC}{S \times PF} \quad (1)$$

$$AC = ACT + ACE \quad (2)$$

$$ACE = (FD \times IE) + (FN \times WC) + AE \quad (3)$$

$$IE = EI \times S \times 10^{-3} \quad (4)$$

$$WC = 0.02 \times IE \text{ (See assumptions.)} \quad (5)$$

$$AE = (3.0 \times S \times PF \times 8760) 10^{-6} \text{ (See assumptions.)} \quad (6)$$

where

- EC = energy cost, \$ million/kWhr
- K = conversion constant
- S = plant size, MW
- PF = plant factor (decimal)
- AC = annual plant cost, \$ million
- ACT = annual TES subsystem cost, \$ million
- ACE = annual electrical generation subsystem cost, \$ million
- FD = fixed charge rate for depreciating investment
- FN = fixed charge rate for nondepreciating investment
- WC = working capital
- AE = annual operating and maintenance cost for electrical generation subsystem, \$ million
- IE = total investment for electrical generation subsystem, \$ million
- EI = electrical generation subsystem cost, \$/kW

combining

$$ACT = \frac{S \times PF \times EC}{K} - [(FD \times IE) + (FN \times WC) + AE] \quad (7)$$

and substituting values

$$ACT = S \{PF[(8.756 \times 10^{-3} \times EC) - 2.628 \times 10^{-2}] - [1.8235 \times 10^{-4} \times EI]\} \quad (8)$$

Assuming the same fixed charge rates and percentage of investment for working capital as before, with maintenance on the TES subsystem taken at 3% of the capital investment, the break-even cost per kilowatt-electric for the TES subsystem can be stated as —

$$ET = \frac{ACT - FC}{(2.1235 \times 10^{-4})S} \quad (9)$$

or

$$ET = \frac{ACT - FC}{2.1235 \times 10^{-2}} \quad (10)$$

where

ET = break-even thermal energy storage cost, \$/kW<sub>e</sub>

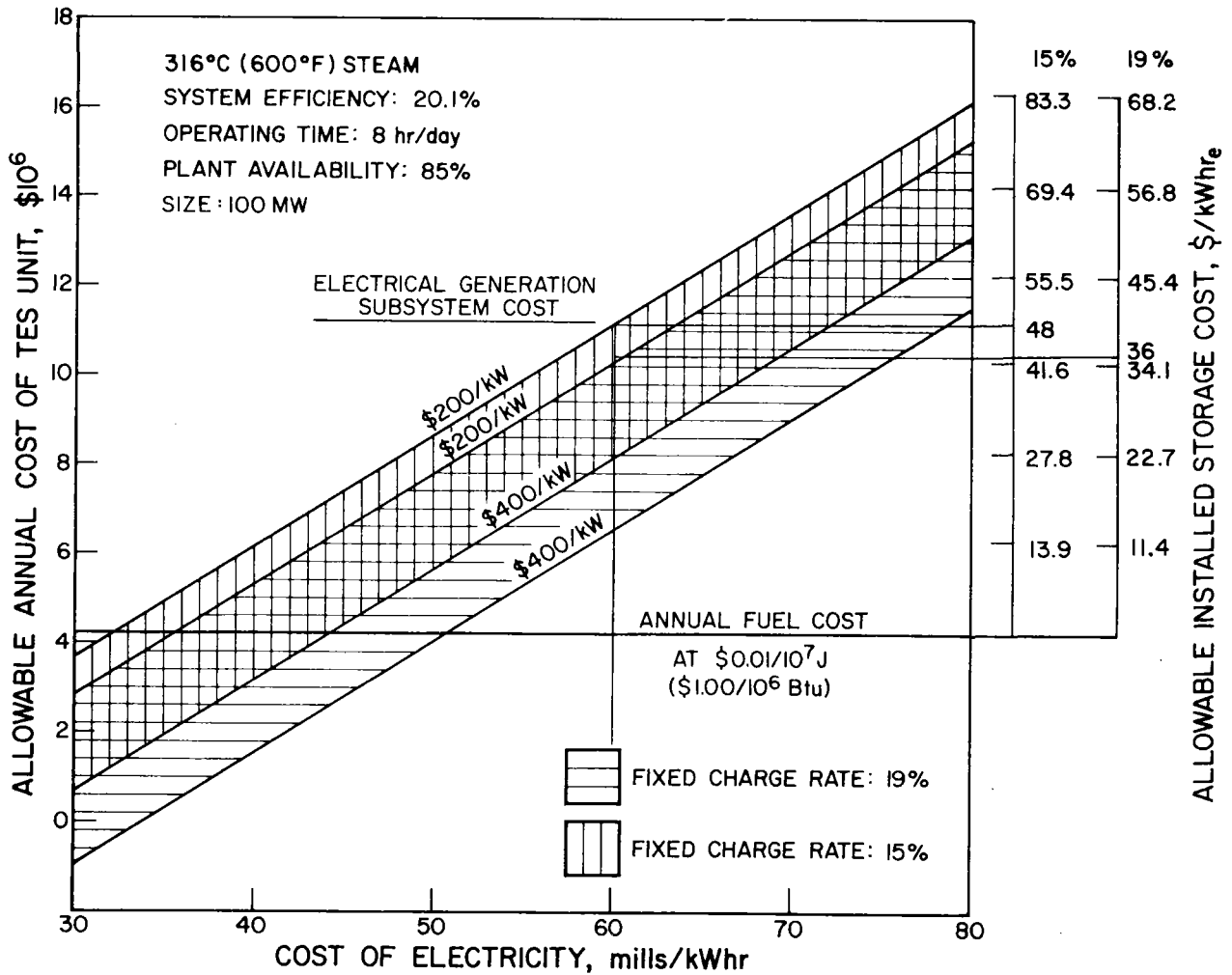
ACT = break-even annual cost of the subsystem, \$ million

S = system size, MW

FC = annual fuel cost for charging TES unit, \$ million

The results are shown in Figures 8, 9, and 10 for the 316°C (600°F), 427°C (800°F) and 454°C (850°F) systems. The left axis shows the total annual break-even cost of the TES subsystem including charging fuel costs. The right axis shows the total break-even capital investment for the TES subsystem per installed kilowatt-hour (electric) for a charging fuel cost of ~\$1/10<sup>9</sup> J (\$1/10<sup>6</sup> Btu) (total charging energy costs). The zero point of the right axis is the point where the allowed annual TES subsystem cost equals the annual fuel cost. The investment costs shown on this axis are equal to \$6.94 and \$5.68 per million dollars of allowed annual cost above the annual fuel cost for the 15% and 19% fixed charged rates, respectively.

For the 454°C (850°F) case, the break-even storage cost with electrical generation subsystem cost of \$200/kW and desired energy costs of \$60 million/kWhr<sub>e</sub> are \$42/kWhr<sub>e</sub> and \$57/kWhr<sub>e</sub> (19% and 15% fixed charged rate). With the 316°C (600°F) case, these costs are reduced to \$36/kWhr<sub>e</sub> and \$48/kWhr<sub>e</sub>. This \$8/kWhr<sub>e</sub> to \$9/kWhr<sub>e</sub> reduction in break-even storage cost for the 316°C (600°F) case results from the \$1.4 X 10<sup>6</sup> increase in annual fuel costs, a result of lower efficiency.



A79114445

Figure 8. TARGET COSTS FOR A TES SUBSYSTEM AS A FUNCTION OF ELECTRICAL GENERATION SUBSYSTEM COST, FIXED CHARGE RATE, AND OUTPUT ELECTRICITY COST WITH 316°C (600°F) OUTLET STEAM

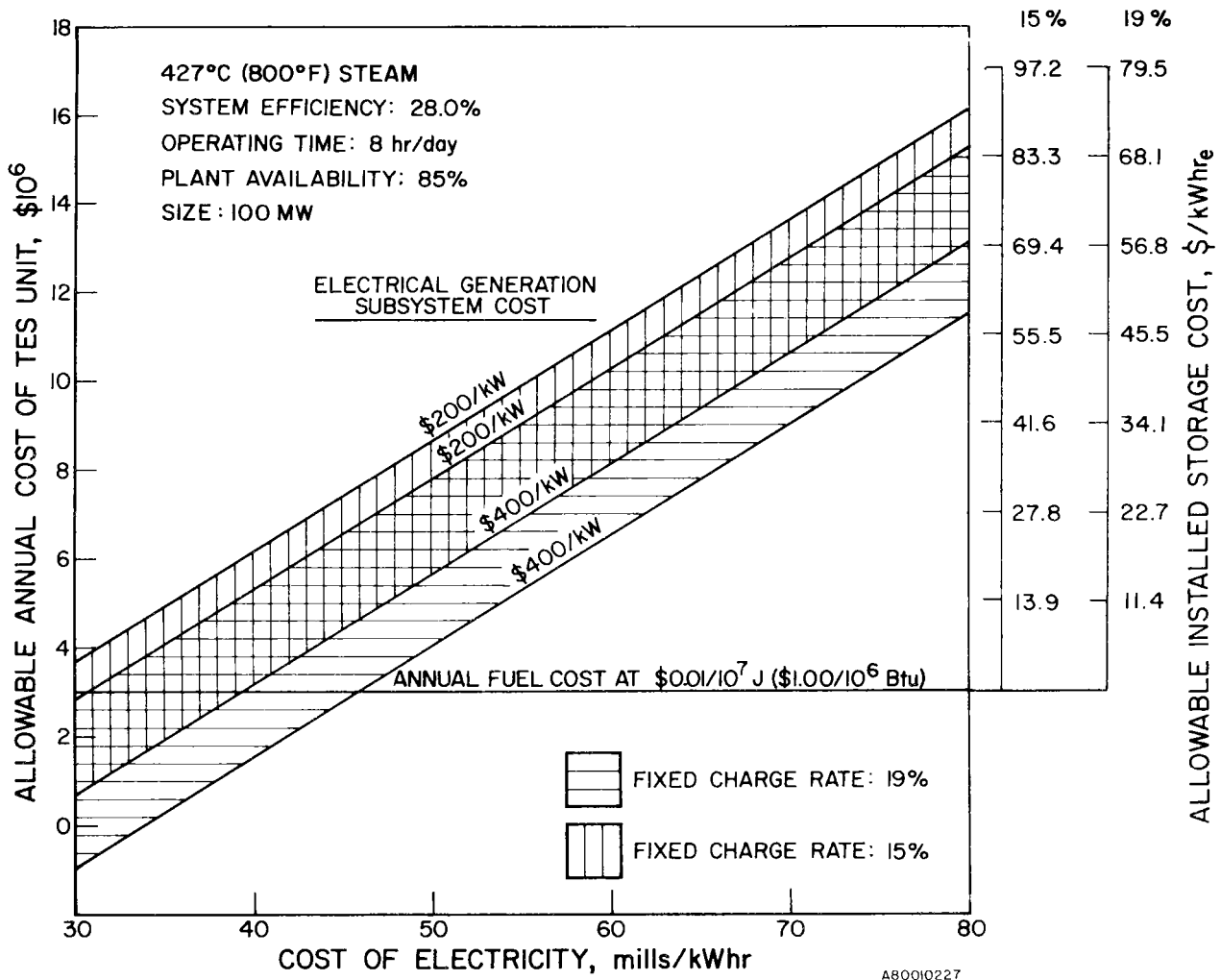


Figure 9. TARGET COSTS FOR A TES SUBSYSTEM AS A FUNCTION OF ELECTRICAL GENERATION SUBSYSTEM COST, FIXED CHARGE RATE, AND OUTPUT ELECTRICITY COST WITH 427°C (800°F) OUTLET STEAM

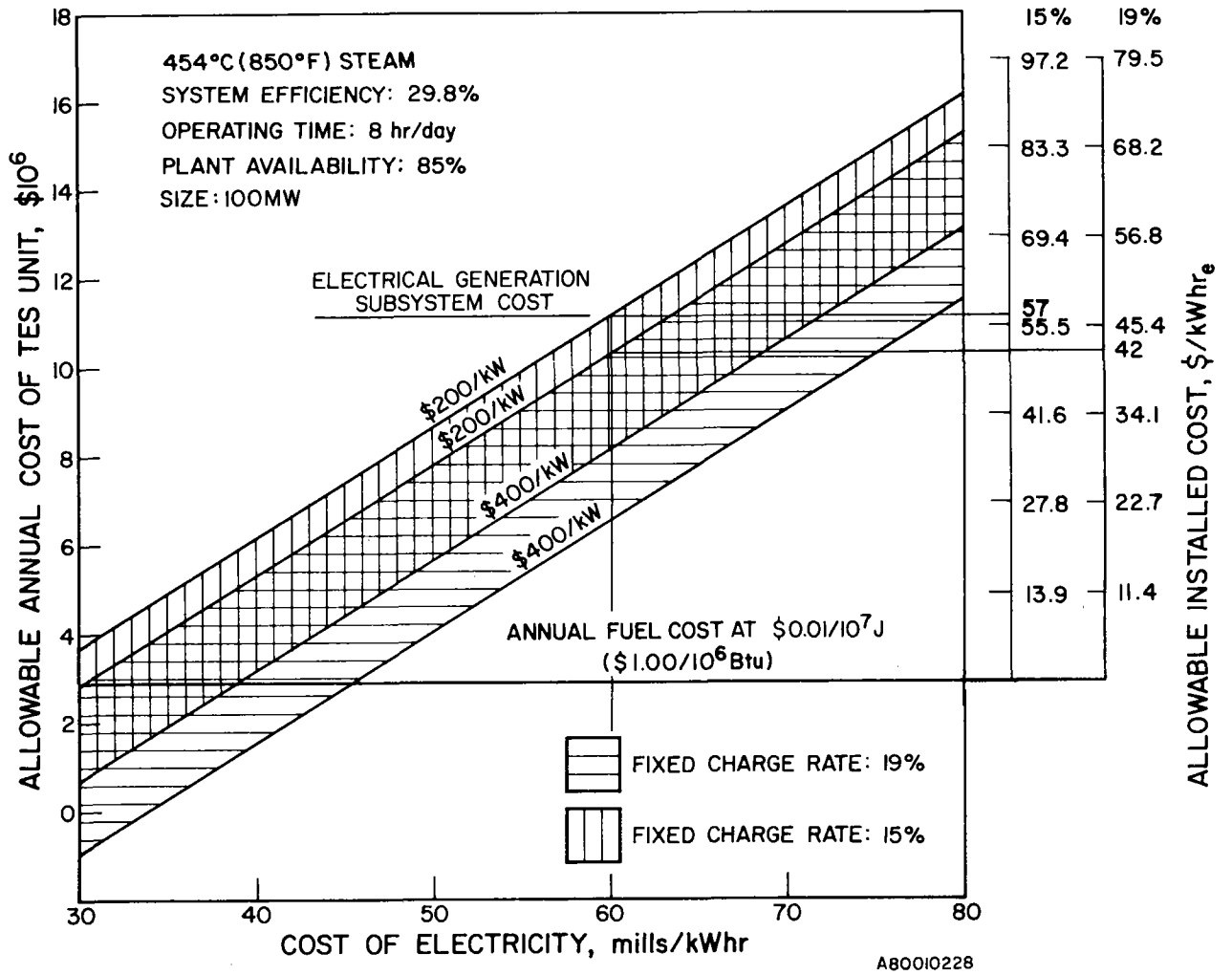


Figure 10. TARGET COSTS FOR A TES SUBSYSTEM AS A FUNCTION OF ELECTRICAL GENERATION SUBSYSTEM COST, FIXED CHARGE RATE, AND OUTPUT ELECTRICITY COST WITH 454°C (850°F) OUTLET STEAM

### Status of Technology

Numerous programs to study the applicability of using the latent heat properties of various inorganic salts to store thermal energy in the respective phase-change temperature regimes are either complete or underway.<sup>1,3,6,10</sup> Storage of thermal energy in PCM is desirable because large quantities of energy are involved in the phase-change process, and this energy is transferred (ideally) at a constant temperature (the phase-change or melting point). As a result of these programs, salts and salt mixtures have been identified for applications spanning a temperature range of 93°C (200°F) to in excess of 1090°C (2000°F). The lower range of this temperature span includes space heating applications, and the upper temperature range includes several solar and vehicular propulsion applications. Storage of thermal energy from cyclic industrial processes and in electric utility steam power plants falls between the two temperature extremes. Each application in this wide temperature range has its own unique set of requirements. For example, in the application where thermal energy is stored and subsequently used to power a vehicle, weight and volume of the storage subsystem is of prime importance. However, in identifying salts for utility applications, the prime factors are cost, reliability, safety, and useful operating lifetimes.

The major portion of the TES subsystem consists of the TES salt and the containment vessel/HX. These two factors must be considered simultaneously because of their various interactions. For example, a salt chosen for its low cost and high heat of fusion may be corrosive toward low cost containment vessel/HX materials, necessitating the use of more expensive and/or complex materials (e.g., linings) or the selection of a different salt. Similarly, if the chosen salt readily reacts with the environment (air or H<sub>2</sub>O), then special containment and sealing arrangements must be provided. Experimental work at several laboratories (IGT, Comstock and Westcott, Minneapolis Honeywell, and Philips)<sup>1,5,10,12,13</sup> has addressed these trade-offs; however, insufficient data are available to provide exact and quantitative numbers, especially long-term salt/containment/HX data.

The design and costs of the HX required in TES systems utilizing PCM are governed by the complexity of the heat transfer processes occurring as well as the corrosivity of the salt. The latter factor can be rather easily accounted

for by materials compatibility testing. But the former presents fundamental and technical constraints that could greatly increase the HX complexity. This complexity results from the fact that as thermal energy is removed from the molten salt, a layer of solidified salt becomes deposited on the HX surface. Because of the poor thermal conductivity of the solidified salt, the heat exchange rate (heat flux) decreases with time as the layer thickness increases. Therefore, although ideally the heat flux from an isothermal source should remain constant, the observed heat flux from a phase-change TES system varies, approaching that more typical of a sensible heat storage source. Programs are now under way to model, predict, and experimentally verify the rates of heat transfer in TES PCM.<sup>10,11</sup> The models developed so far for selected conditions predict quite accurately the observed experimental behavior as the salt layer thickness increases. Currently, most experimental efforts focus on ways to minimize the salt layer thickness or improve its thermal conductivity. Physical as well as chemical means to control the salt layer thickness are being utilized. Some physical means utilize scrapers and others use vibratory techniques to remove the solidified layer. Modifying the chemical composition of the salt, so that a "slush" and weakly crystallized layer rather than a solidified layer is formed, is also being tested. Because the thermal conductivity of most salts is only of the order of 1.73 W/m-K (1 Btu/hr-ft-°F), the addition of a more conductive material having a cellular or directional conductivity is being investigated. Aluminum, for example, is a preferred conductivity promoter because it is approximately two orders of magnitude higher in thermal conductivity. Because of the state of development of some of these advanced heat exchange concepts, comparative quantitative heat flux data are not available.

The technological readiness of passive HX concepts for the TES subsystem discussed in this paper can be assessed if one makes the following simplifying assumption and calculates parametrically the cost breakdown for the TES subsystem components — the containment vessel/HX and TES salt.

- Operational concerns, such as reliability, safety, and useful life, are solvable; these costs are included in the containment vessel/HX cost.

In performing this calculation, we selected the 454°C (850°F) case as the reference design and \$60 million/kWh<sub>e</sub> as the target energy cost. Thus, the break-even installed cost of the TES subsystem is \$52/kWh<sub>e</sub> (average of the 15% and 19% fixed-charge rate break-even costs, with electrical generation subsystem costing \$200/kWh).

Further assumptions were —

- Installed cost is equal to 150% of materials cost. Thus break-even materials cost for 1 kWh<sub>e</sub> of electric storage is about \$34.60.
- Passive heat exchange designs have heat flux rates of 3152 W/m<sup>2</sup> (1000 Btu/hr-ft<sup>2</sup>).
- The TES salt has a heat fusion of 2.326 X 10<sup>5</sup> J/kg (100 Btu/lb), with a cost of \$0.44/kg (\$0.20/lb).

The result of this analysis shows that for passive heat exchangers having a heat flux of 3152 W/m<sup>2</sup> (1000 Btu/hr-ft<sup>2</sup>), the cost ceiling for containment vessel/HX is about \$86/m<sup>2</sup> (\$8/ft<sup>2</sup>) of heat exchange area. Expressing these break-even costs in terms of heat flux, the ceiling cost is \$0.26/100 W/m<sup>2</sup> (\$0.817/100 Btu/hr-ft<sup>2</sup>). Further analysis using different salt costs showed that a \$0.11/kg (\$0.05/lb) change in salt cost results in \$0.13/100 W/m<sup>2</sup> (\$0.40/100 Btu/hr-ft<sup>2</sup>) change in the ceiling cost of the containment vessel/HX. Table 6 shows containment vessel/HX ceiling costs for several salt costs. Overall subsystem costs may be either salt-cost intensive or HX-cost intensive, depending on the application's duty requirements, which dictate selection of salt properties and HX configuration.

Table 6. CONTAINMENT VESSEL/HX CEILING COSTS AS A FUNCTION OF SALT COST\*  
(Expressed in Terms of HX Heat Flux)

Salt Cost				Containment Vessel/HX Cost	
$\$/\text{kg}$	$(\$/\text{lb})^{**}$	$\text{J}/\text{¢}$	$(\text{Btu}/\text{¢})^\dagger$	$\$/100 \text{ W}/\text{m}^2$	$(\$/100 \text{ Btu}/\text{hr}\text{-ft}^2)$
0.22	(0.10)	10,551	(10)	0.513	(1.617)
0.33	(0.15)	7,037	(6.67)	0.386	(1.217)
0.44	(0.20)	5,275	(5)	0.249	(0.817)
0.55	(0.25)	4,220	(4)	0.132	(0.017)

\* Based on a thermal-to-electric conversion efficiency of 29.8% and an allowed storage cost of  $\$52/\text{kWhr}_e$  installed ( $\$34.6/\text{kWhr}_e$  not installed).

\*\* Assumes salt heat of fusion of  $2.326 \times 10^5 \text{ J}/\text{kg}$  (100 Btu/lb).

† Expressing a salt's cost and heat of fusion in this manner permits any combination of salt cost and heat of fusion to be used in this table [e.g.,  $\$0.22/\text{kg}$  ( $\$0.1/\text{lb}$ ) with  $2.326 \times 10^5 \text{ J}/\text{kg}$  (100 Btu/lb) = 10,573 J/¢ (10 Btu/¢);  $\$0.33/\text{kg}$  ( $\$0.15/\text{lb}$ ) with  $3.489 \times 10^5 \text{ J}/\text{kg}$  (150 Btu/lb) = 10,573 J/¢ (10 Btu/¢)].

#### Summary

TES peaking systems for utility applications employing a separate power conversion loop appear viable when interfaced with high-temperature, high-pressure base-load steam-electric plants. Their impact on the primary plant's operation is minimal, but storage efficiency is high. A 30% efficient TES peaking system operating with a 38% efficient primary plant has an effective efficiency equal to that of pumped hydro with an electricity-to-electricity efficiency of about 70%. Nevertheless, with current passive HX costs in the  $\$215$  to  $\$269/\text{m}^2$  ( $\$20$  to  $\$25/\text{ft}^2$ ) range, the economic viability of the TES peaking system clearly rests in the development of reasonably priced containment vessels/heat exchangers with high heat flux rates.

## Task 2. TES Module Testing

### 2.1 Engineering-Scale Testing

#### Introduction

Under IGT's previous thermal energy storage development contract (ERDA EY-76-C-02-2888, "Molten Salt Thermal Energy Storage Systems") three 8 kWh<sub>th</sub>-capacity engineering-scale TES modules were successfully designed, fabricated, and operated with LiKCO<sub>3</sub> PCM with a mid-range melting point of 505°C (941°F).<sup>14</sup> One of these units (Unit 2) was operated for 1400 hours and 30 thermal cycles as part of that effort. The operation of Unit 2 was voluntarily suspended on June 3, 1977 and it was partially disassembled to evaluate the condition of the system. The containment, HX, and salt were found to be in excellent condition. Downtime was approximately five months, during which the solidified LiKCO<sub>3</sub> salt was in contact with ambient air with no detrimental effects. Based on the promising thermal performance results and short-term stability of this TES system, the unit was reassembled and operated to obtain long-term engineering and compatibility data under the present program.

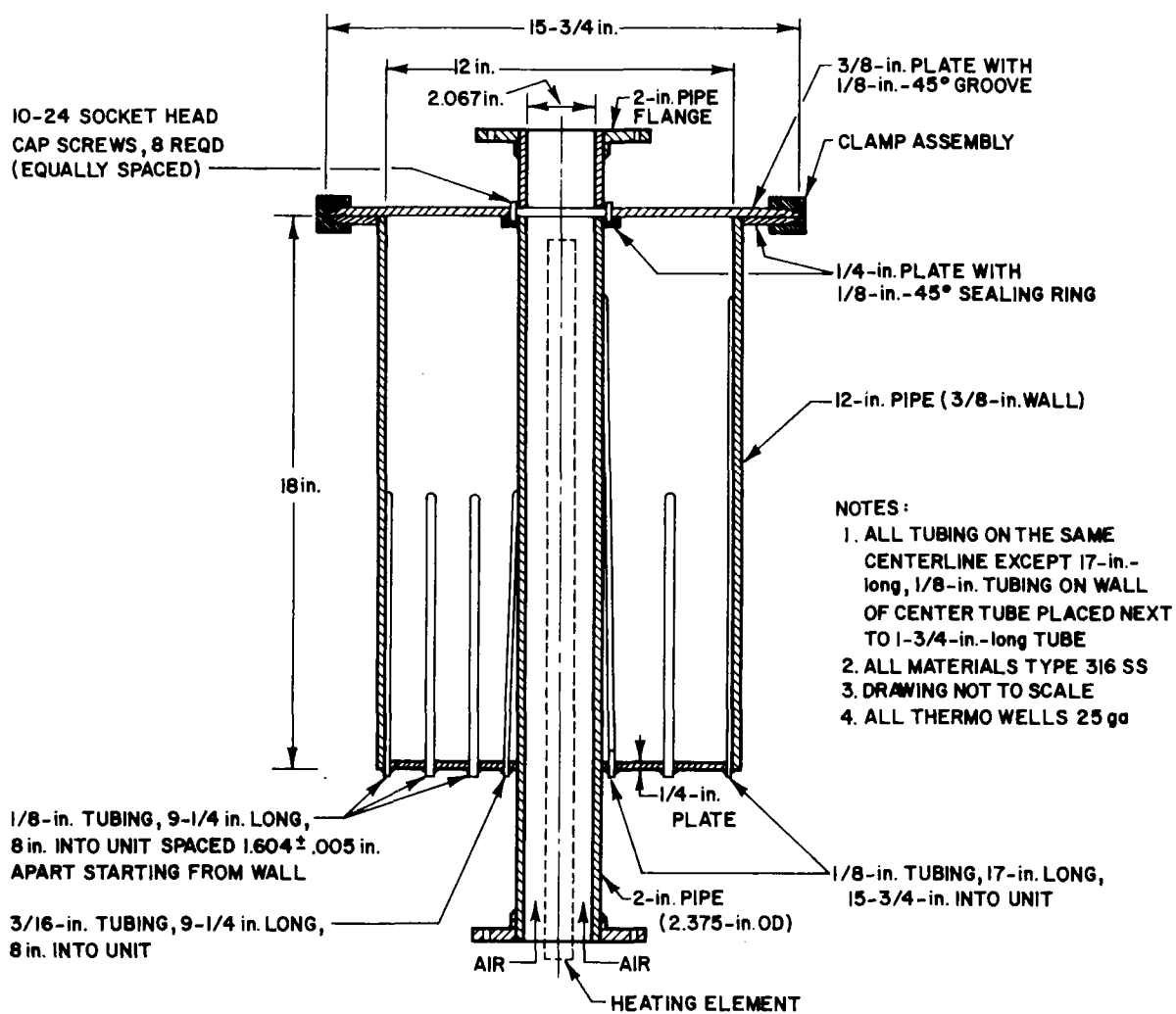
The specific objectives of this subtask were to -

- Establish the endurance and performance of this engineering-scale TES system during prolonged charge/discharge cycling
- Determine the effects of long-term, intermediate temperature exposure and cyclic temperature operation on the phase-change, salt, containment, and HX materials.

The objectives were met after successfully operating Unit 2 for 5650 hours and 129 thermal cycles at 480° to 535° (896° to 995°F). Very good chemical compatibility was demonstrated between the LiKCO<sub>3</sub> salt and the austenitic Type 316 stainless-steel (SS) materials of construction, with the carbonate salt exhibiting no hysteresis effects.

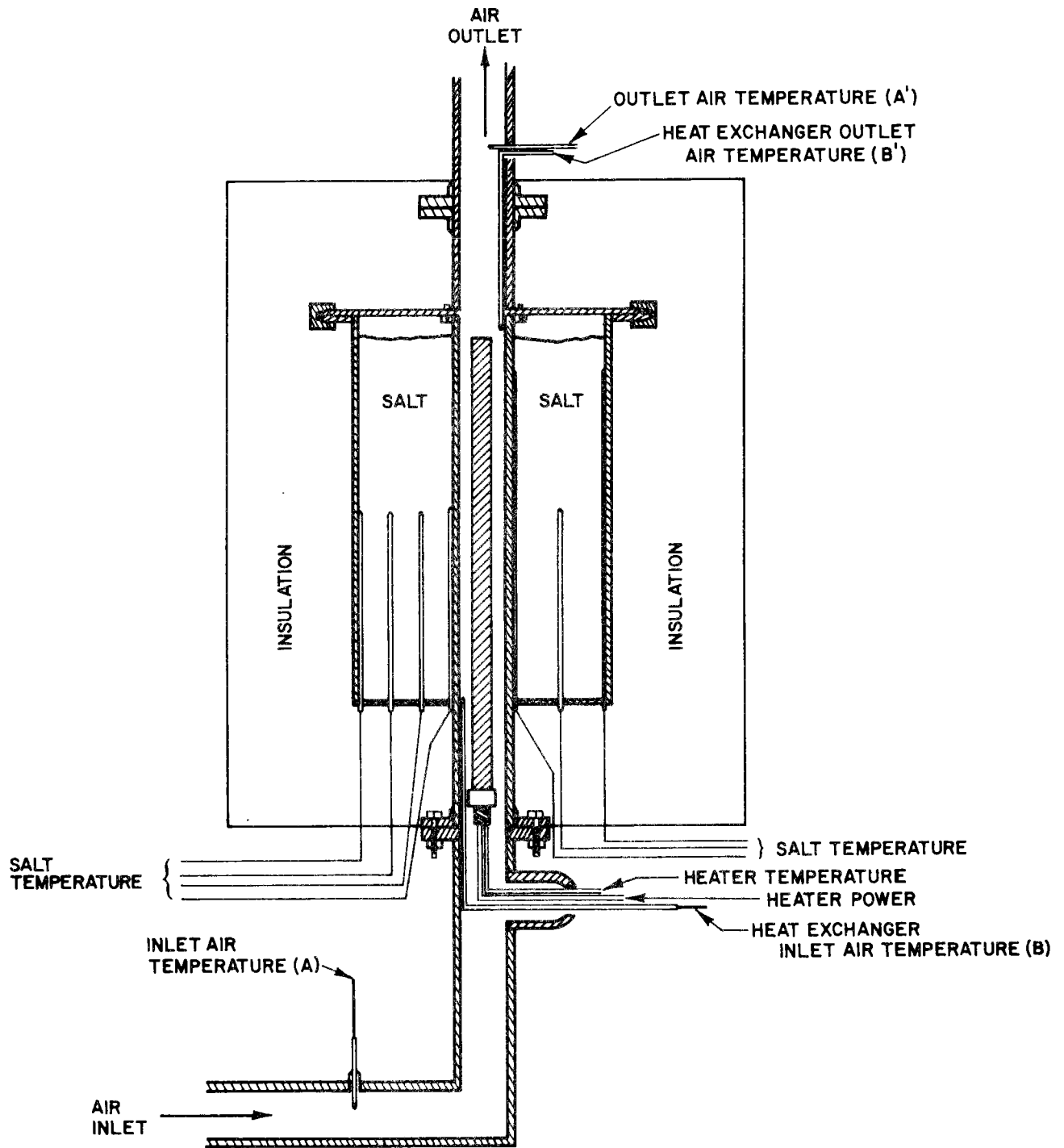
#### Cyclic Endurance Testing

The engineering-scale TES containment design, test-station module, and overall system schematic are shown in Figures 11, 12, and 13. The unit utilizes a single-pass, single-tube HX design and contains 68 kg (150 lb) of reagent-grade LiKCO<sub>3</sub> salt material (35 wt % Li<sub>2</sub>CO<sub>3</sub> - 65 wt % K<sub>2</sub>CO<sub>3</sub>). This salt has a melting point of 505°C (941°F) and a heat of fusion of 3.44 X 10<sup>5</sup> J/kg (148 Btu/lb). More detailed design and fabrication data were presented in a



A78030698

Figure 11. ENGINEERING-SCALE THERMAL ENERGY STORAGE UNIT



A78030701

Figure 12. ENGINEERING-SCALE UNIT MOUNTED IN TESTING STATION

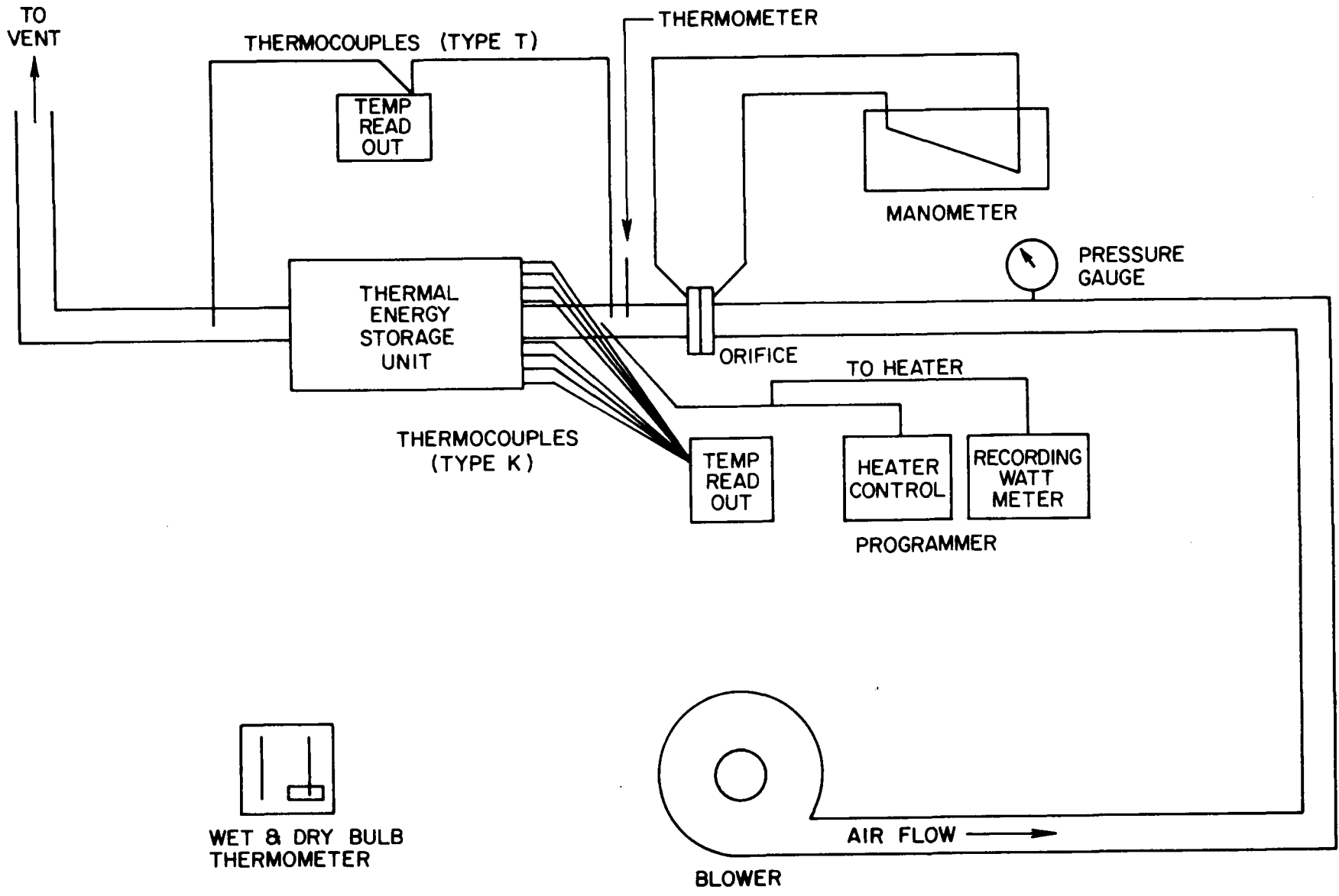


Figure 13. SCHEMATIC DIAGRAM OF THE ENGINEERING-SCALE TES SYSTEM

A77091912

previous report.<sup>14</sup> The system was thermally charged by a resistance heater located in the HX tube until the salt was molten and uniformly heated to 535°C (995°F). The system was discharged when a high-velocity stream of ambient air at a mass flow rate of almost 159 kg/hr (350 lb/hr) was passed up through the HX tube. The LiKCO<sub>3</sub> PCM, which was at a temperature of 535°C (995°F) initially, was thus cooled through the 505°C (941°F) solidification point to a temperature of approximately 480°C (896°F). The unit was then thermally recharged overnight in preparation for another run.

Following the 5 1/2-month shutdown from June to November 1977, the endurance-testing phase for Unit No. 2 was continued on November 16, 1977. Cyclic endurance testing was continued during the following 6 months, when Unit No. 2 accumulated a total of 129 charge/discharge cycles and 5650 hours of operation. The unit was terminated on May 12, 1978.

The discharge performance of Unit 2 was evaluated quantitatively periodically to establish the long-term cycling stability of a molten carbonate TES module. The heat flux,  $Q$ , from the solid/liquid interface in the salt to the air working fluid, was determined as a function of discharge time by monitoring the inlet and outlet air temperatures and calculating  $Q$  from the expression —

$$Q = \frac{\dot{m}C_p\Delta T}{A} \quad (11)$$

where

$Q$  = heat flux, W/m<sup>2</sup> (Btu/hr-ft<sup>2</sup>)

$\dot{m}$  = air mass flow rate, kg/hr (lb/hr)

$C_p$  = heat capacity of air, J/kg-°C (Btu/lb-°F)

$\Delta T$  = air-temperature differential =  $T_{out} - T_{in}$ , °C (°F)

$A$  = heat-transfer area, m<sup>2</sup> (ft<sup>2</sup>)<sup>14</sup>

Results of such analyses are presented in Figure 14, which shows the variation of heat flux with discharge time for five cycles at different points during the lifetime of this unit. Table 7 summarizes the time required to discharge the system and the time-averaged heat flux determined for each of these cycles. Discharge times ranged from 315 to 345 minutes, with time-averaged heat fluxes ranging from 1.17 to 1.31 X 10<sup>4</sup> W/m<sup>2</sup> (3715 to 4160 Btu/hr-ft<sup>2</sup>).

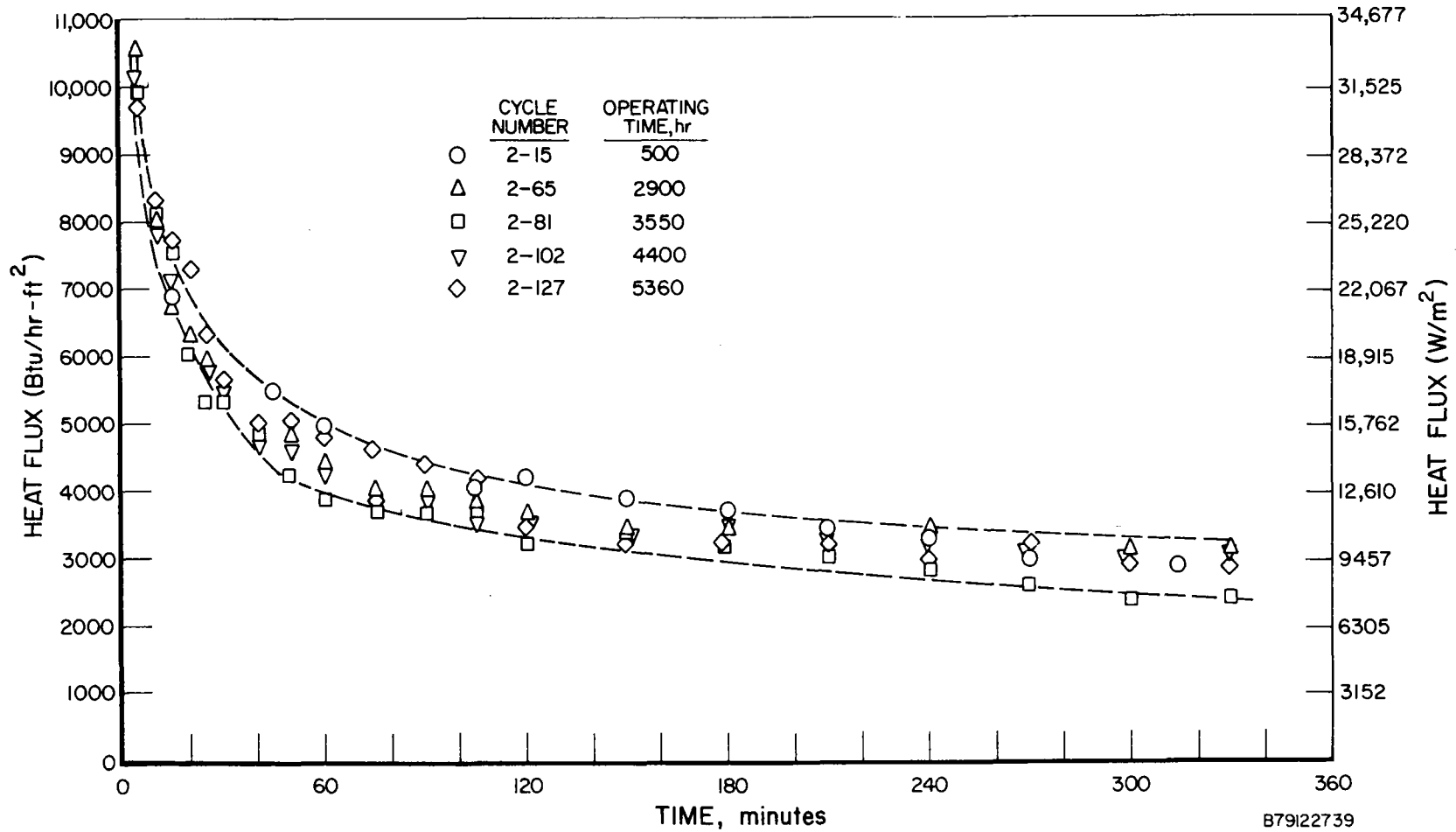


Figure 14. DISCHARGE PERFORMANCE OF ENGINEERING-SCALE TES UNIT (LiKCO<sub>3</sub> Salt)

These data define a rather narrow discharge performance band, indicating no significant loss of thermal energy-storage capacity or heat-transfer capability during more than 5000 hours of operation. This is a significant observation because it indicates dependable performance does occur after a prolonged shutdown, which would occur in a utility application for equipment maintenance.

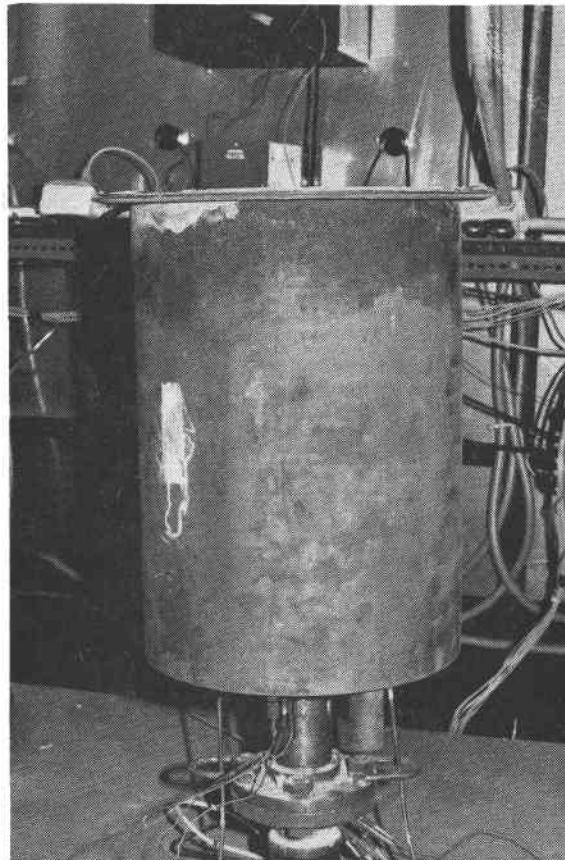
Table 7. EXPERIMENTAL RESULTS FOR DISCHARGING OF ENGINEERING-SCALE TES UNIT 2 (LiKCO<sub>3</sub> Salt)

Discharge Cycle Number	Cumulative Operating Time, hr	Time Required for Discharge, min	Average Heat Flux	
			W/m <sup>2</sup>	(Btu/hr-ft <sup>2</sup> )
2-15	500	315	13,117	(4161)
2-65	2900	330	12,373	(3925)
2-81	3550	330	10,570	(3353)
2-102	4400	330	11,711	(3715)
2-127	5360	345	11,831	(3753)

#### Post-Test Examination

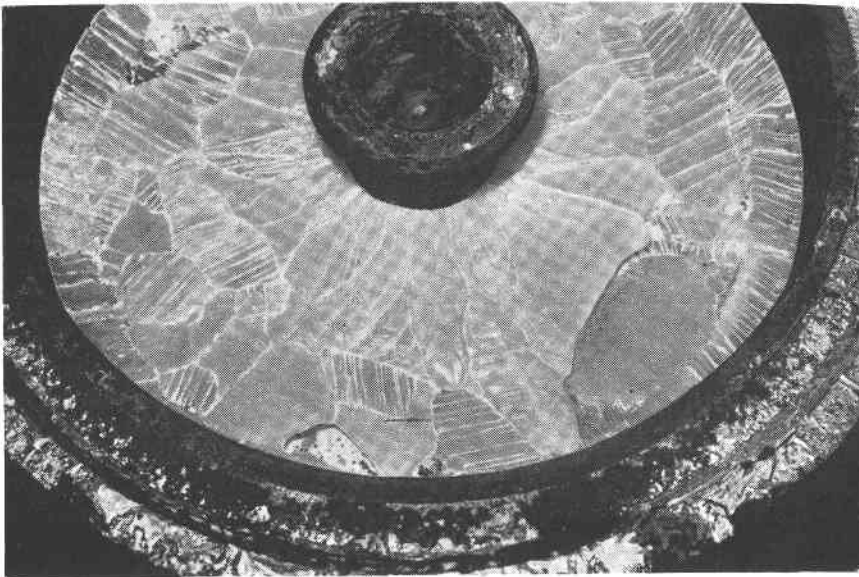
After termination, Unit 2 was dismantled to evaluate the stability of the LiKCO<sub>3</sub> salt and the nature and extent of corrosion of the stainless-steel HX tube and containment vessel. A side-view photograph of the 0.3 m (12 in.) in diameter X 0.46 m (18 in.) -high Unit 2 module after termination and removal of the insulation is shown in Figure 15. The appearance of the upper surface of solidified LiKCO<sub>3</sub> salt after removal of the top cover is shown in Figure 16. The carbonate salt was very clean, free of any significant discoloration from chemical interactions with the stainless-steel HX tube and containment vessel.

A very thin and weakly adherent film of corrosion product was observed on the inner wall of the containment vessel at the salt/gas interface. The film had become detached from some areas and formed a few small localized reddish-brown deposits on the surface of the solid salt. Small samples of the corrosion-product scale were scraped from the containment surface and washed with an acetic acid/acetic anhydride solution to remove the soluble salts. The residue was collected on a millipore filter paper and analyzed by X-ray diffractometry (Cu-K<sub>α</sub> radiation) in an attempt to identify the compound(s) present. As shown in Table 8, six distinct peaks were observed having d-spacings ranging from 4.23 to 2.05 angstroms.<sup>15</sup> Comparison of these peaks with



P80010062

Figure 15. APPEARANCE OF ENGINEERING  
UNIT 2 AFTER 5650 HOURS OF ELEVATED-  
TEMPERATURE OPERATION  
(Insulation and Cover Removed)



P80010063

Figure 16. APPEARANCE OF  $\text{LiKCO}_3$  SALT IN ENGINEERING UNIT 2 AFTER 129 CYCLES AND 5650 HOURS OF ELEVATED-TEMPERATURE OPERATION

available literature data for lithium-containing mixed oxide compounds indicates that  $\text{LiCrO}_2$  or  $\text{LiFeO}_2$  may have formed on the Type 316 SS. This is a plausible finding based on the nominal composition of this steel (17% Cr, 12% Ni, 2.5% Mo, 2% Mn, 1% Si, balance Fe, by weight) although the amount of sample available was too small to obtain a high-precision X-ray diffraction pattern or confirmatory chemical analyses.

Table 8. X-RAY DIFFRACTION ANALYSIS OF CORROSION-PRODUCT SCALE FROM ENGINEERING UNIT 2

Corrosion-Product		$\alpha\text{-LiFeO}_2$ (17-938)*		$\beta\text{-LiFeO}_2$ (17-936)*		$\text{LiCrO}_2$ (24-601)*	
$\overset{\circ}{d}(\text{Å})$	$\overset{\circ}{I}/I_0$	$\overset{\circ}{d}(\text{Å})$	$\overset{\circ}{I}/I_0$	$\overset{\circ}{d}(\text{Å})$	$\overset{\circ}{I}/I_0$	$\overset{\circ}{d}(\text{Å})$	$\overset{\circ}{I}/I_0$
4.23	45					4.800	75
3.81	13						
3.72	8						
2.42	4	2.394	50	2.392	30	2.473	45
2.09	13			2.136	70		
2.05	100	2.073	100	2.043	100	2.060	100

\* Diffraction data for  $\text{LiFeO}_2$  and  $\text{LiCrO}_2$  compounds taken from Reference 15.

The aluminum foil gasket used to form a non-hermetic seal between the interior of the vessel and the ambient atmosphere was in reasonably good condition, having experienced some oxidation, embrittlement, and cracking. (See Figure 16.) Visual examination of the module exterior after removal of the insulation revealed a small deposit of carbonate that was apparently transported by the vapor phase from the melt through this aluminum gasket seal area between the cover and vessel. Visual examination also revealed that a small amount of carbonate was transported (most likely via the vapor phase) from the melt into the upper portion of the HX pipe, resulting in some minor corrosion on the inner surface of this pipe. A very slight leak was observed at one of the thermocouple fittings on the bottom of the vessel. But, in general, visual inspection indicated that the molten carbonate TES module was in very good condition after 5650 hours of elevated-temperature service.

Metallographic analysis of the 316 stainless-steel vessel revealed that a stable oxide scale approximately 25 $\mu$ m (0.001 in.) thick was formed on the inner surface during the 5650 hours of exposure to the carbonate environment. An optical micrograph of the containment inner surface exposed to LiKCO<sub>3</sub> at mid-salt level is shown in Figure 17. In addition to the outer oxide layer, a sub-scale zone of intergranular penetration approximately 76 $\mu$ m (0.003 in.) in extent was also observed. There was no visible evidence of spalling of the outer oxide scale as a result of repeated thermal cycling; the scale appears to have been providing protection against further oxidation of the stainless steel. No significant thermal aging effects were observed in the bulk stainless-steel material.

Samples of the LiKCO<sub>3</sub> salt were taken from various locations in the TES unit for analysis. Differential scanning calorimetry (DSC) was utilized to determine whether any changes in the thermal behavior of the LiKCO<sub>3</sub> salt had occurred as a result of the prolonged operation and cycling at elevated temperature. The melting point of the salt after 5650 hours of testing was found by DSC to consistently be 502.5°C (936.5°F) compared to 505°C (941°F) for the unexposed material, indicating very good salt stability. The chemical analysis of these samples, appearing in Table 9, revealed that there was no change in the composition of the salt due to partial decomposition or chemical reaction with the HX or containment materials.

Table 9. CHEMICAL ANALYSIS OF LiKCO<sub>3</sub> SALT FROM ENGINEERING-SCALE UNIT 2

	COMPOSITION, Wt %					
	Li	K	CO <sub>3</sub>	Fe	Ni	Cr
PRE-TEST	6.57	36.78	56.64	<0.01	<0.01	<0.01
POST-TEST						
2.54cm (1 in.)*	6.58	38.76	55.27	0.01	<0.02	<0.01
5.08cm (2 in.)*	6.43	37.43	57.01	0.01	<0.01	<0.01
6.35cm (2.5 in.)*	6.72	37.54	57.48	0.01	<0.01	<0.01
Average Post-Test	6.58	37.91	56.58	0.01	<0.01	<0.01

\* Samples taken at mid-salt level, 2.54, 5.08, and 6.35 cm (1, 2, and 2.5 in.) away from containment OD.

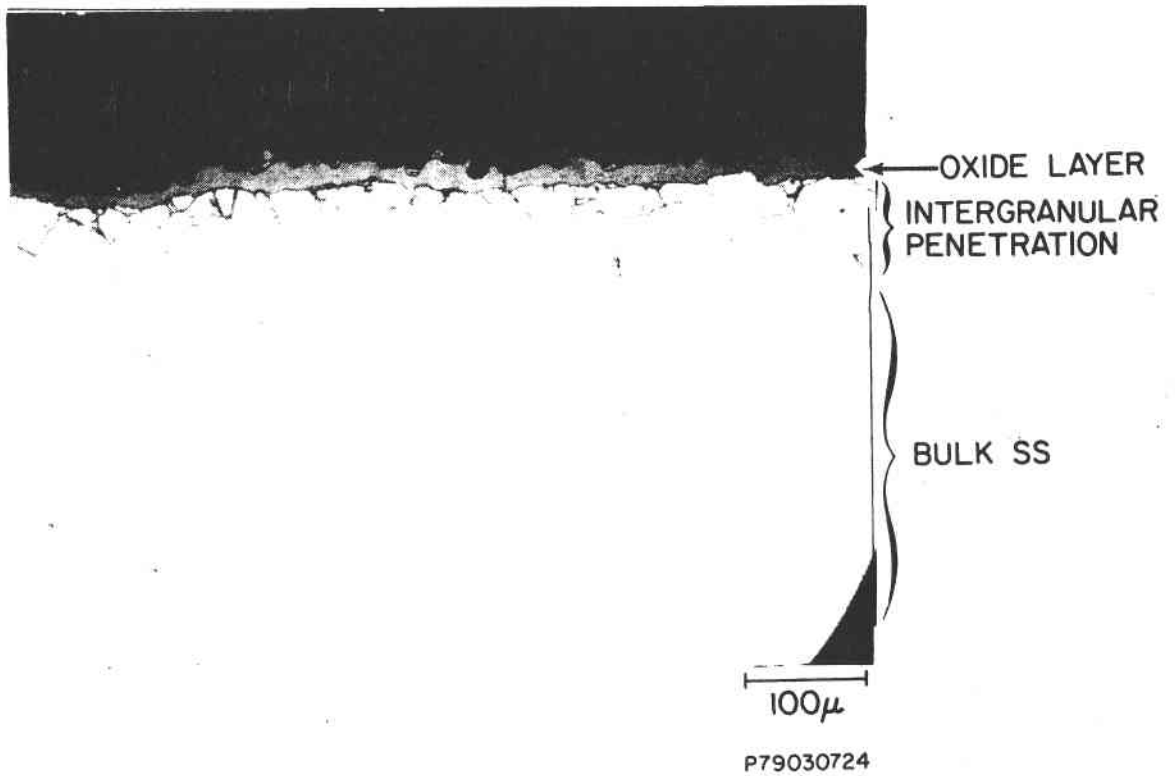


Figure 17. TYPE 316 SS CONTAINMENT FROM ENGINEERING UNIT 2 AFTER 5650 HOURS OF TESTING, SALT SIDE, MID-HEIGHT ( $\text{FeCl}_2\text{-HCl-H}_2\text{O}$  Etchant)

The high degree of stability of this alkali carbonate TES module after 5650 hours of operation is very encouraging, especially since this performance was achieved without a hermetic seal between the ambient and gas phase above the PCM salt and after a 5-month exposure of the salt to ambient during a mid-test shutdown.

## 2.2 Laboratory-Scale Testing

### Introduction

The results of the system studies performed under Task 1 indicated that the PCM for application in a steam-Rankine cycle should have a transformation temperature less than 350°C (662°F). This temperature is defined by the saturation temperature of the steam working fluid at a pressure of  $1.6 \times 10^7$  Pa (2,400 psia). In the possible TES schemes indentified in Task 1, for example, 67 to 77% of the total heat transferred between the PCM and the working fluid would be associated with a unit operating at an approximate temperature of 300°C (570°F). Because this temperature is lower than the lowest melting carbonate eutectic known [43.5 mol %  $\text{Li}_2\text{CO}_3$ /31.5 mol %  $\text{Na}_2\text{CO}_3$ /25.0 mol %  $\text{K}_2\text{CO}_3$  ternary; 397°C melting point (mp)], identification of a suitable PCM for this application would require the investigation of ways to suppress the ternary's mp, possibly by doping it with other carbonates ( $\text{MgCO}_3$ ,  $\text{SrCO}_3$ ,  $\text{CaCO}_3$ ,  $\text{BaCO}_3$ ). Consideration of non-carbonate salts in this temperature regime was outside the scope of the present program.

In view of the aforementioned considerations, the major experimental effort was redirected from the TES application originally intended (steam-Rankine peaking cycle) to solar-thermal systems applications in the temperature range 538° to 870°C (1000° to 1600°F). Carbonate salts are particularly attractive for such high temperature applications because of their relatively high heats of fusion, thermal stability and compatibility with materials of construction. Emphasis was given to salt compositions based on  $\text{Li}_2\text{CO}_3$ ,  $\text{Na}_2\text{CO}_3$ , and  $\text{K}_2\text{CO}_3$ , from which congruently melting carbonate mixtures are available covering the temperature range 397°C (747°F) for the (Li-Na-K) $_2\text{CO}_3$  ternary to 898°C (1648°F) for pure  $\text{K}_2\text{CO}_3$ .

### Salt Selection

The most important salt properties to be considered when selecting a thermal energy storage medium were identified and discussed in detail previously.<sup>16</sup> These factors include —

- Melting temperature
- Heat of fusion
- Heat capacity (solid and liquid)
- Thermal conductivity (solid and liquid)
- Density
- Volume change on fusion
- Volumetric thermal expansion
- Cost and availability
- Chemical stability
- Containment requirements
- Safety

The most reliable thermophysical and thermochemical carbonate property data available are for the pure alkali carbonates,  $\text{Li}_2\text{CO}_3$ ,  $\text{Na}_2\text{CO}_3$ , and  $\text{K}_2\text{CO}_3$ . These data have been reviewed by Janz,<sup>17</sup> Stern and Weise,<sup>18</sup> and most recently by Janz et al.<sup>19</sup> Table 10 provides a summary of pertinent data for these pure carbonates.

The heats of fusion of  $\text{Li}_2\text{CO}_3$  (mp 723°C, 1333°F),  $\text{Na}_2\text{CO}_3$  (mp 858°C, 1576°F), and  $\text{K}_2\text{CO}_3$  (mp 898°C, 1648°F) were measured by Janz, Neuenschwander, and Kelly<sup>20</sup> to be  $6.07 \times 10^5$ ,  $2.65 \times 10^5$ , and  $2.00 \times 10^5$  J/kg (261, 114, and 86 Btu/lb), respectively, using a drop calorimetric technique. Based upon these results and complementary calorimetry work by Rolin and Recapet, Janz et al.<sup>19</sup> most recently recommended the following heat of fusion values:  $\text{Li}_2\text{CO}_3$  —  $5.56 \times 10^5$  J/kg (239 Btu/lb);  $\text{Na}_2\text{CO}_3$  —  $2.81 \times 10^5$  J/kg (121 Btu/lb);  $\text{K}_2\text{CO}_3$  —  $2.00 \times 10^5$  J/kg (86 Btu/lb). However, the former values were used during the course of this work.

Table 10. SELECTED PROPERTIES OF ALKALI CARBONATES

	<u>Li<sub>2</sub>CO<sub>3</sub></u>	<u>Na<sub>2</sub>CO<sub>3</sub></u>	<u>K<sub>2</sub>CO<sub>3</sub></u>
Molecular Weight	73.89	105.99	138.21
Melting Point, °C	723	858	898
Heat of Fusion, J/kg (Btu/lb)	6.07 X 10 <sup>5</sup> (261)	2.65 X 10 <sup>5</sup> (114)	2.00 X 10 <sup>5</sup> (86)
Heat Capacity, J/mol-K (50°C above mp)	188.1	194.8	208.6
Density, kg/m <sup>3</sup> (lb/ft <sup>3</sup> )			
Solid at 25°C	2114 (132)	2531 (158)	2434 (152)
Liquid at 50°C above mp	1810 (113)	1954 (122)	1874 (117)
Volume Change on Melting, %	+6.9	+16.2	+16.4
Thermal Conductivity, W/m-K (Btu/hr-ft-°F)			
Solid at 50°C below mp	1.45 (2.51)	1.27 (2.19)	--
Liquid at 50°C above mp	2.14 (3.70)	1.88 (3.26)	--
Dissociation Constant, Pa (atm) (50°C above mp)	42.6 (4.2 X 10 <sup>-4</sup> )	0.06 (5.9 X 10 <sup>-7</sup> )	0.006 (6.4 X 10 <sup>-8</sup> )
Viscosity, Pa-s (cP) (50°C above mp)	4.65 X 10 <sup>-3</sup> (4.65)	2.8 X 10 <sup>-3</sup> (2.80)	2.22 X 10 <sup>-3</sup> (2.22)
Surface Tension, N/m (50°C above mp)	0.242	0.209	0.166
Technical-Grade Salt Cost, \$/kg (\$/lb)	2.05 (0.93)	0.07 (0.03)	0.42 (0.19)

Expressions for the heat capacities of the molten salts have been presented by Janz et al,<sup>19</sup> with  $C_p$  units\* of J/mol-K.

$$\text{Li}_2\text{CO}_3 \quad C_p = 129.0 + 5.66 \times 10^{-2} T(\text{K}) \quad (12)$$

$$\text{Na}_2\text{CO}_3 \quad C_p = 142.1 + 4.47 \times 10^{-2} T(\text{K}) \quad (13)$$

$$\text{K}_2\text{CO}_3 \quad C_p = 154.5 + 4.45 \times 10^{-2} T(\text{K}) \quad (14)$$

The enthalpy curves shown in Figure 18 represent the sensible and latent heat contents for the pure carbonates and estimates for several carbonate mixtures of interest, based on molar additivity. The sensible heat content curve of MgO is also shown for comparison.

Thermal conductivities of solid and liquid  $\text{Li}_2\text{CO}_3$  and  $\text{Na}_2\text{CO}_3$  have been measured by Egorov and Revyakina<sup>17</sup> using the absolute steady-state radial heat flux method. Conductivity equations have been presented by Janz et al,<sup>19</sup> with units of k in W/m-K.

$$\text{Li}_2\text{CO}_3 \quad k(\text{s}) = 7.59 - 1.29 \times 10^{-2} T(\text{K}) + 6.81 \times 10^{-6} T(\text{K})^2 \quad (700-1000\text{K}) \quad (15)$$

$$k(\text{l}) = 1.36 \times 10^{-3} + 3.33 \times 10^{-3} T(\text{K}) \quad (16)$$

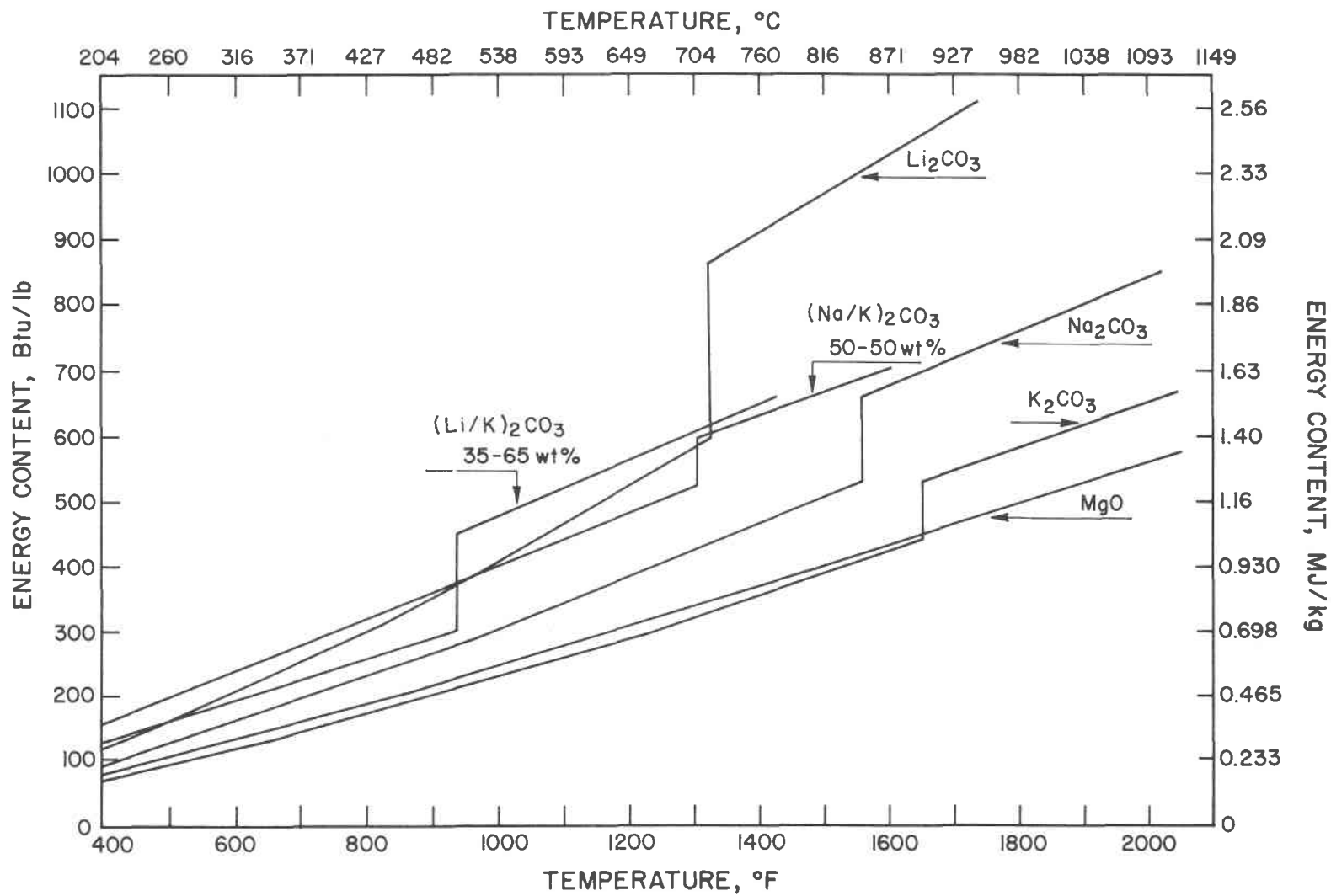
$$\text{Na}_2\text{CO}_3 \quad k(\text{s}) = 8.53 - 1.40 \times 10^{-2} T(\text{K}) + 6.75 \times 10^{-6} T(\text{K})^2 \quad (700-1135\text{K}) \quad (17)$$

$$k(\text{l}) = 4.94 \times 10^{-1} + 1.18 \times 10^{-3} T(\text{K}) \quad (18)$$

No thermal conductivity data have been reported for  $\text{K}_2\text{CO}_3$ .

The densities of carbonate salts at 25°C (77°F) are 2110 kg/m<sup>3</sup> for  $\text{Li}_2\text{CO}_3$ , 2530 kg/m<sup>3</sup> for  $\text{Na}_2\text{CO}_3$ , and 2430 kg/m<sup>3</sup> for  $\text{K}_2\text{CO}_3$ .<sup>21</sup> Densities of the molten salts at a temperature 50°C (90°F) above the melting point are: 1810 kg/m<sup>3</sup> for  $\text{Li}_2\text{CO}_3$  at 773°C (1423°F), 1950 kg/m<sup>3</sup> for  $\text{Na}_2\text{CO}_3$  at 908°C (1666°F), and 1870 kg/m<sup>3</sup> for  $\text{K}_2\text{CO}_3$  at 948°C (1738°F). The volume changes on melting have been estimated to be 6.9%, 16.2%, and 16.4% for  $\text{Li}_2\text{CO}_3$ ,  $\text{Na}_2\text{CO}_3$ , and  $\text{K}_2\text{CO}_3$ , respectively.

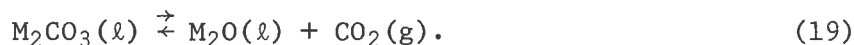
\* An English unit to SI unit conversion table is presented in Appendix A.



A79122749

Figure 18. HEAT CONTENT CURVES FOR SELECTED CARBONATES AND MgO

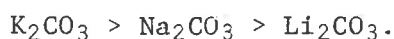
The chemical stability of molten carbonates depends primarily on temperature and the gaseous environment maintained over the melt. Decomposition of the molten metal carbonate  $M_2CO_3(l)$  can be expressed as -



The thermodynamic equilibrium between the melt and the gas phase over it is described in terms of the dissociation constant,  $K_d$  -

$$K_d = \frac{P_{CO_2} a_{M_2O}(l)}{a_{M_2CO_3}(l)} \quad (20)$$

The term  $P_{CO_2}$  in the above equation is the equilibrium  $CO_2$  dissociation pressure, and  $a_{M_2O}(l)$  and  $a_{M_2CO_3}(l)$  are the thermodynamic activities of the metal oxide and metal carbonate, respectively. For ideal solutions, the activity terms may be replaced by the mole fraction (X) of each species. Dissociation constants for  $Li_2CO_3$ ,  $Na_2CO_3$ , and  $K_2CO_3$  at  $50^\circ C$  ( $90^\circ F$ ) above their melting points have been estimated as 42.6 Pa, 0.06 Pa, and 0.006 Pa ( $4.2 \times 10^{-4}$  atm,  $5.9 \times 10^{-7}$  atm, and  $6.4 \times 10^{-8}$  atm), respectively. Thus, for a given oxide content and constant degree of superheat above the melting point, the stability is in the order -



Partial decomposition of molten carbonates with the formation of the oxide ion species, which is more chemically aggressive toward stainless steel than carbonate ion, can be minimized by maintenance of a finite  $CO_2$  partial pressure over the melt. An  $M_2O$  mole fraction of  $10^{-3}$  would be established in molten  $Li_2CO_3$ ,  $Na_2CO_3$ , and  $K_2CO_3$  under  $CO_2$  partial pressures of  $4.3 \times 10^4$  Pa, 59.8 Pa, and 6.48 Pa (0.42 atm,  $5.9 \times 10^{-4}$  atm, and  $6.4 \times 10^{-5}$  atm), respectively, at  $50^\circ C$  ( $90^\circ F$ ) above the melting points. No systematic studies of vaporization have been reported for  $Li_2CO_3$ ,  $Na_2CO_3$  or  $K_2CO_3$  as carbonate -



Expressions have also been presented by Janz et al<sup>19</sup> for the viscosity ( $\eta$ , Pa-s) and surface tension ( $\gamma$ , N/m) of the molten alkali carbonates -

$$\text{Li}_2\text{CO}_3: \quad \eta = 5.259 + 0.015 T(\text{K}) - 13.858 \times 10^{-6} T(\text{K})^2 + 4.313 \times 10^{-9} T(\text{K})^3 \quad (22)$$

$$\gamma = 0.285 - 4.06 \times 10^{-5} T(\text{K}) \quad (23)$$

$$\text{Na}_2\text{CO}_3: \quad \eta = 3.832 \times 10^{-8} \exp [26,260/RT(\text{K})] \quad (24)$$

$$\gamma = 0.269 - 5.02 \times 10^{-5} T(\text{K}) \quad (25)$$

$$\text{K}_2\text{CO}_3: \quad \eta = 1.161 \times 10^{-8} \exp [29,487/RT(\text{K})] \quad (26)$$

$$\gamma = 0.338 - 21.71 \times 10^{-5} T(\text{K}) + 6.25 \times 10^{-8} T(\text{K})^2 \quad (27)$$

Selected values of these properties are summarized in Table 10.

The alkaline earth carbonates  $\text{MgCO}_3$ ,  $\text{CaCO}_3$ ,  $\text{SrCO}_3$ , and  $\text{BaCO}_3$  are of interest as additives to alkali carbonate PCM mixtures because of their ability to modify the melting and solidification behavior. The pure alkaline earth carbonates are generally less stable than the alkali carbonates against thermal decomposition, as indicated by their dissociation constants given in Table 11. As pure compounds they generally decompose to  $\text{M}_2\text{O}$  and  $\text{CO}_2$  rather than melting. Nevertheless, their decomposition in molten mixtures with alkali carbonates can be adequately controlled in certain cases by providing a  $\text{CO}_2$  partial pressure over the melts.

Table 11. SELECTED PROPERTIES OF ALKALINE EARTH CARBONATES

	<u><math>\text{MgCO}_3</math></u>	<u><math>\text{CaCO}_3</math></u>	<u><math>\text{SrCO}_3</math></u>	<u><math>\text{BaCO}_3</math></u>
Molecular Weight	84.32	100.09	147.63	197.35
Density at 25°C, $\text{kg/m}^3$ ( $\text{lb/ft}^3$ )	2963 (185)	2707 (169)	3700 (231)	4437 (277)
Dissociation Constant, $K_d$ , atm				
727°C	539	$6.4 \times 10^{-2}$	$3.1 \times 10^{-4}$	$4.6 \times 10^{-6}$
927°C	--	1.8	$2.9 \times 10^{-2}$	$6.5 \times 10^{-4}$
Technical-Grade Salt Cost, \$/kg (\$/lb)	0.22 (0.10)	0.07 (0.03)	0.49 (0.22)	0.29 (0.13)

The alkali and alkaline earth carbonates of interest as phase-change TES materials are readily available in bulk quantities as technical-grade salts, costing from \$0.07/kg to \$2.05/kg (\$0.03/lb to \$0.93/lb), as indicated in Tables 10 and 11.

Table 12 contains a complete listing of the carbonate-containing salts initially considered as candidate salts, with the experimental or estimated values of properties relevant to their applicability as heat of fusion TES materials. These salts were selected for consideration because their melting points lie within the general 343° to 871°C (650° to 1600°F) range, yet they possess reasonably high heats of fusion. Materials judged to have toxicity, cost, or availability problems were excluded from consideration. The materials considered include single salts and binary and ternary salt mixtures of both eutectic and non-eutectic compositions.

The candidate carbonate compositions were screened at two levels. First, differential scanning calorimetry (DSC)<sup>\*</sup> was employed (when possible) to determine the melting and solidification temperatures and heat of fusion for the mixtures. Since the DSC's maximum operating temperature is 650°C (1200°F), DSC was used only for steam TES applications. Then, based on heat of fusion, stability, and economic considerations, the most promising candidates were tested in laboratory-scale TES modules to determine the cyclic charge/discharge characteristics and short-term stabilities.

Table 13 lists the salt mixtures selected for lab-scale testing, with their pertinent thermophysical properties. Primary emphasis for the salts selected for lab-scale investigations was given to alkali carbonate-based salt compositions with melting points in the solar-thermal range of 538° to 871°C (1000° to 1600°F), although for comparative purposes, fluorides and chlorides, when subjected to identical handling and fabrication procedures, were also considered.

---

\*

Perkin-Elmer DSC-2 differential scanning calorimeter.

Table 12. CANDIDATE CARBONATE-CONTAINING SALTS HAVING MELTING POINTS IN THE RANGE 398° TO 898°C (750° to 1650°F)

Salt System	Composition		Melting Point		Heat of Fusion		Cost	
	Mol %	Wt %	°C	°F	J/kg X 10 <sup>3</sup>	Btu/lb	\$/kg	\$/lb
Li <sub>2</sub> CO <sub>3</sub> -Na <sub>2</sub> CO <sub>3</sub> -K <sub>2</sub> CO <sub>3</sub>	43-32-26	32-33-35	397	747	2.77	119	0.84	0.38
K <sub>2</sub> CO <sub>3</sub> -MgCO <sub>3</sub>	56-44	68-32	460	860	--	--	0.35	0.16
Li <sub>2</sub> CO <sub>3</sub> -K <sub>2</sub> CO <sub>3</sub>	63-37	47-53	488	910	3.91	168	1.19	0.54
Li <sub>2</sub> CO <sub>3</sub> -Na <sub>2</sub> CO <sub>3</sub>	53-47	44-56	496	925	4.16	179	0.95	0.43
Li <sub>2</sub> CO <sub>3</sub> -K <sub>2</sub> CO <sub>3</sub>	43-57	28-72	498	928	3.14	135	0.88	0.40
Li <sub>2</sub> CO <sub>3</sub> -K <sub>2</sub> CO <sub>3</sub>	51-49	35-65	505	941	3.42	147	0.99	0.45
KCl-Na <sub>2</sub> CO <sub>3</sub> -Na <sub>2</sub> SO <sub>4</sub>	55.6-18.4-26	42.4-19.9-37.7	544	1011	2.67	115	0.09	0.04
KCl-K <sub>2</sub> SO <sub>4</sub> -Na <sub>2</sub> CO <sub>3</sub>	47.3-34-18.7	34.6-46.0-19.4	546	1015	2.74	118	0.24	0.11
Li <sub>2</sub> CO <sub>3</sub> -Na <sub>2</sub> CO <sub>3</sub> -K <sub>2</sub> CO <sub>3</sub>	20-60-20	20-60-20	550	1022	3.20	138	0.55	0.25
Li <sub>2</sub> CO <sub>3</sub> -Na <sub>2</sub> CO <sub>3</sub> -K <sub>2</sub> CO <sub>3</sub>	22-16-62	22-16-62	550	1022	3.00	129	0.73	0.33
KCl-K <sub>2</sub> CO <sub>3</sub> -Na <sub>2</sub> CO <sub>3</sub>	42.5-43.3-18.1	28.6-54.0-17.4	558	1037	2.56	110	0.26	0.12
K <sub>2</sub> CO <sub>3</sub> -NaF-Na <sub>2</sub> CO <sub>3</sub>	42-32-26	58.6-13.6-27.8	562	1044	3.02	130	0.35	0.16
BaCO <sub>3</sub> -NaCl-Na <sub>2</sub> CO <sub>3</sub>	21-22-57	36.1-11.2-52.7	562	1044	--	--	0.37	0.17
K <sub>2</sub> CO <sub>3</sub> -NaF	45-55	72.9-27.1	568	1055	3.63	156	0.51	0.23
CaCO <sub>3</sub> -CaF <sub>2</sub> -Ca(OH) <sub>2</sub>	29.7-20.1-50.2	36.0-19.0-45.0	575	1067	--	--	--	--
NaCl-NaF-Na <sub>2</sub> CO <sub>3</sub>	42.5-20.5-37	34.2-11.8-54.0	575	1067	4.04	174	0.13	0.06
CaCO <sub>3</sub> -LiF	29.7-70.3	62.0-38.0	580	1076	--	--	2.14	0.97
KCl-Na <sub>2</sub> CO <sub>3</sub>	50.2-49.8	41.5-58.5	588	1094	3.02	130	0.07	0.03
LiF-Li <sub>2</sub> CO <sub>3</sub>	49-51	25.2-74.8	608	1126	7.16	308	2.93	1.33
NaCl-Na <sub>2</sub> SO <sub>4</sub> -Na <sub>2</sub> CO <sub>3</sub>	51.8-24.1-24.1	33.6-38.0-28.4	612	1134	3.00	129	0.18	0.08
CaCl <sub>2</sub> -CaCO <sub>3</sub>	70-30	72.1-27.9	622	1152	--	--	0.09	0.04
KCl-K <sub>2</sub> CO <sub>3</sub>	61.6-38.4	46.4-53.6	632	1170	2.72	117	0.24	0.11
NaCl-Na <sub>2</sub> CO <sub>3</sub>	76.9-23.1	64.7-35.3	634	1173	4.05	174	0.04	0.02
KCl-K <sub>2</sub> CO <sub>3</sub>	65-35	50-50	636	1177	2.79	120	0.24	0.11
CaCO <sub>3</sub> -Ca(OH) <sub>2</sub>	35.8-64.2	43.0-57.0	653	1207	--	--	0.09	0.04
Cr <sub>2</sub> O <sub>3</sub> -Na <sub>2</sub> CO <sub>3</sub>	45-55	54.0-46.0	658	1216	--	--	1.81	0.82
CaCO <sub>3</sub> -Li <sub>2</sub> CO <sub>3</sub>	37-63	44.3-55.7	662	1224	--	--	1.17	0.53
SrCl <sub>2</sub> -SrCO <sub>3</sub>	74-26	75.3-24.7	671	1240	--	--	--	--
KF-K <sub>2</sub> CO <sub>3</sub>	60-40	38.7-61.3	678	1252	3.12	134	0.84	0.38
BaCO <sub>3</sub> -Na <sub>2</sub> CO <sub>3</sub>	37-63	52.2-47.8	686	1267	--	--	0.18	0.08
KF-K <sub>2</sub> CO <sub>3</sub>	46-54	26.4-73.6	688	1270	2.77	119	0.71	0.32
NaF-Na <sub>2</sub> CO <sub>3</sub>	38.7-61.3	20.0-80.0	690	1274	3.72	160	0.20	0.09
Na <sub>2</sub> CO <sub>3</sub> -Na <sub>2</sub> O	61.3-38.7	73.0-27.0	695	1283	3.95	170	--	--
K <sub>2</sub> CO <sub>3</sub> -Na <sub>2</sub> CO <sub>3</sub>	38.5-61.5	44.9-55.1	695	1283	2.37	102	0.22	0.10
K <sub>2</sub> CO <sub>3</sub> -Na <sub>2</sub> CO <sub>3</sub>	44-56	50.6-49.4	710	1310	2.32	100	0.24	0.11
Li <sub>2</sub> CO <sub>3</sub>	100	100	723	1333	6.07	261	2.05	0.93
BaCl <sub>2</sub> -BaCO <sub>3</sub>	53-47	54.3-45.7	734	1353	--	--	0.31	0.14
BaCO <sub>3</sub> -NaCl	47-53	75.0-25.0	734	1353	--	--	0.24	0.11
CaCO <sub>3</sub> -Na <sub>2</sub> CO <sub>3</sub> -Na <sub>2</sub> SO <sub>4</sub>	37.5-46.5-16	34.3-45.0-20.7	770	1418	--	--	0.11	0.05
CaCO <sub>3</sub> -Na <sub>2</sub> CO <sub>3</sub> -Na <sub>2</sub> SO <sub>4</sub>	38-38-24	33.8-35.8-30.4	795	1463	--	--	0.15	0.07
Cr <sub>2</sub> O <sub>3</sub> -K <sub>2</sub> CO <sub>3</sub>	20-80	21.6-78.4	803	1478	--	--	1.04	0.47
Na <sub>2</sub> CO <sub>3</sub> -Na <sub>2</sub> SO <sub>4</sub>	66.7-33.3	59.9-40.1	812	1494	2.26	97	0.18	0.08
BaCl <sub>2</sub> -BaCO <sub>3</sub>	76-24	86.8-13.2	814	1497	--	--	0.33	0.15
BaCO <sub>3</sub> -NaCl	24-76	35.1-64.9	814	1497	--	--	0.13	0.06
Na <sub>2</sub> CO <sub>3</sub> -Na <sub>2</sub> SO <sub>4</sub>	62-38	54.9-45.1	826	1519	2.21	95	0.20	0.09
Na <sub>2</sub> CO <sub>3</sub>	100	100	858	1564	2.58	111	0.07	0.03
BaCl <sub>2</sub> -BaCO <sub>3</sub>	82.5-17.5	83.3-16.7	860	1580	--	--	0.31	0.14
K <sub>2</sub> CO <sub>3</sub>	100	100	898	1648	2.00	86	0.42	0.19

B80020281

Table 13. FINAL SALTS SELECTED FOR LAB-SCALE TESTING

No.	Salt System	Composition		Melting Point		ΔH <sub>f</sub>		Heat Capacity at Melting Point				Thermal		Density at 25°C		Salt Cost		Capacity Cost		Specific Capacity (a at 25°C)	
		wt %	mol %	°C	°F	J/kg	Btu/lb	c <sub>p</sub> (*) J/kg-K	c <sub>p</sub> (*) Btu/lb-°F	c <sub>p</sub> (†) J/kg-K	c <sub>p</sub> (†) Btu/lb-°F	W/m-K	Btu/hr-°F-ft	kg/m <sup>3</sup>	lb/ft <sup>3</sup>	\$/kg	\$/lb	\$/10 <sup>6</sup> J	\$/10 <sup>6</sup> Btu	J/m <sup>3</sup> ·10 <sup>6</sup>	Btu/ft <sup>3</sup>
1	Li <sub>2</sub> CO <sub>3</sub> -Na <sub>2</sub> CO <sub>3</sub> -K <sub>2</sub> CO <sub>3</sub>	32-33-35	43.3-31.2-25.5	397	747	276,794	119	1674.7	0.40	1632.9	0.39	2.02	1.17	2900.3	143.6	0.73	0.33	2.60	2741	6.65	17,835
2	Li <sub>2</sub> CO <sub>3</sub> -CaCO <sub>3</sub>	55.7-44.3	63-37	662	1224	274,468	118	--	--	--	--	--	--	--	--	1.17	0.53	--	--	--	--
3	Na <sub>2</sub> CO <sub>3</sub> -BaCO <sub>3</sub>	41.8-52.2	63-37	686	1267	172,124	74	--	--	--	--	--	--	--	--	0.18	0.08	--	--	--	--
4	Li <sub>2</sub> CO <sub>3</sub> -Na <sub>2</sub> CO <sub>3</sub> -K <sub>2</sub> CO <sub>3</sub>	1.21-50.0-48.8	1-55-44	706	1303	162,820	70	1674.7	0.40	1549.1	0.37	1.73	1.00	2399.6	149.8	0.24	0.11	1.49	1597	5.30	14,230
5	Na <sub>2</sub> CO <sub>3</sub> -K <sub>2</sub> CO <sub>3</sub>	50-50	56-44	710	1310	162,820	70	1674.7	0.40	1549.1	0.37	1.73	1.00	2399.6	149.8	0.24	0.11	1.49	1597	5.30	14,230
6	NaF-KF	32.5-67.5	40-60	721	1330	586,152	252	--	--	--	--	--	--	2481.3	154.9	1.23	0.56	2.11	2223	14.50	39,007
7	Li <sub>2</sub> CO <sub>3</sub>	100	100	723	1333	607,086	261	2637.7	0.63	2512.1	0.60	1.96	1.13	2108.0	131.6	2.05	0.93	3.38	3563	12.80	34,348
8	CaCl <sub>2</sub>	100	100	772	1422	256,093	110.1	--	--	--	--	--	--	2348.0	134.1	0.09	0.04	0.34	363	5.50	14,764
9	Na <sub>2</sub> CO <sub>3</sub> -K <sub>2</sub> CO <sub>3</sub>	81.3-18.7	85-15	790-737	1454-1360	253,534	109	--	--	--	--	--	--	2313.3	156.9	0.13	0.06	0.52	551	6.37	17,090
10	Na <sub>2</sub> CO <sub>3</sub>	100	100	858	1576	265,164	114	1004.8	0.24	1004.8	0.24	1.83	1.06	2327.7	157.8	0.07	0.03	0.25	264	6.69	17,958
11	K <sub>2</sub> CO <sub>3</sub>	100	100	898	1648	200,036	86	1507.2	0.36	1507.2	0.36	1.73	1.00	2428.4	151.6	0.42	0.19	2.09	2209	4.86	13,038

B80020282

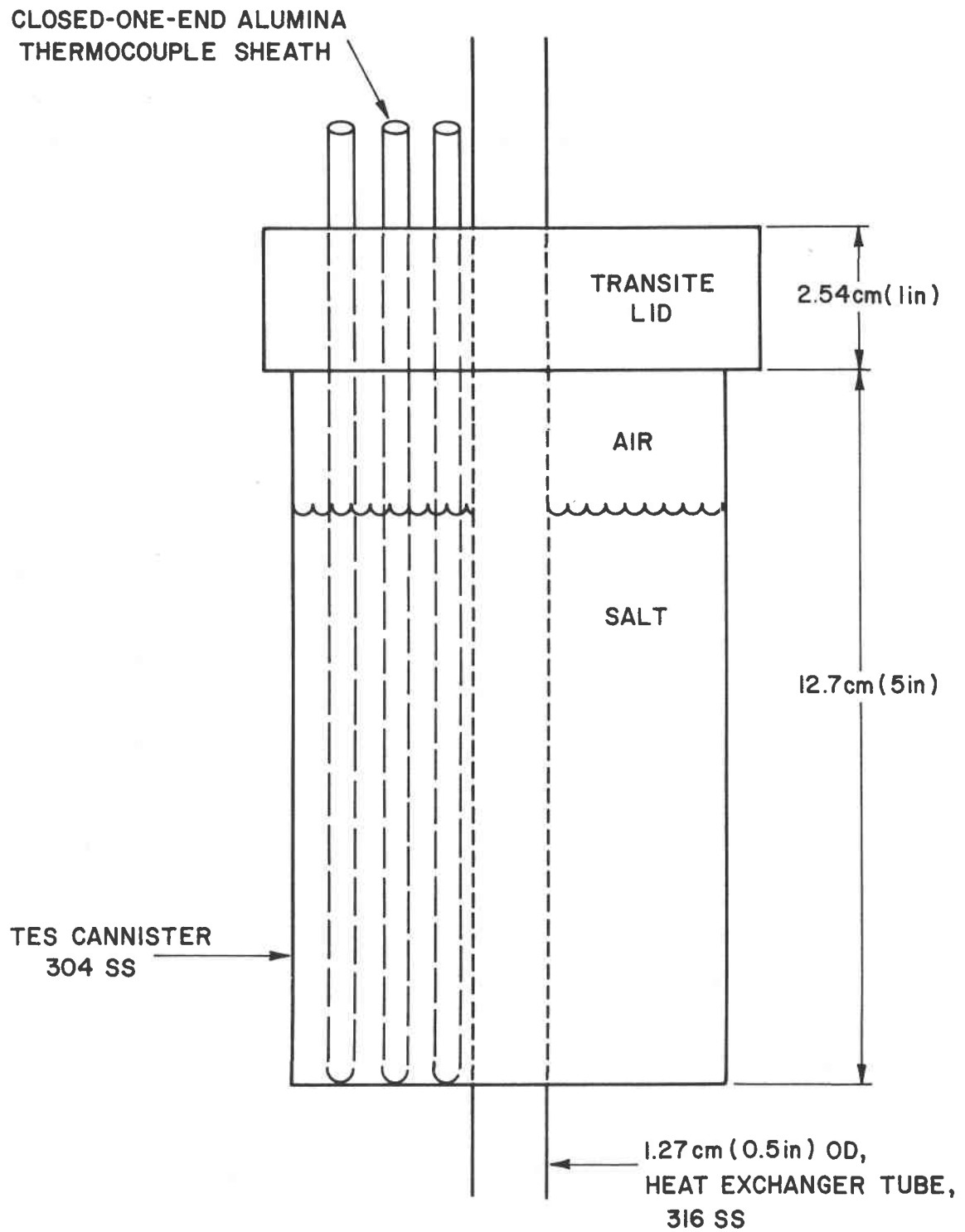
System Components: Construction, Operating Procedures and Data Collection

Construction

Thirteen lab-scale containers, 12.7 cm (5 in.) high, with a 7.62 cm (3 in.) OD, and with a 1.27 cm (0.5 in.) OD single-pass internal HX tube, were fabricated according to the drawing shown in Figure 19. The outside wall of the cannister was Type 304 SS; the HX tube was Type 316 SS. The cannister's top was originally designed as a 1-in.-thick transite disk bored to fit over the central HX tube; the thermocouple (T/C) sheaths were initially installed when 3.18 mm (1/8 in.) holes were drilled in the top and high-quality 4-mm OD, closed-one-end alumina tubes (Ventron Degussit) were inserted slowly into the molten salt. Later this method and design were found unsatisfactory for high-temperature (above 650°C) testing because transite deterioration, salt creepage, and alumina sheath thermal cracking occurred. Therefore the transite cover was replaced with a Type 316 SS cover machined from 6.35 mm (1/4 in.) plate stock that had two holes for SS 316 T/C sheaths and one vent hole. Swagelok fittings were butt-welded onto the cover to seal the stainless-steel sheaths. This arrangement performed well. After the salt mixture was loaded into each cannister, heli-arc welding secured this top to the cannister lip and OD of the HX pipe. A photograph of the final design is shown in Figure 20. Standard 1.27 cm (0.5 in.) Swagelok fittings connected the HX pipe to the TES system's air supply tubing.

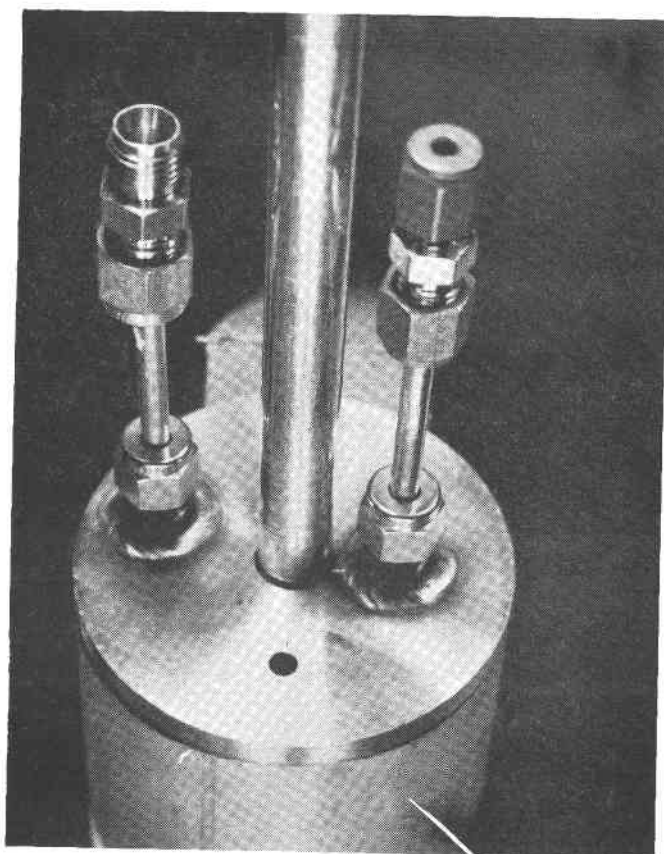
System Operating Procedures and Data Collection

To facilitate lab-scale TES testing, a four-station test stand was constructed, with cooling air supplied through 1.27 cm (0.5 in.) diameter tubing manifolded to each station from a single source (Figure 21). All lab-scale salt containers were inside two clam-shell resistance heaters (Thermal Corp., 825 watts, 1204°C, 2200°F) used to charge the units. The containers and heaters were wrapped with an 20.32 cm (8 in.) radial thickness of Johns-Manville Cerablanket high-temperature insulation (128 kg/m<sup>3</sup>, 8 lb/ft<sup>3</sup> density), rated at a nominal thermal conductivity of 0.12 W/m-K (0.07 Btu/hr-ft-°F) at 540°C (1000°F). The thermal barrier beneath the the unit consisted of 3.81 cm (1.5 in.) of firebricks, 12.7 cm (5 in.) of



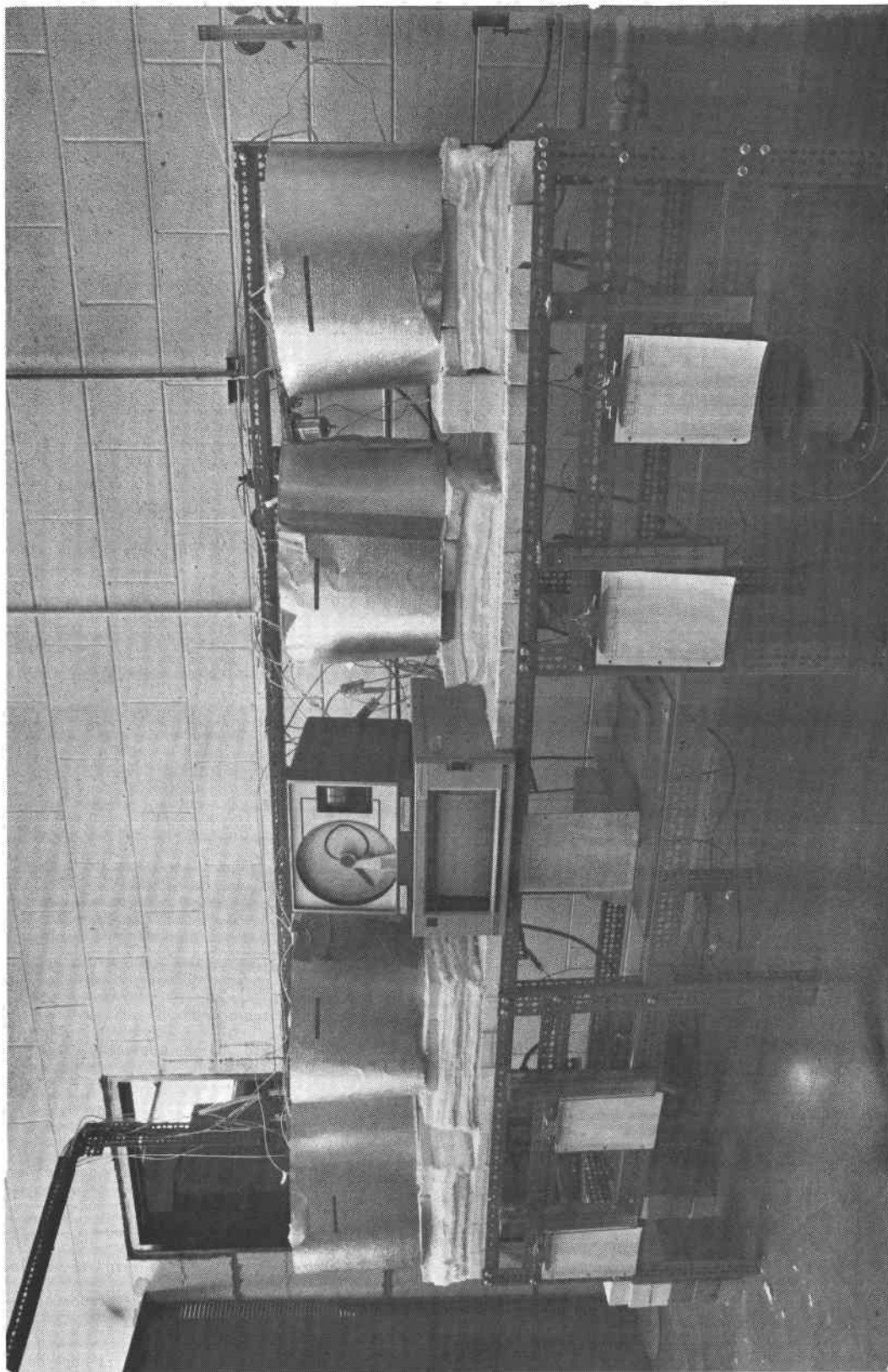
A80010224

Figure 19. CROSS-SECTION OF TYPICAL LAB-SCALE CANNISTER



P80010064

Figure 20. FINAL DESIGN OF TES CANNISTER



P80010065

Figure 21. FOUR-STATION TES LAB-SCALE TEST STAND

insulation and 6.35 cm (2.5 in.) of firebrick as a base. A 17.8 cm (7 in.) thick layer of insulation was also used to minimize radiant heat losses from the top of the unit. A schematic of a TES module, comprised of the TES unit, heater, insulation, instrumentation and controls, is shown in Figure 22.

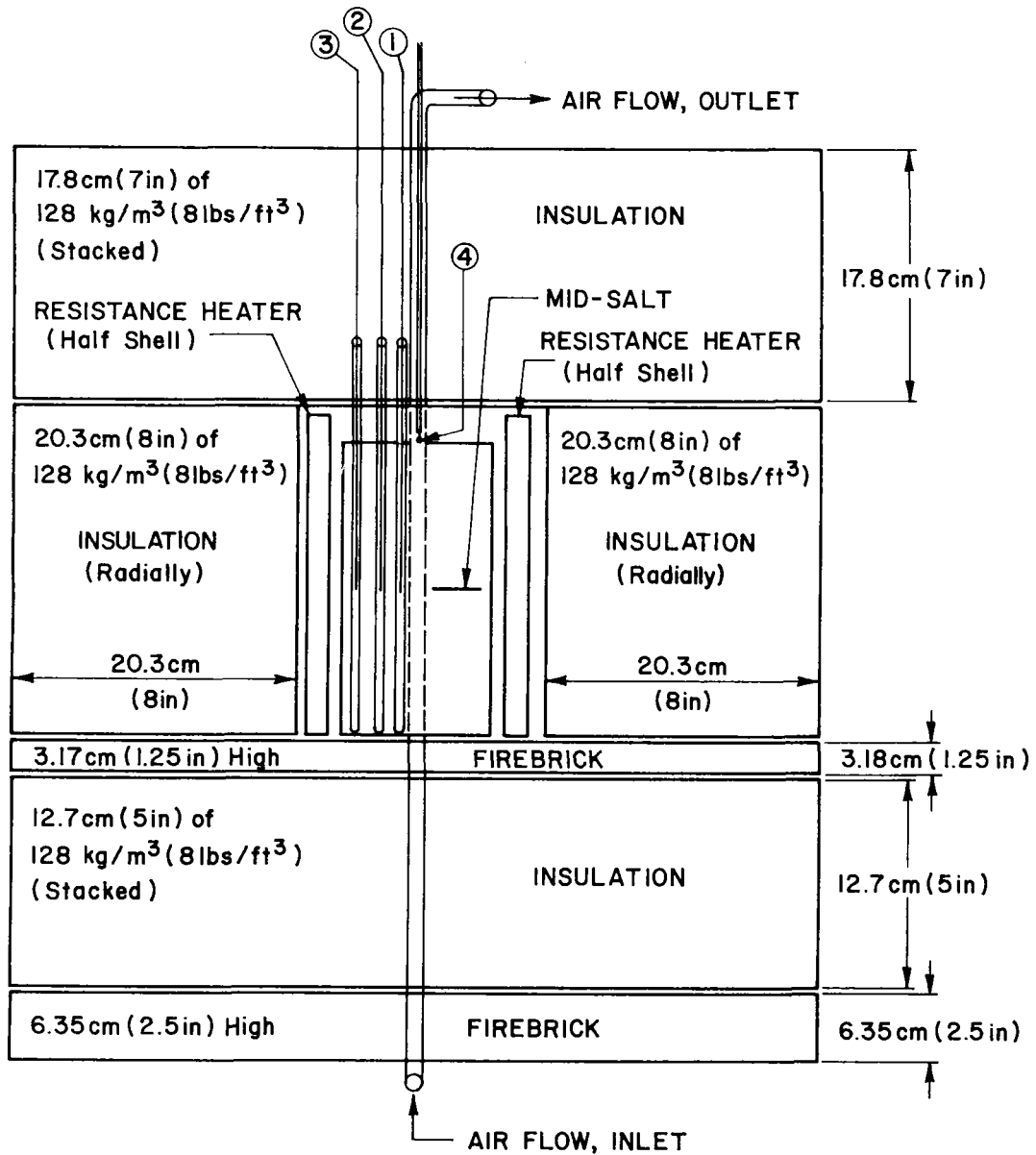
Prior to welding of the top cover and installation into the module setup, each cannister was final filled with approximately 0.91 kg (2 lb) salt powder of the desired composition. Filling was accomplished by the following procedures. First, each container was filled with powdered salt, placed in a HOTPACK resistance box oven, and heated to 50°C (90°F) above the salt melting point. This step was repeated until approximately 80% of the container's volume was filled with molten salt.

The units were operated under varying cycle periods (a cycle consisting of charge, holding time, and discharge). All salts studied in these units were cycled from mp + 50°C (90°F) to mp - 50°C (90°F) for a minimum of 20 cycles, and they were maintained at these operating temperatures from 228 to 1,032 hours.

The salts were discharged with ambient air regulated by a Dwyer flowmeter [range 0 to 11.3 m<sup>3</sup>/hr (400 ft<sup>3</sup>/hr)]. The initial condition for a discharge run was that all T/C's, which were located at mid-salt level, would attain mp + 50°C (90°F). At the end of the holding period, power to the clam-shell heaters was cut, and air was discharged at a constant flow rate, which typically varied from 1.42 to 11.32 m<sup>3</sup>/hr (50 to 400 ft<sup>3</sup>/hr). Mid-salt and air temperatures were continuously recorded on an Esterline Angus 24-point strip chart recorder throughout the cycle. A discharge run was ended when the slowest cooling salt T/C reached the salt's mp - 50°C (90°F) temperature. At this point, air flow was shut off, and the system was re-charged for the next run. The charging sub-cycle was controlled by a T/C at salt mid-level, between the cannister's OD and the heater coils. The temperature controllers were set to bring this location to the holding temperature (mp + 50°C) in less than 2 hours, while initial heat-up rates were maintained between 3.5° and 10°C (6° and 18°F) per minute.

After the end of each test, the containment and salt materials were examined to evaluate their stabilities. The salt composition was chemically analyzed and verified both before installation and after shutdown for CO<sub>2</sub> content, cation composition (Li, K, Na, Ba, Ca, etc.), and relative levels

NO.	THERMOCOUPLE	$r_i$	
		cm	in
①	SALT	1.12	0.44
②	SALT	2.06	0.81
③	SALT	3.02	1.19
④	AIR OUTLET	0	0



A80010226

Figure 22. SCHEMATIC OF LAB-SCALE MODULE

of iron, nickel and chromium (elements indicative of corrosive reaction between salt and stainless-steel containment vessel). Finally, each unit was sectioned at mid-salt level and visually examined to compare salt crystal formation patterns and to note overall compatibility. Selected HX tubes were sectioned in the meniscus region of the salt, mounted, and metallurgically examined to determine the nature and extent of corrosion.

### Salt TES Performance Evaluation

#### Criteria for Performance Evaluation

Numerous factors must be considered in any evaluation of TES system performance. Thus, a particular evaluation should be based on those factors most influential in TES system performance in a specific application (such as solar-thermal power system integration). The following parameters were used in comparatively evaluating the thermal performance of the salts in the lab-scale systems:

- Average discharge heat flux during a discharge run
- Variation of the discharge heat flux with time during a discharge run
- Discharge salt solidification temperature range and characteristics
- Cycling stability - possible variations in discharge behavior resulting from salt/materials instabilities during thermal cycling
- Operational stability - post-test examination of salts' and containment materials' conditions.

Although several other parameters could be added to this list, these form the basis for an assessment of a salt's TES feasibility and for a relative impact analysis of design modifications (such as thermal conductivity enhancement or alternate HX designs).

As with the engineering-scale testing, heat fluxes were calculated using experimental data from Equation 11. The heat-transfer area used to calculate this heat flux was defined as the portion of the central cooling tube in direct contact with the salt. Also, the air outlet temperature was measured at the center of the HX tube near the salt level to yield heat fluxes that are not influenced significantly by radiant heat loss in the extended portions of the HX tube.

Evaluation of Salts for Steam-Rankine Applications 343° to 399°C  
(650° to 750°F)

As discussed in Task 1, the use of a TES subsystem to provide steam superheating can significantly increase the overall efficiency of a steam-Rankine plant. For example, increasing the temperature of the steam entering the turbine from the TES boiler from 316° to 455°C (600° to 850°F) was estimated to result in an increase in system efficiency of from 20% to 30%.

The conceptual TES unit for providing 455°C steam utilized four superheating stages, with salt melt temperatures in the range 349° to 479°C (661° to 894°F). Melting points in this general temperature regime can be attained with mixtures based on  $\text{Li}_2\text{CO}_3$ ,  $\text{Na}_2\text{CO}_3$ , and  $\text{K}_2\text{CO}_3$ . The lowest-melting carbonate eutectic known is the ternary composition 43.5 mole percent (mol %)  $\text{Li}_2\text{CO}_3$ , 31.5 mol %  $\text{Na}_2\text{CO}_3$ , 25 mol %  $\text{K}_2\text{CO}_3$ . As shown in its phase diagram in Appendix B (which contains other available carbonate systems), this eutectic has a melting point of 397°C (747°F) and thus is of interest for steam superheating applications. Also experiments in the U.S.S.R.<sup>22</sup> have indicated that additions of alkaline earth carbonates (5 mol %  $\text{MgCO}_3$ ,  $\text{CaCO}_3$ , or  $\text{BaCO}_3$ ) to the ternary eutectic result in quaternary mixtures with solidus temperatures in the range 355° to 370°C (670° to 700°F). Workers at Battelle Memorial Institute reported<sup>23</sup> that a 19.1 mol % addition of  $\text{CaCO}_3$  to the ternary eutectic resulted in a mixture having a solidus of 335°C (635°F) and a liquidus temperature of 481°C (898°F). Such a mixture would allow heat storage and removal over a range of temperatures close to those identified earlier for the 455°C steam case.

In an attempt to verify these reported melting point depressions, the thermal analysis technique of DSC was used to determine whether a lower melting (<397°C) carbonate will result from the addition of alkaline earth carbonates to the (Li-Na-K) $_2\text{CO}_3$  ternary. Separate additions of 5, 10 and 15 mol % of  $\text{CaCO}_3$  and 5 mol % of  $\text{SrCO}_3$  were made to the ternary eutectic for this study. Upon heating at a rate of 2.5°C (4.5°F) per minute, the ternary eutectic began to melt at 397°C (747°F), in agreement with the published mp value, and melting was completed at 403°C (757°F). Upon cooling at the same rate, a small degree of supercooling was observed; solidification started at 387°C (729°F) and was completed at 384°C (723°F).

No supercooling effects have been observed with this ternary eutectic in the laboratory-scale TES unit. DSC determinations for the ternary and quaternary samples with alkaline earth additions are summarized in Table 14. An addition of 15 mol %  $\text{CaCO}_3$  to the  $(\text{Li-Na-K})_2\text{CO}_3$  ternary lowered its mp from  $397^\circ$  to  $383^\circ\text{C}$  ( $747^\circ$  to  $721^\circ\text{F}$ ), and an addition of 5 mol %  $\text{SrCO}_3$  brought the ternary's mp down to  $389^\circ\text{C}$ .

Table 14. DSC RESULTS FOR THE  $(\text{Li-Na-K})_2\text{CO}_3$  TERNARY AND TERNARY WITH ALKALINE EARTH CARBONATE ADDITIONS

Salt System	Wt %	Melting Point		$\Delta H_f$	
		$^\circ\text{C}$	$^\circ\text{F}$	J/kg	Btu/lb
1. $(\text{Li-Na-K})_2\text{CO}_3$ Ternary	32-33-35	396.2	745.2	$2.67 \times 10^5$	114.7
2. (Ternary) + $\text{CaCO}_3$ (5 mol % $\text{CaCO}_3$ )	95-5	392.8	739.0	$1.95 \times 10^5$	83.7
3. (Ternary) + $\text{CaCO}_3$ (10 mol % $\text{CaCO}_3$ )	90-10	389.4	732.9	$2.51 \times 10^5$	108.1
4. (Ternary) + $\text{CaCO}_3$ (15 mol % $\text{CaCO}_3$ )	85-15	383.0	721.0	$1.90 \times 10^5$	81.8
5. (Ternary) + $\text{SrCO}_3$ (5 mol % $\text{SrCO}_3$ )	92.8-7.2	389.4	732.9	$2.52 \times 10^5$	108.2

These results demonstrate the same general trends as those reported by the Soviets and Battelle Memorial Institute. While the 5, 10 and 15 mol %  $\text{CaCO}_3$  additions exhibited distinct melting points, the Battelle results indicated that a 19.1 mol %  $\text{CaCO}_3$  addition resulted in a system having solidus and liquidus temperature  $146^\circ\text{C}$  ( $263^\circ\text{F}$ ) apart. Further investigation of the melting behavior of the  $(\text{Li-Na-K})_2\text{CO}_3$  eutectic with alkaline earth carbonate additions appears to be needed.

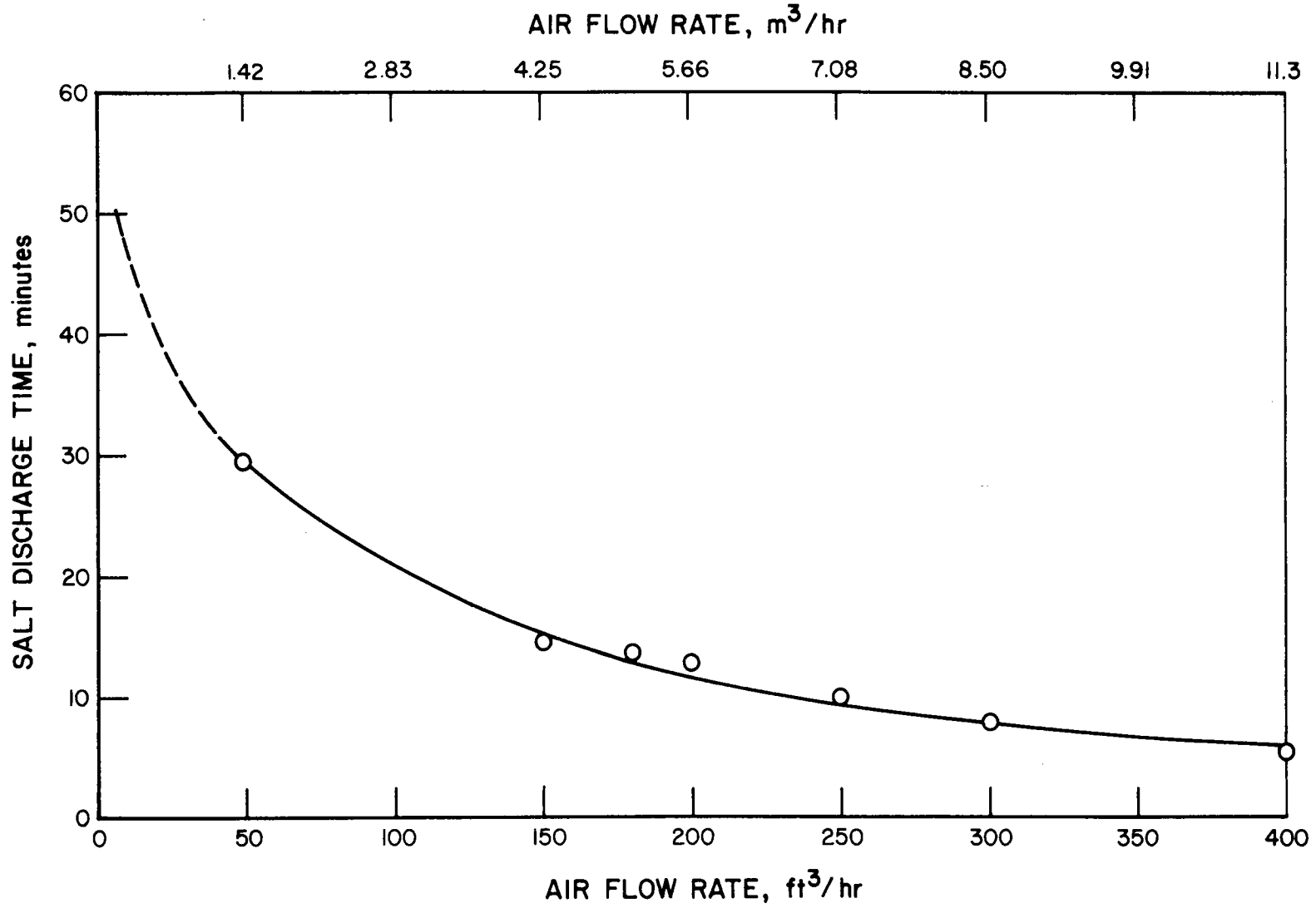
32 wt %  $\text{Li}_2\text{CO}_3$  - 33 wt %  $\text{Na}_2\text{CO}_3$  - 35 wt %  $\text{K}_2\text{CO}_3$  (Module L3-1).

To further investigate the ternary's applicability to steam utility TES subsystems, the thermal behavior of the salt was studied in a lab-scale cannister with the original transite top design, which was found to perform well for this low-temperature salt mixture. In this initial design, salt

temperatures at mid-depth were monitored during discharging with room-temperature air, using Type K (chromel/alumel) T/C's situated at three different radial locations of  $r = 1.1, 2.1$  and  $3.0$  cm ( $0.44, 0.81,$  and  $1.19$  in.). These radii correspond to reduced salt thickness values  $(r/r_o - 1)$  of  $0.76, 2.24,$  and  $3.76,$  which are used in the Megerlin-type heat transfer analysis.<sup>24</sup> Based on the fact that the volume of salt contained between the HX tube and radius ( $r$ ) in the container is proportional to  $r^2 - r_o^2$  (where  $r_o = 6.35$  mm or  $0.25$  in. HX radius,  $r =$  T/C radial distance), these T/C locations correspond to solidifications of  $7%, 33%$  and  $74%$  of the total salt volume when the solid/liquid interface reaches each respective location.

Module L3-1 was loaded with  $611$  grams ( $1.35$  lb) of the ternary eutectic salt. Characteristic discharge curves were determined as a function of discharge air flow rate over the range  $1.42$  to  $11.32$   $m^3/hr$  ( $50$  to  $400$   $ft^3/hr$ ). Figure 23 contains a plot of the discharge time required for the salt to solidify versus air flow rate. At air flow rates greater than  $4.25$   $m^3/hr$  ( $150$   $ft^3/hr$ ), the rate of discharge appears to be controlled mainly by heat transport through the solidified salt. A flow rate of about  $5.1$   $m^3/hr$  ( $180$   $ft^3/hr$ ), which corresponds to a linear flow velocity of  $15.24$  m/second ( $50$  ft/second) through the HX tube, was chosen as the standard, optimum flow condition. This flow rate represents a Reynold's number of  $2.1 \times 10^4$ , thereby satisfying the turbulence criterion. A similar determination of the optimum discharge flow rate was carried out for all salts studied in the lab-scale TES cannisters.

Results obtained during a typical run (No. L3-1-3) of the salt temperature discharge profile for an air flow rate of  $5.1$   $m^3/hr$  ( $180$   $ft^3/hr$ ) are plotted in Figure 24. From the time-temperature response of the salt T/C's, it appeared that the salt was solidifying congruently over the temperature range  $410^\circ$  to  $400^\circ C$  ( $770^\circ$  to  $752^\circ F$ ) taking  $75$  minutes for  $74%$  of the total salt volume to solidify. Figure 25 shows the instantaneous heat flux curve calculated for this salt as a function of discharge time for an air flow rate of  $5.1$   $m^3/hr$  ( $180$   $ft^3/hr$ ). From this, the average discharge heat flux of  $6.95 \times 10^3$   $W/m^2$  ( $2,206$   $Btu/hr-ft^2$ ) was graphically determined, as shown in Table 15 summarizing the experimentally determined data.



A79122748

Figure 23. TYPICAL DISCHARGE PERFORMANCE OF LAB-SCALE MODULE L3-1 CONTAINING TERNARY (Li-Na-K)<sub>2</sub>CO<sub>3</sub> EUTECTIC

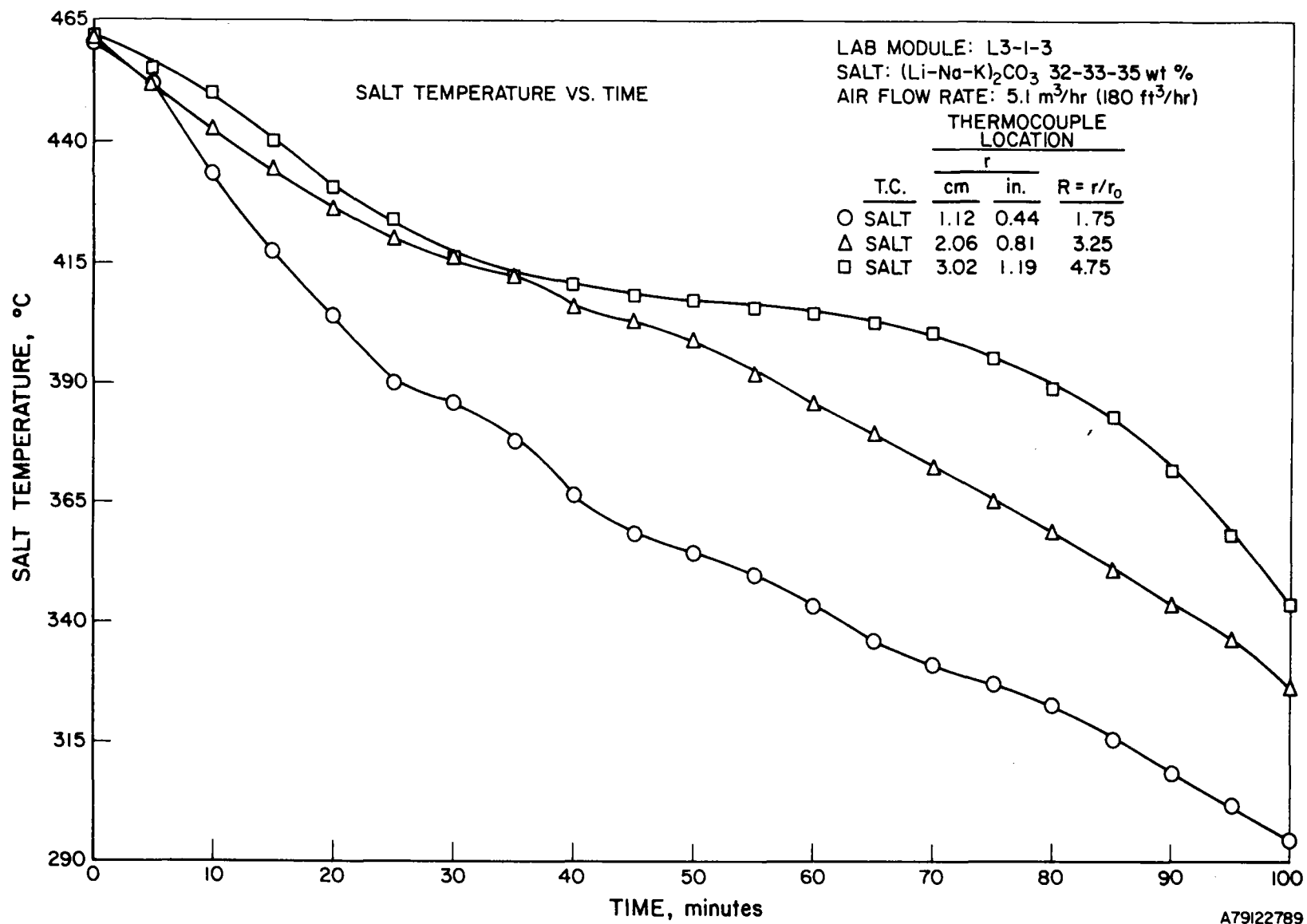
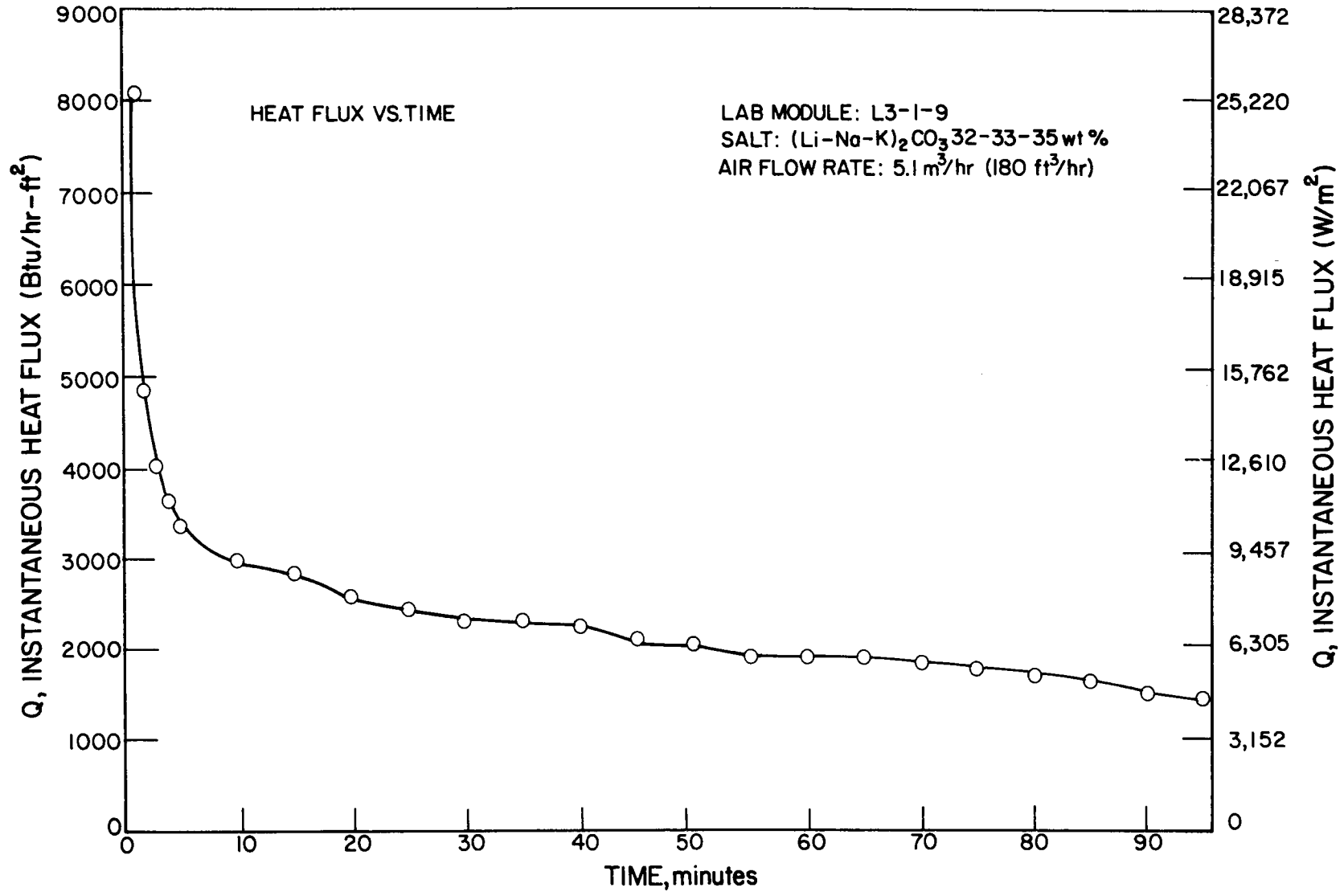


Figure 24. TYPICAL DISCHARGE PERFORMANCE OF  $(\text{Li-Na-K})_2\text{CO}_3$  TERNARY EUTECTIC AT  $5.1 \text{ m}^3/\text{hr}$  ( $180 \text{ ft}^3/\text{hr}$ ) AIR FLOW RATE



B79122783

Figure 25. EXPERIMENTAL HEAT FLUX CURVE FOR (Li-Na-K)<sub>2</sub>CO<sub>3</sub> SYSTEM WITH NO CONDUCTIVITY ENHANCEMENT

Table 15. LAB-SCALE TES EXPERIMENTAL RESULTS

No	Salt Code	Salt System	Composition, wt % (mol %)	Melting Point, °C (°F)	ΔH <sub>f</sub>		Wt. of Salt Loaded		Discharge Solidification Range		Time to Discharge Salt mp + 50°C → mp - 50°C, min	Q̄		No. of Cycles	Hours at Operational Temperature
					J/kg	Btu/lb	gr	lb	°C (°F)	°C (°F)		W/m <sup>2</sup>	Btu/hr-ft <sup>2</sup>		
1	L1-1	Na <sub>2</sub> CO <sub>3</sub> -K <sub>2</sub> CO <sub>3</sub>	50-50 (56-44)	710 (1310)	162,820	70	879.8	1.94	708 (1306)	700 (1292)	34	36,931	11,715	13	336
2	L1-2	Li <sub>2</sub> CO <sub>3</sub> -Na <sub>2</sub> CO <sub>3</sub> -K <sub>2</sub> CO <sub>3</sub>	1.21-49.95-48.84 (56-44)	706 (1303)	162,820	70	880	1.94	706 (1303)	695 (1283)	46	44,422	14,091	22	528
3	L1-3	Na <sub>2</sub> CO <sub>3</sub> -K <sub>2</sub> CO <sub>3</sub>	81.3-18.7 (85-15)	790-737 (454-1360)	253,534	109	821	1.81	790 (1454)	738 (1360)	--	48,375	15,345	38	1032
4	L2-1	Li <sub>2</sub> CO <sub>3</sub>	100 (100)	723 (1333)	607,086	261	720	1.58	727 (1341)	725 (1337)	48	--	--	13	408
5	L2-2	Na <sub>2</sub> CO <sub>3</sub>	100 (100)	858 (1564)	265,164	113	827	1.82	868 (1594)	862 (1584)	27	47,642	14,478	21	288
6	L2-3	K <sub>2</sub> CO <sub>3</sub> (CO <sub>2</sub> Blanket)	100 (100)	893 (1648)	200,036	86	810	1.79	916 (1681)	912 (1674)	21	72,513	23,002	2	96
7	L3-1	(Li-Na-K) <sub>2</sub> CO <sub>3</sub>	32-33-35 (43.3-31.2-25.5)	397 (747)	276,794	119	611.3	1.35	410 (770)	401 (754)	86	6,954	2,206	10	504
8	L3-2	(Li-Na-K) <sub>2</sub> CO <sub>3</sub> w/DuoceI	32-33-35 (43.3-31.2-25.5)	397 (747)	276,794	119	611.3	1.35	408 (766)	404 (759)	53	10,138	3,216	22	312
9	L3-3	BaCO <sub>3</sub> -Na <sub>2</sub> CO <sub>3</sub>	52.2-47.8 (37-63)	686 (1267)	(172,124)	(74)	966	2.63	717 (1323)	712 (1314)	31	41,676	13,220	36	984
10	L3-4	CaCl <sub>2</sub>	100 (100)	772 (1422)	256,093	110	--	--	--	--	--	--	--	--	--
11	L4-1	CaCO <sub>3</sub> -Li <sub>2</sub> CO <sub>3</sub>	44.3-55.7 (37-63)	662 (1224)	(274,468)	(118)	813.6	1.79	662 (1224)	657 (1215)	48	40,405	12,817	25	312
12	L4-2	Li <sub>2</sub> CO <sub>3</sub> (CO <sub>2</sub> Blanket)	100 (100)	726 (1333)	607,086	261	754	1.66	734 (1353)	730 (1346)	54	76,583	24,293	22	672
13	L4-3	KF-NaF	67.5-32.5 (60-40)	721 (1330)	586,152	252	--	--	--	--	--	--	--	--	--

B80020283

After 10 cycles and 504 hours at operational temperatures between 450°C (842°F)(mp + 50°C) and 350°C (662°F)(mp - 50°C), the unit was shut down and used as the TES medium for an analysis of a porous aluminum TCE material that will be discussed in detail in Section 2.3 of this report. The data generated during these 504 hours were utilized to establish a performance baseline for further comparative testing. For this initial set of tests the unit operated with excellent stability, no loss of salt due to creepage, and no equipment failure.

Evaluation of Salts for Solar-Thermal Applications 538° to 871°C  
(1000° to 1600°F)

Advanced concepts for the conversion of solar-thermal energy to electrical power include large central receiver systems employing a closed Brayton power cycle, as well as small dispersed power systems with Stirling heat engines. TES subsystems are desirable in these applications to provide energy to the turbine or heat engine during periods of low solar insolation - early morning, late afternoon, and periods of cloud cover. Latent heat storage is particularly attractive because of its potential for attaining high-energy storage densities and its ability to receive and release heat over a narrow temperature range.

The salts investigated in this subtask for their applicability to latent heat storage were in the temperature range 538° to 871°C (1000° to 1600°F), which represents the expected regime of storage temperature requirements for storage-coupled advanced solar systems.<sup>25,26,27</sup> These high design temperatures are being used to ultimately obtain higher thermal conversion efficiencies.

The following account details the operational life of the first three high-temperature salts selected for lab-scale evaluation. It was during these initial tests that some of the significant problems associated with molten salt systems in this high-temperature regime were encountered and solutions identified. The first salts tested were 49.4 wt % Na<sub>2</sub>CO<sub>3</sub> - 50.6 wt % K<sub>2</sub>CO<sub>3</sub>; 1.21 wt % Li<sub>2</sub>CO<sub>3</sub> - 49.95 wt % Na<sub>2</sub>CO<sub>3</sub> - 48.84 wt % K<sub>2</sub>CO<sub>3</sub>; and pure Li<sub>2</sub>CO<sub>3</sub>.

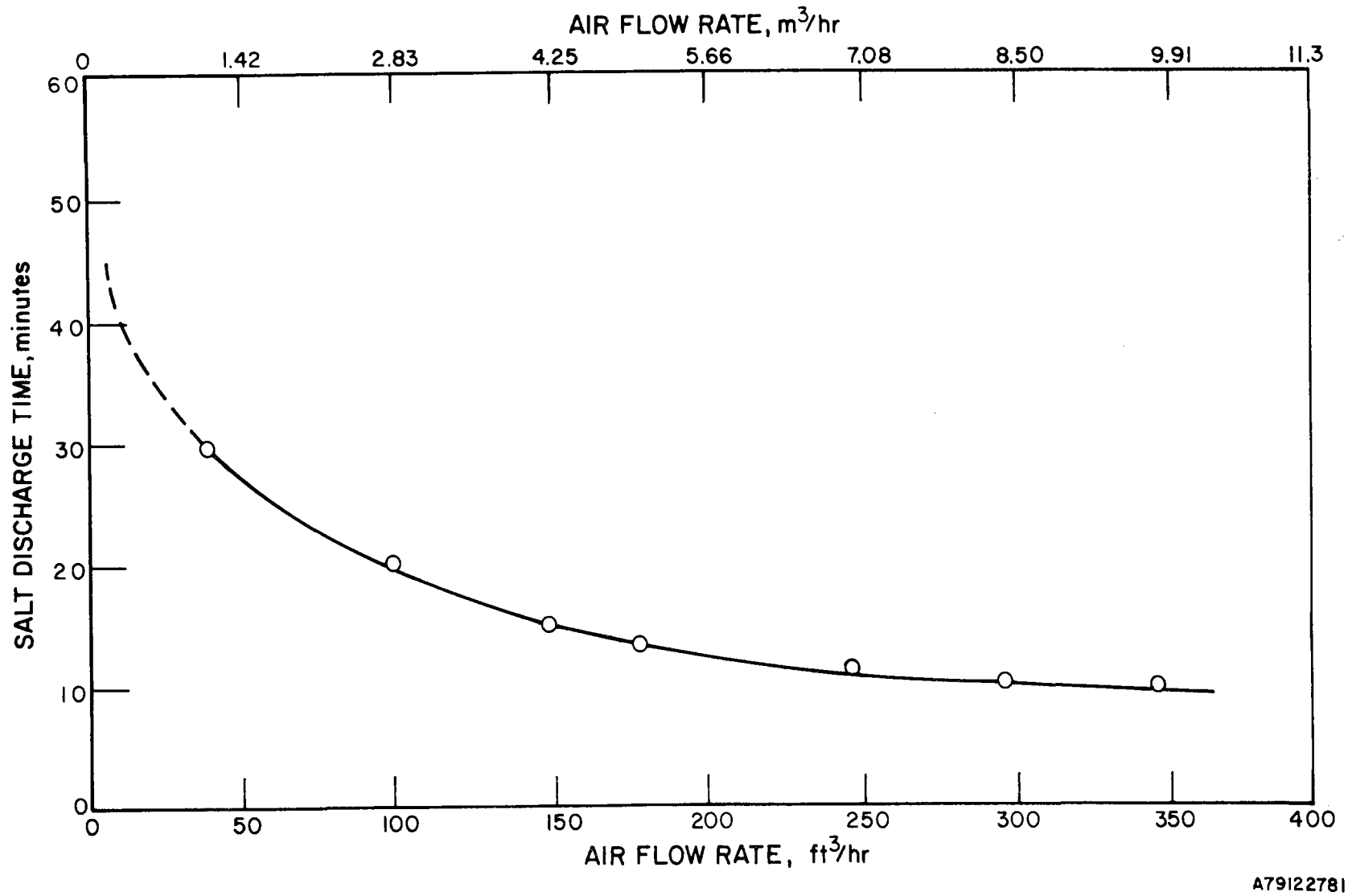
49.4 wt % Na<sub>2</sub>CO<sub>3</sub> - 50.6 wt % K<sub>2</sub>CO<sub>3</sub> (Module L1-1). This Na<sub>2</sub>CO<sub>3</sub>-K<sub>2</sub>CO<sub>3</sub> mixture was expected to correspond to a congruently melting salt with a melting point of 710°C (1310°F), the lowest-melting composition in this binary system. The phase diagram for this, and other available carbonate systems, are included in Appendix B.

A cannister was loaded with 880 grams (1.94 lb) salt of composition 49.4 wt %  $\text{Na}_2\text{CO}_3$  - 50.6 wt %  $\text{K}_2\text{CO}_3$  and assembled with the original cannister design of transite cover and high quality alumina T/C sheaths as previously described. The molten salt level in these lab-scale units was approximately 1.27 cm (0.5 in.) below the top of the vessel; the salt volume in a cannister was approximately  $426 \text{ cm}^3$  ( $26 \text{ in.}^3$ ).

As for the ternary, and for all salts studied in this subtask, characteristic discharge curves were initially obtained as a function of discharge air flow rate over the range 1.42 to  $11.32 \text{ m}^3/\text{hr}$  (50 to  $400 \text{ ft}^3/\text{hr}$ ) to determine the optimum flow condition for that unit, so that the rate of discharge (salt solidification) is controlled mainly by the heat flux through the solidifying salt. The plot of salt solidification time versus air flow rate appears in Figure 26, from which  $180 \text{ ft}^3/\text{hr}$  was chosen as the standard flow rate for this system.

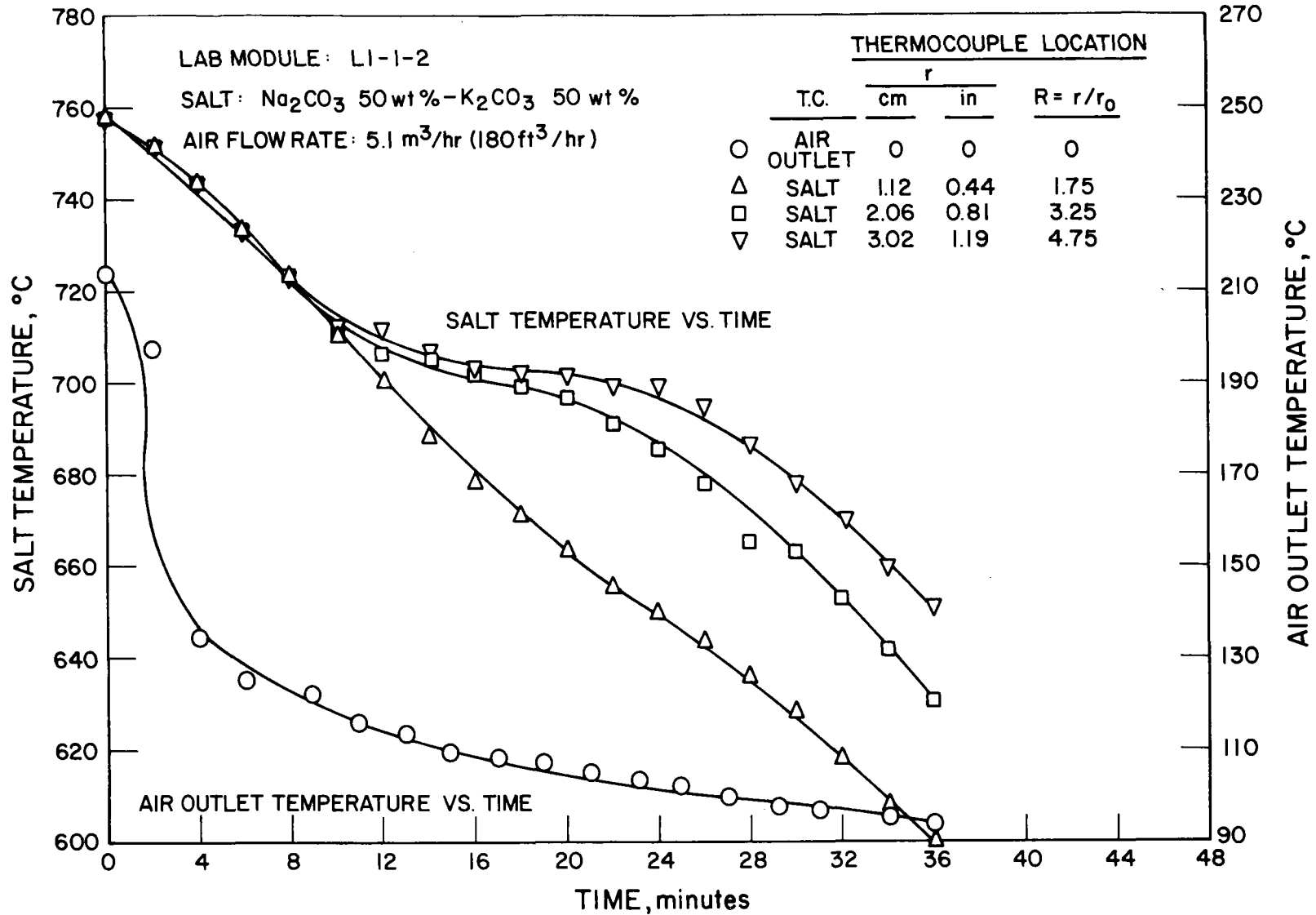
Discharge results obtained during a typical run (No. L1-1-2) for an air flow rate of  $5.1 \text{ m}^3/\text{hr}$  ( $180 \text{ ft}^3/\text{hr}$ ) are plotted in Figure 27. This time-temperature response of salt T/C's confirmed that the salt was indeed solidifying congruently over the temperature range  $708^\circ$  to  $701^\circ\text{C}$  ( $1306^\circ$  to  $1294^\circ\text{F}$ ). No significant thermal gradients were observed through the still molten salt regions during solidification, indicating strong convective mixing effects consistent with previous TES results. Figure 28 shows the instantaneous heat flux curve calculated for this salt as a function of discharge time for an air flow rate of  $5.1 \text{ m}^3/\text{hr}$  ( $180 \text{ ft}^3/\text{hr}$ ).

After 13 charge/discharge cycles and 336 hours of operation of Module L1-1 with the  $\text{Na}_2\text{CO}_3$ - $\text{K}_2\text{CO}_3$  salt, the heaters became nonfunctional. Upon disassembly of the unit, it was discovered that a significant amount of salt had crept up the inner container wall and outer HX tube surfaces, reacting with the insulation and corroding the metal furnace leads. The transite cover initially used over the container had also deteriorated as a result of the severe temperatures and chemical environment. The color of the solidified salt had changed from white to blue, possibly from corrosion of the stainless-steel container. Because of these experimental difficulties, the following cannister design modifications were made:



A79122781

Figure 26. TYPICAL DISCHARGE PERFORMANCE OF MODULE L1-1, 49.4 wt % Na<sub>2</sub>CO<sub>3</sub> - 50.6 wt % K<sub>2</sub>CO<sub>3</sub>



B79122729

Figure 27. TYPICAL DISCHARGE PERFORMANCE OF MODULE L1-1, 49.4 wt % Na<sub>2</sub>CO<sub>3</sub> - 50.6 wt % K<sub>2</sub>CO<sub>3</sub> AT 5.1 m<sup>3</sup>/hr (180 ft<sup>3</sup>/hr) AIR FLOW RATE

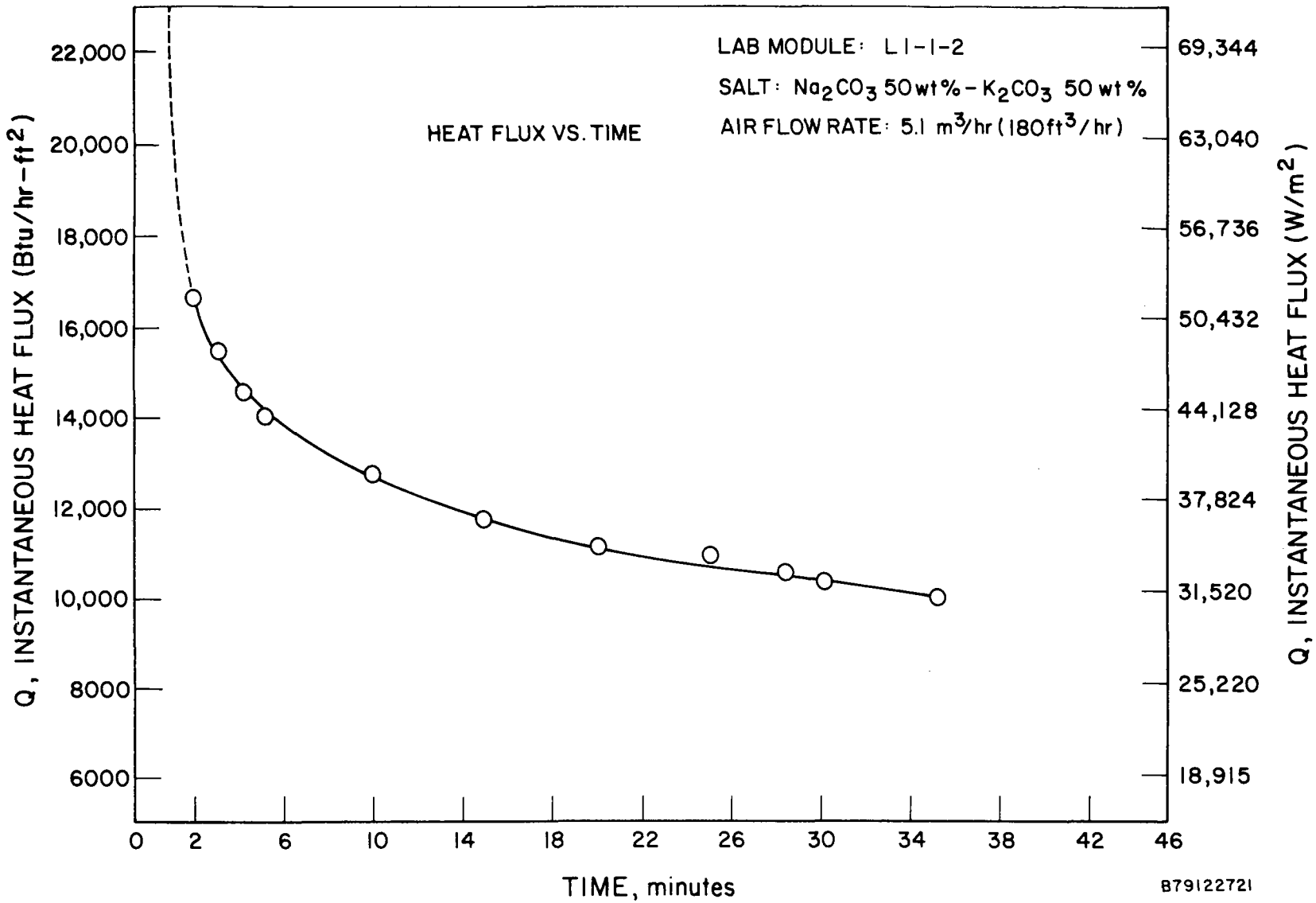


Figure 28. EXPERIMENTAL HEAT FLUX CURVE FOR MODULE L1-1, 49.4 wt % Na<sub>2</sub>CO<sub>3</sub> - 50.6 wt % K<sub>2</sub>CO<sub>3</sub> AT 5.1 m<sup>3</sup>/hr (180 ft<sup>3</sup>/hr) AIR FLOW RATE

1. The transite cover was replaced with a machined stainless-steel cover, containing three holes for T/C sheaths and one vent hole. This cover was welded onto the container wall and HX tube, greatly reducing the area that allowed salt to creep out the container, yet still utilizing the alumina T/C sheaths.
2. Lost  $\text{Na}_2\text{CO}_3\text{-K}_2\text{CO}_3$  salt was replenished, and 1 mol %  $\text{Li}_2\text{CO}_3$  was added to this same cannister to reduce corrosion of stainless steel by possibly forming a  $\text{LiCrO}_2$  protective layer on container and HX walls. This unit was then run as L1-2.

1.21 wt %  $\text{Li}_2\text{CO}_3$  - 49.95 wt %  $\text{Na}_2\text{CO}_3$  - 48.84 wt %  $\text{K}_2\text{CO}_3$  (Module L1-2. After the above modifications were completed, the cannister contained 888 grams (1.96 lb) of the salt mixture and was operated as Module L1-2. The discharge and heat flux curves obtained at a flow rate of  $5.1 \text{ m}^3/\text{hr}$  ( $180 \text{ ft}^3/\text{hr}$ ) are shown in Figures 29 and 30 respectively. From the time-temperature response of the salt T/C's, it appeared that the doping of the Na-K system with  $\text{Li}_2\text{CO}_3$  slightly altered the melting behavior of the system by causing it to solidify incongruently over the temperature range  $710^\circ$  to  $695^\circ\text{C}$  ( $1310^\circ$  to  $1283^\circ\text{F}$ ). Figure 31 shows the variation of heat flux with discharge time for four cycles at different points during the lifetime of this unit. The general shape of the curves remained unchanged while defining a narrow lifetime discharge performance band, indicating no significant loss of thermal storage capacity or heat transfer capability during more than 500 hours of operation.

Problems were encountered with thermal cracking of the recrystallized alumina T/C protection sheaths after 140 hours of operation. Failure of the alumina sheaths allowed salt contact with the 0.51 mm (0.02 in.) thick-walled Type 304 SS clad T/C's and led to eventual T/C failure. Because ceramic sheath failure was a recurring problem, the T/C design was modified to incorporate three 0.76 mm (0.03 in.) thick-walled Type 316 SS sheaths that were directly welded to the stainless-steel cover.

This unit was restarted and finally terminated after 23 cycles and 528 hours in operation, with no loss of salt or change in chemical composition of the mixture.

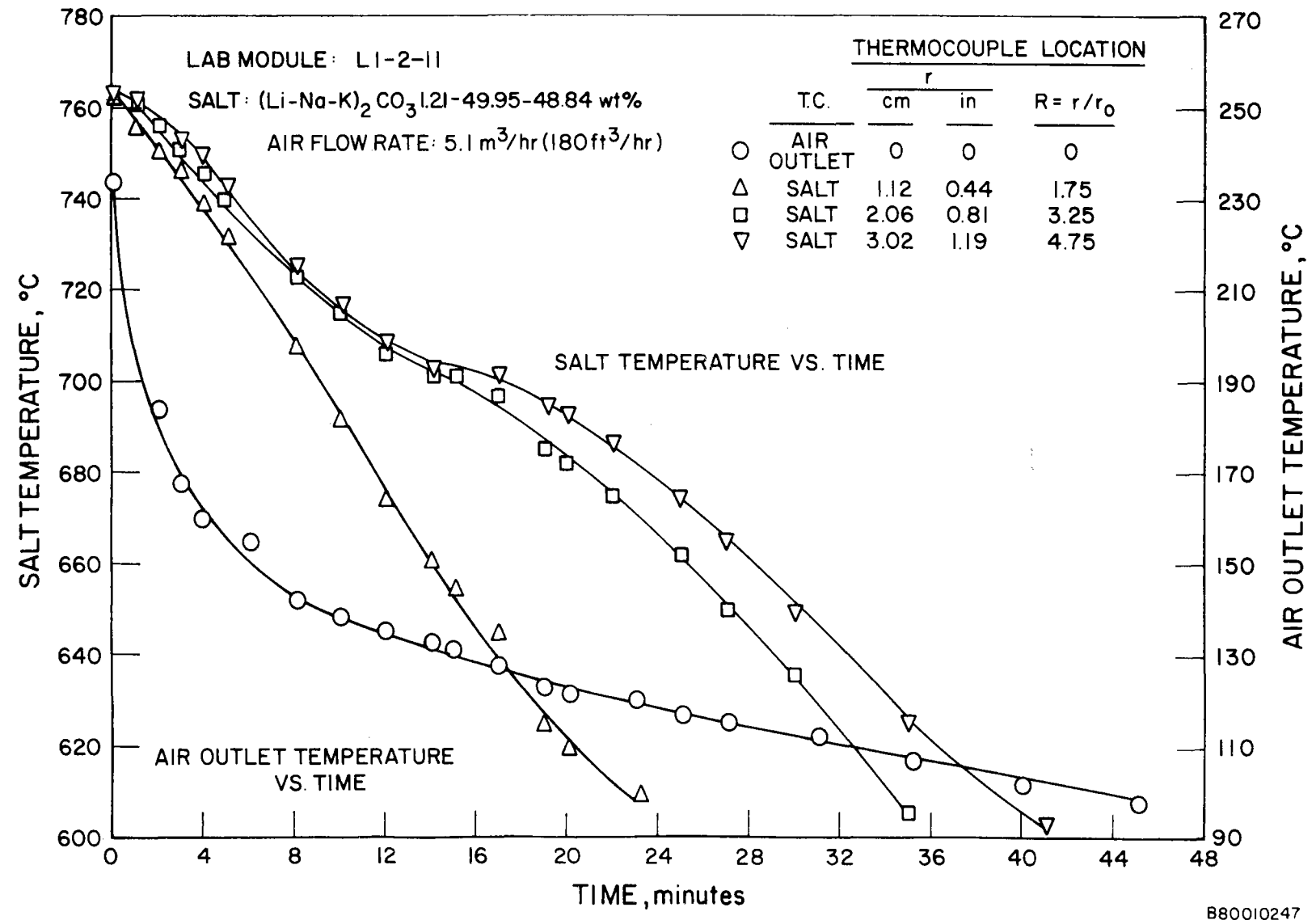
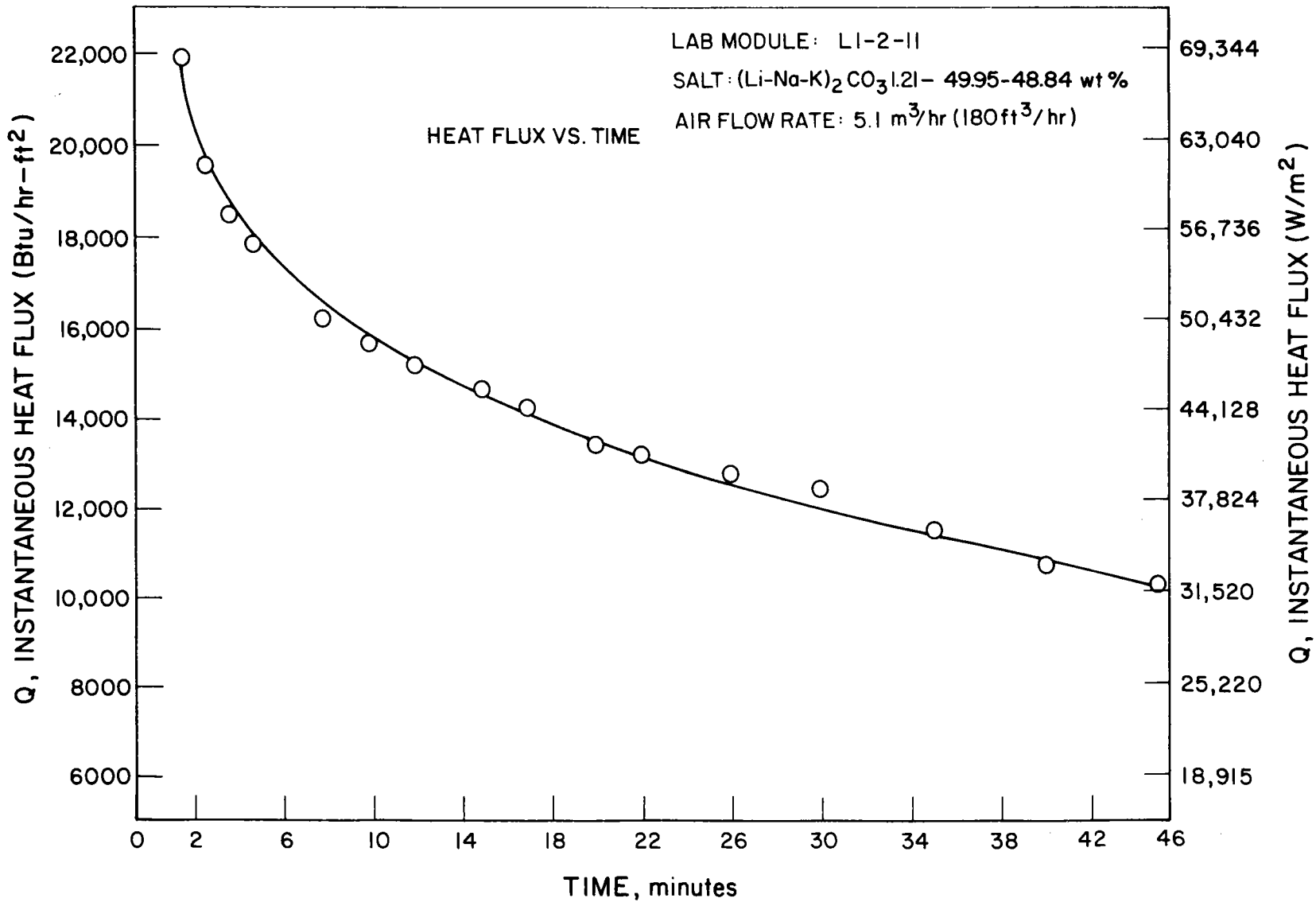
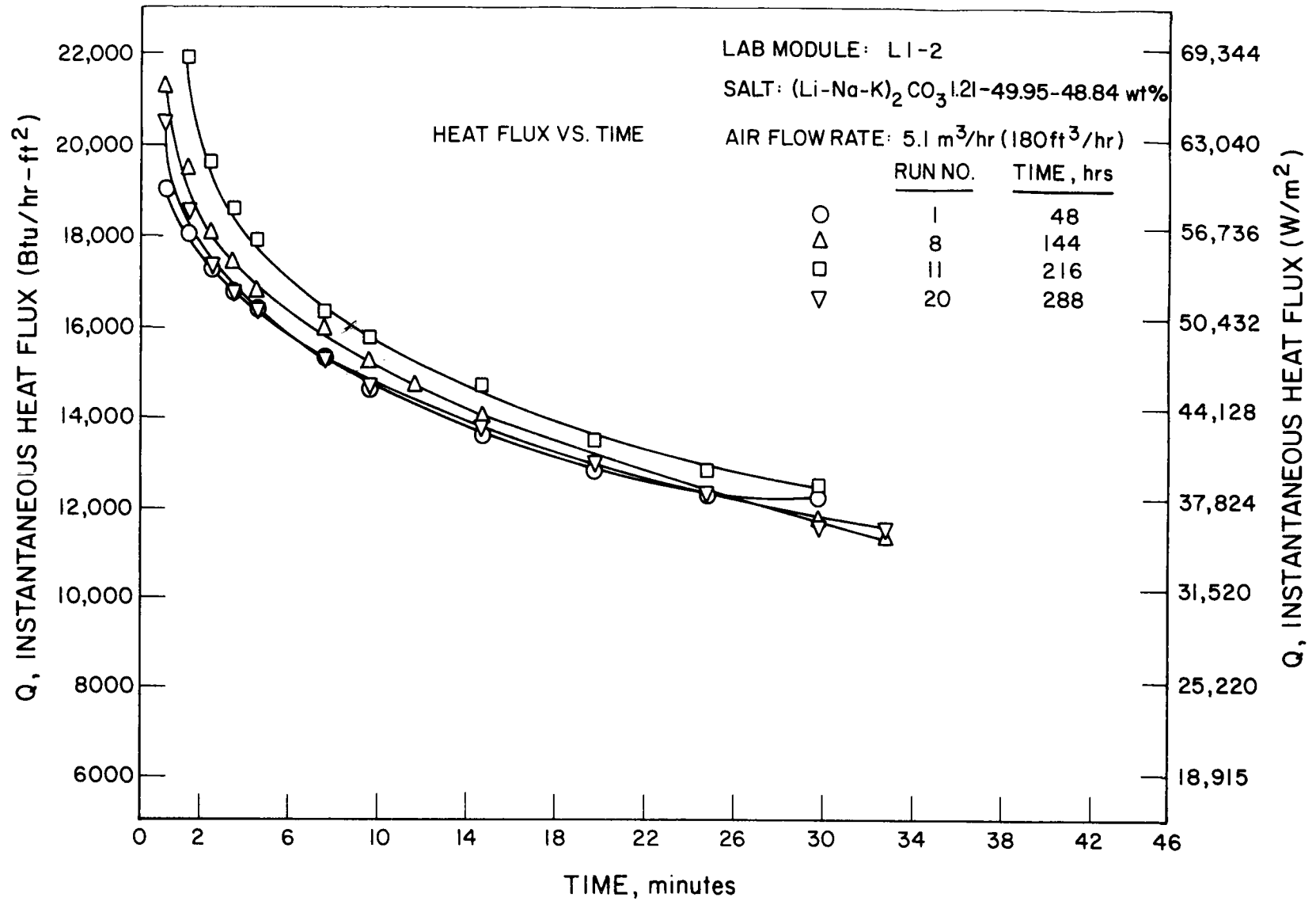


Figure 29. TYPICAL DISCHARGE PERFORMANCE OF (Na-K)<sub>2</sub>CO<sub>3</sub> SYSTEM WITH Li<sub>2</sub>CO<sub>3</sub> ADDED



B80010249

Figure 30. EXPERIMENTAL HEAT FLUX CURVE FOR (Na-K)<sub>2</sub>CO<sub>3</sub> SYSTEM WITH Li<sub>2</sub>CO<sub>3</sub> ADDED



B80010248

Figure 31. LIFETIME DISCHARGE PERFORMANCE OF (Na-K)<sub>2</sub>CO<sub>3</sub> SYSTEM WITH Li<sub>2</sub>CO<sub>3</sub> ADDED

Li<sub>2</sub>CO<sub>3</sub> (Modules L2-1 and L4-2). Originally Module L2-1 contained 720 grams (1.6 lb) of Li<sub>2</sub>CO<sub>3</sub> and operated with the transite top design during the same period as the Li-doped (Na-K)<sub>2</sub>CO<sub>3</sub> system.

Typical discharge and heat flux curves are shown in Figures 32 and 33, respectively. Solidification of the Li<sub>2</sub>CO<sub>3</sub> was observed to occur within  $\pm 3^{\circ}\text{C}$  (5.4°F) of its quoted mp of 723°C (1333°F). The salt at the outer T/C location solidified before that at the middle T/C because of heat loss through the outer container wall.

This system encountered difficulties with alumina T/C sheath failures simultaneously with the Li-doped (Na-K)<sub>2</sub>CO<sub>3</sub> system. After 13 cycles and 408 hours the unit was shut down for post-test examination. Visual examination revealed salt leakage through a small pinhole in the bottom weld and a similar defect in the container wall at about mid-salt level. Post-test analysis of the salt revealed an increase in iron content from 0.03 to 0.36 wt % and an increase in nickel from >0.01 to 0.03 wt %.

Based on the successful results obtained when the design of the Li-doped (Na-K)<sub>2</sub>CO<sub>3</sub> system was modified, a new final can design was established. This final design incorporated two 10.22 mm (0.4 in.) thick-walled open-one-end Type 316 SS sheaths and 3.18 mm (0.125 in.) OD T/C's with 1.02 mm (0.04 in.) thick Type 304 SS cladding. It avoided direct welding of the T/C sheaths by using butt-weld tube fittings (Swagelok), with a welded vent tube that could also serve to provide an environment of CO<sub>2</sub> above the salt (as in Figure 20). This design proved generally satisfactory for subsequent laboratory-scale testing.

In Module L4-2, 754 grams (1.7 lb) of Li<sub>2</sub>CO<sub>3</sub> was retested in the modified cannister described above with a cover-gas environment of CO<sub>2</sub> over the melt.

From the salt discharge plot of Figure 34 one can see that this system solidified between 734° and 730°C (1353° to 1346°F). Also, from the instantaneous heat flux profile of Figure 35, the average heat flux to the air was calculated to be 76,574 W/m<sup>2</sup> (24,290 Btu/hr-ft<sup>2</sup>). This was the largest heat transfer exhibited by any salt, regardless of temperature regime. The consistency of this unit's performance becomes evident on inspection of Figure 36, which plots the discharge heat flux from four different cycles in the unit's lifetime.

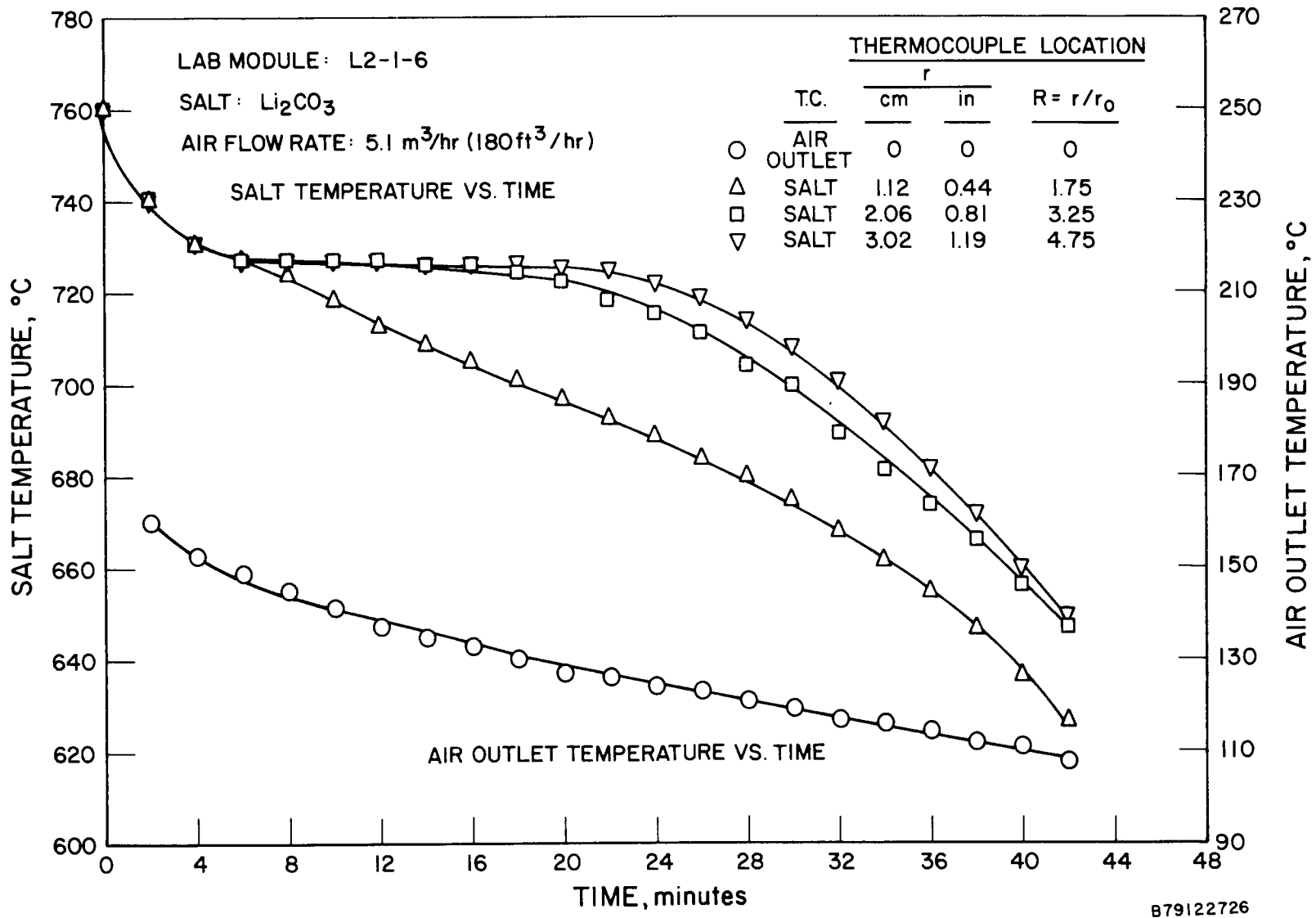


Figure 32. TYPICAL DISCHARGE PERFORMANCE OF  $\text{Li}_2\text{CO}_3$  SYSTEM (MODULE L2-1: AIR COVER GAS) AT  $5.1 \text{ m}^3/\text{hr}$  ( $180 \text{ ft}^3/\text{hr}$ ) AIR FLOW RATE

B79122726

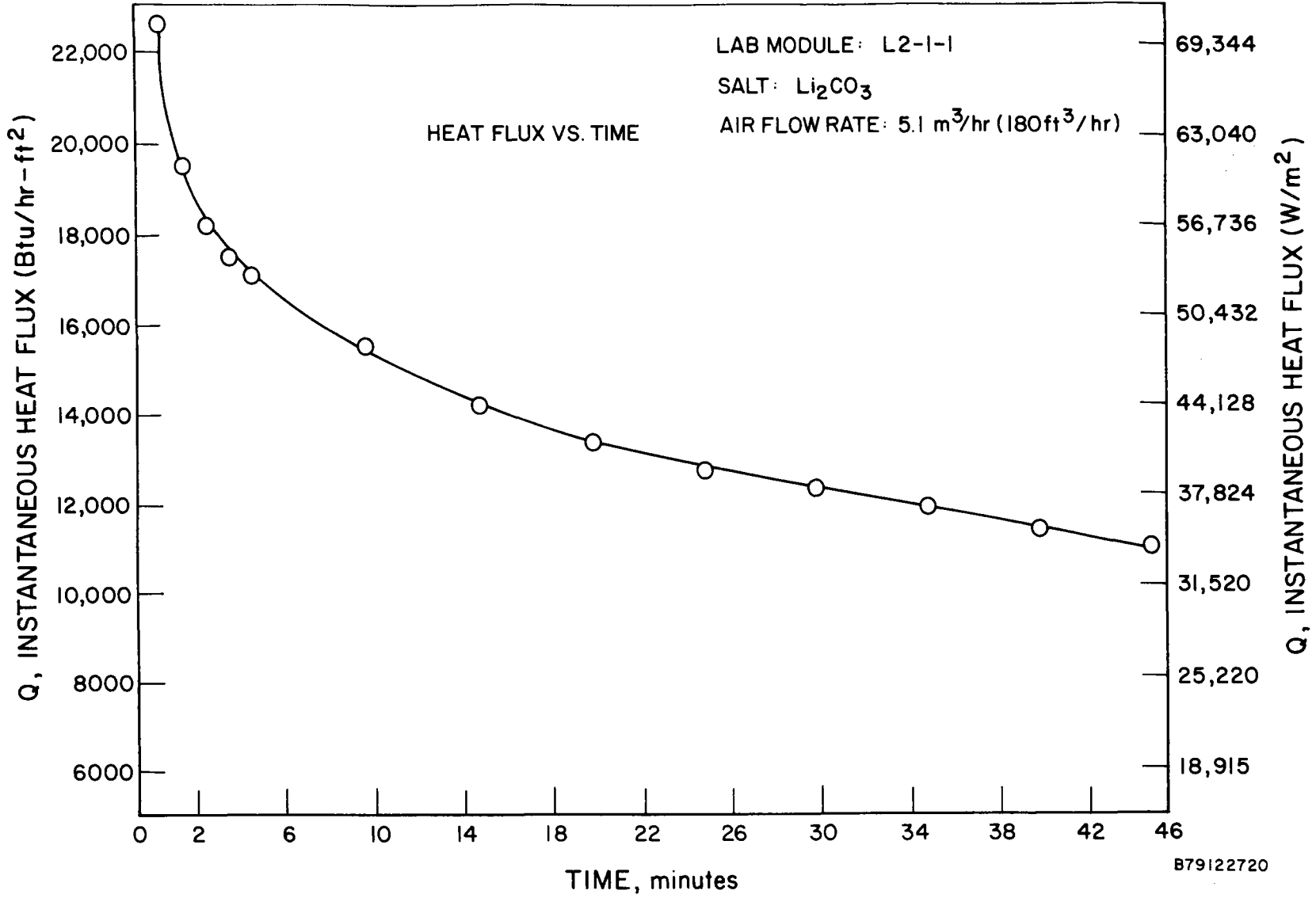
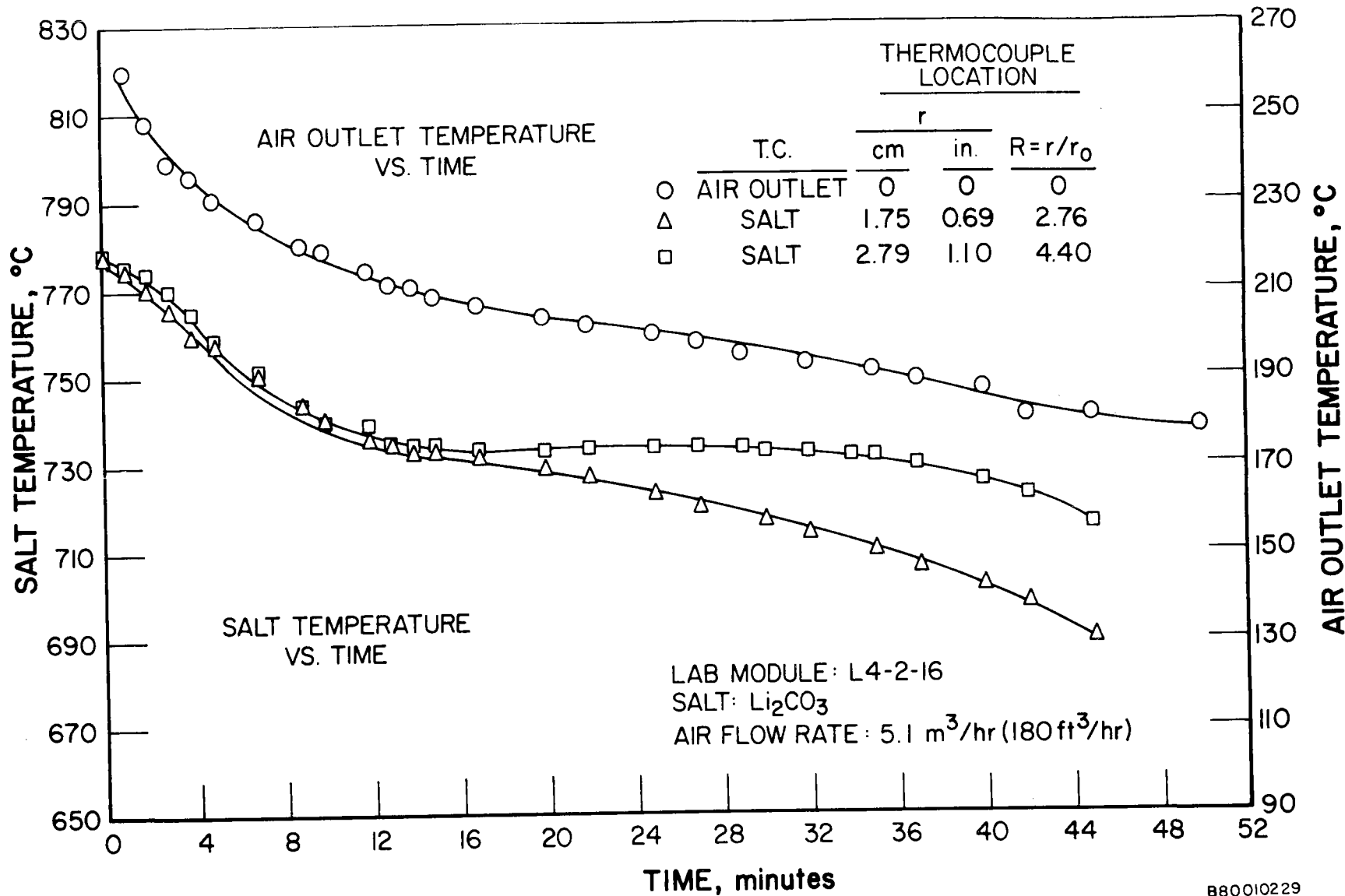


Figure 33. EXPERIMENTAL HEAT FLUX CURVE FOR  $\text{Li}_2\text{CO}_3$  SYSTEM (MODULE L2-1: AIR COVER GAS) AT  $5.1 \text{ m}^3/\text{hr}$  ( $180 \text{ ft}^3/\text{hr}$ ) AIR FLOW RATE



B80010229

Figure 34. TYPICAL DISCHARGE PERFORMANCE OF  $\text{Li}_2\text{CO}_3$  SYSTEM WITH  $\text{CO}_2$  COVER GAS AT  $5.1 \text{ m}^3/\text{hr}$  ( $180 \text{ ft}^3/\text{hr}$ ) AIR FLOW RATE

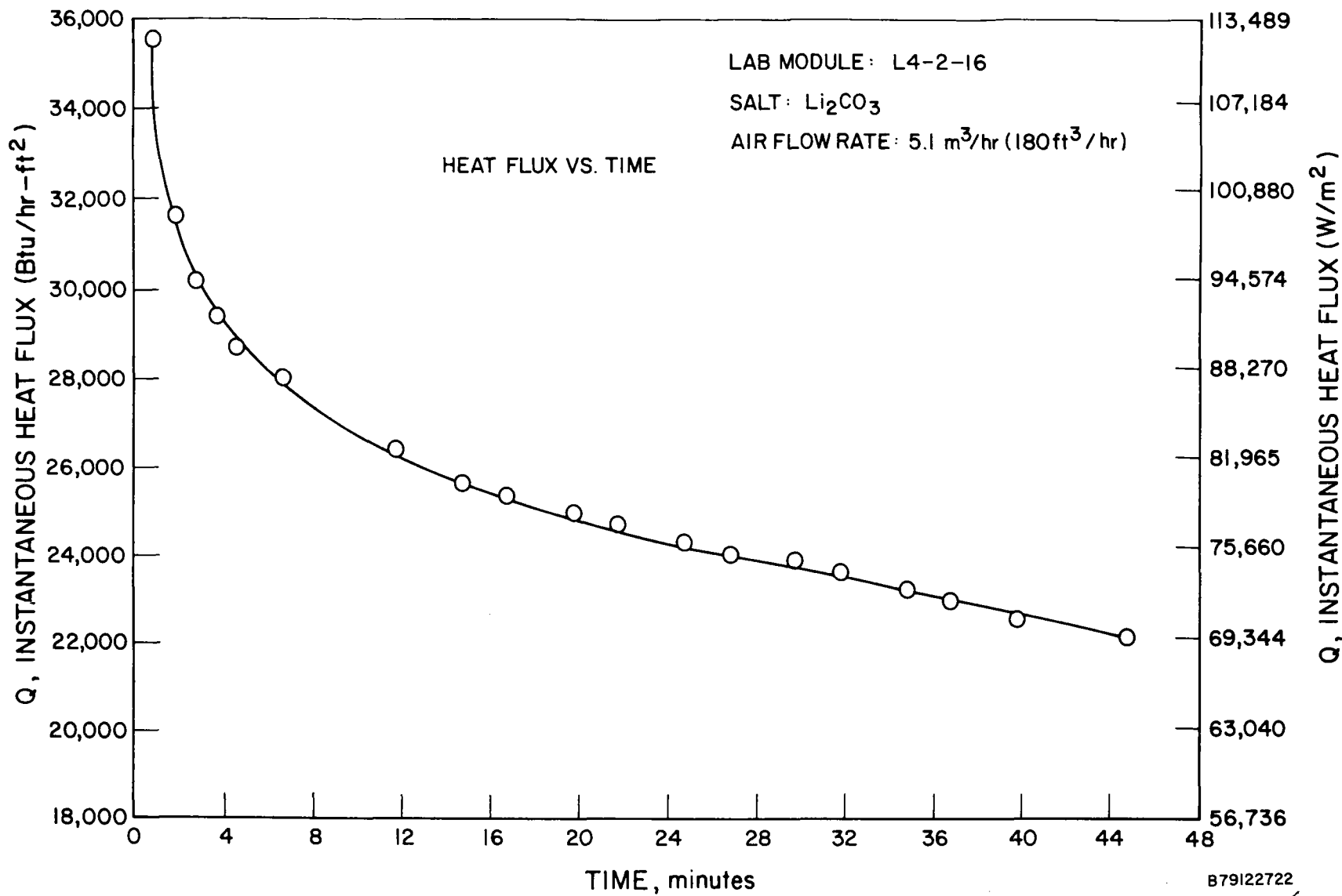


Figure 35. EXPERIMENTAL HEAT FLUX CURVE FOR  $\text{Li}_2\text{CO}_3$  SYSTEM WITH  $\text{CO}_2$  COVER GAS AT  $5.1 \text{ m}^3/\text{hr}$  ( $180 \text{ ft}^3/\text{hr}$ ) AIR FLOW RATE

B79I22722

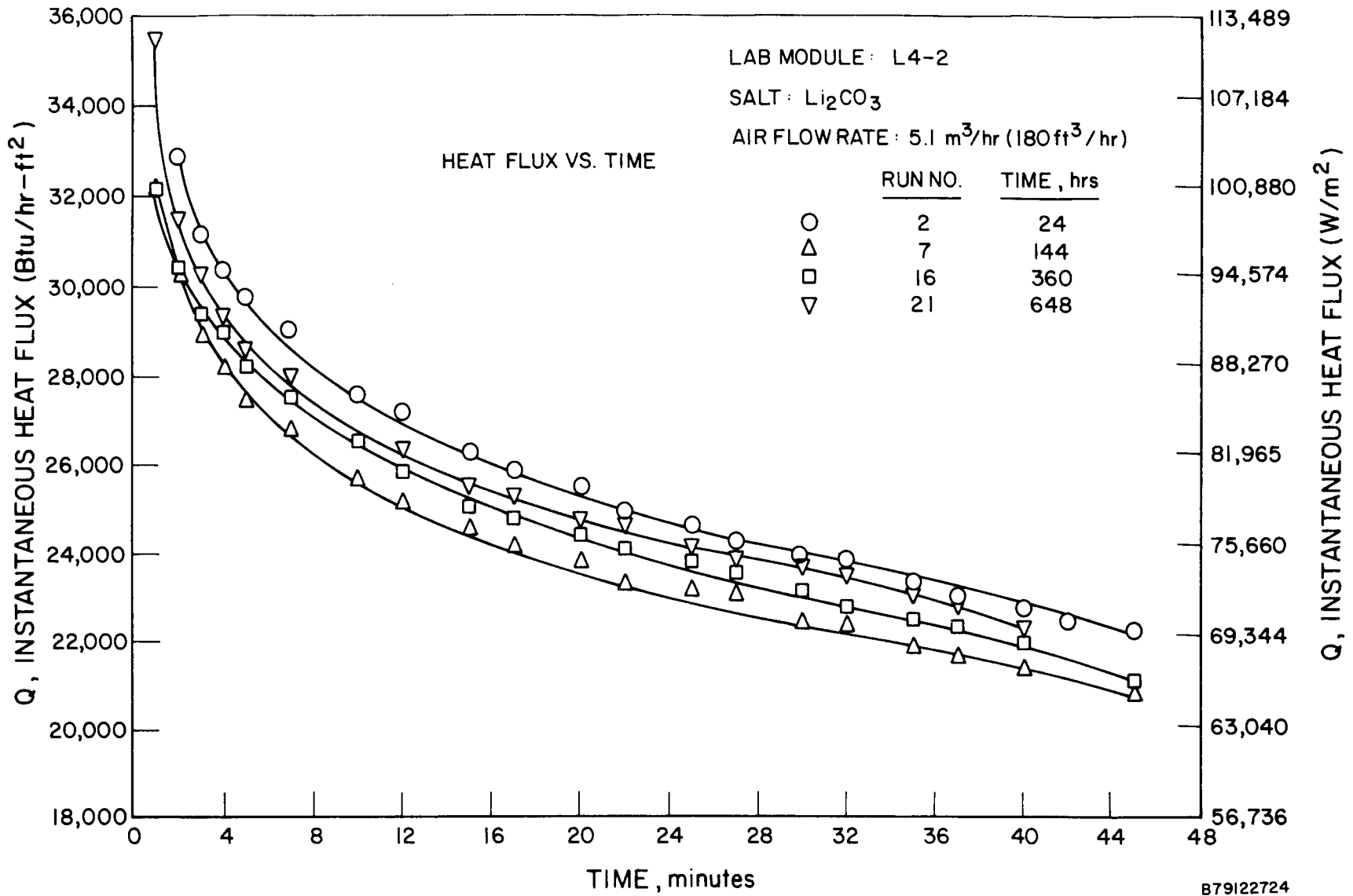


Figure 36. LIFETIME DISCHARGE PERFORMANCE OF  $\text{Li}_2\text{CO}_3$  SYSTEM WITH  $\text{CO}_2$  COVER GAS

These profiles not only define a narrow discharge performance band but also seem to exhibit a performance stabilization period during the first seven cycles.

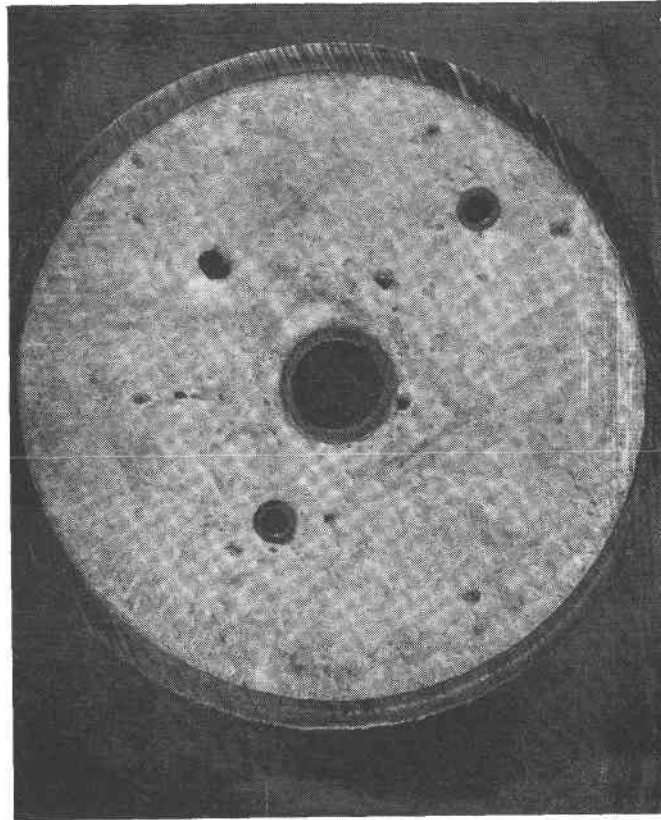
This unit was maintained at operating temperatures for 672 hours and 22 charge/discharge cycles, at which time it was shut down and sectioned for post-test evaluations. The solidified mid-salt cross section is shown in Figure 37. The size and morphology of solid salt crystals in this and other sectioned modules could be correlated with the manner in which the final cooldown was performed. In this particular instance, the salt's last discharge run was a free-cool run, in which the salt was allowed to cool from 50°C (90°F) above its mp to ambient with no air-cooling discharge. From this photograph, one may observe the somewhat fine radially-oriented columnar crystals that formed near the outer edge. This growth pattern is the result of fairly rapid outward cooling through radiant heat loss to the ambient. From this outer edge inward, the crystals become larger and randomly oriented, a result of slower cooling.

The new cannister design was successful in that no salt creepage was observed throughout the cannister's operational life. From Table 16 one can see that this unit's post-test analysis revealed no increase in iron or nickel. Also, the CO<sub>2</sub> cover gas aided in reducing the corrosion rate compared with an air cover gas, most likely by minimizing Li<sub>2</sub>CO<sub>3</sub> decomposition to Li<sub>2</sub>O and CO<sub>2</sub>.

Table 16. PRE- AND POST-TEST CHEMICAL ANALYSIS OF Li<sub>2</sub>CO<sub>3</sub> SYSTEM

Chemical Analysis, Wt %	<u>Li</u>	<u>CO<sub>3</sub></u>	<u>Fe</u>	<u>Ni</u>	<u>Cr</u>
Pre-Test	19.08	79.26	0.03	<0.01	<0.01
Post-Test (Air)	18.89	80.23	0.36	0.03	0.01
Post-Test (CO <sub>2</sub> )	19.39	80.53	0.02	<0.01	<0.01

The following synopses highlight the most important experimental results of the remaining six salts selected for possible solar-thermal applications. All utilized the final welded containment design.



P80010066

Figure 37. TRANSVERSE CROSS SECTION THROUGH  
MODULE L4-2  $\text{Li}_2\text{CO}_3$  SYSTEM AFTER 672 HOURS AND  
22 CYCLES

Na<sub>2</sub>CO<sub>3</sub> (L2-2). Although Na<sub>2</sub>CO<sub>3</sub> possesses a lower heat of fusion ( $2.6 \times 10^5$  J/kg, 113 Btu/lb) than Li<sub>2</sub>CO<sub>3</sub> ( $6.1 \times 10^5$  J/kg, 261 Btu/lb), this salt is attractive because its mp of 858°C (1576°F) approaches the upper end of the solar temperature range being studied, and it may become cost effective (\$0.07/kg, \$0.03/lb) in a large-scale solar-power system for which the mass of TES medium is not restricted.

With this in mind, a lab-scale unit containing 827 grams (1.82 lb) of Na<sub>2</sub>CO<sub>3</sub> was tested in a welded container. This discharge profile of Figure 38 shows that the salt nominally solidified at 865°C (1589°F), while maintaining an average discharge heat flux of 45,648 W/m<sup>2</sup> (14,480 Btu/hr-ft<sup>2</sup>), as calculated from the heat flux graph of Figure 39. This curve shows the instantaneous heat flux for Na<sub>2</sub>CO<sub>3</sub> to be decreasing at a rate of 788 W/m<sup>2</sup> (250 Btu/hr-ft<sup>2</sup>) per minute, as compared to Li<sub>2</sub>CO<sub>3</sub>'s decrease of 451 W/m<sup>2</sup> (143 Btu/hr-ft<sup>2</sup>) per minute. The lifetime performance of the unit exhibited relative stability throughout Run 17, with a decrease by Run 22. Post-test examination revealed slight leaks around the T/C fittings, which resulted in a loss of approximately 15 grams (0.03 lb) of salt.

The free-cool shut down occurred after 21 cycles and 288 hours of operation. Chemical analysis of the terminated salt indicated no change in nominal composition and a slight increase in iron (from 0.03 to 0.06 wt %), a result of hot corrosion, as summarized in Table 17. When the cannister was sectioned and photographed (Figure 40), micro-cracks and voids ranging from 0.025 to 6.35 mm (0.001 to 0.25 in.) were found in the salts along very evident radially-oriented salt solidification patterns. These patterns are very different from the typical free-cool crystallization patterns found in the Li<sub>2</sub>CO<sub>3</sub> unit. If these voids and cracks were also formed in the solid phase under the "forced-cooling" of the standard operating procedures, they would act as thermal resistances and reduce the effective heat flux. If such defects were filled with air or CO<sub>2</sub> during discharge, they would have a thermal conductivity of 0.07 W/m-K ( $\sim 0.04$  Btu/hr-ft<sup>2</sup>-°F), compared to 1.73 W/m-K ( $\sim 1$  Btu/hr-ft<sup>2</sup>-°F) for solid Na<sub>2</sub>CO<sub>3</sub>. These apparent factors could ultimately lower Na<sub>2</sub>CO<sub>3</sub>'s effective thermal conductivity through the solid salt and partially explain the much lower heat fluxes observed for Na<sub>2</sub>CO<sub>3</sub>, compared to Li<sub>2</sub>CO<sub>3</sub>.

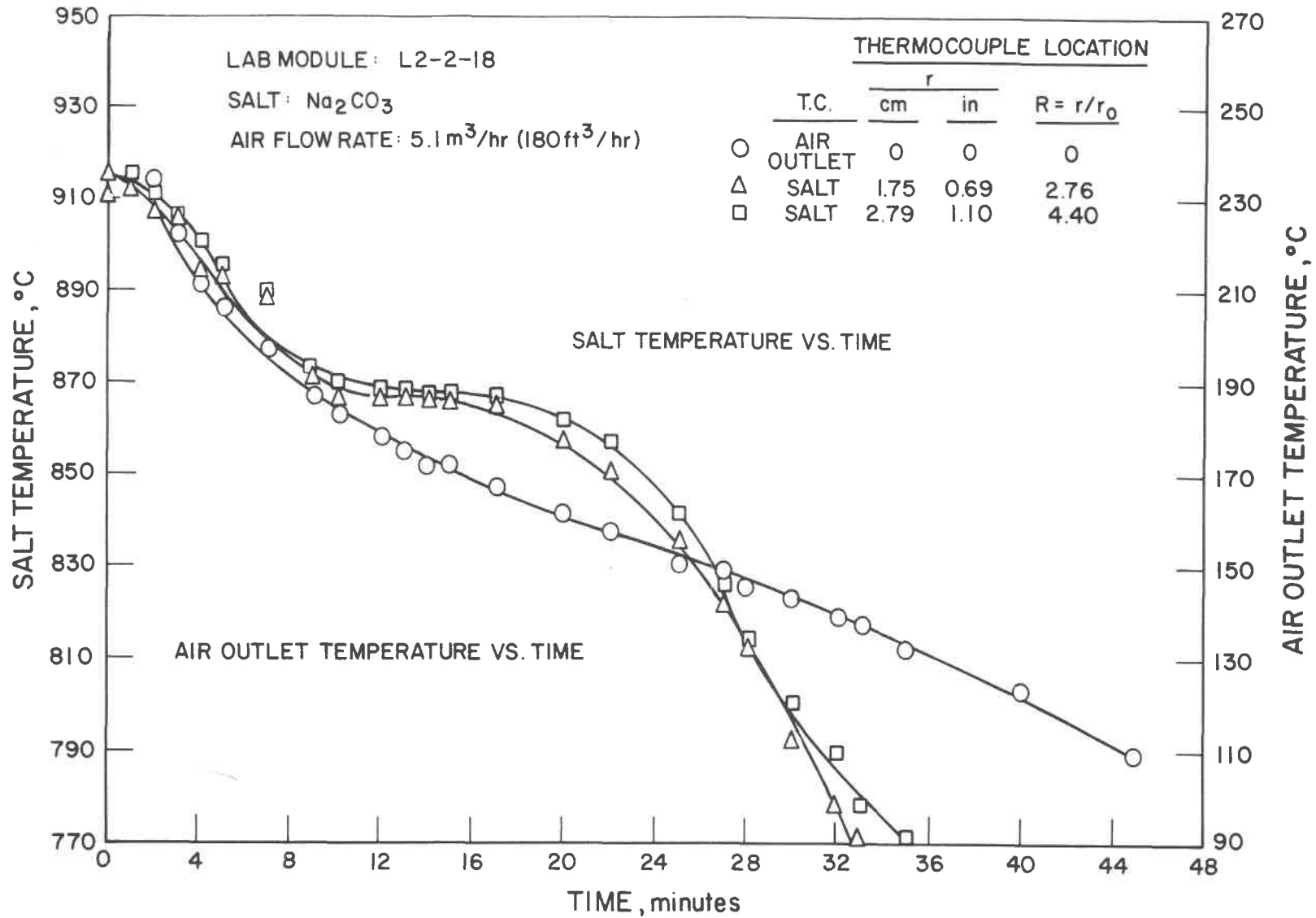
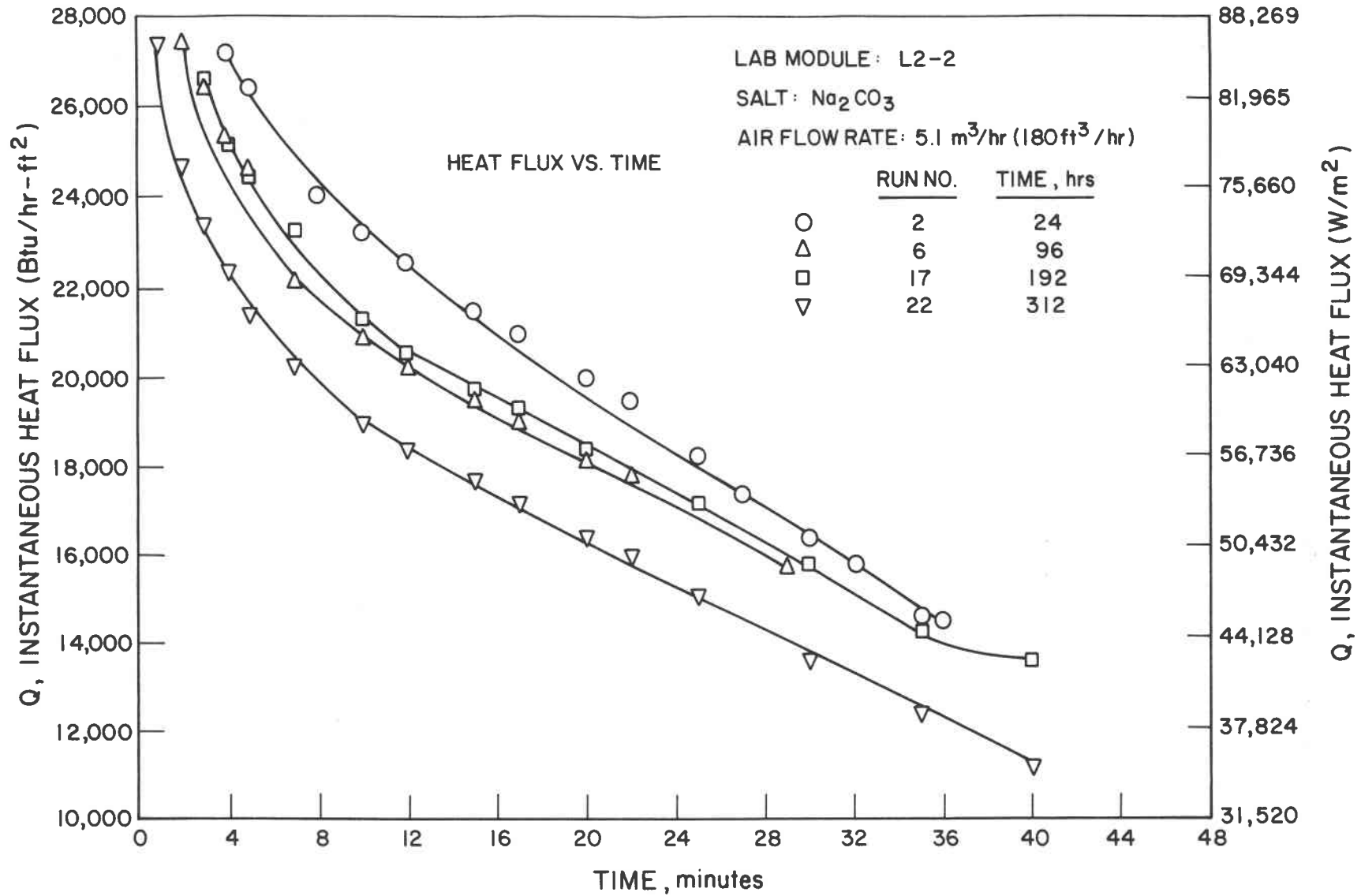


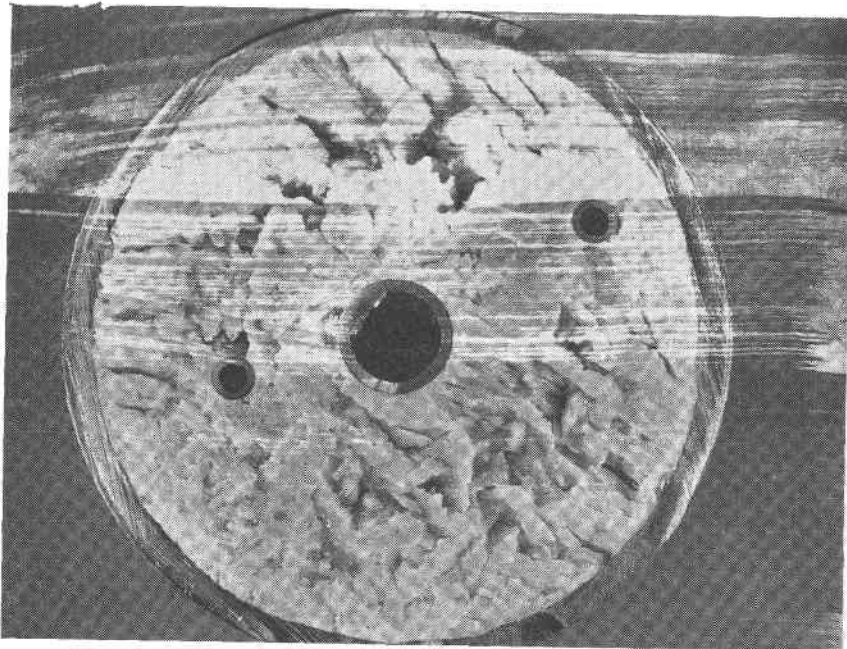
Figure 38. TYPICAL DISCHARGE PERFORMANCE OF Na<sub>2</sub>CO<sub>3</sub> SYSTEM AT 5.1 m<sup>3</sup>/hr (180 ft<sup>3</sup>/hr) AIR FLOW RATE

B80010254



879122725

Figure 39. LIFETIME DISCHARGE PERFORMANCE OF Na<sub>2</sub>CO<sub>3</sub> SYSTEM



P80010067

Figure 40. TRANSVERSE CROSS SECTION THROUGH MODULE L2-2  
 $\text{Na}_2\text{CO}_3$  SYSTEM AFTER 288 HOURS AND 21 CYCLES

Table 17. PRE- AND POST-TEST CHEMICAL ANALYSIS OF Na<sub>2</sub>CO<sub>3</sub> SYSTEM

Chemical Analysis, Wt %	<u>Na</u>	<u>CO<sub>3</sub></u>	<u>Fe</u>	<u>Ni</u>	<u>Cr</u>
Pre-Test	44.29	56.40	0.03	<0.01	<0.01
Post-Test	43.07	57.39	0.06	<0.01	0.01

Metallurgical analysis of the Type 316 SS HX tube at the meniscus of the salt-side surface revealed the formation of an outer, porous, hot corrosion layer and sub-scale carburization of both the bulk grains and grain boundaries as a result of salt interactions. Air-side oxidation of the HX was also observed. Additionally, precipitated particles of what appeared to be brittle inter-metallic sigma phase were observed throughout the bulk stainless-steel matrix. Sigma phase formation, a result of the prolonged high-temperature exposure and not of salt corrosion, is deleterious to the strength and related mechanical properties of stainless steel. Figure 41 shows a micrograph of this Type 316 SS which was exposed to Na<sub>2</sub>CO<sub>3</sub> for 288 hours at 807° to 907°C (1485° to 1665°F). Of particular note are the 150 to 200 μm ( 6 to 8 mil) thick porous, hot corrosion zone at the surface and the precipitated sigma phase particles within grains and grain boundaries. These clearly indicate that selection and testing of alternate containment materials are required for these high-temperature solar-thermal applications, not only on the basis of salt compatibility, but also on the basis of possible interactions with actual working fluids (air, He, molten sodium).

K<sub>2</sub>CO<sub>3</sub> (L2-3). Potassium carbonate, with a melting point of 898°C (1648°F), is the highest melting carbonate of interest in the upper temperature range for the solar-thermal applications. Therefore, to completely and thoroughly span this entire temperature range, this salt was selected for testing.

This unit also utilized a CO<sub>2</sub> cover gas environment at the salt surface. Its discharge profile and its rapidly decreasing heat flux curve (Figures 42 and 43, respectively) are highly suspect, though, because they represent only two cycle runs prior to system failure. A high discharge solidification temperature of 912°C (1674°F), and calculated average heat flux of 72,507 W/m<sup>2</sup> (23,000 Btu/hr-ft<sup>2</sup>) were observed, but additional confirmatory data would be desirable.

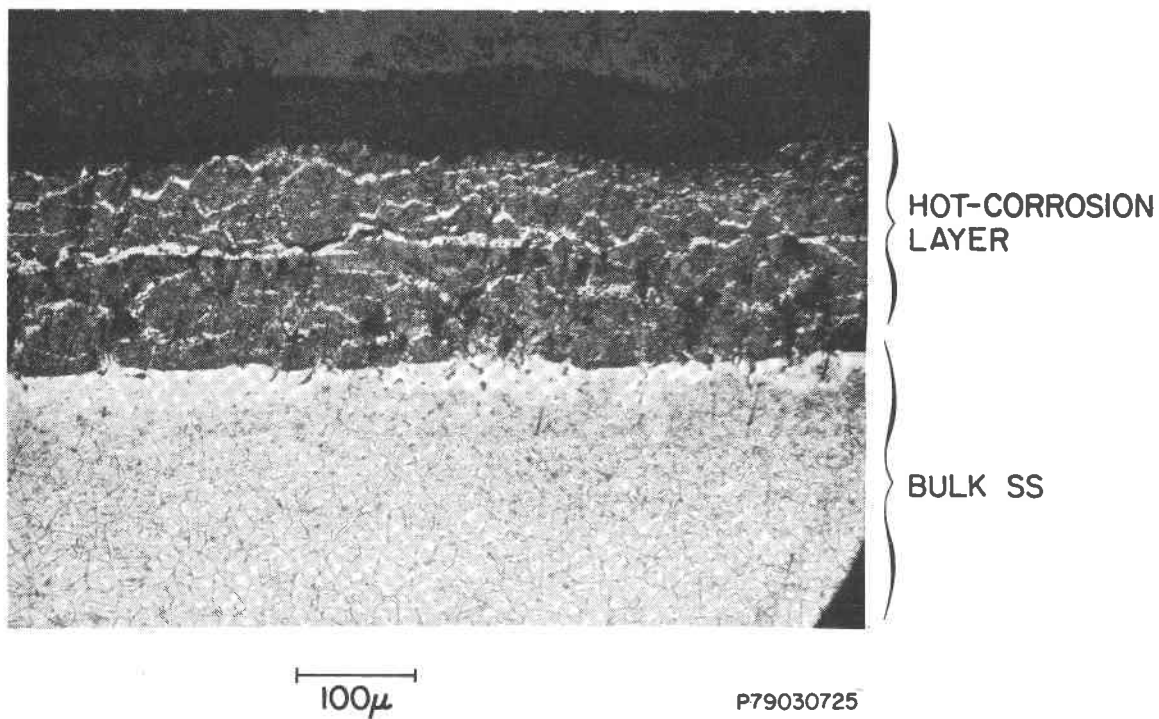


Figure 41. TYPE 316 SS CONTAINMENT AFTER 288 HOURS EXPOSURE TO  $\text{Na}_2\text{CO}_3$  AND 21 CYCLES AT  $807^\circ$  TO  $907^\circ\text{C}$  ( $1485^\circ$  to  $1665^\circ\text{F}$ ) UNDER  $\text{CO}_2$  COVER GAS ( $\text{FeCl}_3\text{-HCl-H}_2\text{O}$  Etchant)

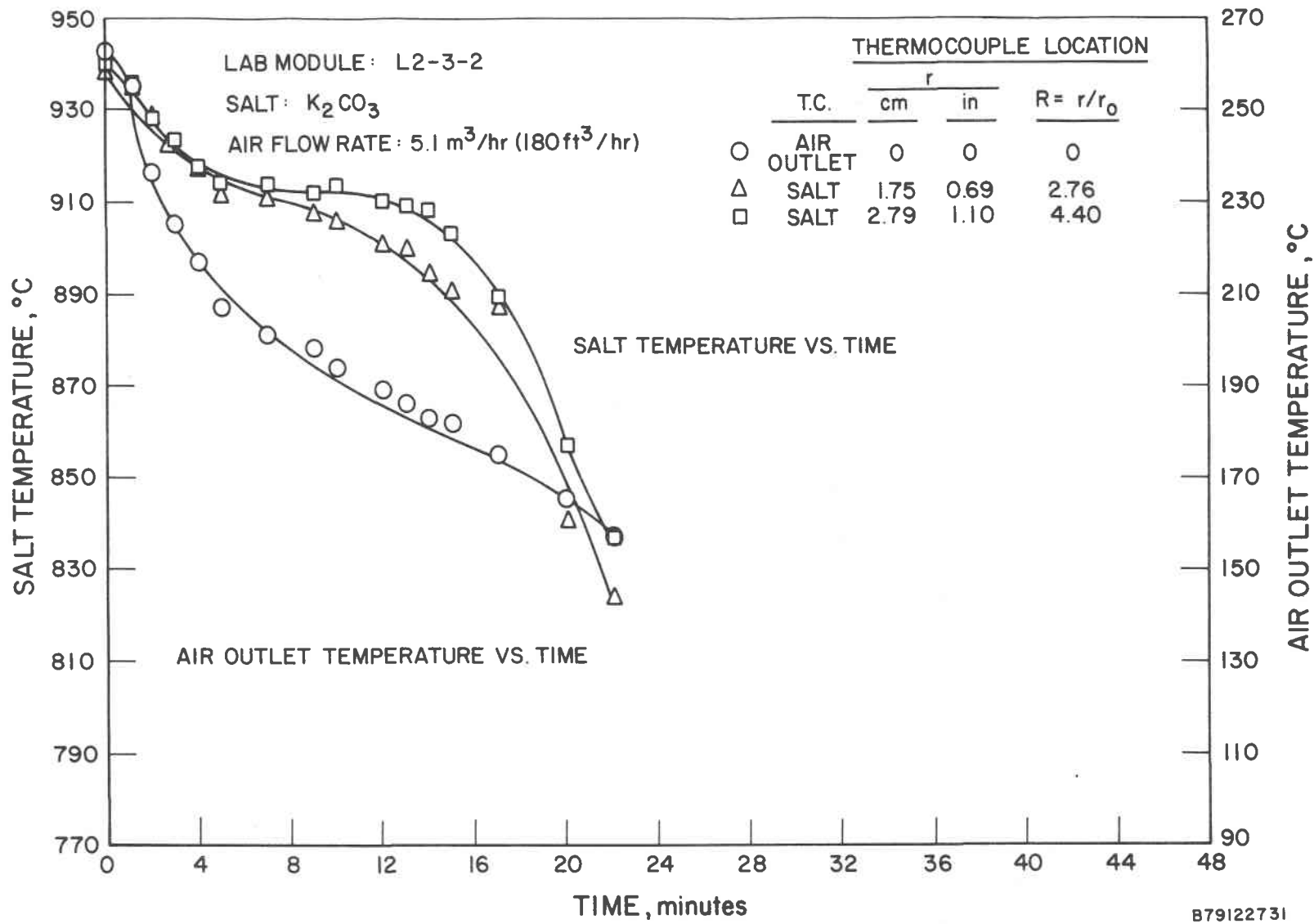
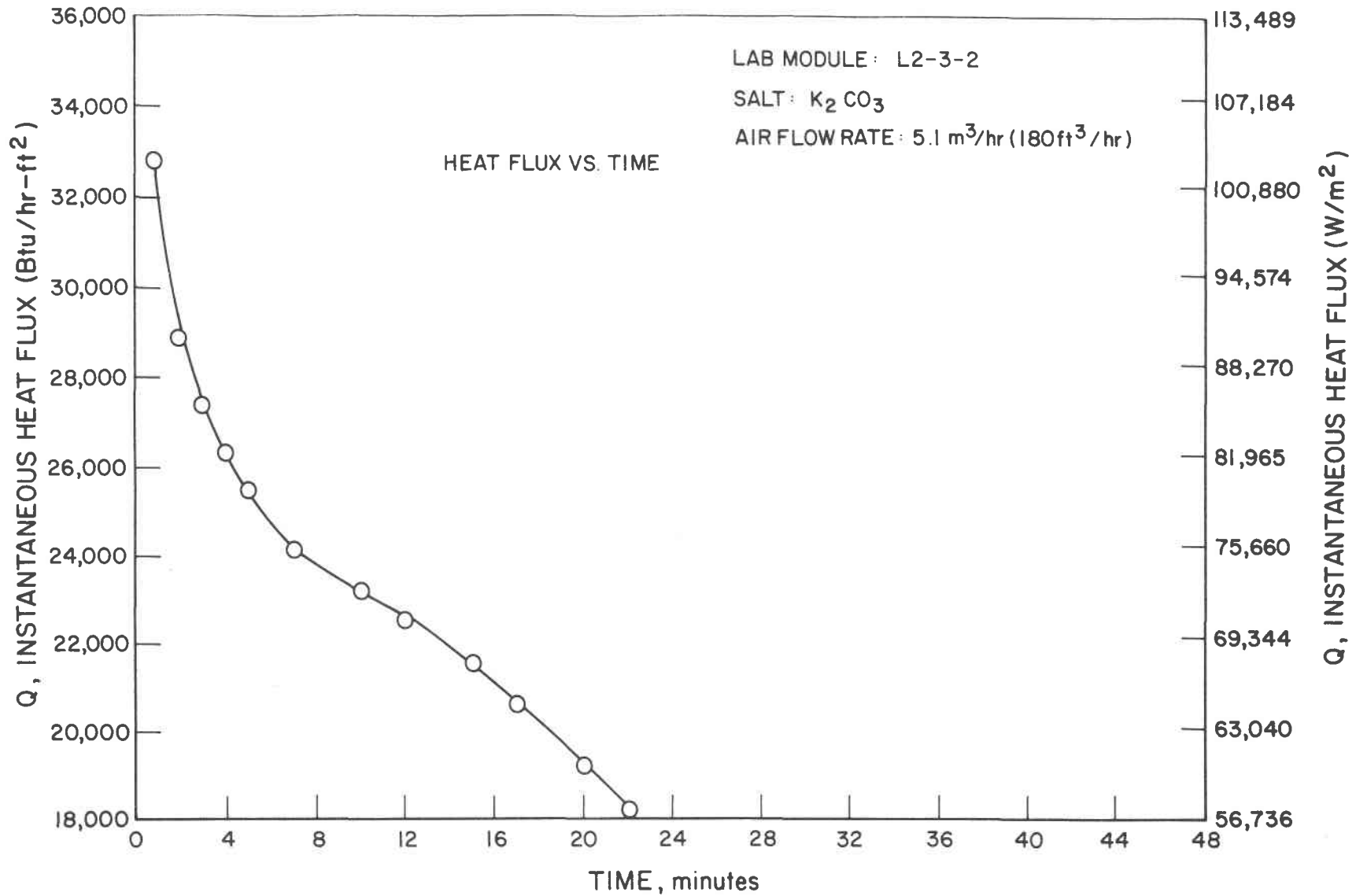


Figure 42. TYPICAL DISCHARGE PERFORMANCE OF MODULE L2-3  $K_2CO_3$  SYSTEM AT  $5.1 \text{ m}^3/\text{hr}$  ( $180 \text{ ft}^3/\text{hr}$ ) AIR FLOW RATE



B79122723

Figure 43. EXPERIMENTAL HEAT FLUX CURVE FOR MODULE L2-3  $K_2CO_3$  SYSTEM AT  $5.1 \text{ m}^3/\text{hr}$  ( $180 \text{ ft}^3/\text{hr}$ ) AIR FLOW RATE

It appears that this salt defined the maximum useful operating temperature of AISI 304 and 316 for TES applications. After two cycles and 96 hours at 948°C (1738°F), the HX tube failed, allowing no air to flow through it on discharge. As a result of this, the unit was terminated prematurely and sectioned lengthwise along the cooling tube. The salt surface and embedded fragments of HX tubing are shown in Figure 44. Examination of this section revealed that the tube had become extremely oxidized and embrittled from the continuous high-temperature exposure. This eventually led to a complete loss of structural integrity, resulting in a HX breach that allowed salt to enter and fill the HX tube.

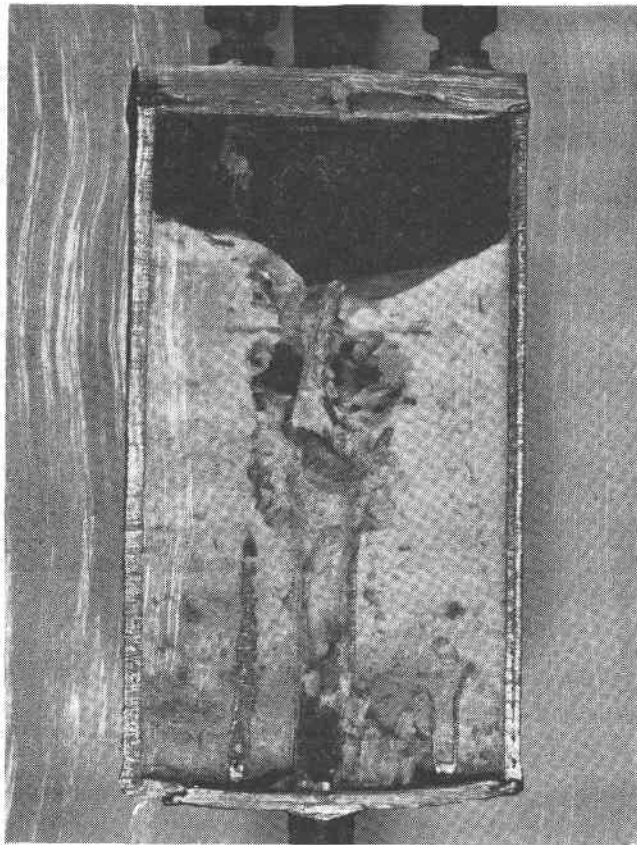
Post-test chemical analyses revealed that the detectable amount of hot corrosion products containing iron, nickel, and chromium were deposited in the bottom on the cannister. Lower concentrations of these elements were found at the top (Table 18).

Table 18. PRE- AND POST-TEST CHEMICAL ANALYSIS OF K<sub>2</sub>CO<sub>3</sub> SYSTEM

Chemical Analysis, Wt %	<u>K</u>	<u>CO<sub>3</sub><sup>-</sup></u>	<u>Fe</u>	<u>Ni</u>	<u>Cr</u>
Pre-Test	56.15	43.05	0.02	<0.01	<0.01
Post-Test (Bottom)	54.91	42.76	2.27	0.03	0.24
Post-Test (Top)	55.73	44.28	0.03	<0.01	<0.01

47.8 wt % Na<sub>2</sub>CO<sub>3</sub> - 52.2 wt % BaCO<sub>3</sub> (L3-3). Very little thermo-physical property data were available for this system, other than that showing there was a congruently melting eutectic (reportedly at 686°C, 1267°F)<sup>21</sup> at this composition. As a prospective TES medium, this, and the next Li<sub>2</sub>CO<sub>3</sub>-CaCO<sub>3</sub> system (mp ~662°C, 1224°F), represent the only carbonates with melting points in the 650°C (1202°F) region.

Since this system was attractive from an economic standpoint (\$0.18/kg, \$0.08/lb), and little past work was conducted with it, 966 grams (2.1 lb) of this Na<sub>2</sub>CO<sub>3</sub>-BaCO<sub>3</sub> mixture was cycle-tested for extended operations. It is important to note from Figure 45 that the thermal arrest in the salt's temperature versus time curve occurred at 717° to 712°C (1323° to 1314°F) instead of the published value of 686°C. The consistency with which this solidification occurred



P80010071

Figure 44. LONGITUDINAL CROSS SECTION THROUGH  
MODULE L2-3  $K_2CO_3$  SYSTEM THAT FAILED AFTER 96  
HOURS AT  $841^\circ$  TO  $941^\circ C$  ( $1546^\circ$  to  $1726^\circ F$ ) AND 2 CYCLES

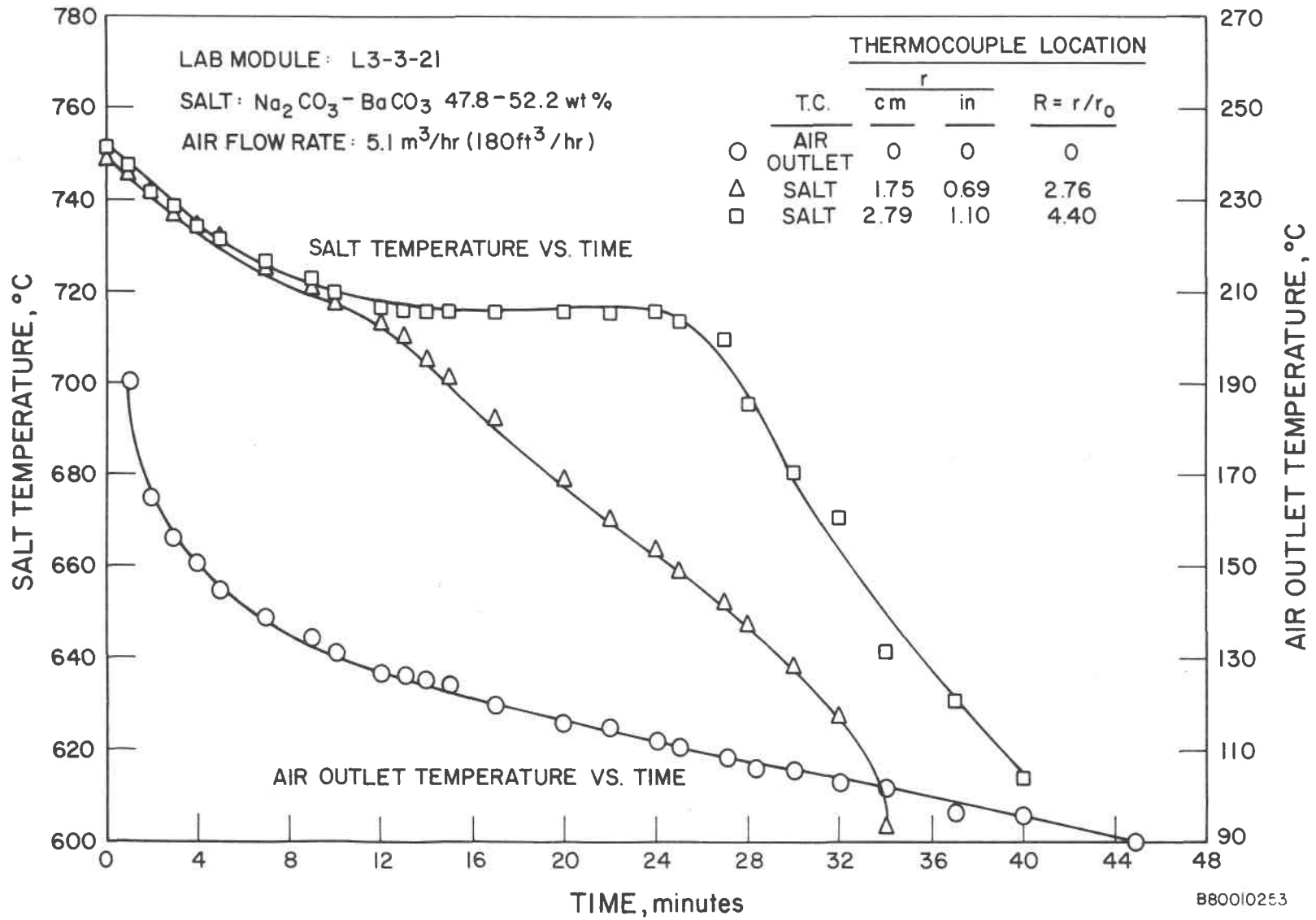


Figure 45. TYPICAL DISCHARGE PERFORMANCE OF  $\text{Na}_2\text{CO}_3 - \text{BaCO}_3$  SYSTEM AT  $5.1 \text{ m}^3/\text{hr}$  ( $180 \text{ ft}^3/\text{hr}$ ) AIR FLOW RATE

indicates that this  $\text{Na}_2\text{CO}_3\text{-BaCO}_3$  eutectic may be used for phase change TES applications in the higher  $700^\circ$  to  $735^\circ\text{C}$  ( $1290^\circ$  to  $1340^\circ\text{F}$ ) range. An experimental heat flux of  $41,676 \text{ W/m}^2$  ( $13,220 \text{ Btu/hr-ft}^2$ ) was graphically calculated from Run 21 (Figure 46). This plot also outlines the relatively stable discharge performance exhibited by this salt throughout 27 cycles of its operating life.

After 36 cycles and 984 hours of operation, this unit was shut down by forced cooling with air at a typical working flow rate ( $5.1 \text{ m}^3/\text{hr}$ ,  $180 \text{ ft}^3/\text{hr}$ ) down to ambient. The sectioned photograph of Figure 47 illustrates the crystal size formation patterns characteristic of this type of discharge. As is expected, near the cooling tube the crystals are fine, with columnar shapes, exhibiting a distinct radial orientation with respect to the cooling tube. This type of growth pattern is the result of very rapid cooling. Midway between the cooling tube and outer wall, the crystals are larger and randomly oriented because of slower cooling. Near the outer edge, the crystals are somewhat finer again but have no preferred orientation, indicating a higher cooling rate than that in the middle, but much slower than that near the HX tube. These observations are consistent with the temperature profile through the salt as a function of cooling time, as shown in Figure 45.

Post-test analysis revealed no salt decomposition or significant containment corrosion.

55.7 wt %  $\text{Li}_2\text{CO}_3$  - 44.3 wt %  $\text{CaCO}_3$  (L4-1). With its reported mp of  $662^\circ\text{C}$  ( $1224^\circ\text{F}$ ),<sup>21</sup> this was the lowest melting carbonate mixture tested for solar-thermal applications. A quantity of 814 grams (1.79 lb) of this mixture was loaded and run in a welded container, with extremely stable results. From Figure 48, it was observed that no super-cooling occurred and that the  $\text{Li}_2\text{CO}_3\text{-CaCO}_3$  salt consistently solidified within  $\pm 5^\circ\text{C}$  ( $9^\circ\text{F}$ ) of its reported mp of  $662^\circ\text{C}$  ( $1224^\circ\text{F}$ ).

Although the module contained 56 wt %  $\text{Li}_2\text{CO}_3$ , its average heat flux to the air of  $40,415 \text{ W/m}^2$  ( $12,820 \text{ Btu/hr-ft}^2$ ) is one of the lowest tested. This value was calculated from Run 25 (Figure 49, which also displays a very narrow lifetime performance band for Runs 2, 12, 22, and 25.)

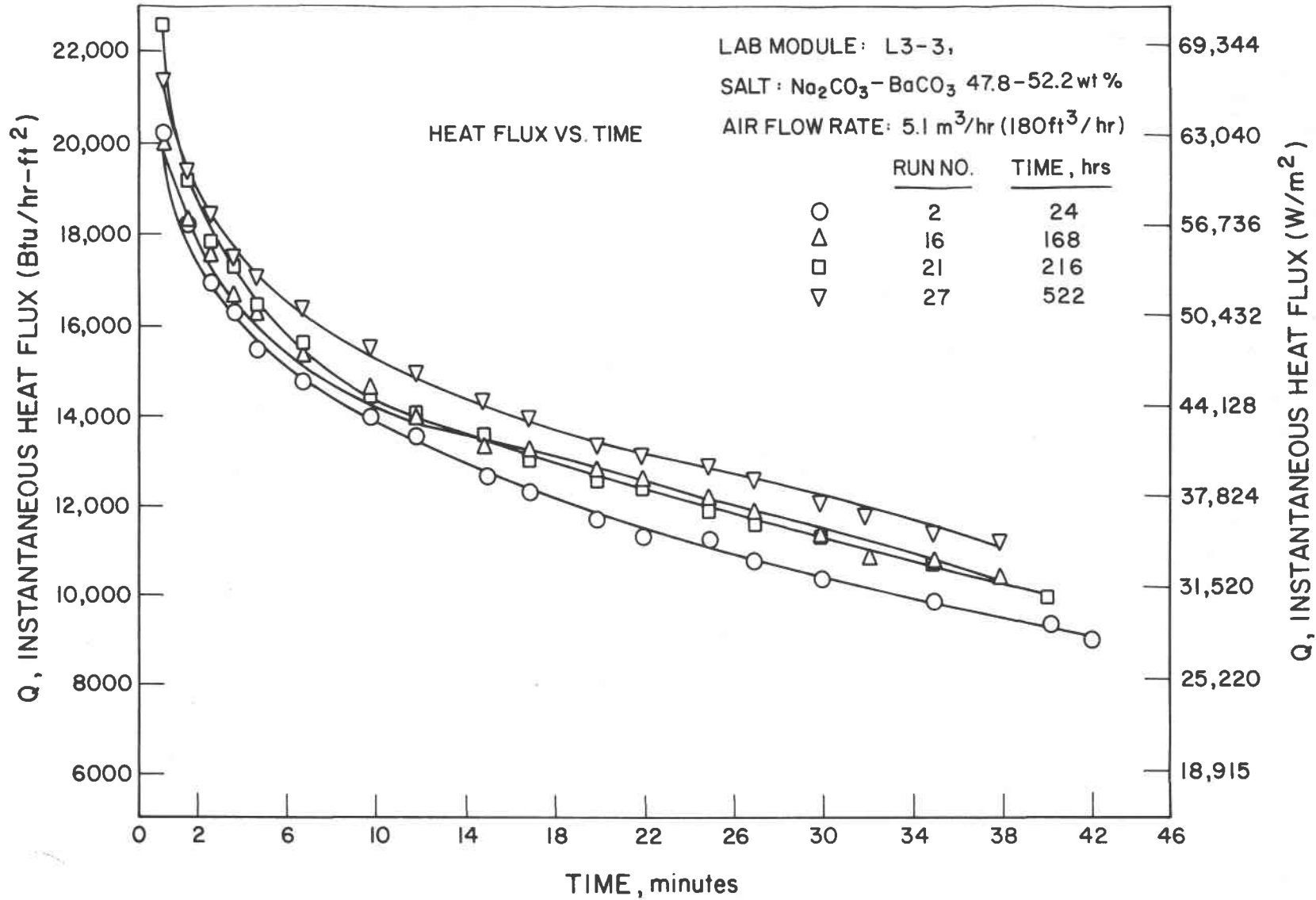


Figure 46. LIFETIME DISCHARGE PERFORMANCE OF Na<sub>2</sub>CO<sub>3</sub> - BaCO<sub>3</sub> SYSTEM OVER 984 HOURS

B80010251

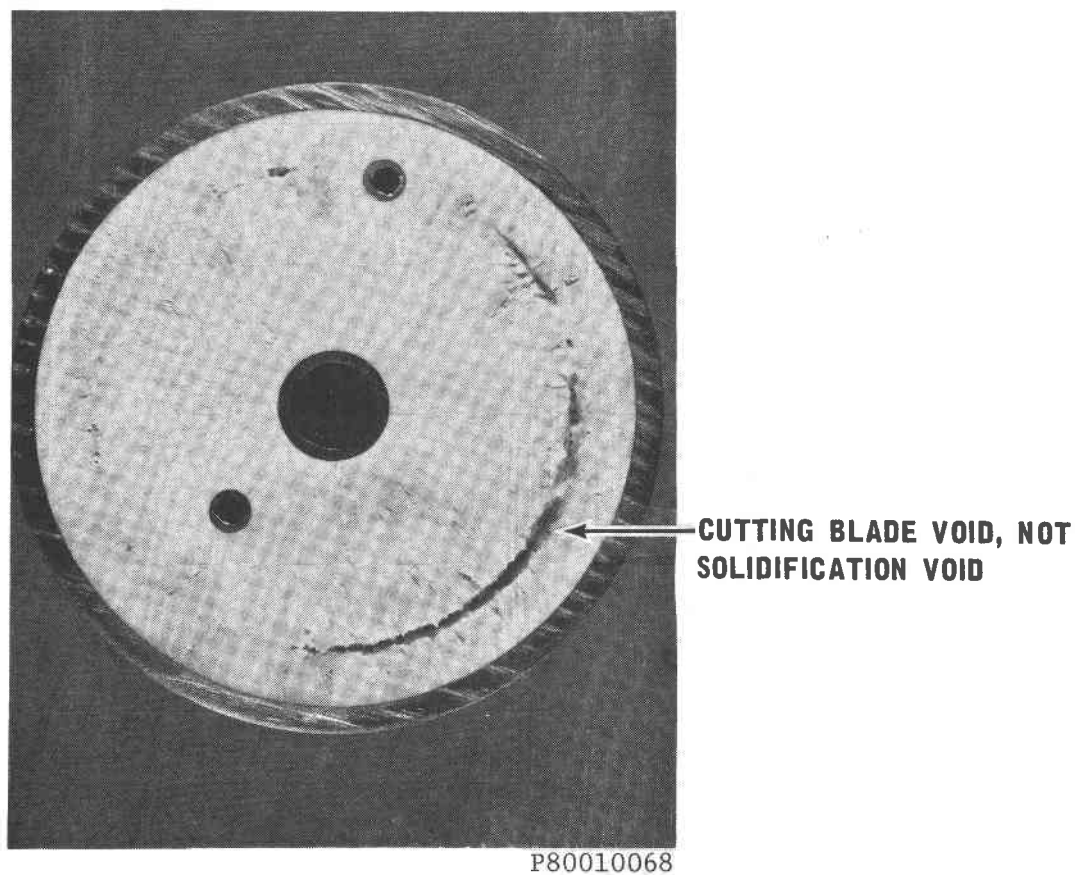
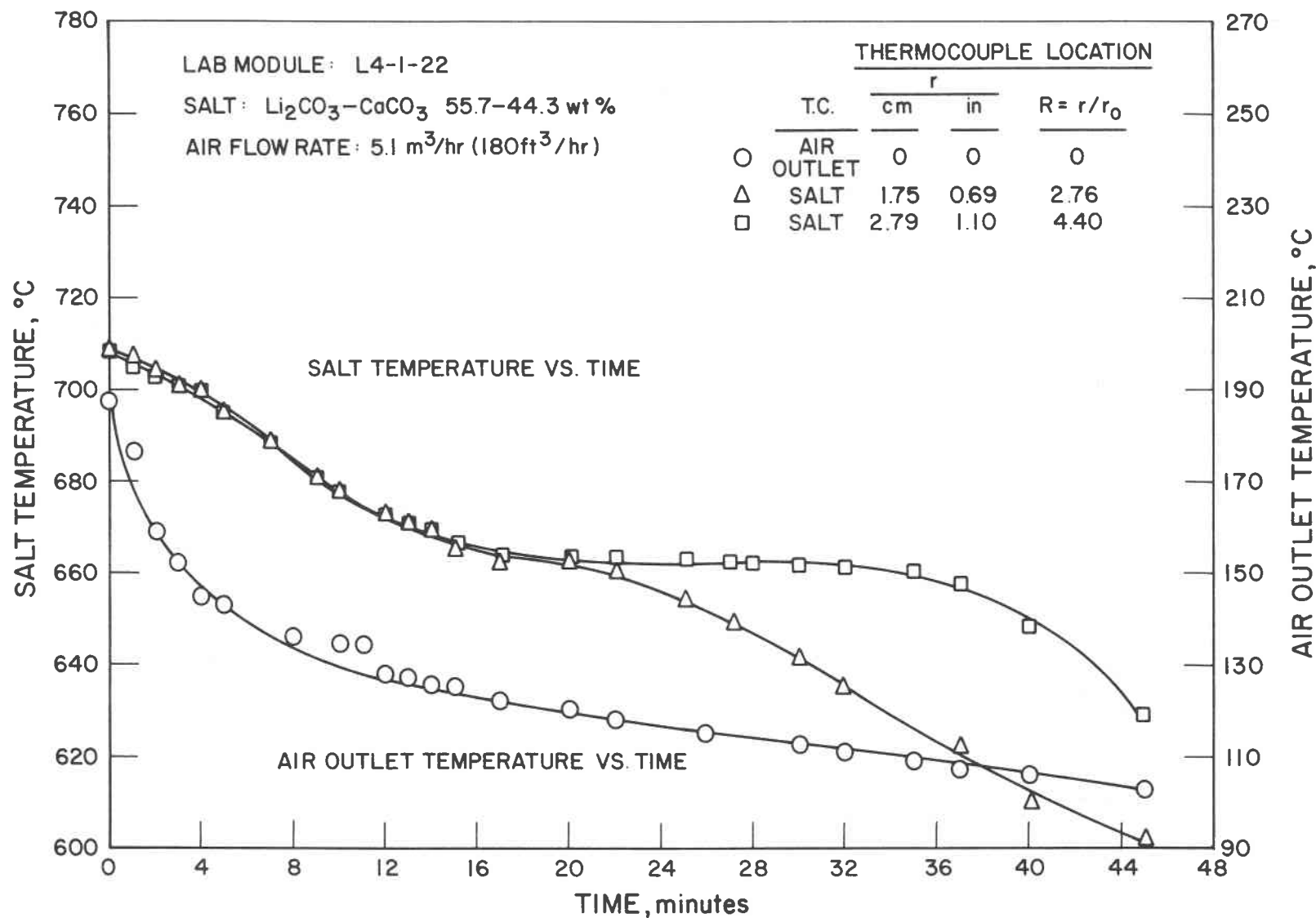
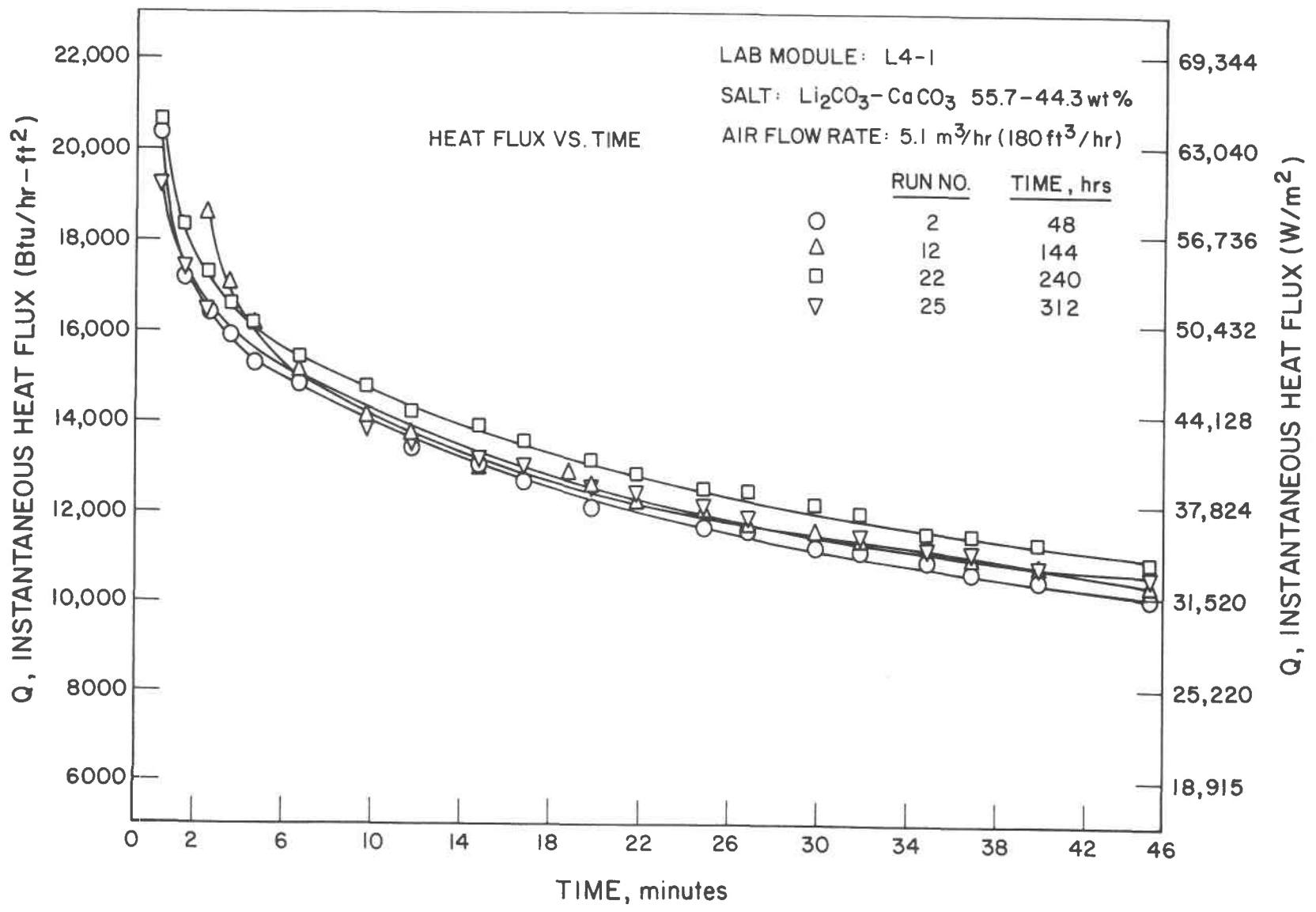


Figure 47. TRANSVERSE CROSS SECTION THROUGH MODULE L3-3 47.8 wt %  $\text{Na}_2\text{CO}_3$  - 52.2 wt %  $\text{BaCO}_3$  AFTER 984 HOURS AND 36 CYCLES



B79I22728

Figure 48. TYPICAL DISCHARGE PERFORMANCE OF  $\text{Li}_2\text{CO}_3$  -  $\text{CaCO}_3$  SYSTEM AT  $5.1 \text{ m}^3/\text{hr}$  ( $180 \text{ ft}^3/\text{hr}$ ) AIR FLOW RATE



B80010250

Figure 49. LIFETIME AVERAGE INSTANTANEOUS HEAT FLUX CURVE FOR  $\text{Li}_2\text{CO}_3\text{-CaCO}_3$  SYSTEM

Since no heat of fusion values were available in literature for either the  $\text{Na}_2\text{CO}_3\text{-BaCO}_3$  or the  $\text{Li}_2\text{CO}_3\text{-CaCO}_3$  system, estimated values were obtained by comparing the integrated quantity of heat removed from these salts with that removed from  $\text{Li}_2\text{CO}_3$  and  $\text{Na}_2\text{CO}_3$ , whose heats of fusion are known. The results appeared previously in Table 15 (parenthetically).

More reliable heat of fusion and thermal conductivity measurements are required to accurately analyze the thermal performance and attractiveness of the  $\text{Na}_2\text{CO}_3\text{-BaCO}_3$  and  $\text{Li}_2\text{CO}_3\text{-CaCO}_3$  systems as PCM's for further TES development work.

This  $\text{Li}_2\text{CO}_3\text{-BaCO}_3$  system was terminated in a free-cool after 312 hours and 25 cycles. Post-test examinations revealed no salt decomposition and no increase in concentration of metallic containment elements from corrosion.

83.1 wt %  $\text{Na}_2\text{CO}_3$  - 18.7 wt %  $\text{K}_2\text{CO}_3$  (Module L1-3). This salt served a dual purpose during its lab-scale testing. Although investigated as a candidate TES medium in the solar-thermal 538° to 871°C (1000° to 1600°F) temperature range, its more important ramifications were as a TCE concept. A detailed account of this unit's experimental results is presented in Section 2.3, testing of thermal conductivity enhancement concepts.

#### Non-Carbonate Salts

It is a recognized fact that no single salt, or family of salts, possesses superior properties in all important categories (such as low cost, high heat-of-fusion, ease of handling, low corrosivity, and high-temperature stability). It is obvious that trade-offs in these parameters are necessary when selecting a salt for a given application and its particular duty requirements. Thus it is probable that carbonate salts may someday be an optimum selection for one application, with a fluoride, chloride, or other salt being a better choice for another application having different system performance and cost limitations.

In keeping with this logic, and to establish a baseline of comparative thoroughness, two non-carbonate mixtures were tested in the lab-scale cannisters. These salts were treated with the same handling, loading, and operating procedures that proved successful for the carbonates. A closed cannister system was to be used, with an inert environment above the salt, as required.

CaCl<sub>2</sub> (L3-4). This chloride system was chosen because its 772°C (1422°F) mp was compatible to the temperature requirements of the study, and its medium heat of fusion ( $2.56 \times 10^5$  J/kg, 110 Btu/lb) and low unit cost (\$0.09/kg, \$0.04/lb) made it an attractive TES candidate.

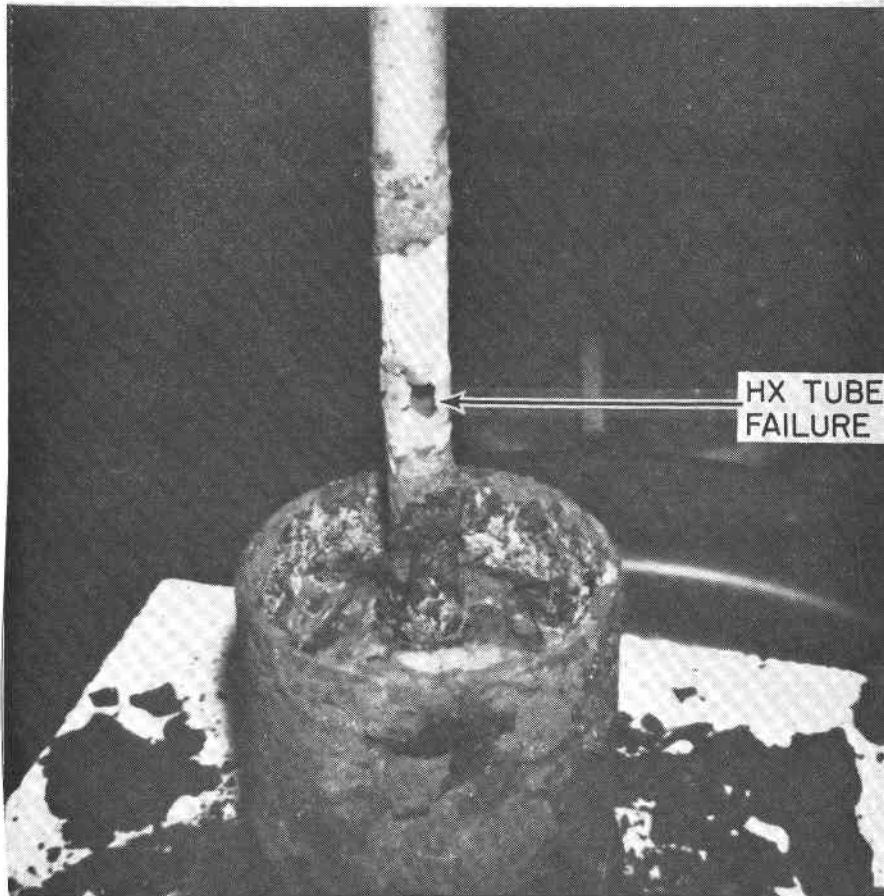
Because of CaCl<sub>2</sub>'s hygroscopicity, the mixture was handled in an air dry-room and dehydrated overnight in a Hotpack oven purged with dry CO<sub>2</sub>. Gravimetric analyses indicated nearly complete removal of the water of hydration. In keeping with the standard procedures, 727 grams (1.6 lb) of the salt were then loaded into a cannister and melted in the Hotpack oven in two fillings. In less than 6 hours (at 822°C, 1512°F) in this oven, a large amount of salt crept out of the cannister. Upon immediate removal and visual inspection of the cannister, it was found that excessive hot corrosion had scaled off a 180 μm (~7 mils) layer from the OD of the SS Type 304 cannister.

The unit was finally filled to 2.54 cm (1 in.) from the top of the can with molten salt and maintained at 725°C (1337°F) for 20 hours (overnight), prior to welding of the top and closing of the system. Although this was often done with carbonates, the chloride cannister was found to have lost its operational integrity entirely, with a corrosion scaling loss of 635 μm (25 mils) from the cannister OD, and an eroded hole in the SS 316 HX tube, as pictured in Figure 50.

Unlike carbonates, the failure of this salt during loading demonstrated that chlorides require a dry, monitored O<sub>2</sub>-free inert environment throughout the entire handling, loading, and operating procedures to prevent extensive corrosion of metallic containment.

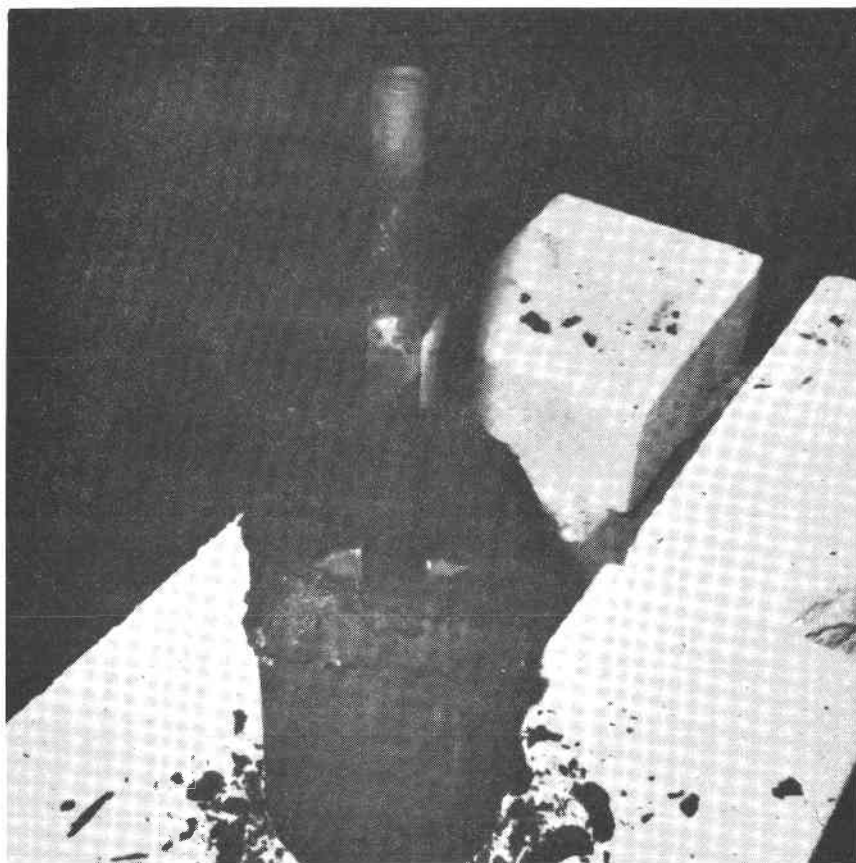
32.5 wt % NaF - 67.5 wt % KF (L4-3). This NaF-KF system is an attractive TES candidate because of its high heat of fusion ( $5.86 \times 10^5$  J/kg, 252 Btu/lb) and its melting point (721°C, 1330°F). Also, it was selected as the most cost-effective fluoride for TES applications in the 700° to 725°C (1292° to 1337°F) temperature range in a Pennwalt Corporation report by J. L. Eichelberger.<sup>28</sup>

As with the chloride salt, this salt was to be operated eventually in a closed system under a high-purity argon environment. After two fillings and 4 hours at ~770°C (1418°F), significant amounts of salt crept out of the containers and corrosively scaled off a 254 μm (~10 mil) layer of stainless steel from the outer surface of the cannister (Figure 51).



P80010069

Figure 50. MODULE L3-4 AFTER FILLING WITH  $\text{CaCl}_2$   
AND HOLDING AT  $725^\circ\text{C}$  ( $1337^\circ\text{F}$ ) FOR 20 HOURS



P80010070

Figure 51. MODULE 14-3 AFTER FILLING WITH NaF-KF  
AND HOLDING AT 770°C (1418°F) FOR 6 HOURS

Aluminum powder was to be a "getter" at this point, but too much of the cannister had corroded after this first 4 hours at operational temperatures to consider it functional. Once again, the necessity for a dry, O<sub>2</sub>-free environment above fluorides and chlorides to load and weld the containers became visibly apparent.

If one considers these facts, it becomes clear that the application of either of these two non-carbonate TES mixtures on a large industrial scale would entail the use of sophisticated atmosphere control during loading, operation, and maintenance. The added expense for salt handling alone could significantly decrease the cost effectiveness of either the energy-dense fluorides or inexpensive chloride salts. These points, together with the uncertainty of personnel safety in the event of a system leak, become important institutional considerations of these salts' ultimate TES applicability.

#### Experimental Verification of Megerlin Analysis

An accurate heat transfer model describing the melting and solidification of PCM salts is necessary if one is to adequately interpret the results from experimental TES modules and to meaningfully extrapolate these results to large-scale systems that use actual fluids at elevated temperature and pressure. The analytical model developed at the Institute of Gas Technology (IGT) during the original contract was based on Megerlin's analysis of the solidification of a cylindrical melt via an internal HX.<sup>16</sup> The general mathematical approach adopted was obtained by modifying some existing solutions for phase-change thermal behavior. One of the more appropriate solutions was that originally developed by Megerlin.<sup>24</sup> Using a cylindrical geometry, a finite heat-transfer coefficient, and the liquid (salt) at its melting point, the time required to solidify a given thickness of salt can be expressed in a relationship containing a number of dimensionless parameters:

$$N_{Fo} = \int_1^R \frac{r \ln r^* (N_{Bi} \ln r^* + 2) dr^*}{\sqrt{(N_{Bi} \ln r^* + 1)^2 + 2 \frac{N_{Bi}}{N_{ph}} \ln r^* (N_{Bi} \ln r^* + 2) - (N_{Bi} \ln r^* + 1)}} \quad (28)$$

where —

$N_{Fo}$  (the Fourier number) gives the dimensionless time required to solidify a given thickness of salt,

$$N_{Fo} = k\tau/c_p \rho a^2 \quad (29)$$

$N_{Bi}$  (Biot number) gives the ratio of the surface conductance to interior solid conductivity,

$$N_{Bi} = ha/k_s \text{ or } Ua/k_s \quad (30)$$

$N_{ph}$  (phase change number) gives the ratio of the heat of fusion to the sensible heat between the melting point and a reference temperature (temperature of cooling/heating media),

$$N_{ph} = \frac{\Delta H_f \rho_l}{c_p (t_m - t_a) \rho_s} \quad (31)$$

The term  $R$  is a reduced thickness: the ratio of the thickness of the annular layer of solid salt to the radius of the HX pipe.

- $a$  = characteristic thickness, m (ft), (half thickness of a slab, radius of a cylinder or a sphere)
- $c_p$  = heat capacity, J/kg-K (Btu/lb<sub>m</sub>-°F)
- $h$  = surface heat-transfer coefficient, W/m<sup>2</sup>-K (Btu/hr-ft<sup>2</sup>-°F)
- $\Delta H_f$  = heat of fusion, J/kg (Btu/lb<sub>m</sub>)
- $k_s$  = thermal conductivity of solid, W/m-K (Btu/hr-ft-°F)
- $r^*$  = radial integration variable,  $r_{\text{interface}}/r_o$
- $t_a$  = ambient temperature, °C (°F)
- $t_m$  = melting point, °C (°F)
- $U$  = overall heat-transfer coefficient, W/m<sup>2</sup>-K (Btu/hr-ft<sup>2</sup>-°F)
- $\rho_l$  = density liquid, kg/m<sup>3</sup> (lb<sub>m</sub>/ft<sup>3</sup>)
- $\rho_s$  = density solid, kg/m<sup>3</sup> (lb<sub>m</sub>/ft<sup>3</sup>)
- $\tau$  = time, hr

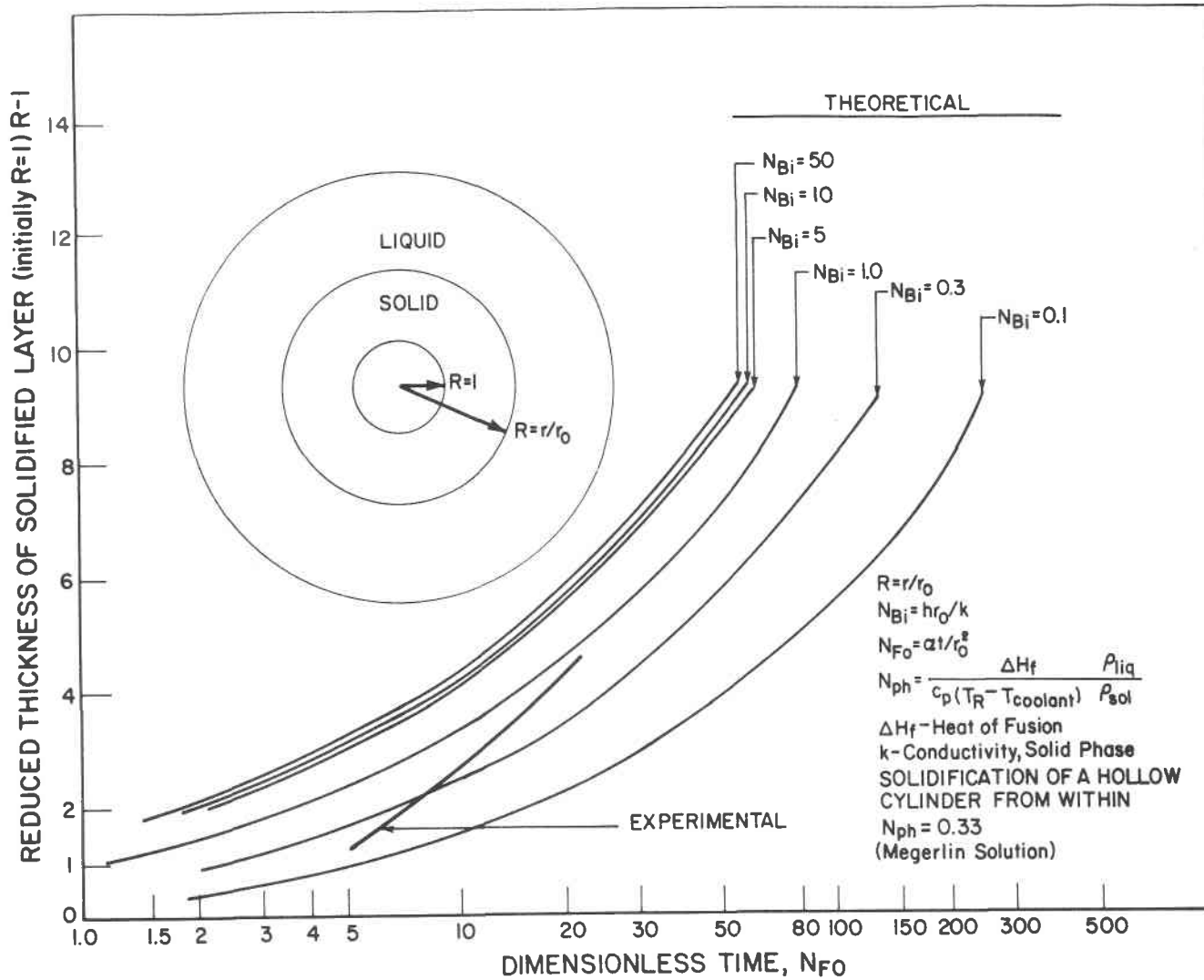
Two salts were used to compare their lab-scale experimental performance with that predicted by the Megerlin solution. The average discharge performances of the pure salts  $\text{Li}_2\text{CO}_3$  (mp = 723°C, 1333°F;  $\Delta H_f = 6.07 \times 10^5$  J/kg, 261 Btu/lb) and  $\text{Na}_2\text{CO}_3$  (mp = 858°C, 1576°F;  $\Delta H_f = 2.65 \times 10^5$  J/kg, 114 Btu/lb) were selected for this analysis.

Solidification of Pure  $\text{Li}_2\text{CO}_3$  and  $\text{Na}_2\text{CO}_3$ ; Movement of the Solid-Liquid Interface During System Discharge

As previously mentioned, T/C's were located at mid-depth in the salt at two radial locations [1.8 and 2.3 cm (0.69 and 1.10 in.)] from the HX, and their response with time was recorded during discharging. The time required for the solidifying front to reach the location of a T/C was determined from the traces at the point where the T/C began to indicate a temperature below the mp and subsequently yielded a descending cooling curve (characteristic of a solid being cooled). The average times required for the solid front to reach the T/C's isolated from edge effects (such as heat loss) for  $\text{Li}_2\text{CO}_3$  and  $\text{Na}_2\text{CO}_3$  are summarized in Table 19, which shows the radial locations of the T/C's and the calculated Fourier numbers. The theoretical solidification profiles determined by numerical evaluation of the Megerlin solution for  $\text{Li}_2\text{CO}_3$  ( $N_{ph} = 0.33$ ,  $N_{Bi} = 0.3$ ) and  $\text{Na}_2\text{CO}_3$  ( $N_{ph} = 0.14$ ,  $N_{Bi} = 0.3$ ) are shown in Figures 52 and 53, respectively, with the experimental profile. The observed behavior shows the solidification proceeding slower than expected during the early stages of discharge and proceeding faster than predicted during the later stages, which may be partially attributable to the convective mixing currents present in the molten salt. Considering the small size of the unit being examined, these numbers agree surprising well with the theoretical model.

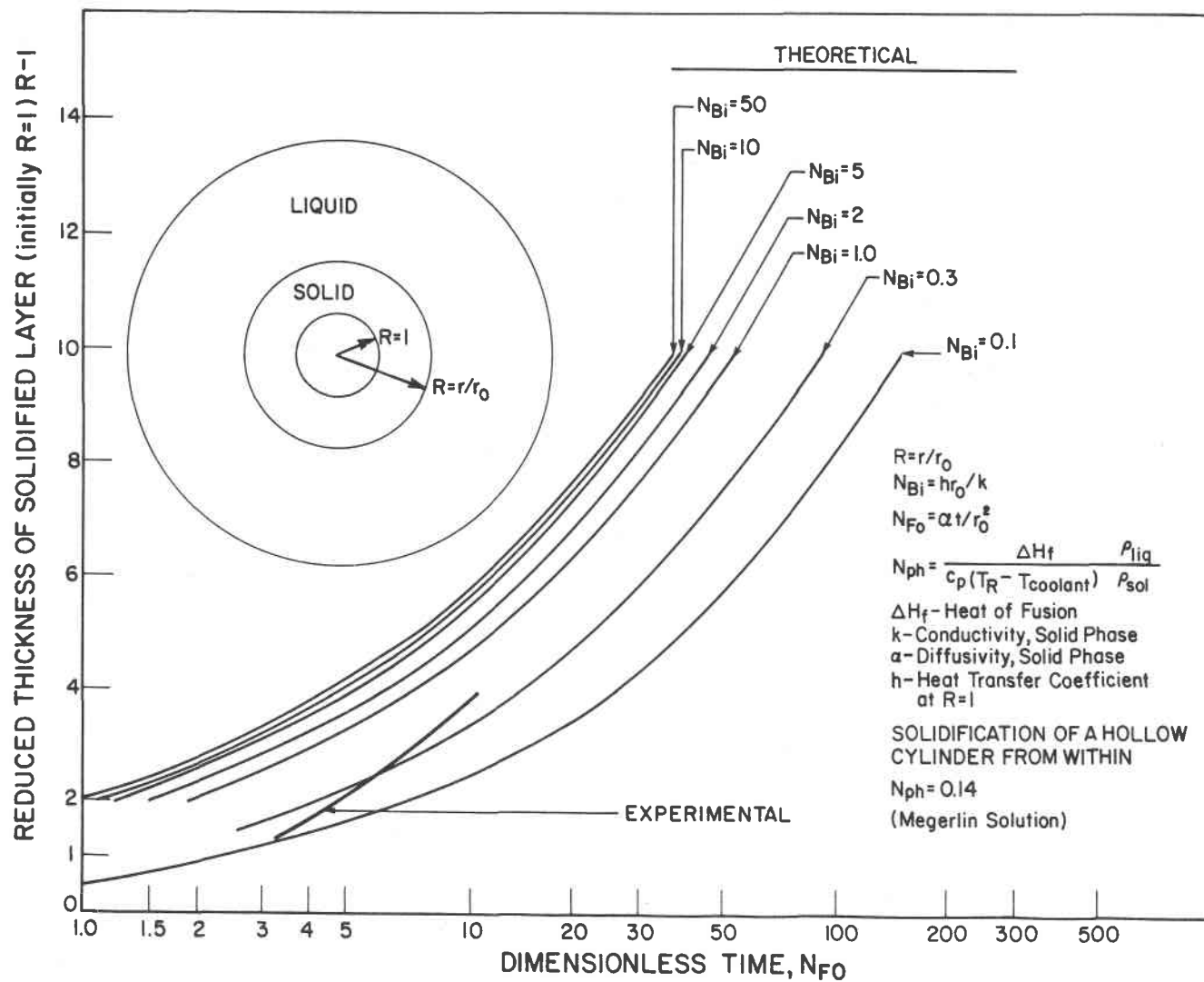
Table 19. COMPARISON OF THEORETICAL AND OBSERVED SOLIDIFICATION BEHAVIOR ( $\text{Li}_2\text{CO}_3$  and  $\text{Na}_2\text{CO}_3$ )

Salt System	Radial Location (R-1)	Average Time, min	$N_{Fo}$ Observed	$N_{Fo}$ Theoretical
$\text{Li}_2\text{CO}_3$	1.76	17.0	6.68	5.8
$\text{Li}_2\text{CO}_3$	3.40	35.0	14.00	19.0
$\text{Na}_2\text{CO}_3$	1.76	10.0	4.07	3.6
$\text{Na}_2\text{CO}_3$	3.40	21.4	8.72	10.8



B79122787

Figure 52. COMPARISON OF  $Li_2CO_3$  EXPERIMENTAL SOLIDIFICATION PROFILES WITH PREDICTIONS OF THE MEGERLIN SOLUTION



B79I22786

Figure 53. COMPARISON OF  $Na_2CO_3$  EXPERIMENTAL SOLIDIFICATION PROFILES WITH PREDICTIONS OF THE MEGERLIN SOLUTION

The primary source of error for the early-discharge discrepancies is in the excess enthalpy of superheat stored as sensible heat in the molten salt at the operating temperatures (mp + 50°C). The differences in the later stages of discharge are probably a result of the continual radiant heat losses to the ambient.

It follows from these considerations that the model efficiently predicts small as well as larger-scale (engineering units) TES salt performance, as found in previous work.<sup>16</sup>

#### Assessment of Salt TES Applicability

Because of the complex and diverse trade-offs involved in selecting a salt for a given application and duty cycle, simple comparisons can be uncertain, and numbers can often serve only as guidelines when one assesses a salt's experimental data for TES applicability. With this in mind, the following summaries of salts for solar-thermal applications were prepared, based on thermophysical and experimentally determined data.

- $\text{Li}_2\text{CO}_3\text{-CaCO}_3$  55.7-44.3 wt %

This salt exhibited excellent compatibility with the AISI 304 SS cannister and AISI 316 HX tube. Accurate determinations of its heat of fusion, thermal conductivity and other thermophysical properties are essential, though, for an accurate analysis of its experimental performance. It appears to be an attractive PCM for TES applications in the 650° to 700°C (1202° to 1292°F) temperature range.

- $\text{Na}_2\text{CO}_3\text{-BaCO}_3$  41.8-52.2 wt %

Reliable thermophysical and transport data are lacking for this system also. Excellent long-term (484 hours) compatibility with SS 304 and 316 containment and stable thermal performance were demonstrated. With its higher experimental solidification point of ~715°C (1320°F) (instead of its reported mp of 656°C), this salt may be utilized in 700° to 750°C (1292° to 1382°F) applications.

- $(\text{Li-Na-K})_2\text{CO}_3$  1.21-49.95-48.84 wt % and  $(\text{Na-K})_2\text{CO}_3$  50-50 wt %

The  $(\text{Na-K})_2\text{CO}_3$  binary system exhibited (even during loading) strong surface tension creepage properties and was relatively corrosive. Upon doping this system with  $\text{Li}_2\text{CO}_3$  to lower its corrosivity, its heat flux increased, though melting somewhat incongruently. Accurate thermal conductivity determinations through both solid salts would greatly aid in assessing this apparent improvement.

- $\text{Li}_2\text{CO}_3$

The  $\text{Li}_2\text{CO}_3$  unit with the  $\text{CO}_2$  blanket exhibited the highest heat flux of any salts and operated stably for more than 650 hours with no hysteresis. Good compatibility with the stainless-steel containment was demonstrated, although investigations should be conducted into other alloys for long-term (30 years) applications. Its high heat of fusion ( $6.07 \times 10^5$  J/kg, 261 Btu/lb), stable experimental performance, and melting point of  $723^\circ\text{C}$  ( $1339^\circ\text{F}$ ) make this salt a prime versatile candidate for both large central receiver and small dispersed power systems applications in the  $700^\circ$  to  $750^\circ\text{C}$  ( $1292^\circ$  to  $1382^\circ\text{F}$ ) temperature regime.

- $(\text{Na-K})_2\text{CO}_3$  81.3-18.7 wt %

This interesting composition requires more in-depth study for one to completely understand its discharge solidification characteristics. Only then can the total impact of its apparent slush behavior on the thermal performance and its subsequent applicability be clearly evaluated. As one will find in Section 2.3, though operating  $50^\circ\text{C}$  ( $90^\circ\text{F}$ ) higher, generally, than the  $(\text{Na-K})_2\text{CO}_3$  50-50 wt % system, this salt delivered 31% more heat ( $\text{Btu/hr-ft}^2$ ) over the same operating cycle. Its long-term (1032 hours) compatibility with stainless-steel containment and  $\$0.13/\text{kg}$  ( $\$0.06/\text{lb}$ ) unit cost again indicate a strong potential for cost-effective commercial TES applicability in the broad range of  $700^\circ$  to  $800^\circ\text{C}$  ( $1292^\circ$  to  $1472^\circ\text{F}$ ).

- $\text{Na}_2\text{CO}_3$

With its high mp of  $858^\circ\text{C}$  ( $1576^\circ\text{F}$ ), medium heat of fusion of  $2.65 \times 10^5$  J/kg (114 Btu/lb), and extremely low cost of  $\$0.07/\text{kg}$  ( $\$0.03/\text{lb}$ ), this salt seems capable of immediately lending itself to high-temperature solar applications in the  $800^\circ$  to  $900^\circ\text{C}$  ( $1472$  to  $1652^\circ\text{F}$ ) range, in which the mass of TES medium is not restricted. Our initial experimental results revealed nothing to negate this. They did, nevertheless, clearly illustrate the present need to select and test alternate TES containment materials. This selection should be performed not only on the basis of salt compatibility, but also on the basis of possible interactions with actual working fluids (high-temperature air, helium, and molten sodium) or their impurities and on the basis of the physical and microstructural stabilities of these alternate materials (super alloys) at high temperatures for extended periods (anticipated 25 to 30-year plant goal lifetimes).

- $\text{K}_2\text{CO}_3$

Although it exhibited a high average heat flux of  $72,507 \text{ W/m}^2$  (23,000  $\text{Btu/hr-ft}^2$ ) through two cycles, these numbers are questionable because the time at which the HX tube was breached is unknown.  $\text{K}_2\text{CO}_3$ 's lower heat of fusion ( $2.0 \times 10^5$  J/kg, 86 Btu/lb) and steeply decreasing heat flux profile result in an uncertain outlook for this salt's ultimate utilization as a TES medium in the  $850^\circ$  to  $925^\circ\text{C}$  ( $1562^\circ$  to  $1697^\circ\text{F}$ ) range. Once again, the need for investigating new containment materials for these high-temperature applications was illustrated. Potassium carbonate should be reinvestigated when adequate high-temperature containment materials are identified.

- $\text{CaCl}_2$  100 wt % and NaF-KF 32.5-67.5 wt %

It was found that chlorides and fluorides could not be handled, loaded, and operated as easily and safely as carbonates. As previously mentioned, the use of either of these salt types on a large scale would require the maintenance of a dry,  $\text{O}_2$ -free inert environment over them to prevent extensive corrosion of metallic materials. For the purpose of this investigation, testing of chlorides and fluorides, using much the same procedure as that used for carbonates, resulted in the loss of containment integrity and total system failure.

### 2.3 Evaluation of TCE Materials

#### Introduction

An extremely important aspect of TES module performance is the development of a means of increasing the average rate of heat transfer between the salt and HX, particularly during discharge. Inspection of any salt thermal discharge curve reveals a trend of decreasing instantaneous heat flux as the thickness of solidified salt between the liquid/solid interface and HX increases. Therefore, the limiting factor for the thermal performance of any TES system during discharge is controlled largely by the rate at which the latent heat of fusion released at the solid/liquid interface is transported to the HX surface, through the growing layer of solid salt. Incorporation of a TCE medium within the PCM can significantly influence the performance, design, and ultimate cost of the TES system. It allows achievement of relatively high average discharge heat fluxes and possibly more uniform thermal input to subsequent generators.

Considerations for the selection of suitable conductivity promoters include -

- Thermal conductivity and heat capacity
- Compatibility with carbonates
- Cost
- Availability
- Fabrication to desired configuration.

#### Experimental Testing

Table 20 contains a list of potential TCE materials. This table spans the range of thermal conductivities of available TCE materials, from

Table 20. POTENTIAL HEAT CONDUCTION ENHANCEMENT MATERIALS

Material	Melting Point		Thermal Conductivity at 500°C (932°F)		Heat Capacity Room Temp		Materials Cost			
	°C	(°F)	W/m-K	Btu/hr-ft-°F	J/kg-K	Btu/lb-°F	\$/kg	\$/lb	\$/m <sup>3</sup>	\$/ft <sup>3</sup>
Aluminum	660	(1220)	220	127	921	0.22	1.74	0.79	4,732	134
Copper	1083	(1981)	308	178	385	0.09	1.65	0.75	14,726	417
Iron	1536	(2797)	38	22	461	0.11	3.02	1.37	23,766	673
Molybdenum	2610	(4730)	116	67	255	0.06	9.70	4.40	99,128	2807
Nickel	1453	(2647)	57	33	502	0.12	4.76	2.16	42,448	1202
316 Stainless Steel	1370	(2478)	21	12	502	0.12	2.80	1.27	22,531	638
ATJ Graphite	sublimes		78	45	837	0.20	9.85	4.47	22,107	626
Pyrolytic Graphite	sublimes		208	120	837	0.20	--	--	--	--
Silicon Carbide	2700	(4892)	87	50	836	0.20	--	--	--	--
CS Graphite	sublimes		76	44	837	0.20	1.10	0.50	2,401	68

\* Costs based on 100% of theoretical density.

B80020284

21 W/m-K (12 Btu/hr-ft-°F) for 316 SS to 308 W/m-K (178 Btu/hr-ft-°F) for copper.

Of particular note are aluminum (mp 660°C, 1220°F; thermal conductivity 220 W/m-K, 127 Btu/hr-ft-°F) and copper (mp 1083°C, 1981°F; thermal conductivity 308 W/m-K, 178 Btu/hr-ft-°F), both of which possess thermal conductivities 10 times larger than austenitic stainless steels, and 2 to 6 times greater than the major constituents of these steels.

#### Corrosion Tests

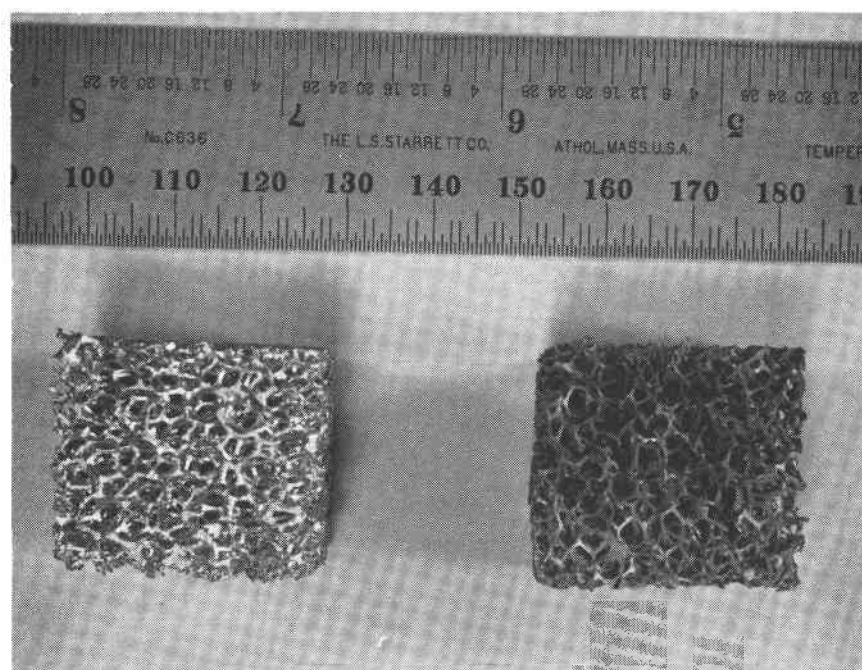
Aluminum Duocel. Based on the attractive thermal conductivity of aluminum, a compatibility test of a 95 volume percent porous, continuous aluminum matrix (brand named Duocel)\* was performed in a (Li-Na-K)<sub>2</sub>CO<sub>3</sub> ternary eutectic for over 4000 hours at 450°C (840°F). (The mean pore size and volume fraction of porosity can be varied over broad ranges during the manufacturing of this particular matrix.)

The carbonate melts were contained in alumina crucibles, and a flow of dry CO<sub>2</sub> gas was maintained over them during testing in Hotpack ovens. Table 21 summarizes the results of this corrosion test. Shown in Figure 54 are an unexposed aluminum Duocel cube and one tested for 528 hours. Although one may readily observe the slight discoloration, only negligible weight changes occurred after 4180 hours of testing. Metallography of a polished cross-section after testing revealed a very thin, passive corrosion-product layer, very likely LiAlO<sub>2</sub>.

Table 21. RESULTS OF CORROSION TESTING OF ALUMINUM DUOCEL IN  
TERNARY EUTECTIC 43.5 mol % Li<sub>2</sub>CO<sub>3</sub>, 31.5 mol % Na<sub>2</sub>CO<sub>3</sub>,  
25.0 mol % K<sub>2</sub>CO<sub>3</sub>, 450°C

Sample No.	Exposure Time, hr	Weight, g		Weight Change	
		Initial	Final	g	%
1	168	2.9693	2.9663	- 0.0030	- 0.1
2	528	3.1034	3.1014	- 0.0020	- 0.06
3	1522	2.9903	2.9777	- 0.0126	- 0.4
4	4180	3.0159	3.0138	- 0.002	- 0.07

\* Produced by Energy Research and Generation Inc., Oakland, California.



P78041074

Figure 54. DUOCEL ALUMINUM MATERIAL AS RECEIVED (Left) AND AFTER 528 HOURS EXPOSURE TO MOLTEN  $(\text{Li-Na-K})_2\text{CO}_3$  AT  $450^\circ\text{C}$  ( $842^\circ\text{F}$ ) (Right)

Although it has been demonstrated in IGT's fuel cell research<sup>29</sup> that aluminum is stable in molten carbonates at temperatures remarkably near its mp (600°C, 1112°F), aluminum can only be considered as a TCE material for low-temperature TES applications because of its 660°C (1220°F) mp.

Reticulated Vitreous Carbon. Samples of another candidate enhancement material, porous reticulated vitreous carbon (RVC)<sup>\*</sup>, were also chosen for testing. Corrosion tests were conducted in platinum crucibles with the RVC immersed in the 50-50 wt % (Na-K)<sub>2</sub>CO<sub>3</sub> salt at 750°C (1382°F). The initial results indicated incompatibility of the RVC and the salt. This was then conclusively determined in a second 400 hour test in which the RVC was continuously and totally submerged in the molten salt. The RVC sample completely disintegrated, settling into a carbonaceous deposit at the bottom of the platinum crucibles. This salt/material incompatibility also eliminated RVC from TCE applicability in the high solar-thermal (538° to 871°C) temperature range.

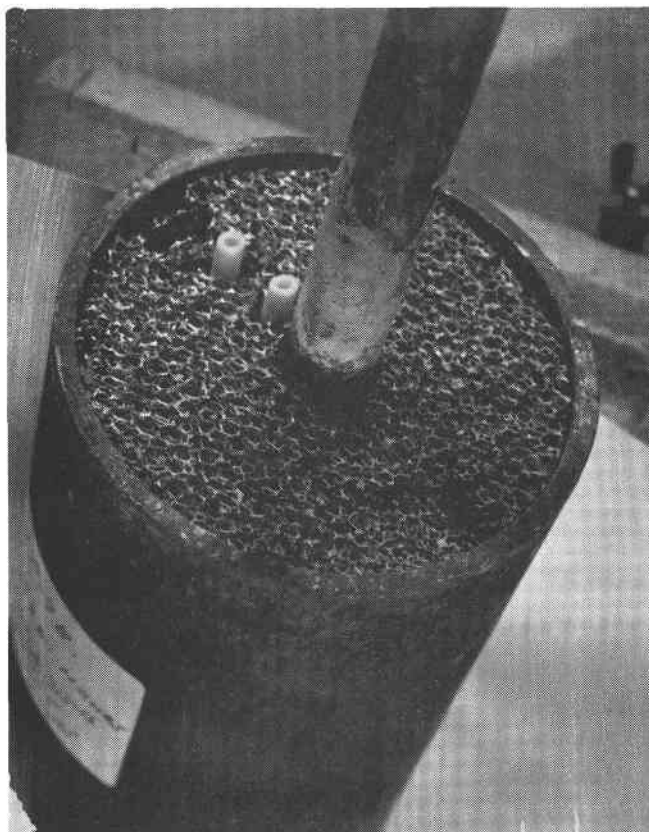
Based on the promising Duocel compatibility results and on its high thermal conductivity, this highly porous body of aluminum was then evaluated in a lab-scale TES unit. The results of this test and the evaluation of one other TCE concept are presented here.

#### Lab-Scale TCE Evaluation

Aluminum Duocel in (Li-Na-K)<sub>2</sub>CO<sub>3</sub> 32-33-35 wt % (L3-2). As mentioned in Section 2.2, 611 grams (1.3 lb) of the (Li-Na-K)<sub>2</sub>CO<sub>3</sub> eutectic were initially tested in the absence of enhancement material to provide a performance baseline to use when comparing the results obtained with Duocel. This unit utilized the original lab-scale design for low temperature, which included a slip-fit transite top and three salt T/C's shrouded in high-quality alumina sheaths. From this initial test, a baseline average heat flux of 6,954 W/m<sup>2</sup> (2,206 Btu/hr-ft<sup>2</sup>) was determined.

After 10 cycles and 504 hours of operation, a cylindrically fabricated block of Duocel was installed into the molten salt, force-fit onto the HX tube. Figure 55 shows the Duocel after installation. The unit was re-installed and the test proceeded in this same cannister an additional 312 hours and 22 cycles.

\* RVC Products Co., Ann Arbor, Michigan.



P80010072

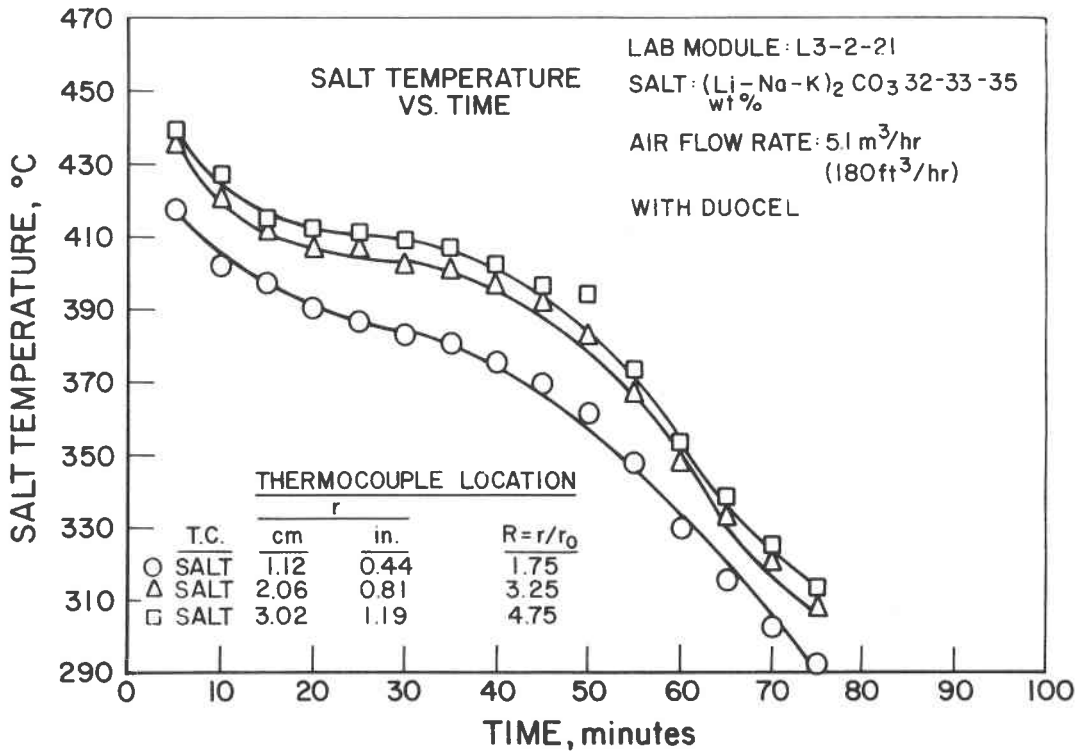
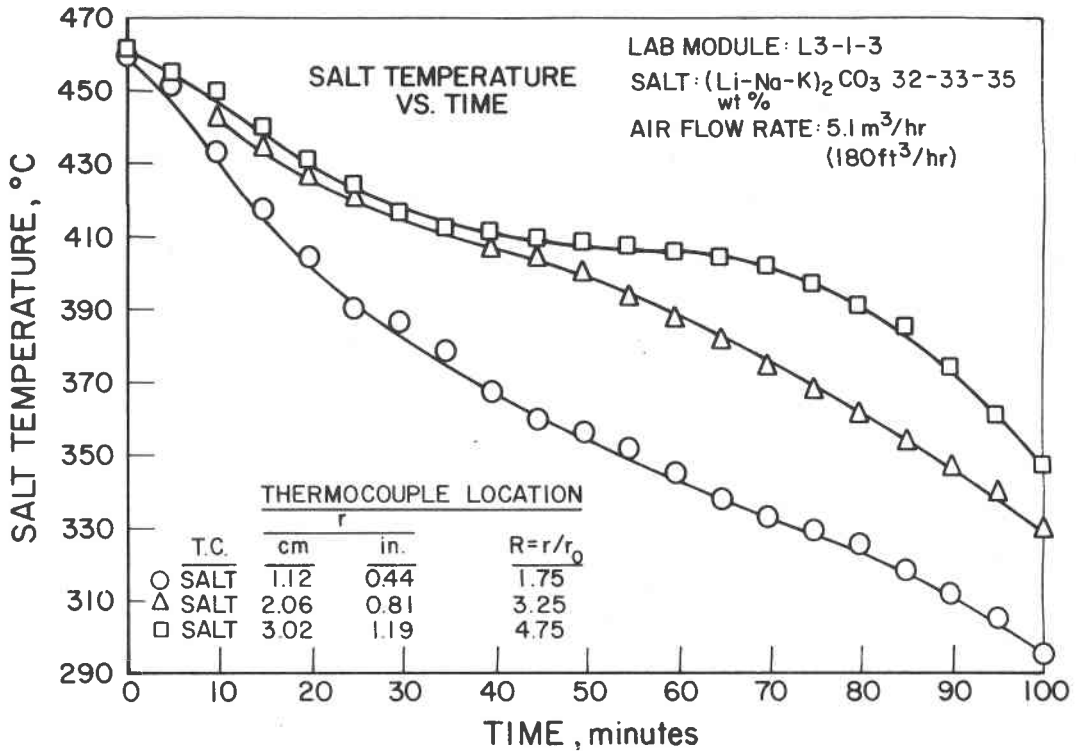
Figure 55. FORCE-FIT INSTALLATION OF DUOCEL  
ENHANCEMENT MATERIAL INTO CANNISTER CONTAINING  
(Li-Na-K)<sub>2</sub>CO<sub>3</sub> EUTECTIC

Discharge profiles with and without Duocel are compared in Figure 56. Although the discharge solidification point remained unchanged ( $\sim 409^{\circ}\text{C}$ ,  $768^{\circ}\text{F}$ ), the graphs are nonetheless significantly different. The time required to solidify the ternary out to the T/C at  $r = 3.02\text{ cm}$  (1.19 in.) decreased from 70 minutes to 40 minutes with the porous aluminum Duocel material, a 43% decrease in solidification time. Also, the unit with Duocel took 33% less time to discharge from  $450^{\circ}$  to  $350^{\circ}\text{C}$  ( $842^{\circ}$  to  $662^{\circ}\text{F}$ ) than the baseline module, and it reduced the time period of apparent salt temperature thermal arrest by 57%. Effective TCE is also illustrated by the fact that Duocel caused a 55% decrease in salt radial thermal gradient at the end of discharge from  $13^{\circ}\text{C}/\text{cm}$  to  $29^{\circ}\text{C}/\text{cm}$  ( $61^{\circ}\text{F}/\text{in}$  to  $133^{\circ}\text{F}/\text{in}$ ). This fact is significant when one considers that such a decrease occurred across the relatively small radius of 1.5 inches.

The change in the discharge heat flux profiles from no enhancement to 95 percent porous Duocel is also marked, as shown in Figure 57. The average heat flux of  $10,135\text{ W}/\text{m}^2$  ( $3,215\text{ Btu}/\text{hr}\text{-ft}^2$ ) with Duocel represents a 45% increase in heat conduction through the solid salt to the air working fluid over the same operating temperatures.

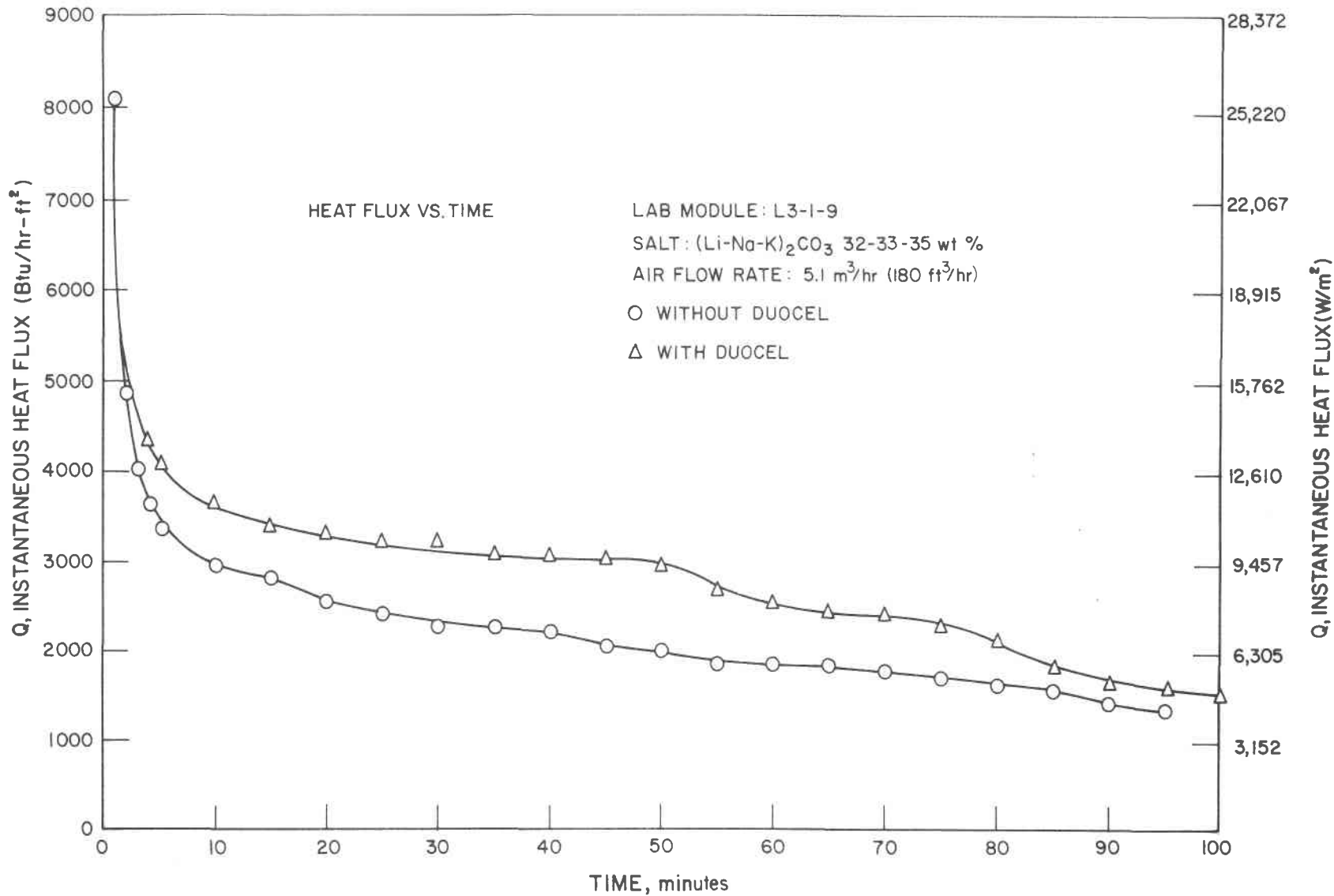
After 32 cycles and 816 hours of combined operation, this unit was then shut down for post-test evaluation. As shown in Figure 58, the unit was sectioned lengthwise, revealing a good salt/TCE-material filling pattern on solidification, with little inter-matrix void formation. Visual inspection also revealed varying degrees of contact between the Duocel and HX tube, varying from direct contact to as much as  $2,388\text{ }\mu\text{m}$  (94 mils) separation at one point. Despite the force fit achieved during initial installation, the Duocel appeared to have relaxed away from the HX during operation.

One of the primary difficulties in using any reticulated conductivity promoter is obtaining a good contact with the HX surface. An alternative to force-fitting is to braze the aluminum block to the HX tube. But this alternative proved too costly and time-consuming, because further work must still be done to develop a braze for use with aluminum and stainless steel that is also compatible with carbonate salts.



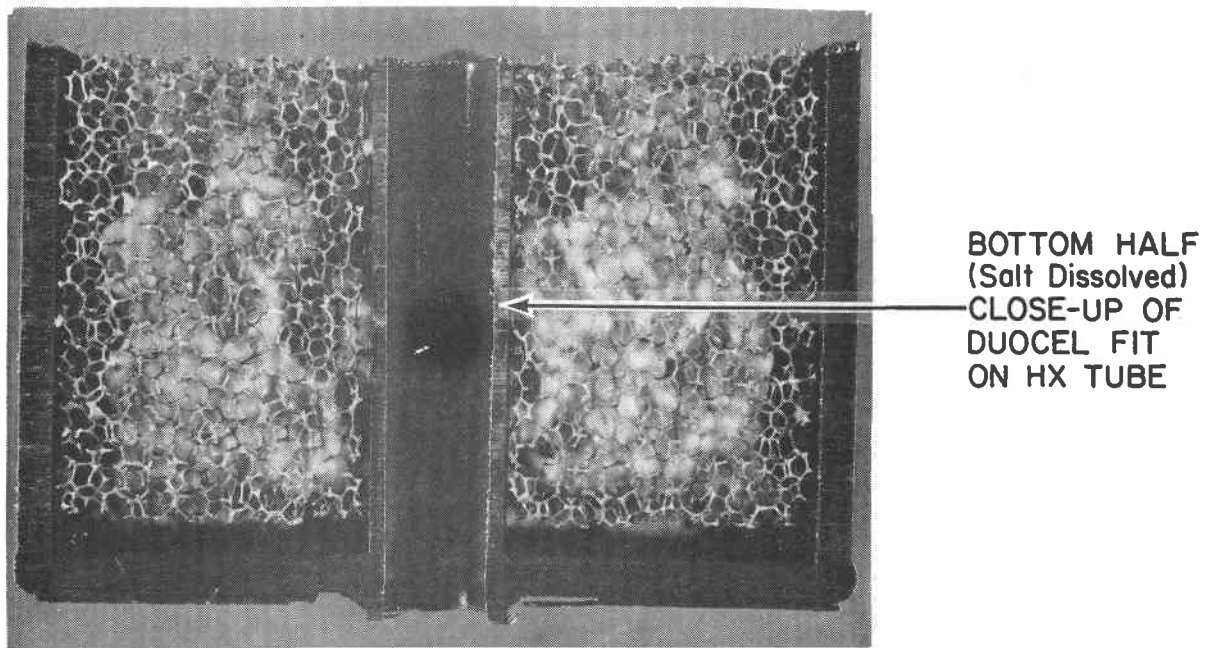
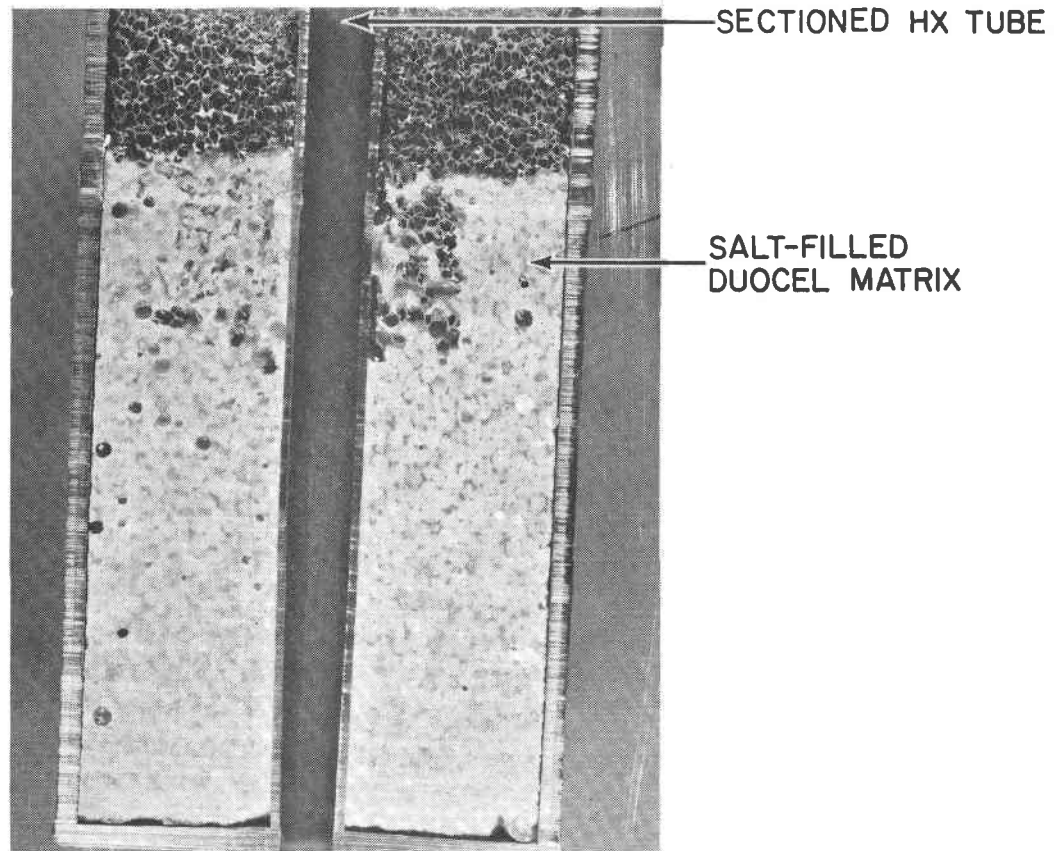
B80010252

Figure 56. (Li-Na-K)<sub>2</sub>CO<sub>3</sub> (32-33-35 wt %) DISCHARGE PROFILE WITHOUT AND WITH DUOCEL TCE MATERIAL



A80010246

Figure 57. COMPARISON OF (Li-Na-K)<sub>2</sub>CO<sub>3</sub> DISCHARGE HEAT FLUX PERFORMANCE WITHOUT AND WITH CONDUCTIVITY ENHANCEMENT



P80010073

Figure 58. LONGITUDINAL CROSS SECTION THROUGH MODULE L3-1 AND L3-2  
(Li-Na-K)<sub>2</sub>CO<sub>3</sub> (32-33-35 wt %) AFTER 816 HOURS AND 32 CYCLES

81.3 wt % Na<sub>2</sub>CO<sub>3</sub> - 18.7 wt % K<sub>2</sub>CO<sub>3</sub> (Module L1-3). It has been determined from previous TES work performed at IGT<sup>16</sup> that heat transfer resistance in the PCM is the major TES performance-limiting factor. This effect, which results from the low thermal conductivity in the solid phase, reduces the heat flux through the solid PCM that forms on the salt-side heat-transfer surface. It is the primary limitation to using a passive HX in the TES system. With these problems in mind, this particular (Na-K)<sub>2</sub>CO<sub>3</sub> system was chosen as the third TCE concept to evaluate. From this system's phase diagram, a mixture of 85-15 mol % Na<sub>2</sub>CO<sub>3</sub>-K<sub>2</sub>CO<sub>3</sub> appeared to represent a system that would solidify incongruently over the range 790° to 740°C (1454° to 1364°F) upon discharging.

It was considered that such incongruent solidification could result in a "slush-type" salt behavior, perhaps eliminating the formation of a continuous crust of solid salt on the HX surface. In this way, heat transfer could be enhanced by convection in the remaining dispersed liquid phase.

To this end, 821 grams (1.8 lb) of this salt mixture was loaded and run as both a prospective high-temperature solar-thermal TES medium and TCE material. Examination of the salt temperature profile as a function of time (Figure 59) reveals that no actual thermal arrest occurs in the temperature range 790 to 740°C (1454° to 1364°F); instead, two slight inflection points are exhibited in this area. This apparent behavior is consistent with the incongruent character of the published phase diagram.

Also, from Run 21 (Figure 60), the average heat flux of 48,375 W/m<sup>2</sup> (15,345 Btu/hr-ft<sup>2</sup>) was calculated. This represents a 31% increase in heat flux to the air working fluid by this mixture over that of Module L1-1, containing 50-50 wt % Na<sub>2</sub>CO<sub>3</sub>-K<sub>3</sub>CO<sub>3</sub> over the same "working cycle." Also, throughout its experimental life, this system's performance was consistent and stable.

This salt system was subjected to prolonged cycling of 38 charge/discharge runs and 1032 hours at operating temperatures of 813 to 713°C (1495° to 1315°F), with no system failures or salt leakages. After a forced cooldown at 5.1 m<sup>3</sup>/hr (180 ft<sup>3</sup>/hr), the cannister was sectioned at mid-salt.

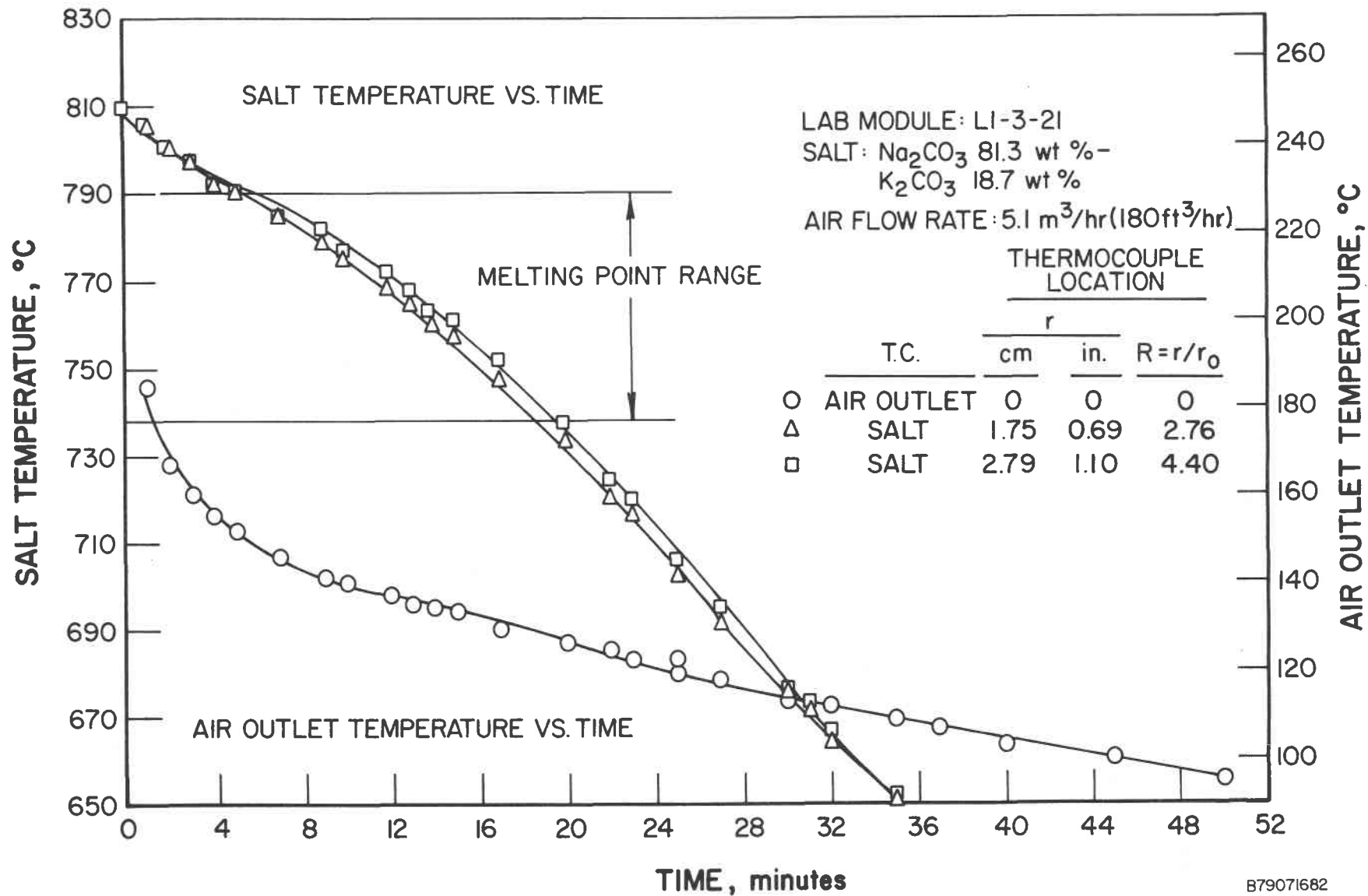
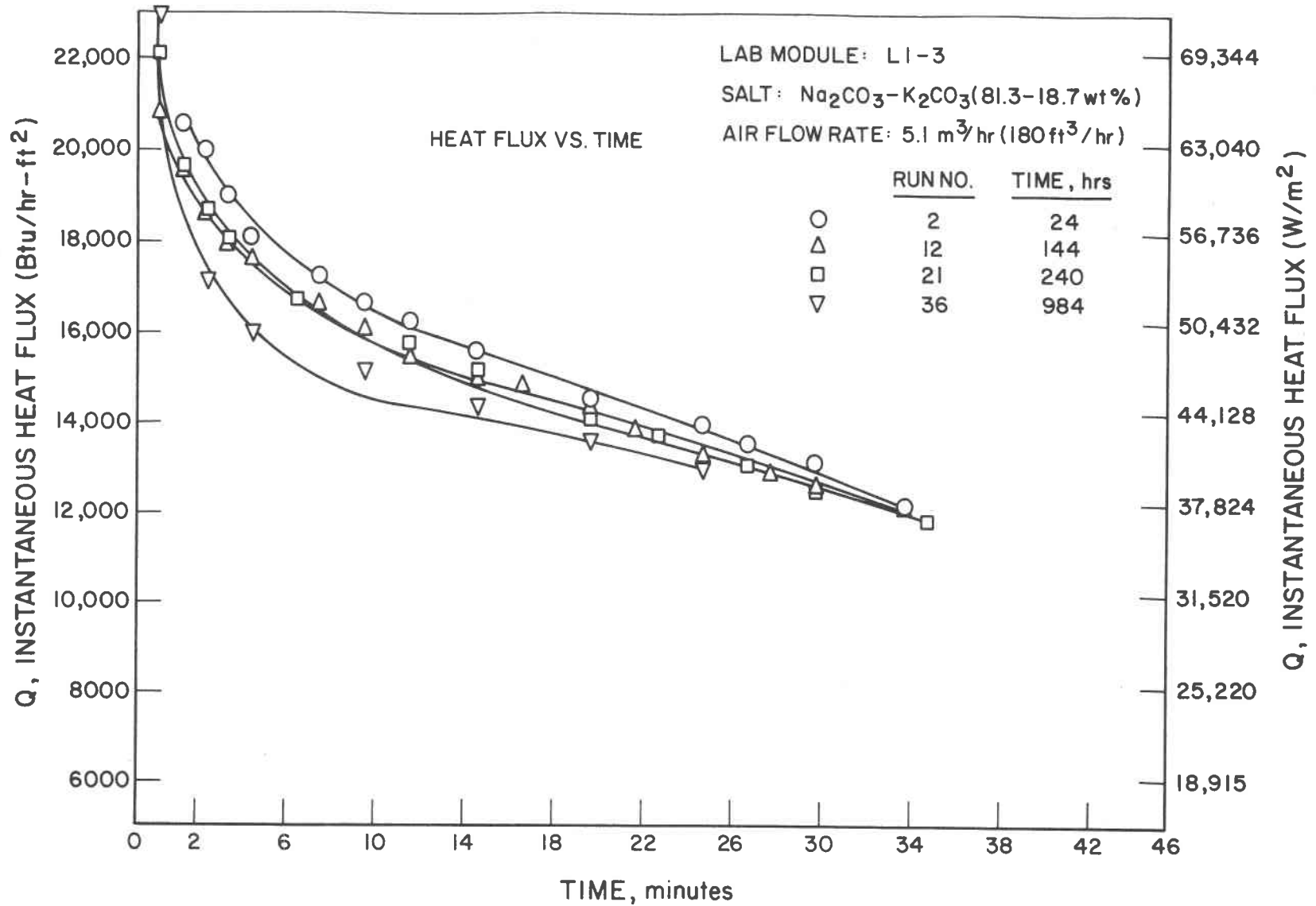


Figure 59. TYPICAL DISCHARGE PERFORMANCE OF (Na-K)<sub>2</sub>CO<sub>3</sub> SLUSH  
AT 5.1 m<sup>3</sup>/hr (180 ft<sup>3</sup>/hr) AIR FLOW RATE



879122715

Figure 60. LIFETIME DISCHARGE HEAT FLUX OF (Na-K)<sub>2</sub>CO<sub>3</sub> SLUSH

Some interesting observations come to light when this salt's crystal patterns (Figure 61) are compared to the solidified surface of the similarly cooled  $\text{Na}_2\text{CO}_3\text{-BaCO}_3$  congruently melting eutectic of Module L3-3. Rather than the pattern of crystals indicative of rapid cooling (Figure 47), one encounters unoriented crystals of similar size and geometry occurring from the HX tube to the can inside-diameter.

In view of these facts, the thermal conductivity enhancing "slush" behavior of the  $(\text{Na-K})_2\text{CO}_3$  mixture is notably confirmed by the —

- Absence of thermal arrest in its salt temperature discharge profile
- Incongruent solidification patterns
- 31% increase in average heat flux over the 50-50 wt % congruently melting  $(\text{Na-K})_2\text{CO}_3$  eutectic.

The post-test chemical analysis of this salt, which revealed no decomposition after 1032 hours and little corrosion, is summarized in Table 22.

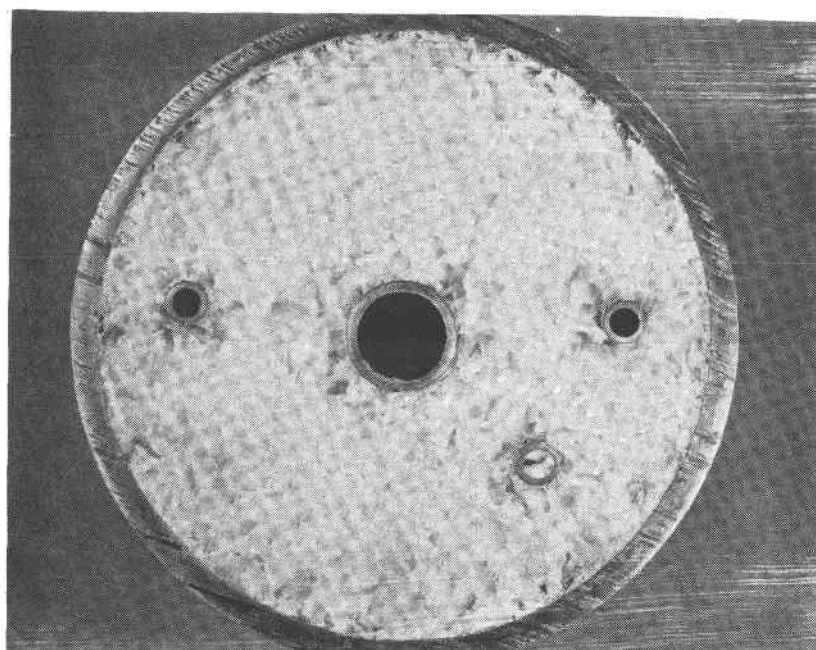
Table 22.  $(\text{Na-K})_2\text{CO}_3$  81.3-18.7 wt % "SLUSH" PRE- AND POST-TEST CHEMICAL ANALYSIS

Chemical Analysis, Wt %	<u>Na</u>	<u>K</u>	<u>CO<sub>3</sub></u>	<u>Fe</u>	<u>Cr</u>	<u>Ni</u>
Pre-Test	35.27	10.58	54.16	<0.01	<0.01	<0.01
Post-Test (r = 0.23 in.)	35.16	10.02	54.59	0.05	<0.01	<0.01
(r = 0.68 in.)	35.00	11.65	55.35	0.02	<0.01	<0.01
(r = 0.95 in.)	35.07	11.99	55.15	0.01	<0.01	<0.01

#### Techno-Economic Considerations of TCE Materials

When considering the feasibility of TCE concepts, one must evaluate both the technical and economic aspects of the problem, that is, the cost/performance trade-offs. In costing an actual TES subsystem, the major component costs to be considered include —

- Salt PCM
- Containment and HX materials
- Fabrication and assembly



P80010074

Figure 61. TRANSVERSE CROSS SECTION THROUGH  
MODULE L1-3 81.3 wt %  $\text{Na}_2\text{CO}_3$  - 18.7 wt %  $\text{K}_2\text{CO}_3$   
AFTER 1032 HOURS AND 38 CYCLES

- Insulation
- Instrumentation and controls
- TCE materials or active HX system.

Economic analyses indicate that TES subsystem costs are dominated by salt and containment/HX costs. Yet the overall subsystem cost may be either salt-cost intensive or HX-cost intensive, depending on the application's duty requirements, which dictate selection of salt properties and HX configuration. Although TCE materials do indeed add an incremental cost, such an approach may reduce the required heat transfer area in HX-cost-intensive cases enough to result in a net decrease in total TES subsystem cost by reducing HX materials and fabrication costs. Other items to consider when one is selecting TCE materials and designing subsystems are the sensible heat storage capability added to the subsystem and the nominal increase in required TES volume caused by displacement of salt and its latent heat.

#### Conductivity Enhancement Factor

The most practical porous aluminum densities for TES application are in the range of 5% to 20% of theoretical density (i.e., 0.95 to 0.80 volume fraction porosity). In this range, the porosity is essentially completely interconnected, so that both the salt and aluminum enhancement form continuous phases throughout each segment of the TES. To a first approximation, then, the effective thermal conductivity of the two-phase mixture can be expressed as -

$$k_{\text{eff}} = f_s k_s + f_{\text{Al}} k_{\text{Al}} = (1 - f_{\text{Al}}) k_s + f_{\text{Al}} k_{\text{Al}} \quad (32)$$

where -

$f_{\text{Al}}$  = volume fraction of aluminum enhancement material

$f_s$  = volume fraction of salt

$k_{\text{Al}}$  = thermal conductivity of aluminum enhancement material at theoretical density

$k_s$  = thermal conductivity of solid salt.

The manufacturers of the Duocel material experimentally measured the thermal conductivity of porous aluminum as a function of density and obtained the solid curve shown in Figure 62. This curve can be compared with the calculated dashed curve, which is based on Equation 32 and neglects any contribution to conductivity by the air in the pores. In the high-porosity range investigated, the term  $(f_{Al} k_{Al})$  overpredicts the actual conductivity of the porous aluminum. Correcting for the difference between measured and calculated values, Equation 32 can be modified to —

$$k_{eff} = (1-f_{Al})k_s + 0.56 f_{Al} k_{Al} \quad (33)$$

A thermal conductivity enhancement factor,  $F$ , was defined as the ratio of effective conductivity of the solid salt/porous aluminum composite material to the conductivity of solid salt alone, as shown in Equation 34:

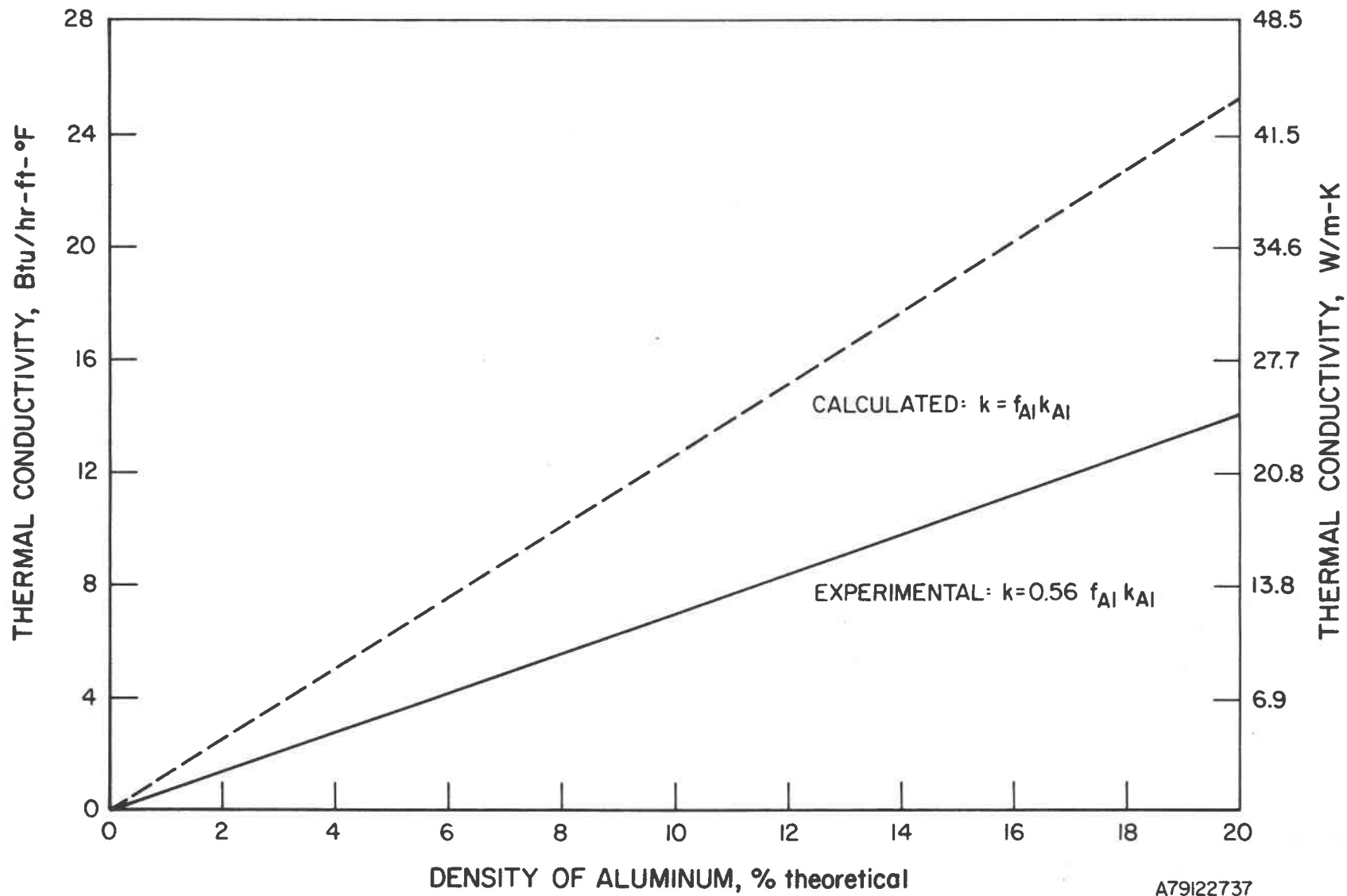
$$F = \frac{k_{eff}}{k_s} = \frac{(1-f_{Al})k_s + 0.56 f_{Al} k_{Al}}{k_s} \quad (34)$$

Equation 33 was used to calculate values of  $k_{eff}$  for a series of assumed values of  $k_s$  and  $f_{Al}$ , and the results appear in Figure 63. For salts having  $k_s$  values in the range of 0.87 to 8.65 W/m-K (0.5 to 5 Btu/hr-ft-°F), use of a high porosity aluminum enhancement material would be expected to result in an increase in  $k_{eff}$ , corresponding to approximately 1.12 W/m-K (0.65 Btu/hr-ft-°F) for each percent of theoretical density of the aluminum used. For a given aluminum density, however, the largest degree of enhancement (larger  $F$ ) is realized for salts of lowest conductivity.

#### Cost, Performance and Design Implications

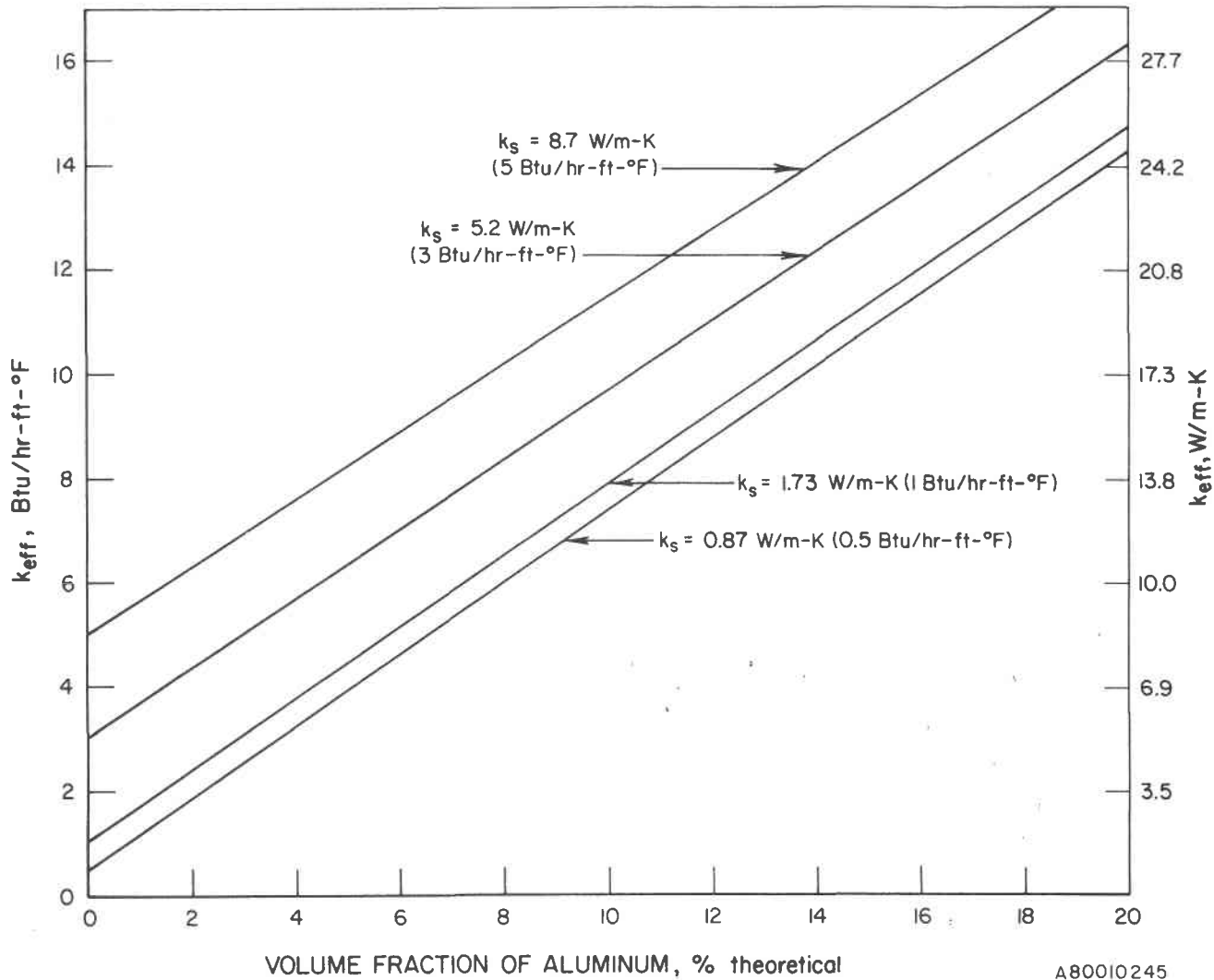
Use of a TCE material will impact on an actual TES system in several areas that must be evaluated:

- Increase in the effective thermal conductivity,  $k_{eff}$ , through the solid salt layer
- Decrease in the required HX surface area
- Supplement of sensible heat storage capacity to the TES system
- Increase in required system volume, a result of displacement of the salt
- Increase in capital costs associated with TCE medium.



A79I22737

Figure 62. THERMAL CONDUCTIVITY OF POROUS ALUMINUM DUOCEL MATERIAL



A80010245

Figure 63. EFFECTIVE THERMAL CONDUCTIVITY OF POROUS ALUMINUM/SALT COMPOSITE MATERIAL (Calculated From Equation 33)

Additional costs are undeniably associated with any enhancement material. It must be realized that certain counterbalancing trade-offs do exist: the increased  $k_{\text{eff}}$  will also lead to a need for less HX area. This may significantly offset the cost of enhancement when the net TCE cost is viewed as being approximately equal to the cost of enhancement material minus the cost of savings of reduced HX area, considering the salt storage volume displaced by TCE is negligible.

As a first-cut estimate of the performance-cost trade-offs involved in the use of conductivity enhancement materials, it is useful to consider the relationship between the enhancement factor,  $F$  ( $F = k_{\text{eff}}/k_s$ ), and the capital cost of the materials.  $F$  factors based upon the curves of Figure 63 have been calculated and are plotted in Figure 64 as the ratio of enhancement factor to unit price,  $F:\$/\text{m}^3$  ( $F:\$/\text{ft}^3$ ), as a function of percent theoretical density of aluminum for a range of assumed  $k_s$  values. These curves are based on a theoretical density of aluminum of  $2,712 \text{ kg}/\text{m}^3$  ( $169.3 \text{ lb}/\text{ft}^3$ ) and an estimated bulk-quantity cost for the fabricated porous aluminum structure of twice the raw material cost [i.e.,  $2 \times \$1.1/\text{kg}$  ( $\$0.50/\text{lb}$ ); see Figure 65 for assumed cost versus density]. As expected, the enhancement factor-to-cost ratio decreases with increasing  $k_s$  values. It also decreases somewhat with increasing aluminum density, although this trend mostly reflects the assumed shape of the cost versus density curve, shown in Figure 65.

The effect of an enhancement material on performance is best shown through use of the heat transfer model based on Megerlin's solution to the moving boundary problem.<sup>24</sup>

Parametric curves previously derived for the engineering-scale units, which contain  $\text{LiKCO}_3$  and are cooled by high-velocity ambient air, are shown in Figure 66. These curves show dimensionless time ( $N_{\text{FO}}$ ) required to solidify the  $\text{LiKCO}_3$  salt of Engineering Unit 2 to a dimensionless thickness ( $R-1$ ). For these units,  $N_{\text{ph}} = 0.57$  and  $N_{\text{Bi}} = 0.76$ , in the absence of any conductivity enhancement. Approximately 5 hours are required to discharge these units; this time corresponds to  $N_{\text{FO}} = 20.7$  before correcting for removal of superheat prior to the start of solidification. Such a discharge results in a solid salt layer of reduced thickness,  $R-1 = 3.7$ , and appears as Case IV in Figure 66 for  $k_s = 2.25 \text{ W}/\text{m}\cdot\text{K}$  ( $1.3 \text{ Btu}/\text{hr}\cdot\text{ft}\cdot^\circ\text{F}$ ). But if porous aluminum

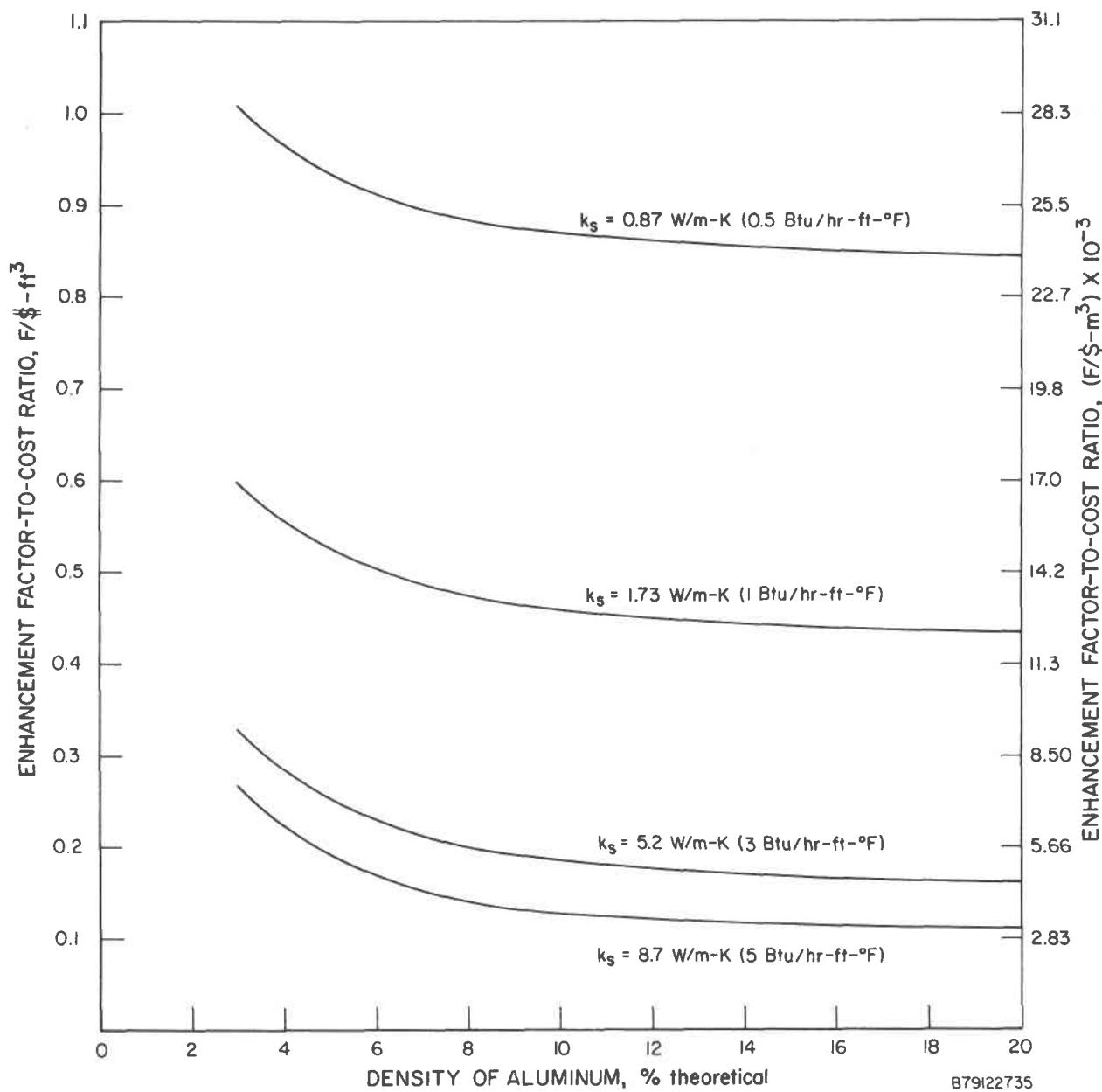


Figure 64. ENHANCEMENT FACTOR-TO-COST RATIO VERSUS DENSITY OF POROUS ALUMINUM FOR SEVERAL ASSUMED VALUES OF  $k_s$

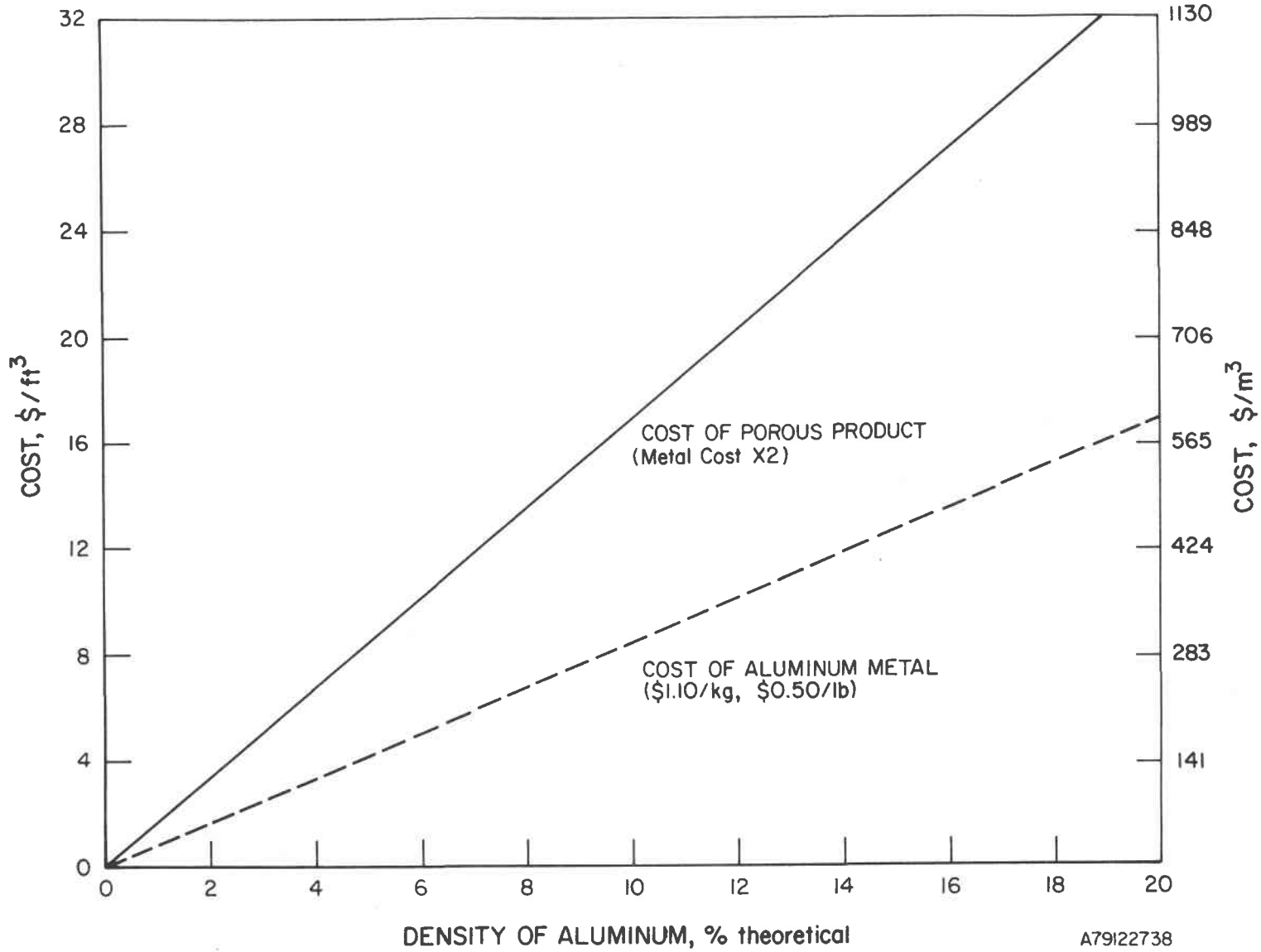
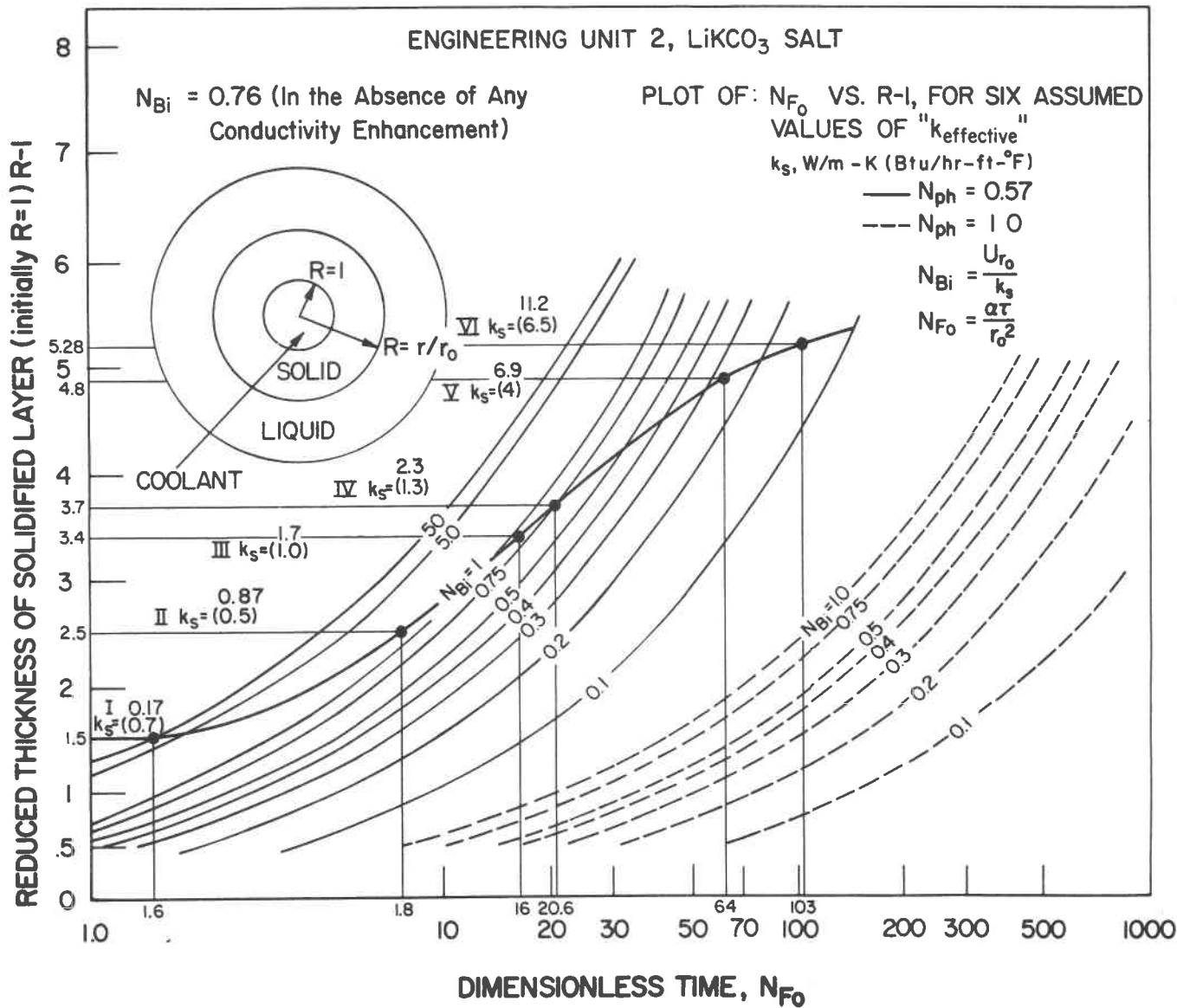


Figure 65. ASSUMED COST OF POROUS ALUMINUM ENHANCEMENT MATERIAL

A79I22738



B80010255

Figure 66. KINETICS OF SOLIDIFICATION OF ANNULAR PCM LAYER FROM WITHIN

enhancement of 8% density were introduced into the system,  $k_{eff}$  would be expected (by Equation 33) to increase from 2.25 W/m-K (1.3 Btu/hr-ft-°F) ( $k_s$  for solid  $LiKCO_3$  without enhancement) to 11.2 W/m-K (6.5 Btu/hr-ft-°F), and an F-factor of 5 (Case VI). Figure 66 also shows that the parameters  $N_{Bi}$  and  $N_{Fo}$  have different dependences on  $k_{eff}$ :

$$N_{Bi} \propto \frac{1}{k_{eff}}$$

and

$$N_{Fo} \propto k_{eff}$$

so that now  $N_{Bi} = 0.15$  and  $N_{Fo} = 103$ . As indicated, this 5-hour discharge with an enhancement factor of 5 would allow solidification of a layer of thickness  $R-1 = 5.3$ . With the relative solidified volume being proportional to  $r^2$  (from  $R = r/r_o$ ,  $r_o = 1$  in.), the enhancement material could increase the average heat flux so that approximately twice (1.8 X) the salt volume could be solidified in the same time. In a large TES unit with multiple HX's, this is equivalent to reducing the required HX surface area by a factor of two, and it results in corresponding cost reductions.

Because of this potential for increasing the thermal performance and/or decreasing the cost of TES substyems by incorporating TCE materials, it becomes apparent that an extensive search for and evaluation of such materials for use in molten carbonate environments should be extended to the 700° to 870°C (1300° to 1600°F) solar-thermal regime.

## 2.4 Conceptual Design of TES Module for Solar-Thermal Power System

### Use of the Heat Transfer Model in Large-Scale TES Solar-Thermal Power System

#### Introduction

The phase-change heat-transfer model developed by Megerlin and modified during our previous TES program at IGT can also be used in large-scale system design.<sup>16</sup> The existing model can be used to determine the thickness of solidified salt around a cylindrical internal HX tube that carries a working fluid as a function of the time it has cooled from its mp. This solidification is measured in terms of the radius of the internal well.

For a conceptual system design that has a large molten salt bath with a number of pipes parallel to each other in a well-formed matrix, carrying the working fluid through the salt bath, the model will determine the pipe spacing, the number of pipes required, and the length needed (given the pipe radius) for a particular storage requirement. Thus, the energy discharged from a unit is related to the physical design of the system, allowing a balance between the energy required by the working fluid and the energy that is discharged as a result of the system design.

TES Sub-System for Large-Scale Solar-Thermal Power Plant (Air Fluid)

The heat transfer model has been applied to the scale-up design of a storage sub-system of a central-receiver solar-thermal power-plant that utilizes a high-temperature Brayton cycle with high-temperature, high-pressure air as the heat transport fluid.

Such a central-receiver solar power-plant concept has been proposed by Boeing,<sup>26</sup> utilizing a high-temperature, closed, Brayton-cycle thermal engine, with helium or air as the heat transport fluid. Figure 67 is an overall view of the central receiver and heliostat field, with the power plant and storage subsystem at the base of the receiver tower.

Figure 68 illustrates a solar-thermal power plant schematic incorporating the TES unit. The primary flow circuit from the receiver is through the turbine(s), the recuperator (low-pressure side), the precooler, the compressor(s), the recuperator (high-pressure side), and back to the receiver. The alternative thermal-energy storage loop extends solar-plant electrical-power production into non-insolation hours. The resultant phase-change TES conceptual design is summarized in Figure 69. The phase-change medium is contained in an insulated underground vessel. The working fluid is channeled through the specified design number of straight superalloy tubes and collected by manifolds at the top and bottom of the vertical vessel. The carbonate salt can then be contained as a bath immersing the HX tubes. The vertical flow arrangement, with the hot working fluid entering the top manifold during charging and the cold fluid entering the bottom manifold during discharging, will maintain the solidified salt below the liquified portion. This arrangement will provide for unrestrained volume expansion during salt melting, reducing stresses on the system containment and HX tubes.

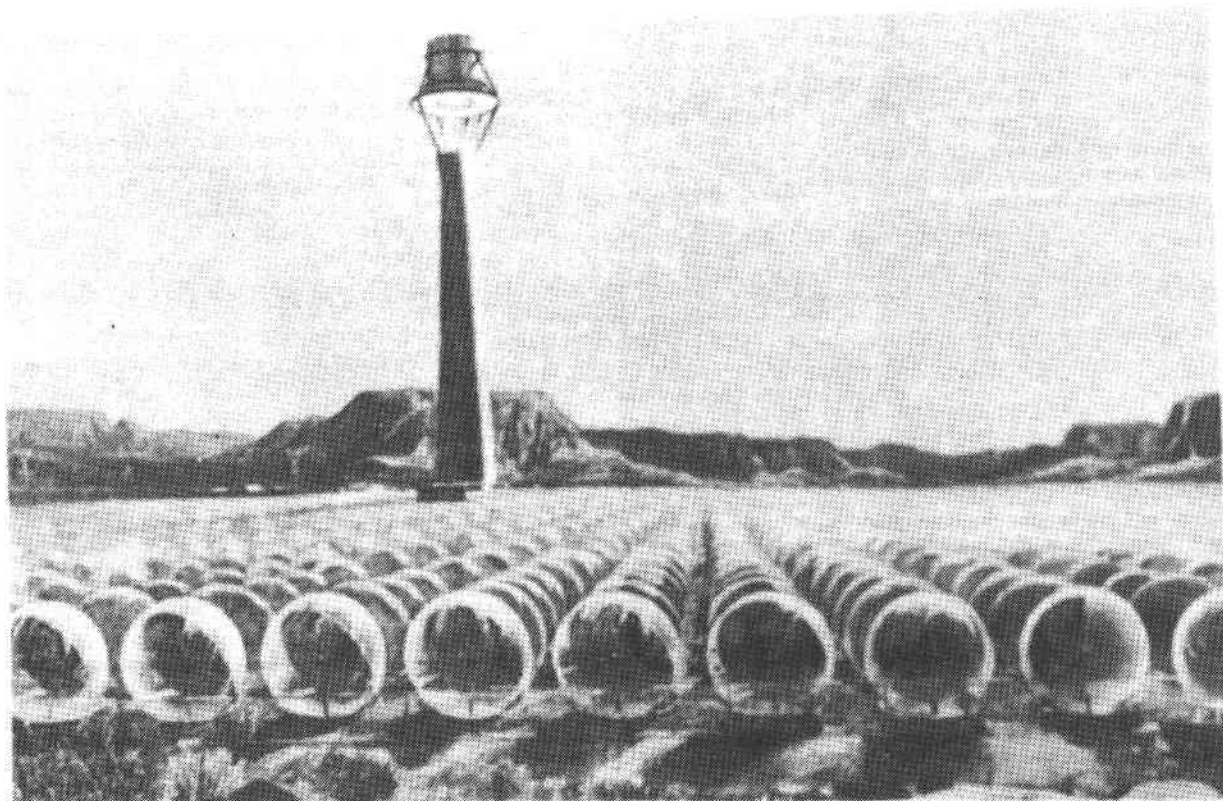
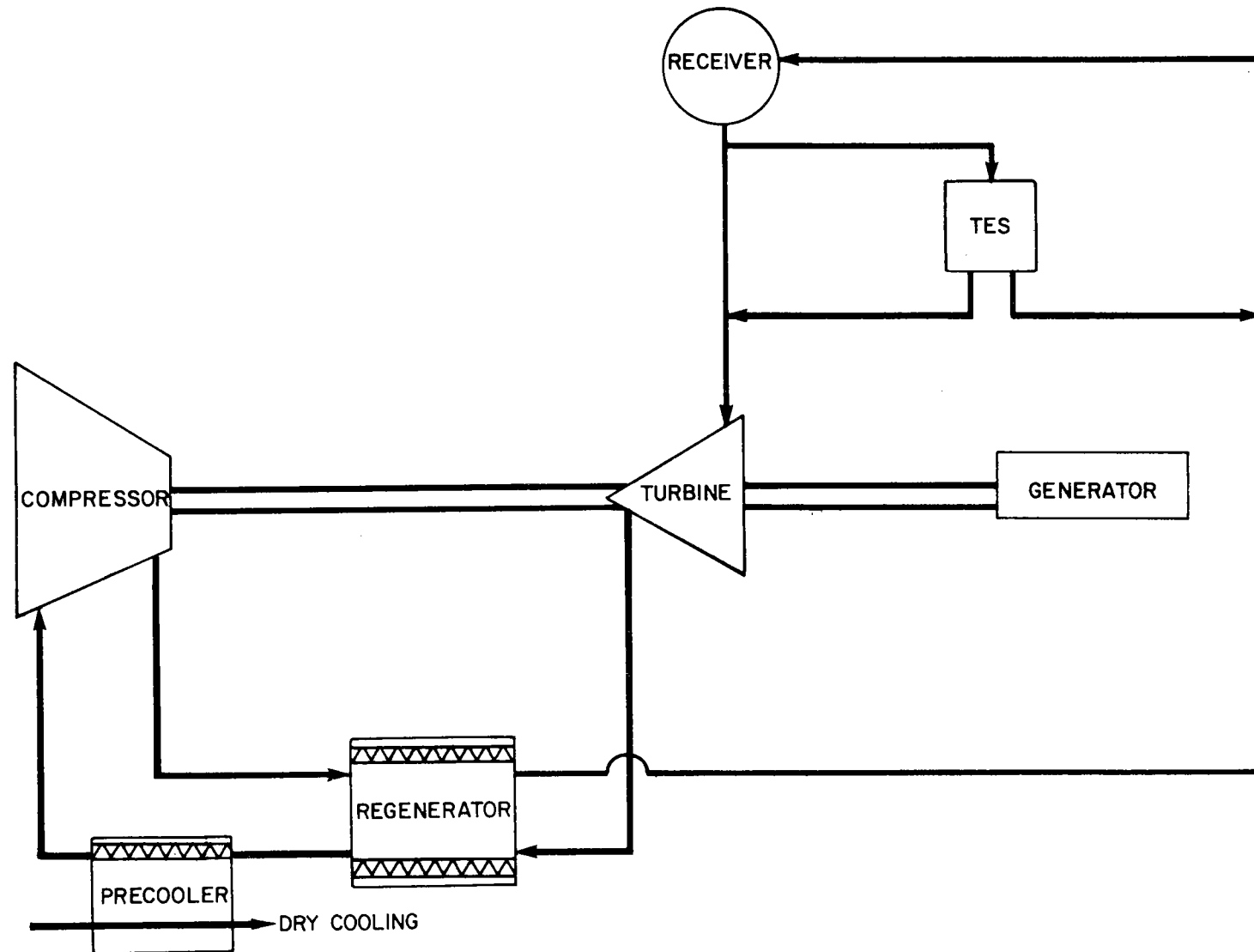
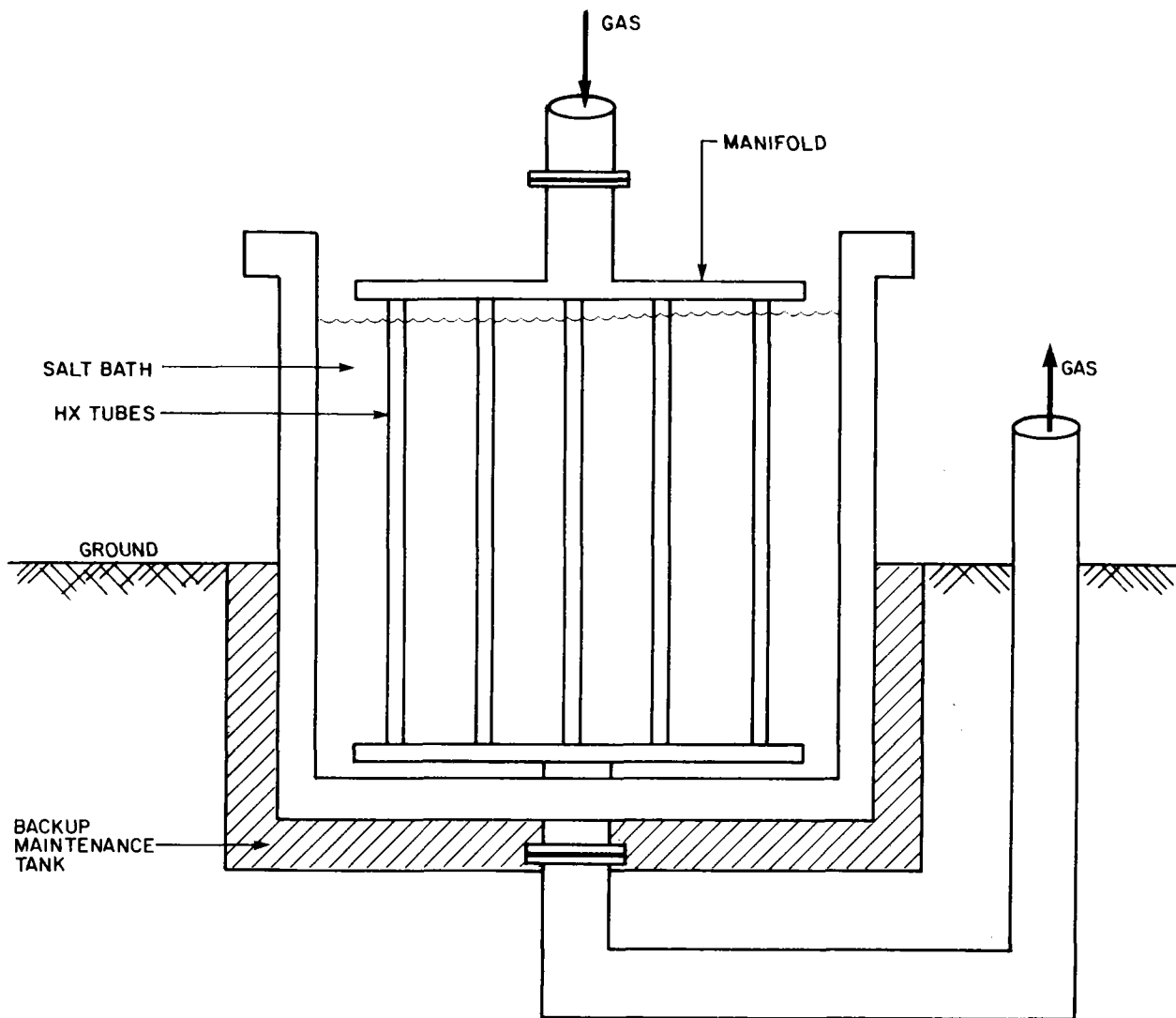


Figure 67. CENTRAL RECEIVER SOLAR POWER PLANT CONCEPT<sup>26</sup>



A79122779

Figure 68. STORAGE/PLANT SCHEMATIC<sup>26</sup>



A79122780

Figure 69. PHASE-CHANGE TES CONCEPT

The system is designed to deliver  $50 \text{ MW}_{\text{th}}$  over a 6-hour period, thus requiring a system capacity of  $1.08 \times 10^{12} \text{ J}$  ( $1.02 \times 10^9 \text{ Btu}$ ).

Conceptual design of the TES subsystem is based on use of pure  $\text{Li}_2\text{CO}_3$  (mp of  $723^\circ\text{C}$ ,  $1333^\circ\text{F}$ ) as the PCM for the purpose of heating the 3.45 MPa (500 psia) air from  $538^\circ\text{C}$  ( $1000^\circ\text{F}$ ) at the inlet to  $704^\circ\text{C}$  ( $1300^\circ\text{F}$ ) at the outlet.

For a  $50 \text{ MW}_{\text{th}}$  TES delivery, the air flow rate then must be —

$$\begin{aligned} \dot{m}_f &= 50 \text{ MW} \times (1.08 \times 10^{19} \text{ J/MW}) \left( \frac{1}{6\text{hr}} \right) (1/1.87 \times 10^5 \text{ J/kg}) = \\ &= 9.66 \times 10^5 \text{ kg/hr} = 2.13 \times 10^6 \text{ lb}_m/\text{hr} \end{aligned} \quad (35)$$

Also, from the thermal capacity —

$$\begin{aligned} m_s &= (1.08 \times 10^{12} \text{ J}) (1/6.07 \times 10^5 \text{ J/kg}) \\ &= 1.78 \times 10^6 \text{ kg} = 3.93 \times 10^6 \text{ lb}_m \end{aligned} \quad (36)$$

of salt (heat of fusion only) are required for storage. The volume of salt that must then be solidified (using the room temperature density for a first approximation) is —

$$V_s = (1.78 \times 10^6 \text{ kg}) / (2108 \text{ kg/m}^3) = 843.8 \text{ m}^3 = 2.98 \times 10^4 \text{ ft}^3 \quad (37)$$

This now determines the "fixed volume" requirement that the heat transfer model will be applied to solve. The phase-change number determined for a mean air temperature of  $621^\circ\text{C}$  ( $1150^\circ\text{F}$ ) is —

$$N_{ph} = \frac{(\Delta H_f)(\rho_k)}{C_{p(s)}(t_m - t_a)\rho_s} = 1.94 \approx 2 \quad (38)$$

where

$$\begin{aligned}\Delta H_f &= 6.07 \times 10^5 \text{ J/kg (261 Btu/lb}_m\text{)} \\ \rho_l &= 1834.1 \text{ kg/m}^3 \text{ (114.5 lb/ft}^3\text{)} \\ \rho_s &= 2108 \text{ kg/m}^3 \text{ (131.6 lb/ft}^3\text{)} \\ C_{p(s)} &= 2625.1 \text{ J/kg-K (0.627 Btu/lb-}^\circ\text{F)} \\ t_m &= \text{melting point temperature} = 723^\circ\text{C (1333}^\circ\text{F)} \\ t_a &= \text{mean air temperature} = 621.1^\circ\text{C (1150}^\circ\text{F)}\end{aligned}$$

The Megerlin plots for  $N_{ph} = 2$  and a range of Biot numbers appear in Figure 70.

In this example, pipes 3.81 cm (1.5 in.) in diameter were chosen; the number of pipes required, their spacing, and their length had to be determined. The Fourier number corresponding to a 1.9 cm (0.75 in.) radius and 6-hour discharge time ( $\tau$ ) is -

$$N_{Fo} = \frac{\alpha \tau}{r_o^2} = 15.67 \quad (39)$$

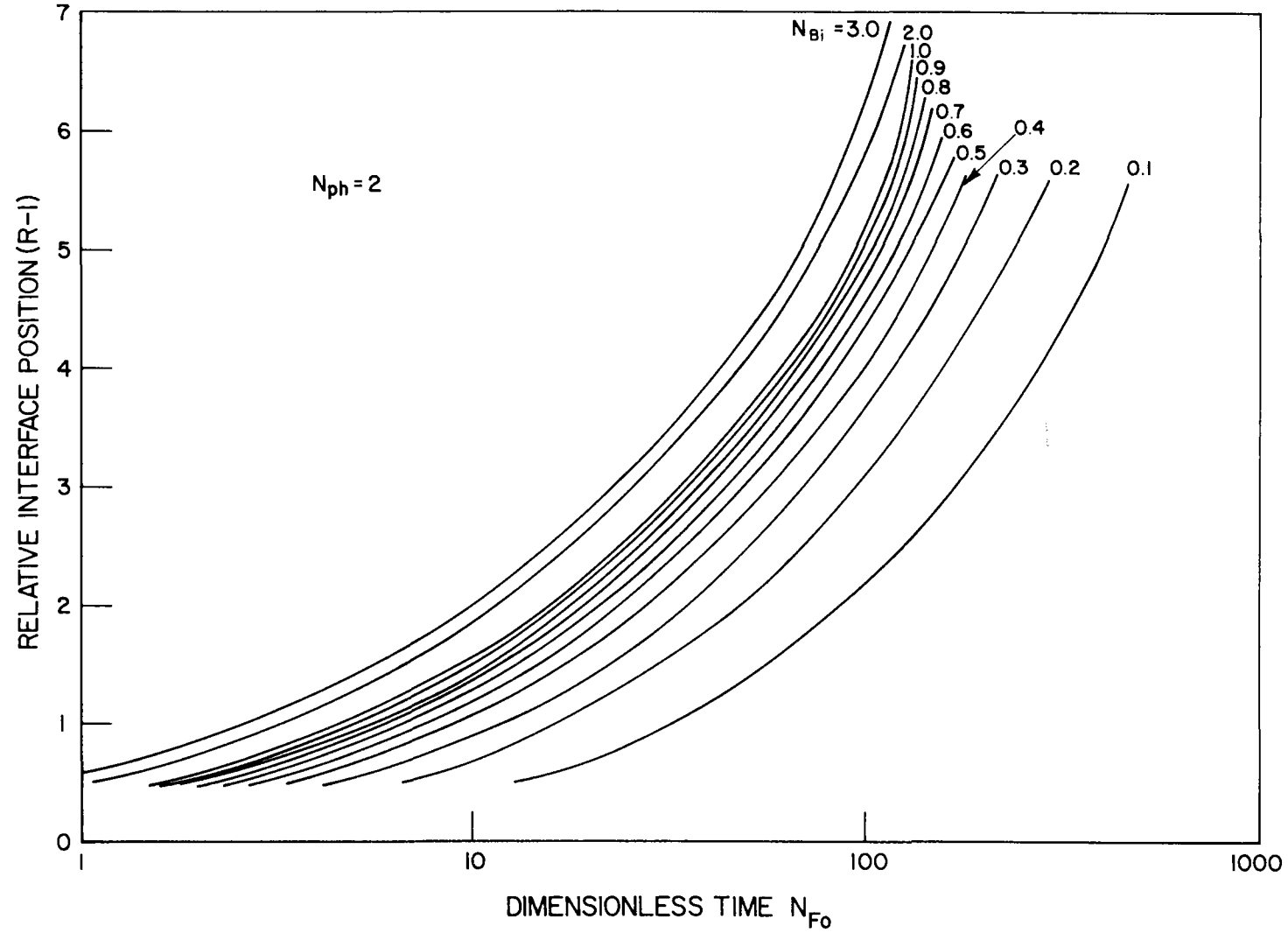
$$\text{where } \alpha = \frac{k}{c_p \rho_s}$$

Given the pipe diameter, ( $d = 3.81 \text{ cm, } 1.5 \text{ in.}$ )  $2r_o$ , the Biot number  $N_{Bi}$  is specified for using the Megerlin plots in Figure 70 to determine  $r_1$ , which will yield the thickness of solidified salt ( $r_1 - r_o$ ) and the pipe spacing ( $2r_1$ ). The pipe length is determined from the fixed volume requirement -

$$\begin{aligned}L_1 &= \frac{V_s}{(r_1^2 - r_o^2) n\pi} = 43.8 \text{ m}^3 / (r_1^2 - r_o^2) n\pi \\ &= [2.98 \times 10^4 \text{ ft}^3 / (r_1^2 - r_o^2) n\pi]\end{aligned} \quad (40)$$

With the Biot number being given by -

$$N_{Bi} = \frac{h_f r_o}{k_s} \quad (41)$$



A78030706

Figure 70. MEGERLIN PLOTS FOR DETERMINING SOLIDIFIED PCM THICKNESS

an expression for the air-side heat transfer coefficient,  $h_f$ , must be derived. In general, one may assume fully turbulent flow in the air tubes. This assumption thus permits use of the Nusselt equation -

$$N_{Nu} = 0.023 N_{Re}^{0.8} N_{Pr}^{0.2} = \frac{h_f d}{k_f} \quad (42)$$

to derive the expression for  $h_f$ . Solving Equation 42 for  $h_f$  yields -

$$h_f = \left[ 0.02 N_{Pr}^{0.2} k_f \right] \left[ \frac{\dot{m}_f}{\pi \mu_f} \right]^{0.8} (r_o^{-1.8}) (n^{-0.8}) \quad (43)$$

where  $n$  = number of pipes with radius  $r_o$ . Substituting into Equation 43 the appropriate properties for air at 621°C (1150°F) and 3.45 MPA (500 psia), while setting  $r_o = 1.9$  cm (0.75 in.) and  $\dot{m}_f = 9.66 \times 10^5$  kg/hr ( $2.13 \times 10^6$  lb<sub>m</sub>/hr) yields -

$$h_f = 47,363/n^{0.8} (\text{W/m-K}) \quad [27,366/n^{0.8} (\text{Btu/hr-ft } ^\circ\text{F})] \quad (44)$$

It can be seen from Equation 44 that  $L_1$  and  $r_1$  are both dependent on the number of pipes to be used. The pipe length,  $L_1$ , can be determined for any number of pipes by selecting  $n$  and calculating  $h_f$  from Equation 44, determining  $N_{Bi}$  and using it to find  $r_1$  from the Megerlin plots, then substituting  $r_1$  and  $n$  into Equation 40, and solving for  $L_1$ .

When one has calculated a pipe length consistent with a given number of tubes,  $n$ , that are sufficient to remove the heat from the salt volume, he must consider if sufficient heat-transfer surface is present to heat the air to the required outlet temperature.

Assuming that the PCM remains at its melting point, the enthalpy change in the air working fluid as it progresses through the pipe is described by -

$$\frac{\dot{m}_f C_{pf}}{n \pi d} \frac{dt}{dL} = h_f (t_m - t) = h_f (726^\circ\text{C} - t) \quad [h_f (1338.8^\circ\text{F} - t)] \quad (45)$$

Rearranging Equation 45, integrating, and evaluating [given that at  $L = 0$ ,  $t = 538^\circ\text{C}$  ( $1000^\circ\text{F}$ ), and at  $L = L_2$ ,  $t = 704^\circ\text{C}$  ( $1300^\circ\text{F}$ )], leads to -

$$L_2 = 1.838 \frac{\dot{m}_f C_{Pf}}{n \pi h_f d} \quad (46)$$

The total heat transfer requirement will be satisfied when  $n$  is chosen so that  $L_1 = L_2$ , thus meeting both the fixed-volume and air-temperature requirements.

The solution is obtained graphically by using Equations 40, 44, and 46, and the Megerlin plots of Figure 70 to derive Table 23.

The values of  $L_1$  and  $L_2$  are shown as a function of  $n$  in Figure 71. The intersection of the two curves, representing the design solution, occurs at  $n = 52,000$  and  $L_1 = L_2 = 3.38$  m (11.1 ft). This design operates with  $h_f = 7.96$  W/m-K (4.6 Btu/hr-ft<sup>2</sup>-°F) and  $r_1 = 4.34$  cm (1.71 in.). Therefore, the design conditions for the TES operation can be met by solidifying  $1.8 \times 10^6$  kg (3.9 million lb) of  $\text{Li}_2\text{CO}_3$  cylindrically around 52,000 pipes, 3.81 cm (1.5 in.) in diameter and 3.38 m (11.1 ft) long, spaced 8.7 cm (3.42 in.) apart, over a 6-hour period. A top view of this TES subsystem, with hexagonally arrayed tubes, appears in Figure 72. As a final check, the total area open to air flow is -

$$\begin{aligned} A &= n\pi r_o^2 = (52,000) (\pi) \left(\frac{1.9}{100}\right)^2 = 59.3 \text{ m}^2 \\ &= (52,000) (\pi) \left(\frac{0.75}{12}\right)^2 = 638.1 \text{ ft}^2 \end{aligned} \quad (47)$$

The linear air velocity is -

$$\begin{aligned} v &= \frac{(9.66 \times 10^5 \text{ kg/hr}) (\text{hr}/3600 \text{ sec}) (0.0699 \text{ m}^3/\text{kg})}{59.3 \text{ m}^2} = 0.32 \text{ m/sec} \\ &= \frac{(2.13 \times 10^6 \text{ lb/hr}) (\text{hr}/3600 \text{ sec}) (1.12 \text{ ft}^3/\text{lb})}{638.1 \text{ ft}^2} = 1.04 \text{ ft/sec} \end{aligned} \quad (48)$$

Where the specific volume of air at 3.45 MPa (500 psia),  $621^\circ\text{C}$  ( $1150^\circ\text{F}$ ) is  $0.0699$  m<sup>3</sup>/kg (1.12 ft<sup>3</sup>/lb), the Reynolds number is -

$$\begin{aligned} N_{Re} &= dv\rho_f/\mu_f n = \frac{(1.5/12 \text{ ft})(1.04 \text{ ft/sec})(0.891 \text{ lb/ft}^3)(3600 \text{ sec/hr})}{0.0466 \text{ lb/ft-hr}} \\ &= 4.65 \times 10^8/n = 8,945 \quad (n = 52,000) \end{aligned} \quad (49)$$

Table 23. DESIGN PARAMETERS FOR AIR UPGRADING, USING  $\text{Li}_2\text{CO}_3$  AS THE PCM\*

	n	$h_f$		$N_{Bi}$	$r_2$		$L_1,$ Salt Volume Requirement		$L_2,$ Air Temperature Requirement	
		$\text{W/m}^2\text{-K}$	$\text{Btu/hr-ft}^2\text{-}^\circ\text{F}$		cm	in.	m	ft	m	ft
1.	20,000	56.2	9.90	0.734	5.30	2.10	5.55	18.20	4.08	13.40
2.	25,000	47.1	8.30	0.61	5.16	2.03	4.69	15.40	3.90	12.80
3.	30,000	40.9	7.20	0.53	4.90	1.93	4.39	14.40	3.75	12.30
4.	35,000	35.8	6.30	0.47	4.70	1.85	4.15	13.60	3.64	11.95
5.	40,000	32.3	5.70	0.42	4.62	1.82	3.78	12.40	3.55	11.64
6.	45,000	29.5	5.20	0.38	4.50	1.77	3.61	11.84	3.47	11.37
7.	50,000	27.0	4.76	0.35	4.38	1.73	3.45	11.32	3.39	11.13
8.	52,000	26.2	4.61	0.34	4.34	1.71	3.38	11.08	3.36	11.04
9.	55,000	25.0	4.41	0.3269	4.28	1.69	3.31	10.87	3.33	10.92
10.	60,000	23.4	4.12	0.30	4.19	1.65	3.21	10.53	3.27	10.73
11.	65,000	21.9	3.86	0.29	4.11	1.62	3.12	10.22	3.22	10.56
12.	70,000	20.7	3.64	0.27	4.01	1.58	3.07	10.08	3.17	10.40

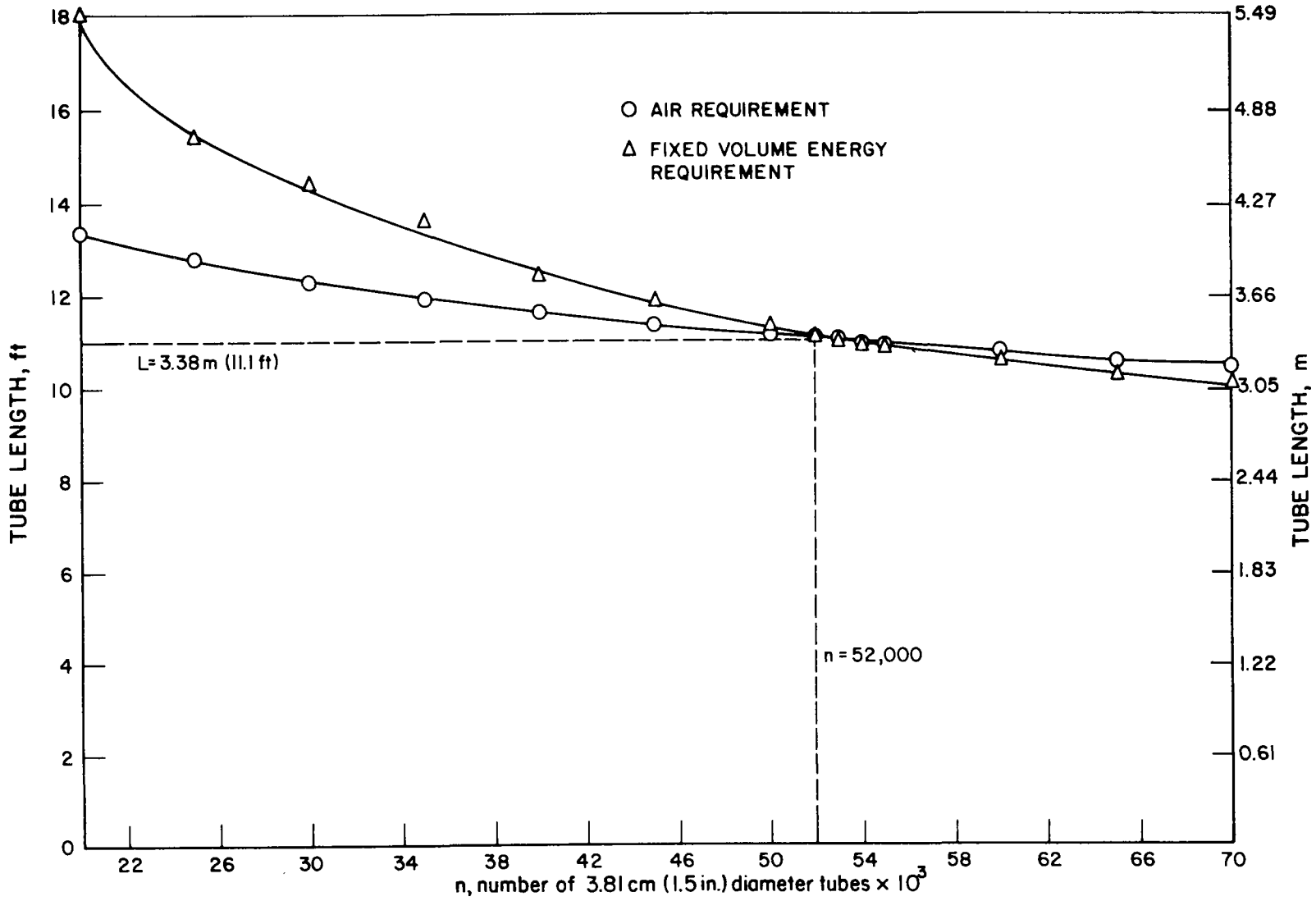
B80020285

\*  $N_{ph} = 2$

$N_{Fo} = 15.67$

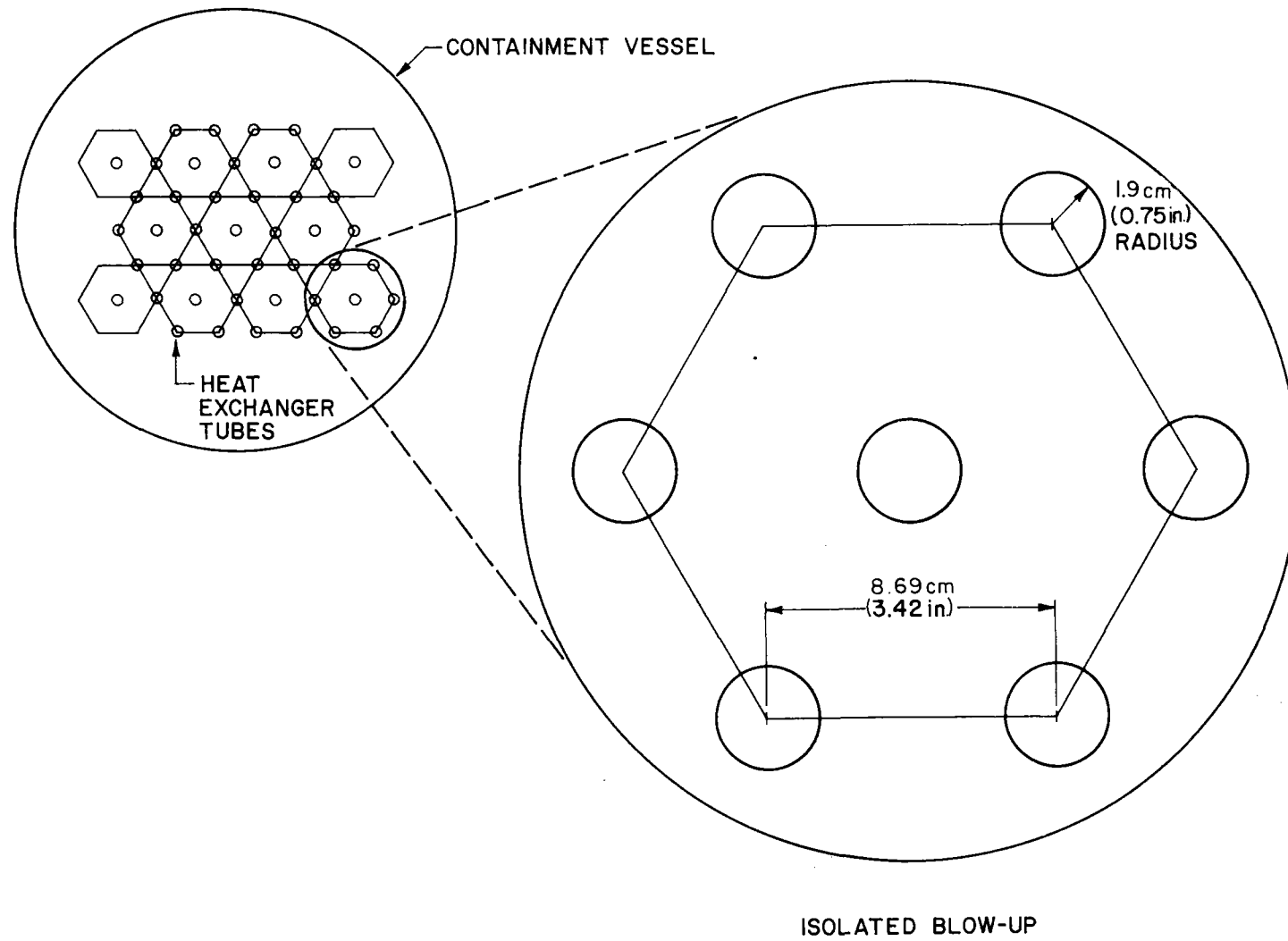
$r_o = 1.91 \text{ cm (0.75 in)}$

$\dot{m} = 9 \times 10^5 \text{ Kg/hr (2} \times 10^6 \text{ lb/hr)}$



A79122785

Figure 71. GRAPHIC SOLUTION FOR THE DESIGN OF A MULTITUBE HX TES SUBSYSTEM USING Li<sub>2</sub>CO<sub>3</sub>



A80010244

Figure 72. CROSS-SECTION OF LATENT-HEAT PHASE-CHANGE TES SUBSYSTEM (Top View)

which confirms the turbulent flow assumption and verifies the use of the Nusselt equation to derive the air-side heat transfer coefficient.

It is to be kept in mind that while the above design does indeed satisfy the performance requirements, it is not necessarily the optimum design. An optimization analysis must include studies of the effects of pipe sizing and of the use of conduction enhancement and determination of the cost-effectiveness of each design, which is beyond the scope of this project. Nevertheless this example does show the importance of the heat-transfer model and does identify the key parameters involved in designing a latent-heat TES subsystem for solar-thermal applications.

## CONCLUSIONS

Steam-Electric Power System Definition

In this project, we —

- Defined a TES utilization concept of an electrical generation subsystem, composed of a multistage condensing steam turbine and a TES subsystem with a separate power conversion loop. [The primary plant provides steam at 538°C (1000°F) and 16.5 MPa (2400 psia).]
- Evaluated conceptual designs for a 100 MW<sub>(e)</sub> TES peaking system providing steam at 316°C (600°F), 427°C (800°F), and 454°C (850°F) at 3.79 MPa (550 psia).

316°C case: Three stages; charge-to-discharge mass ratio of 1.12 with a 20% system efficiency. Average break-even storage cost, with electrical generation subsystem cost of \$200/kW and desired energy costs of 60 mills/kWhr<sub>(e)</sub> is \$43.5/kWhr<sub>(e)</sub>.

427°C case: Six isothermal sections; charge-to-discharge mass ratio of 1.2 with a 28% system efficiency.

454°C case: Seven isothermal stages; charge-to-discharge mass ratio of 1.3 with a system efficiency of 30%. Average break-even storage cost is \$52/kWhr<sub>(e)</sub>.

- Concluded TES-peaking-system utility applications that employ a separate power-conversion loop appear technically viable when interfaced with high-temperature, high-pressure base-load steam-electric plants.
- Concluded the economic feasibility of the TES peaking system depends on the development of reasonably priced containment vessels/HX's with high heat flux rates.

Salts

- Carbonate salts are attractive candidates for thermal energy storage applications.
  - They have excellent thermal, chemical and physical properties and stabilities.
  - Safe, simple handling procedures can be used.
- The feasibility of using alkali/alkaline earth carbonates as latent-heat thermal-storage materials over the temperature range 397° to 898°C (747° to 1648°F) was demonstrated.
- LiKCO<sub>3</sub> (mp 505°C, 941°F) exhibited excellent chemical, physical and thermal stability for over 5600 hours and 130 cycles and was compatible with Type 316 SS. No change in salt chemistry occurred.

- Pure  $\text{Li}_2\text{CO}_3$  [ $6.07 \times 10^5$  J/kg (261 Btu/lb), \$2.05/Kg (\$0.93/lb)] and  $\text{Na}_2\text{CO}_3$  [ $2.63 \times 10^5$  J/kg (113 Btu/lb), \$0.07/Kg (\$0.03/lb)] appear attractive as PCM's in approximate temperature regimes of  $700^\circ\text{C}$  ( $1300^\circ\text{F}$ ) and  $815^\circ\text{C}$  ( $1500^\circ\text{F}$ ), respectively.
- The  $\text{Na}_2\text{CO}_3$ - $\text{BaCO}_3$  mixture is an attractive, low-cost (\$.18/Kg, \$0.08/lb) mixture for  $\sim 700^\circ\text{C}$  ( $\sim 1300^\circ\text{F}$ ) applications.
- Salt of 85 mol %  $\text{Na}_2\text{CO}_3$  - 15 mol %  $\text{K}_2\text{CO}_3$  solidified incongruently over the temperature range  $785^\circ$  to  $740^\circ\text{C}$  ( $1445^\circ$  to  $1364^\circ\text{F}$ ).
- Salts of  $\text{CaCO}_3$  and  $\text{BaCO}_3$  were chemically stable as mixtures with alkali carbonates over the  $650^\circ$  to  $700^\circ\text{C}$  ( $1200^\circ$  to  $1300^\circ\text{F}$ ) range.
- Addition of 15 mol %  $\text{CaCO}_3$  to  $(\text{Li-Na-K})_2\text{CO}_3$  ternary eutectic lowered the melting point from  $397^\circ$  to  $383^\circ\text{C}$  ( $747^\circ$  to  $721^\circ\text{F}$ ).
- Carbonates can be melted and loaded in air environment safely and acceptably.
- Chlorides and fluorides require more sophisticated handling fabrication and operation procedures.
  - Vapors are toxic in air.
  - They must be handled and cycled in dry, inert environments to avoid accelerated containment corrosion by oxygen/moisture contamination.

#### Containment and HX Materials

- Types 304 and 316 SS demonstrated good compatibility over a range of  $370^\circ$  to  $650^\circ\text{C}$  ( $700^\circ$  to  $1200^\circ\text{F}$ ). Salt-side oxidation of Type 316 SS 25  $\mu\text{m}$  (1 mil) after 5650 hours in contact with  $\text{LiKCO}_3$  at  $482^\circ$  to  $524^\circ\text{C}$  ( $900^\circ$  to  $975^\circ\text{F}$ ) occurred.
- Prolonged operation above  $650^\circ\text{C}$  ( $1202^\circ\text{F}$ ) results in greater salt creepage and increased oxidation, carburization, grain boundary, carbide precipitation and brittle sigma-phase formation in austenitic stainless steels. Use of superalloys should be investigated.
- Use of  $\text{CO}_2$  blanket over molten carbonates above  $650^\circ\text{C}$  reduces the rate of oxidation and carburization of stainless-steel materials.

#### TCE Materials

- Porous aluminum material is attractive in carbonates to near its mp of  $\sim 650^\circ\text{C}$ . It demonstrated long term stability at  $450^\circ\text{C}$  ( $840^\circ\text{F}$ ).
- Addition of 5 vol % aluminum Duocel increased the average discharge heat flux in ternary  $(\text{Li-Na-K})_2\text{CO}_3$  eutectic (mp  $397^\circ\text{C}$ ,  $747^\circ\text{F}$ ) by  $\sim 45\%$ .

- Reticulated carbon matrix is not compatible with carbonates under air at 750°C (1382°F).
- An incongruent slush concept of 85 mol % Na<sub>2</sub>CO<sub>3</sub> - 15 mol % K<sub>2</sub>CO<sub>3</sub> salt exhibited a heat flux 31% higher than the 45-56 mol % (Na-K)<sub>2</sub>CO<sub>3</sub> system.
- Cost/benefit trade-off of TCE materials for solar-thermal systems depends on system design and duty cycle, and salt and TCE material characteristics. Further work is required for applications above 650°C (1202°F).

#### TES Module Thermal Performance

- Over 1000 hours of stable laboratory-scale and 5000 hours of stable engineering-scale performance have been demonstrated with carbonates.
- Repeated thermal cycling (20-130 cycles) did not affect physiochemical properties or cyclic thermal performance of any carbonate salts studied.
- Baseline thermal discharge characteristics and heat fluxes for salts considered for solar-thermal applications [37,830 - 75,660 W/m<sup>2</sup> (12,000 - 24,000 Btu/hr-ft<sup>2</sup>) in 0.1 KWhr<sub>th</sub> units] were established.
- The heat-transfer model based on Megerlin's solution shows agreement between predicted and observed interfacial location during heat removal from PCM.
- The heat-transfer model for scale-up to multi-tube 50 MW<sub>th</sub> HX configuration at 704°C (1300°F) was utilized.
- The thermal enhancement concept provides more efficient utilization of heat-transfer area.

## RECOMMENDATIONS FOR FUTURE RESEARCH

- Screen and evaluate high-temperature alloys as carbonate containment materials for 650° to 870°C (1200° to 1600°F) applications.
- Pursue development of cost-effective salt, containment, and insulation materials.
- Scale up to 10 KWhr<sub>th</sub> modules and conduct endurance testing of the most promising salts identified in lab-scale (0.1 kWhr<sub>th</sub>) studies, utilizing working fluids considered for commercial applications.
- Continue cost/benefit trade-off analyses and compatibility/performance studies on TCE materials in a 650° to 870°C (1200° to 1600°F) temperature range.
- Further develop and experimentally verify the heat-transfer model to account for TCE materials, high-temperature working fluids, alternate HX configuration, and superheating and convective mixing effects on solidification and melting behavior.
- Maintain cognizance of and active interaction with ongoing TES systems design and analysis studies to provide effective feedback to salt/HX R&D efforts.

## REFERENCES CITED

1. Cohen, B. M., "Development of a Phase Change Thermal Energy Storage Unit Utilizing Modified Anhydrous Sodium Hydroxide." Report prepared under Contract No. NAS3-20615 for the National Aeronautics and Space Administration. Cambridge, Mass.: Comstock & Wescott, Inc., April, 1977 - January, 1978.
2. Public Service Electric and Gas Co., "An Assessment of Energy Storage Systems Suitable for Use by Electric Utilities." Report prepared under Contract No. E(11-1)-2501 for the U. S. Energy Research and Development Administration. July, 1976.
3. Carlson, J. A. and Clayton, J. L., "Research on Energy Storage for Solar Thermal Conversion." Report prepared under Contract No. NSF-C7522234 for the National Science Foundation. Pasadena, Calif.: Xerox Electro-Optical Systems, September, 1977.
4. Bechtel Corp., "Retrofitted Feedwater Heat Storage for Steam Electric Power Stations Peaking Power Engineering Study." Final report prepared under Contract No. EY-76-C-02-2863-00 for the U. S. Energy Research and Development Administration. San Francisco: 1976.
5. Honeywell, Inc., "Solar Pilot Plant. Phase I. Conceptual Design Report." Report prepared under Contract No. E(04-3)-1109 for the U. S. Energy Research and Development Administration. Minneapolis: May 1976.
6. Ferarra, A. et. al., "Thermal Energy Storage Heat Exchanger." Final report prepared under Contract No. NAS3-20117 for the National Aeronautics and Space Administration. Bethpage, N. Y.: Grumman Aerospace Corp., October, 1977.
7. Steeve, E. J., Commonwealth Edison's Zion, Ill. facility - Westinghouse, private communication of October, 1977.
8. Steeve, E. J., Commonwealth Edison's Dresden, Ill. facility - General Electric, private communication of October, 1977.
9. Electric Power Research Institute, EPRI Technical Assessment Guide. Palo Alto, Calif.: August, 1977.
10. Dullea, J. and Maru, H. C. "Molten Salt Thermal Energy Storage Systems." Report prepared under Contract No. EY-76-C-02-2888 for the U. S. Energy Research and Development Administration. Chicago: Institute of Gas Technology, June, 1976 - May, 1977.
11. Shamsundar, N., "Heat Transfer in Thermal Storage Systems." Draft of final report prepared under Contract No. EG-77-C-04-3974/EFT-5 for the U. S. Energy Research and Development Administration. Houston: University of Houston Press, May 15, 1978.

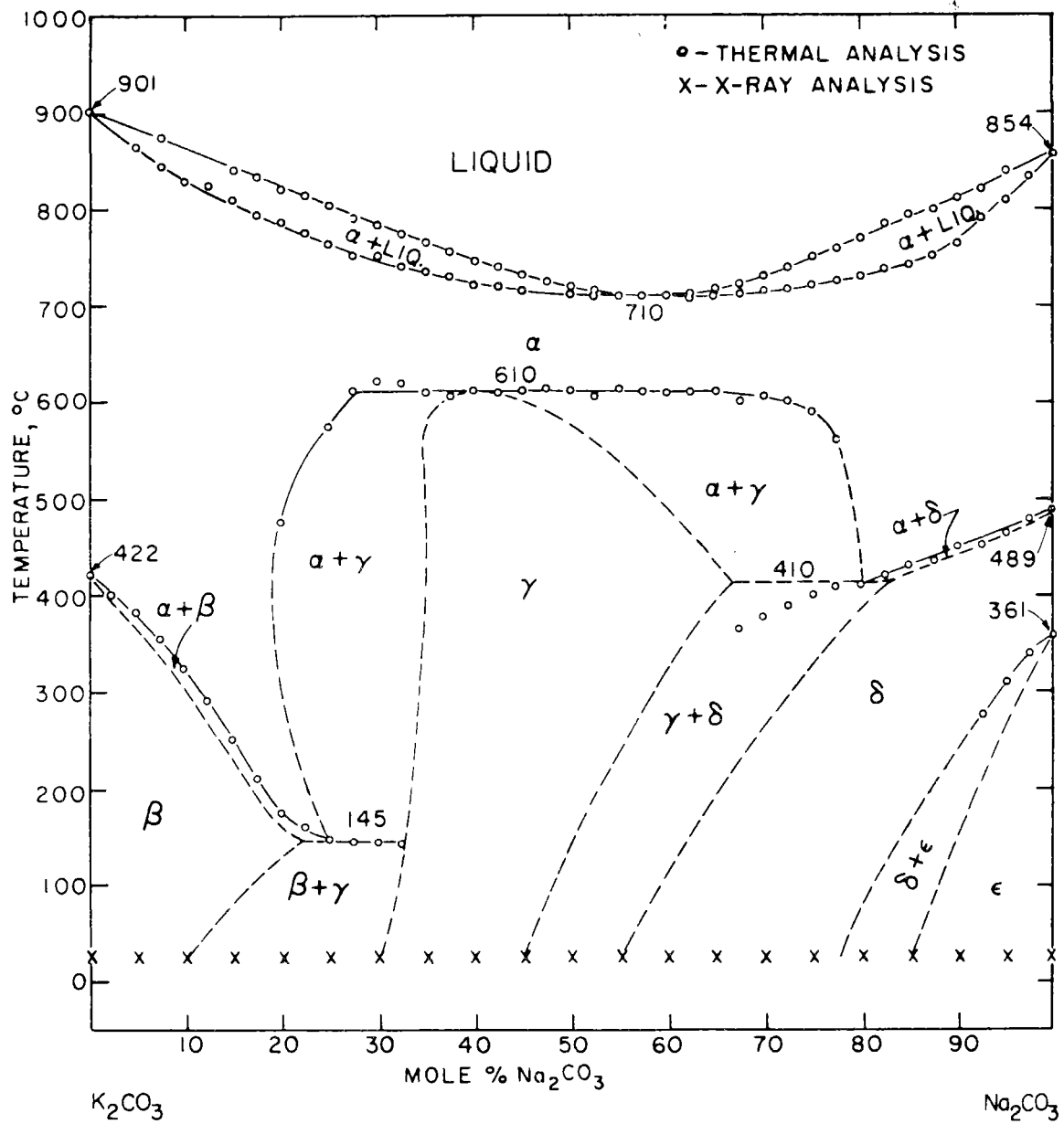
12. Meijer, R. J. and Spigt, C. L., "The Potential of the Philips Stirling Engine for Pollution Reduction and Energy Conservation." Paper presented at the 2nd Symposium on Low Pollution Power Systems Development organized by the Committee on the Challenges of Modern Society, NATO, Dusseldorf, West Germany, November 4-8, 1974.
13. Schroder, J., "Thermal Energy Storage and Control." Paper No. 74-WA/OTD-1 presented at the 95th Winter Annual Meeting of the American Society of Mechanical Engineers, New York, November 17-22, 1974.
14. Maru, H. C., Dullea, J. F., Kardas, A. and Paul, L., "Molten Salt Thermal Energy Storage Systems." Report prepared under Contract No. EY-76-C-02-2888 for the U. S. Energy Research and Development Administration. Chicago: Institute of Gas Technology, March, 1978.
15. International Center for Diffraction Data, "Powder Diffraction File." JCPDS Publication SMA-27. Swarthmore, Penn.: 1977.
16. Maru, H. C., Dullea, J. F., Kardas, and Paul, L., "Molten Salt Thermal Energy Storage Systems." Report prepared under Contract No. EY-76-C-02-2888 for the U. S. Energy Research and Development Administration. Chicago: Institute of Gas Technology, March, 1978.
17. Janz, G. J., Molten Salts Handbook. New York: Academic Press, 1967.
18. Stern, K. H. and Weise, E. L., "High Temperature Properties and Decomposition of Inorganic Salts, Part 2. Carbonates." Report prepared under Contract NSRDS-NBS30. Washington, D. C.: November, 1969.
19. Janz, G. J. et. al., "Physical Properties Data Compilations Relevant to Energy Storage. II. Molten Salts: Data on Single and Multi-Component Salt Systems." Report prepared under Contract NSRDS-NBS 61, Part II for the U. S. Department of Commerce/National Bureau of Standards. Troy, N. Y.: Rensselaer Polytechnic Institute, April, 1979.
20. Janz, G. J., Neuenschwander, E. and Kelly, F. J., "High-Temperature Heat Content and Related Properties for  $\text{Li}_2\text{CO}_3$ ,  $\text{Na}_2\text{CO}_3$ . and  $\text{K}_2\text{CO}_3$ , Trans. Faraday Soc. 59, 841 (1963).
21. Janz, G. J., et. al., "Eutectic Data: Safety, Hazards, Corrosion, Melting Points, Compositions and Bibliography." Report prepared under Contract No. TID-27163-P1 for U. S. Energy Research and Development Administration. Troy, N. Y.: Rensselaer Polytechnic Institute, July, 1976.
22. Davtyan, O. K., Teterin, G. A. and Uminskii, M. V., Sov. Electrochem. 6, 773 (1970).

23. Moore, H. H. et. al., "A Process for Cleaning and Removal of Sulfur Compounds from Low-Btu Gases." Interim Report No. 1. Richland, Wash.: Battelle Memorial Institute, Pacific Northwest Laboratories, August, 1974.
24. Megerlin, F., "Geometrically One-Dimensional Heat Conduction During Melting and Solidification," Forsch. Ingenieurwes 34 (2), 40-60 (1968).
25. Calogeras, J. E. and Gordon, L. H., "Storage Systems for Solar Thermal Power." Technical paper prepared under Contract DOE/NASA/1034-78/1 and NASA TM-78952 for the Department of Energy presented at 13th IECEC, San Diego, Calif., August 20-25, 1978.
26. Boeing Engineering and Construction, "Advanced Thermal Energy Storage Concept Definition Study for Solar Brayton Power Plants. Vol. 1." Report prepared under Contract No. EY-76-C-03-1300 for the U. S. Department of Energy. Seattle, Wash.: November, 1977.
27. Zimmerman, W. F., "Liquid Metal Thermal Transport." Paper presented at Focus on Solar Technology: A Review of Advanced Solar Thermal Power Systems, Golden, Colo., November, 1978.
28. Eichelberger, J. L., "Investigation of Metal Fluoride Thermal Energy Storage Materials." Report prepared under Contract No. EY-76-C-02-2990-00 for the Energy Research and Development Administration. King of Prussia, Penn.: Pennwalt Corp., December, 1976.
29. Institute of Gas Technology, "Development of Molten Carbonate Fuel Cells." Final report, A.G.A. Project DC-4-1. Chicago: 1967.
30. Levin, E. M., McMurdie, H. F. and Hall, F. D., Phase Diagrams for Ceramists. Columbus, Ohio: The American Ceramic Society, 1956.

MM/HH

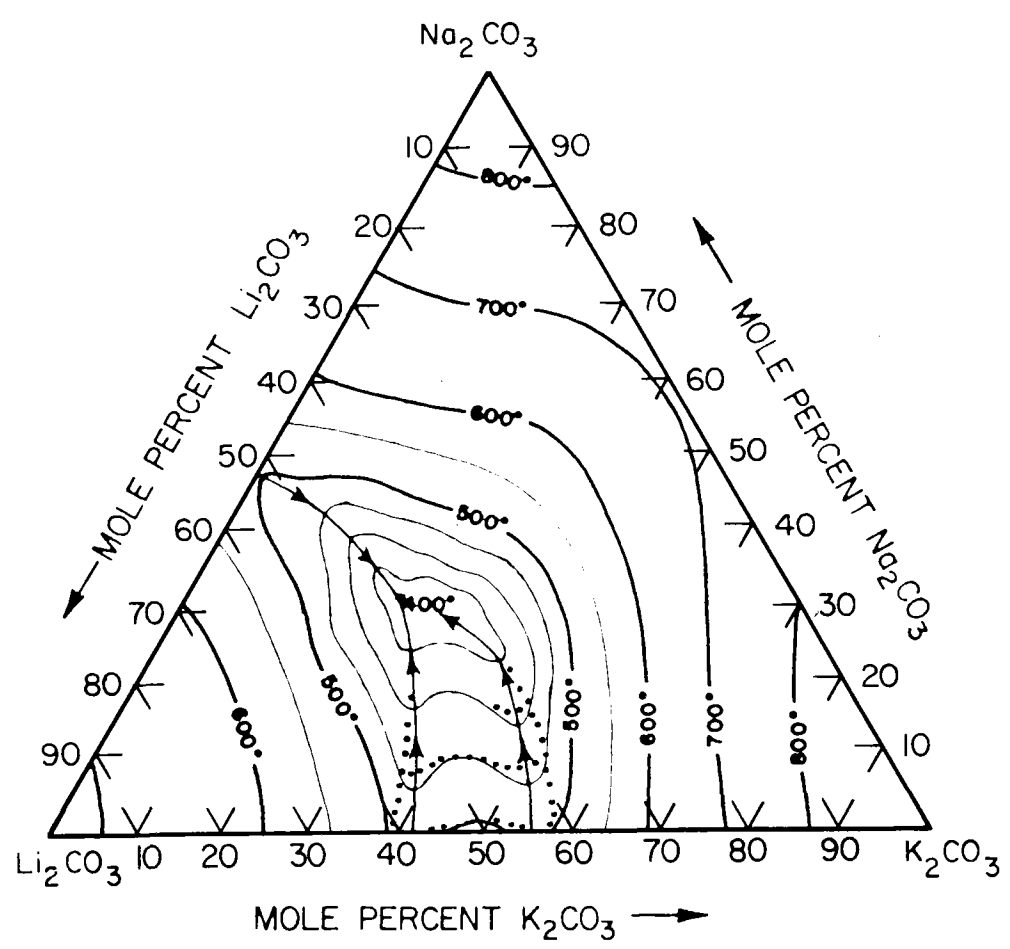
Table A-1. CONVERSION FACTORS

<u>Non-SI Unit</u>	<u>Operation</u>	<u>SI Unit</u>
atm	X $1.013 \times 10^5$	Pa
Btu	X 1055.06	J
Btu/lb	X 2326.00	J/kg
Btu/lb-°F	X 4186.80	J/kg-K
Btu/hr-ft-°F	X 1.731	W/m-K
Btu/hr-ft <sup>2</sup> -°F	X 5.678	W/m <sup>2</sup> -K
Btu/hr-ft <sup>2</sup>	X 3.154	W/m <sup>2</sup>
Cal	X 4.18	J
°C	+ 273.15	K
cP	X 0.001	Pa-s
°F	(5/9) (°F-32)	°C
ft	X 0.3048	m
ft <sup>2</sup>	X 0.0929	m <sup>2</sup>
ft <sup>2</sup> /hr	X 0.0000258	m <sup>2</sup> /s
ft <sup>3</sup>	X 0.0283	m <sup>3</sup>
in.	X 0.0254	m
in. <sup>2</sup>	X 0.00064516	m <sup>2</sup>
lb	X 0.4536	kg
lb/ft <sup>3</sup>	X 16.018	kg/m <sup>3</sup>
lbm/ft <sup>2</sup> -s	X 4.882	kg/m <sup>2</sup> -s
mil	X 0.0000254	m
psia	X 6894.8	Pa



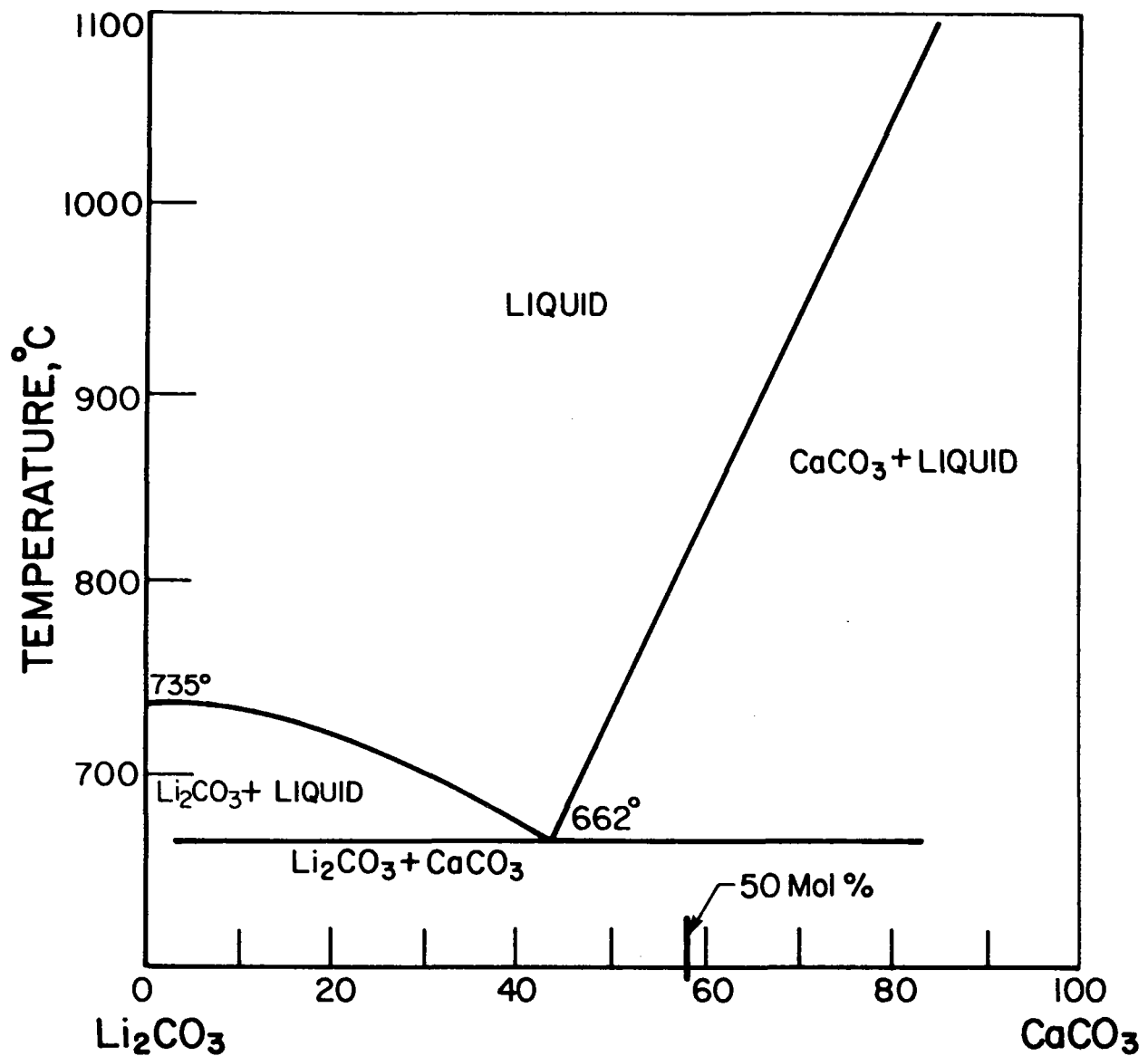
A76122833

Figure B-1. PHASE DIAGRAM FOR THE  $(\text{Na-K})_2\text{CO}_3$  SYSTEM<sup>30</sup>



A76122832

Figure B-2. PHASE DIAGRAM FOR THE  $(\text{Li-Na-K})_2\text{CO}_3$  SYSTEM<sup>30</sup>



A79122784

Figure B-3. PHASE DIAGRAM FOR THE  $\text{Li}_2\text{CO}_3$  -  $\text{CaCO}_3$  SYSTEM<sup>30</sup>

**DOCUMENT RELEASE AUTHORIZATION**

NASA Scientific and Technical Information Facility P.O. Box 8757, Balt/Wash International Airport, Maryland 21240		Control No. _____ Date: _____		
D E S C R I P T I O N	TITLE: <b>HIGH-TEMPERATURE MOLTEN SALT THERMAL ENERGY STORAGE SYSTEMS</b>			
	AUTHOR(S): <b>R. J. Petri, T. D. Claar, R. R. Tison</b>			
	ORIGINATING ORGANIZATION: <b>Institute of Gas Technology</b>		COGNIZANT NASA CENTER  <b>Lewis Research Center</b>	
	CONTRACT NO: <b>NAS3-20806</b>			
	SECURITY CLASSIFICATION: TITLE: <u>Unclassified</u> DOCUMENT: <u>Unclassified</u>			
	REPORT NO: _____			
	DATE: _____			
	NASA CR NO. <u>159663</u>	WORK UNIT NO: <b>YKR-7870</b>	NASA TECHNICAL MONITOR <b>E. R. Furman</b> <b>R. W. Vernon</b>	OFFICE CODE <b>4340</b>
NASA TMX NO. _____				
THE FOLLOWING TO BE COMPLETED BY THE RESPONSIBLE NASA PROGRAM OFFICER OR HIS DESIGNEE (Further information is available in SP-7034 entitled R & D Reporting Guidance for Technical Monitoring of NASA Contracts)				
I. Document may be processed into the NASA Information System as follows <input checked="" type="checkbox"/> May be announced in STAR (or CSTAR if a limited availability is checked below) <input type="checkbox"/> May not be announced (The attached letter may be consulted for information pertaining to the NASA non-announcement series) <input type="checkbox"/> May not be entered into the System because _____ (Provide a brief statement to be quoted in answering requests for the referenced document)				
II. Document may be made available as checked below: <input checked="" type="checkbox"/> Publicly Available <input type="checkbox"/> Classified but Unlimited to Security Qualified Requesters <input type="checkbox"/> U.S. Government Agencies and Contractors Only <input type="checkbox"/> U.S. Government Agencies Only <input type="checkbox"/> U.S. Government Agencies, NASA and NASA Contractors Only <input type="checkbox"/> NASA and NASA Contractors Only <input type="checkbox"/> NASA Headquarters and Centers Only <input type="checkbox"/> Other Limitations (Specify) _____				
Signature (Program Officer, or Designee): <i>Richard W. Vernon</i>		Office Code: <u>4340</u> Telephone No: <u>FTS 294-6266</u>		
Date Signed: <b>8/30/79</b>				
<b>MAILING LABEL</b> Use open window envelope or Clip out and paste		TO:  NASA Scientific and Technical Information Facility Attn: Accessioning Department P.O. Box 8757 Balt/Wash International Airport Maryland 21240		

FF 427 FEB 75

Enclosure 1  
Distribution List for Final Report  
NAS3-20806

	<u>No. of Copies</u>
Albuquerque Operations Office P. O. Box 5400 Albuquerque, NM 87115 Attn: D. K. Nowlin	1
Argonne National Lab 9700 South Cass Avenue Argonne, IL 60439 Attn: Dr. Magdy Farahat	1
Arizona Public Service 411 North Central Phoenix, AZ 85036 Attn: E. R. Weber	1
Badger Energy, Inc. 1 Broadway Cambridge, MA 02142 Attn: Fred Gardner	1
Bechtel Corporation 50 Beale Street San Francisco, CA 94119 Attn: T. E. Walsh	1
Biphase Energy Systems 2800 Airport Boulevard Santa Monica, CA 90405 Attn: Walter Studhalter	1
Black & Veatch P. O. Box 8405 Kansas City, MO 64114 Attn: Sheldon L. Levy	1

## Distribution List - Cont.

	<u>No. of Copies</u>
Boeing Engineering & Construction Division of The Boeing Company P. O. Box 3707 Seattle, WA 98124 Attn: J. Shroeder	1
W. Beverly	1
W. Engle	1
Central Electricity Generating Board Research Division Marchwood Engineering Laboratories Marchwood, Southampton Hampshire SO4 4ZB, England Attn: Dr. Ian Glendenning	1
Comstock & Wescott, Inc. 765 Concord Avenue Cambridge, MA 02138 Attn: Richard E. Rice	1
DOE/ETS Division of Planning & Technical Transfer 600 E. Street Washington, D. C. 20545 Attn: Leslie S. Levine	1
U.S. Department of Energy Division of Energy Storage Systems Washington, D. C. 20545 Attn: G. F. Pezdirtz	1
J. Swisher	1
J. Gahimer	1
W. Frier	1
R. Holliday	1
L. Holt	1

3

## Distribution List - Cont.

	<u>No. of Copies</u>
U.S. Department of Energy San Francisco Operations Office 1333 Broadway Oakland, CA 94612 Attn: D. Elliot	1
R. Hughey	1
U.S. Department of Energy Division of Central Solar Technology Washington, D. C. 20545 Attn: M. U. Gutstein	1
Dynatech R/D Company 99 Erie Street Cambridge, MA 02139 Attn: Dr. R. P. Tye	1
Edison Electric Institute 90 Park Avenue New York, NY 10016 Attn: J. Karp	1
Electric Power Research Institute 3412 Hillview Avenue P. O. Box 10412 Palo Alto, CA 94303 Attn: Dr. T. Schneider	1
Dr. F. Kalhammer	1
W. A. Stevens	1
Exxon Research and Engineering Company P. O. Box 45 Linden, NJ 07036 Attn: R. P. Cahn	1

## Distribution List - Cont.

	<u>No. of Copies</u>
General Atomic Company P. O. Box 81608 San Diego, CA 92138 Attn: D. Vrable	1
General Electric Company - TEMPO P. O. Drawer QQ Santa Barbara, CA 93102 Attn: W. Hausz	1
General Electric Company 1 River Road Schenectady, NY 12345 Attn: Eldon Hall	1
General Electric Company Advanced Energy Programs P. O. Box 15132 Cincinnati, OH 45215 Attn: W. F. Zimmerman	1
Geoscience Ltd 410 South Cedros Avenue Solana Beach, CA 92075 Attn: Dr. H. Poppendiek	1
Graz University of Technology Obere Teichstrasse 21/i A-8010 Graz, Austria Attn: Prof. P. V. Gilli	1
Grumman Aerospace Corporation Bethpage, NY 11714 Attn: Robert Haslett	1

5

## Distribution List - Cont.

	<u>No. of Copies</u>
Honeywell, Inc. Energy Resources Center 2600 Ridgeway Parkway Minneapolis, MN 55413 Attn: R. LeFrois	1
Indian Institute of Technology Department of Mechanical Engineering Madras 600036, India Attn: Dr. M. V. Krishna Murthy	1
Jet Propulsion Laboratory California Institute of Technology 4800 Oak Grove Drive Pasadena, CA 91103 Attn: J. Stearns	1
Midwest Research Institute 425 Volker Boulevard Kansas City, MO 64110 Attn: K. P. Ananth	1
National Aeronautics and Space Administration Lewis Research Center 21000 Brookpark Road Cleveland, OH 44135 Attn: Arno W. Nice, MS: 500-202 Norman T. Musial, MS: 500-311 Leonard W. Schopen, MS: 500-305 Linda M. Finke, MS: 500-202 Report Control Office, MS: 5-5 Library, MS: 60-3 Richard W. Vernon, MS: 500-202	1 1 1 1 1 2 48
National Aeronautics and Space Administration Headquarters Washington, D. C. 20546 Attn: RG-14/W. Johnson	1

6

## Distribution List - Cont.

No. of  
Copies

NASA Scientific & Technical Information Facility  
 P. O. Box 8757  
 Baltimore/Washington International Airport, MD 21240  
 Attn: Accessioning Department 30

Naval Research Laboratories  
 Washington, D. C. 20375  
 Attn: Dr. T. A. Chubb 1

Northern States Power Company  
 414 Nicollet Avenue  
 Minneapolis, MN 55401  
 Attn: Les Weber, Vice Pres. of Research 1

Oak Ridge National Laboratory  
 Building 9204-1, Mail Stop 3  
 P. O. Box Y  
 Oak Ridge, TN 37830  
 Attn: David M. Eissenberg 1

Ontario Hydro  
 700 University Avenue  
 Toronto, Ontario M5G1X6, Canada  
 Attn: A. G. Barnstaple 1

R&D Associates  
 P. O. Box 9695  
 Marina del Rey, CA 90291  
 Attn: R. P. Hammond 1

Rocket Research Company  
 York Center  
 Redmond, VA 98052  
 Attn: D. D. Huxtable 1

## Distribution List - Cont.

	<u>No. of Copies</u>
Rockwell International Rocketdyne Division 6633 Canoga Avenue Canoga Park, CA 91304 Attn: Richard Morgan	1
Rockwell International Energy Systems Group 11716 Monogram Avenue Granada Hills, CA 91344 Attn: Jack Rosemary	1
Sandia Laboratories Albuquerque Albuquerque, NM 87115 Attn: J. F. Banas	1
Sandia Laboratories Livermore P. O. Box 969 Livermore, CA 94550 Attn: A. C. Skinrod	1
L. Radosevish	1
T. D. Brumleve	1
W. S. Winter, Jr.	1
J. D. Gilson	1
SERI 1536 Cole Boulevard Golden, CO 80401 Attn: R. Copeland	1
C. Wyman	1
Sigma Research, Inc. 2950 George Washington Way Richland, WA 99352	1
Solar Resources Inc. 5401 McConnell Avenue Los Angeles, CA 90066 Attn: Ralph E. Bartera	1

## Distribution List - Cont.

	<u>No. of Copies</u>
Stone & Webster 245 Summer Street P. O. Box 2325 Boston, MA 02107 Attn: K. E. Hogeland	1
Swiss Federal Institute of Reactor Research 5303 Wurenlinged Switzerland Attn: Professor M. Taube	1
Tennessee Valley Authority 1360 Commerce Union Bank Building Chattanooga, TN 37401 Attn: Dr. A. Manaker	1
University of Delaware Department of Chemical Engineering Newark, DE 19711 Attn: C. E. Birchenall	1
University of Stuttgart Institute for Nuclear Energy & Energy Systems (IKE) Pfaffenwaldring 31, Postfach 80 11 40 7000 Stuttgart 80, Federal Republic of Germany Attn: Manfred Groll	1
Westinghouse Electric Corporation P. O. Box 10864 Pittsburgh, PA 15236 Attn: M. K. Wright W. Lundberg	1 1
Xerox Electro-Optical Systems 300 North Halstead Street Pasadena, CA 91107 Attn: William Mortenson	1

1. Report No. DOE/NASA/0806-79/1 NASA CR 159663		2. Government Accession No.		3. Recipient's Catalog No.	
4. Title and Subtitle High-Temperature Molten Salt Thermal Energy Storage Systems				5. Report Date February 1980	
				6. Performing Organization Code	
7. Author(s) Randy J. Petri, Terry D. Claar, Ray R. Tison, Leonard G. Marianowski				8. Performing Organization Report No.	
9. Performing Organization Name and Address Institute of Gas Technology IIT Center, 3424 S. State St. Chicago, Illinois 60616				10. Work Unit No.	
				11. Contract or Grant No. NAS 3-20806	
12. Sponsoring Agency Name and Address National Aeronautics and Space Administration Washington, DC 20546				13. Type of Report and Period Covered Contractor Final Report 9/14/77 -- 12/14/78	
				14. Sponsoring Agency Code	
15. Supplementary Notes Project Manager, Edward R. Furman, NASA Lewis Research Center, Cleveland, Ohio					
16. Abstract Experimental results of comparative screening studies of candidate molten carbonate salts as phase-change materials (PCM) for advanced solar-thermal energy storage applications at 540° to 870°C (1004° to 1600°F) and steam-Rankine electric generation at 400° to 540°C (752° to 1004°F) are presented. Alkali carbonates are attractive as latent-heat storage materials because of their relatively high storage capacity and thermal conductivity, low corrosivity, moderate cost, and safe and simple handling requirements. Salts were tested in 0.1 kWhr lab-scale modules and evaluated on the basis of discharge heat flux, solidification temperature range, thermal cycling stability, and compatibility with containment materials. The feasibility of using a distributed network of high-conductivity material to increase the heat flux through the layer of solidified salt was experimentally evaluated. The thermal performance of an 8 kWhr thermal energy storage (TES) module containing LiKCO <sub>3</sub> remained very stable throughout 5650 hours and 130 charge/discharge cycles at 480° to 535°C (896° to 995°F). A TES utilization concept of an electrical generation peaking subsystem composed of a multistage condensing steam turbine and a TES subsystem with a separate power conversion loop was defined. Conceptual designs for a 100 MW <sub>e</sub> TES peaking system providing steam at 316°, 427°, and 454°C (600°, 800°, and 850°F) at 3.79 X 10 <sup>6</sup> Pa (550 psia) were developed and evaluated. Areas requiring further investigation have also been identified.					
17. Key Words (Suggested by Author(s)) Thermal storage Phase-change media Solar thermal storage Carbonates			18. Distribution Statement Unclassified - unlimited Star Category 44 DOE Category UC-94a		
19. Security Classif. (of this report) Unclassified		20. Security Classif. (of this page) Unclassified		21. No. of Pages 190	22. Price*

\* For sale by the National Technical Information Service, Springfield, Virginia 22161